Agenzia nazionale per le nuove tecnologie,
l'energia e lo sviluppo economico sostenibile

MINISTERO DELLO SVILUPPO ECONOMICO

Ricerca di Sistema elettrico

Qualifica di codici di calcolo dedicati alle analisi di sistemi avanzati quando applicati nella simulazione di impianti a metallo liquido

A Del Nevo, C. Venturi, E. Martelli, D. Rozzia, F. Castiglia, M. Giardina, F. Mascari, M.L. Richiusa, G. Vella

Report RdS/2013/025

QUALIFICA DI CODICI DI CALCOLO DEDICATI ALLE ANALISI DI SISTEMA AVANZATI QUANDO APPLICATI NELLA SIMULAZIONE DI IMPIANTI A METALLO LIQUIDO

A. Del Nevo, C. Venturi, E. Martelli, D. Rozzia (ENEA), F. Castiglia, M. Giardina, F. Mascari, M.L. Richiusa, G. Vella (UNIPA)

Settembre 2013

Report Ricerca di Sistema Elettrico

Accordo di Programma Ministero dello Sviluppo Economico - ENEA
Piano Annuale di Realizzazione 2012
Area: Produzione di energia elettrica e protezione dell'ambiente
Progetto: Sviluppo competenze scientifiche nel campo della sicurezza nucleare e collaborazione ai programmi internazionali per il nucleare di IV Generazione
Obiettivo: Sviluppo competenze scientifiche nel campo della sicurezza nucleare
Responsabile del Progetto: Mariano Tarantino, ENEA

Il presente documento descrive le attività di ricerca svolte all'interno dell'Accordo di collaborazione "Sviluppo competenze scientifiche nel campo della sicurezza nucleare e collaborazione ai programmi internazionali per il nucleare di IV generazione"
Responsabile scientifico ENEA: Mariano Tarantino
Responsabile scientifico CIRTEN: Giuseppe Forasassi

Titolo

Qualifica di codici di calcolo dedicati alle analisi di sistema avanzati quando applicati nella simulazione di impianti a metallo liquido

Descrittori

Tipologia del documento: Rapporto Tecnico

Collocazione contrattuale: Accordo di programma ENEA-MSE su sicurezza nucleare e reattori di IV generazione

Argomenti trattati:
Analisi incidentale
Termoidraulica dei reattori nucleari
Termoidraulica del nocciolo
Generation IV reactors

Sommario

Il presente report rappresenta un contributo allo sviluppo e alla qualifica di codici e metodi per l'analisi di sicurezza di reattori di IV generazione refrigerati a metalli liquidi. Il report si divide in due parti: una prima parte (A) nella quale sono presentati lo sviluppo di due modelli RELAP5-3D© di reattori veloci a piscina refrigerati a metallo liquido: 1) CP-ESFR ed 2) EBR-II. La prima nodalizzazione relativamente semplice e fast running sarà finalizzata attraverso l'uso dei dati neutronici d'impianti calcolati nell'ambito della stessa task LP2 A3. La seconda nodalizzazione, molto dettagliata e complessa, fa uso di compoenenti tridimensionali e sarà utilizzata nell'ambito del progetto IAEA coordinated research project (CRP) on EBR-II Shutdown Heat Removal Tests (SHRT). Il report descrive l'ambito, le nodaliazzazioni, la strategia e i principali step dei qualifica.
La seconda parte (B) riguarda uno studio sull'applicabilità degli attuali codici termoidraulici di sistema per l'analisi di sicurezza di reattori di IV generazione refrigerati a metalli liquidi (piombo e sodio). Tale attività segue il seguente schema logico. 1) Identificazione dei fenomeni termoidrualici rilevanti per la sicurezza prendendo a riferimento il progetto prototipico di un reattore refrigerato a metallo liquido (es. ELSY o ALFRED). 2) L'identificazione dei principali modelli e correlazioni rilevanti per la simulazione del codice. 3) La valutazione di tali modelli e correlazioni. 4) L'identificazione dei possibili miglioramenti che possono essere implementati e di quali modelli addizionali sarebbero necessari.

Note

Lavoro eseguito in collaborazione con Università di Palermo (UNIPA)

Autori:

A. Del Nevo, C. Venturi, E. Martelli, D. Rozzia (ENEA)
F. Castiglia, M. Giardina (UNIPA)
F. Mascari, M. L. Richiusa, G. Vella (UNIPA)

Copia n. **In carico a:**

REV.	DESCRIZIONE	DATA		REDAZIONE	CONVALIDA	APPROVAZIONE
0	EMISSIONE	24/09/13	NOME	A. Del Nevo	I. Di Piazza	M. Tarantino
			FIRMA			

(Page intentionally left blank)

SUMMARY

The report is a contribution on activities related to the development and the qualification of thermal-hydraulic system codes and of methods for safety analyses of liquid metals Gen. IV reactors. The report is divided into two parts.

The former (A) presents the development of two RELAP5-3D© nodaliztions of pool type sodium cooled fast reactors. The CP-ESFR nodalization is rather simple and fast running, and will be finalized using the neutronic data calculated in the framework of the same task LP2 A3. The EBR-II is detailed. Indeed, it models the overall pool system and the reactor zone with a 3D component, and the driver core fuel assemblies, fed by the high flow line, one by one. This is developed and set-up in the framework of IAEA coordinated research project (CRP) on EBR-II Shutdown Heat Removal Tests (SHRT). The report describes the framework of the activities, the nodalization and the first steps of qualification.

The second part (B) deals with studies on the applicability of current thermal-hydraulic system codes when applied to safety analyses of pool type Gen. IV fast reactors, cooled with liquid metals (i.e. ELSY o ALFRED). The study is based on the following rationale: 1) identification of thermal-hydraulic phenomena relevant for the safety; 2) identification of the main models and correlations relevant for the code simulation; 3) a qualitative evaluation of the reliability and limitations of those models and correlations; 4) the identification of possible model improvements.

LIST OF CONTENTS

PART A: DEVELOPMENT AND SETUP OF RELAP5-3D© NODALIZATIONS OF LIQUID METAL POOL FAST REACTORS

LIST OF FIGURES

LIST OF TABLES

1 DEVELOPMENT AND SET UP OF CP-ESFR NODALIZATION BY RELAP5-3D© V4.0.3 CODE

1.1 Framework

The development of the CP-ESFR has a twofold objective: 1) the set up and application of a chain of codes for supporting the design and safety analysis of liquid metals pool types Gen. IV reactors; 2) the assessment of core thermal-hydraulic parameters (i.e. cladding temperature, coolant temperature at core outlet and fuel centerline temperatures) of two different fuel design (i.e pelletized and sphere-packed). The activity is connected with the EC project PELGRIMM.

1.1.1 Description of CP-ESFR

CP ESFR is a large integrated Collaborative Project on European Sodium Fast Reactor realized under the ages of the EURATOM 7th Framework Programme, which merges the contribution of 25 European partners[1]. The ESFR plant design is based on an industrial sodium cooled pool reactor of 1500 MWe with a plant's efficiency of 42%.

The CP-ESFR (Fig. 1) designed comprises the core, the above core structure, the Fuel Handling System (FHS), three mechanical primary pump, six secondary loops, each had one Intermediate Heat Exchangers (IHX) on the reactor side and six modular sodium/water Steam Generators (SG). In addiction there are six Deacay Heat Exchangers (DHX) connected to six Direct Reactor Cooling loops (DRC) to ensure decay heat removal of the reactor when it is shut down. In Fig. 1 is represented a plant layout for twinned reactors and in Fig. 1 a 3D view of the CP-ESFR pool with theirs components.

The project design was made base on specified objectives:

- Simplification of structure
- Improved In Service Inspection and Repair
- Improved manufacturing conditions for cost reduction and increased quality
- Reduction of risks related to sodium fires and to the water/sodium reaction
- Improved robustness against external hazards.

The main characteristics of CP-ESFR are summarized in the Tab. 1.

The oxide core consists of 225 inner and 228 outer fuel sub assembly (Fig. 2). Three rows of reflector sub-assemblies, not reported in the figure, can be used to place one fertile or MA fuel assembly and two additional rows of steel blocks. The "control" rod system is composed by 9 DSD (Diverse Shutdown Device) assemblies and 24 CSD (Control and Shutdown Device) assemblies.

The inner and outer sub-assembly, in Fig. 3, consist of a hexagonal wrapper tube made of ferritic martensitic steel (EM10). Within, it is located a fuel bundle and ,a reflector and absorber layers. The fuel bundle consists of 271 pins (see Fig. 4). The clad is fabricated in ODS steel with outer diameter of 10.73 mm and 0.5 mm of thickness. Pins are placed in a triangular arrangement with helical wire wrap spacer. The overall length of the fuel pin bundle is 2.363 meter. The active core region is 1 meter long. The uranium oxide fuel pellets have a outside diameter equal to 9.43 mm. The gap has a thickness 0.15 mm filled with helium.

A fertile blanket region (300 mm) that contains only depleted uranium oxide, a lower gas plenum filled by helium and a plug with ODS steel pellets are placed below the active core region. The fuel rod has an upper gas plenum and an upper plug with the same characteristics.

Each sub-assembly fits in the diagrid support sub-assembly plate by the foot sub-assembly for a length of 600 mm. The inner and outer fuel sub-assembly have the same axial sub-assembly structure but they differs in Pu mass content. 14.05% for inner fuel region and 16.35% for the outer.

Over fuel pin bundle there is a sodium region, then the absorber and reflector regions. These regions have 19 pins in the same configuration of fuel region but without the helical wire wrap spacer. The external radius of each pin is 40 mm. In the absorber and reflector region, clads are made in EM10 material (1 mm of thick) and pellets are made in B4C and steel F17 respectively. Between clad and pellet there is a gap of 1 mm.

Outside the core, three rings of reflectors are installed. Only 84 sub-assemblies are cooled. The central assembly of the core is a reflector.
Reflector pins placed in the inner region have the same characteristics of the UPS region, described above.

The core and the neutron shielding are fixed on a diagrid, which is supported on the strongback. The strongback is laid on the main vessel bottom and transfers the total core weight.

The diagrid is a stainless steel cylindrical structure with a diameter of 7.4 m. It contains a large number of vertical circular shroud tubes where the core subassemblies are inserted. These shroud tubes provide the positioning and support for the subassemblies and allow the sodium feed from the strongback through holes. The detailed flow arrangements are such that the hydraulic forces acting on the subassemblies serve to hold them down in the diagrid. This structure is entirely welded. The absence of bolts removes any risk of loose parts inside the primary circuit. The diagrid structure needs high stability (thermal and mechanical) to avoid changes in core geometry that may cause excursions of reactivity.

The strongback is a stainless steel pressurized (5 bar) box-type structure comprising two circular plates linked by welded webs. It is resting on the vessel bottom (no welding). A pivot centers the strongback and provides an ultimate redundant support in case of core structure collapse. It could also offer a natural path to corium. Absence of welding between strongback and vessel is favorable regarding seismic and inspectability issues.

The pump is connected to the strongback and not to the diagrid (like in Superphenix), see Fig. 5. The new design allows a shorter and more robust pipe connection, reducing the risk of a break. Sodium flows (Fig. 6) first through the strongback with a pressure of 5 bar. Then, it flows through the diagrid by means of 18 flexible sleeves (500 mm diameter). The sleeves are welded on the lower surface of the diagrid. A share of flow sodium, 830 Kg/s, entering in diagrid through sleeves is directed to core catcher to cooling vessel. They may undergo high thermomechanical constraints during transients, and their behavior is to be considered with great care for design improvements. Monitoring is necessary to detect deterioration of the support structures.

The ACS (Above Core Structure) is a conical structure located over the core. The main functions are: 1) the support of control rod drive mechanisms and core instrumentation, and 2) the control of the primary sodium flow distribution into the hot pool to achieve the required thermal-hydraulic conditions and quality of the sodium free surface. The ACS supports the Direct Lift Charge Machine (DLCM) is installed in the center. It is used for handling of core center fuel assemblies. The ACS also provides the thermal protection of the equipment within the ACS and the SRP (Small Rotating Plug).

The main components of the ACS (Fig. 7) are listed hereafter.

- The outer shell.
- The baffle plate.
- The porous plate (flat plate at the base of ACS with holes for sodium flow and penetration of the shroud and instrumentation guide-tubes).
- Shroud tubes (tubes to drive absorber rods (CSD and DSD), the Direct Lift Charge Machine (DLCM), the Failed Fuel Location system (FFL), Core Thermocouples, core measuring and ISI monitoring systems).
- Instrument Guide Tubes (IGT).
- The Thermocouples and Failed Fuel Location (FFL) pipework.
- The Multiple Layer Insulation (to reduce the heat transfer to the small rotating plug, and control the axial temperature gradient in the external shell of the ACS).

The ACS extends over one row of steel reflectors and is immersed in the sodium to a height of 6 m. The environment above the sodium comprises a layer of argon, which may contain sodium vapor and aerosols and 0.85 m depth of multiplate insulation to reduce the heat transfer from the ACS to the SRP. Most of the ACS structures are immersed in the stream of sodium emerging from the core, at a temperature ranging from 560°C at the core outlet to 545°C at the sodium surface. The top part of the structure, approximately 1.160 m, however, is located in the cover gas region where the temperature ranges from 130°C at the interface between the insulation plates and the underside of the SRP, to 545°C at the sodium level. Instrumentation is routed via straight instrumentation guide tubes below the baffle plate. The tubes provide access to the core for Thermocouples (TC), Failed Fuel Location sampling systems (FFL), Fission Chambers (FC), and nucleonic instruments.

A flow baffle is incorporated to slow down the velocity of the coolant emerging from the core and to direct the flow into the hot pool, in a way that meets the thermal hydraulic objectives, such as mixing, flow and temperature distribution and hot pool surface quiescence. One of the most important problems to be solved, by the ACS, is to get a structure rigid enough to resist the core emerging flow impingement and seismic movements, and flexible enough to accommodate thermal differential stresses, due to core coolant emerging flow temperature variations and gradients. The ACS is integrated in the SRP. As such, it can only be removed as a complete unit. It takes part in the primary argon cover gas containment. It also forms a part of the primary circuit.

Three primary pumps are installed with a nominal flow mass of 6512 kg/s each. Every pump comprises a cylindrical casing and vertical shaft machine inserted into the primary circuit via a penetration in the reactor roof, on which it is mounted.

The bottom end of the pump, the outlet, is connected with a sphere to the strongback, whilst the pump suction side/inlet to the impeller communicates directly with the reactor's cold pool. The design has been kept as simple as possible, without valve. Pumps are located on a common pitch circle diameter and forming a parallel circuit with the same pump head and specific energy requirement.
The design (Fig. 8) includes the following main features:

- Single mixed flow impeller.
- Top inlet entry flow to the impeller.
- Subcritical hollow drive-shaft, designed to get the first critical whirling speed above the maximum operating speed with a comfortable margin.

- Synchronous motor to allow easy operation of the pump over the whole range of required speeds (with specific regulations).

The impeller is mounted on the drive shaft. A flywheel is implemented in order to extend the rundown time. The shaft is supported at the top end by a magnetic axial thrust bearing and a radial bearing.
A hydrostatic sodium radial bearing is located at the bottom of the shaft above the impeller and is fed with high pressure sodium from the outlet collecting sphere (Fig. 8).

Six IHX (intermediate heat exchange) on 600 MWth are installed in reactor vessel (Fig. 9). It is a counter flow heat exchanger with the secondary sodium flowing downwards through a central duct before turning upwards in the bottom header and flowing vertically inside the heat exchanger tubes, where it is heated by the primary sodium flowing downwards on the shell side. The IHX unit is connected physically and functionally to both the primary and secondary sodium circuits. The design requirements are:

- Maximum allowed pressure drop imposed by the primary and secondary systems (~17 kPa on the primary sodium side, ~0.1 MPa on the secondary side).
- Maximum secondary circuit pressure in case of steam generator unit design based accident (about 55 bar on the IHX in case of a Sodium/Water reaction resulting from the failure of all the tubes of a modular SG).
- The seal between the IHX and the inner vessel must accommodate thermal movements between the components and the conical part (redan). A gas seal is not recommended (risk of gas entrainment into the core).

The IHX has a valve on the primary sodium side allowing the inlet window to be closed and the secondary circuit and steam plant to be isolated from the primary circuit. The reactor might be operated with one or two IHX isolated.

The inner vessel is an axisymmetrical shell fabricated structure, comprising: conical part (redan), a cylindrical inner vessel upper skirt, a cylindrical core barrel welded on the strongback. In the conical skirt, there are a minimum set of 9 penetrations: 6 fot the IHX penetrations and 3 for primary pump penetrations.

The inner vessel separates the hot pool which contains the core subassemblies and the IHX inlets from the cold pool where are located the IHX outlets and the primary pumps inlets. It provides a leaktight barrier between the hot and cold pools and provides geometric and hydraulic guide to the pump inlets. It participates with the other internal structures in the distribution of the primary sodium flow inside the main vessel.

A conical skirt (redan) is proposed in place of the ogival skirt of EFR to simplify manufacturing. The core barrel is welded on the strongback (and not on the diagrid). As a result, the conical skirt is less sensitive to buckling by plastic ruin. It also decreases the surface subjected to the difference in pressure between collectors, and it provides a natural protection of the diagrid against hot shocks at the exit of the IHX. The inner vessel upper part is subject to high thermo mechanical constraints at the free surface (sodium at 545°C, argon at 400°C), leading to minimize thickness in that region to lower thermal fatigue. On the other hand, it must also sustain high mechanical and fluid loads during an earthquake, and its thickness must be large enough to ensure its stability.

The main vessel is fabricated in austenitic steel (316LN). It is hanged to the civil work by means of a forged piece. The upper cylindrical part is cooled by a small sodium flow taken from the cold plenum below the diagrid. An immersed weir (Fig. 10) limits the risk of gas entrainment and ensures creep and fatigue

resistance of the main vessel over 60 years. The strongback is laid on a forged structure in the vessel wall, which improves the integrity and inspectability both during manufacturing and reactor life.

The main vessel is completely surrounded by a leak tight safety vessel. A nitrogen atmosphere is maintained between the two vessels. The safety vessel may be fabricated in another grade than main vessel to avoid common mode failure. The main function of the safety vessel is to avoid core uncovering in case of a leakage of the main vessel. The interspace between the main vessel and safety vessel is large enough to accommodate a wheeled ISI vehicle for inter-vessel inspection, but small enough to ensure a sufficient sodium level in the event of a main vessel leakage – to allow decay heat removal via the normal IHX and DRC systems.

GENERAL CHARACTERISTICS PLANT	
Reactor heat output	3600 MWth
Net electrical output	1500 MWe
Plant lifetime	60 years
Global efficiency	42%
Availability objective	90%
Number of IHX	6
Number of DHX	6
Number of pumps	3
Number of secondary loops	6
Number of DRC loops	6

Tab. 1 – CP-ESFR: plant characteristics.

FUEL SUB-ASSEMBLY DESIGN	oxide
Sub assembly pitch [mm]	0.2108
sodium gap with inter assembly [mm]	0.0045
wrapper tube outer flat-flat width [mm]	0.2063
wrapper tube thickness [mm]	0.0045
wrapper tube material	FM steel (EM10)
WIRE	
wire wrap spacer diameter [mm]	0.001
wire wrap helical pitch [mm]	225
wire wrap spacer material	ODS steel
FUEL PINS	
number of fuel pins for sub-assembly	271
outer clad diameter [mm]	0.01073
inner clad diameter [mm]	0.00973
cladding material	ODS steel
fuel pellet diameter [mm]	0.00943
fuel pellet material	$(U,Pu)O_2$
fuel average density	88% TD
O/M	1.98

Tab. 2 – CP-ESFR: fuel pin characteristics

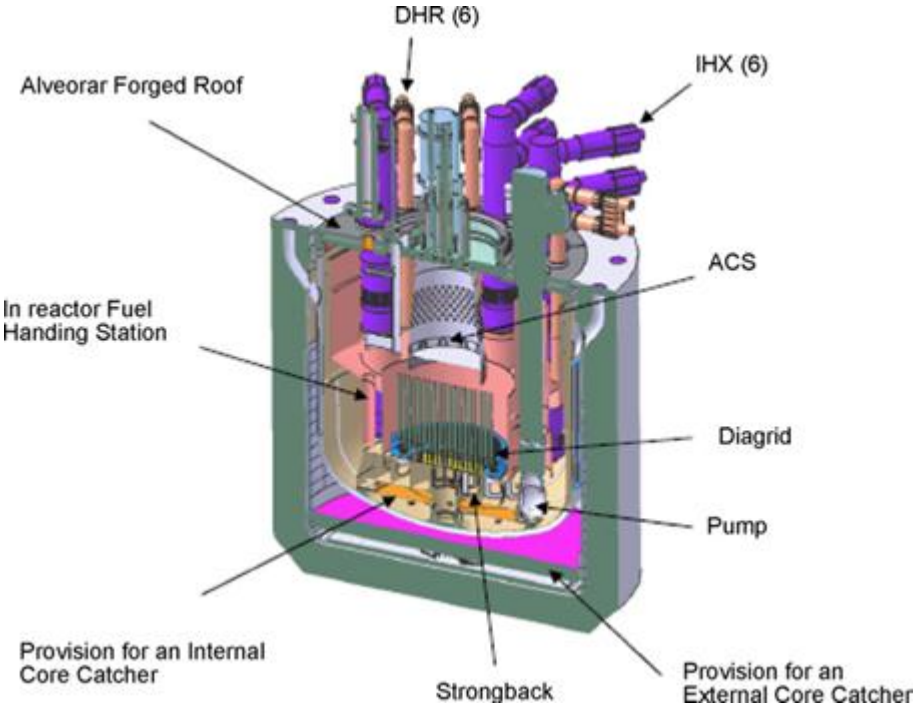

Fig. 1 – CP-ESFR: 3D view of the pool and internals.

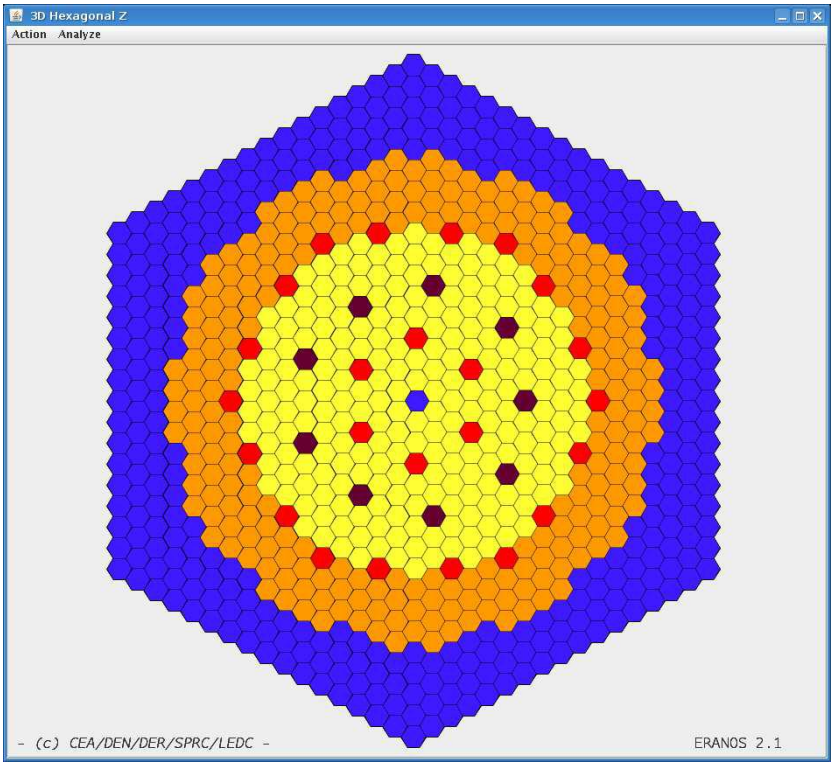

Fig. 2 – CP-ESFR: radial cross-section of the SFR core with oxide fuel

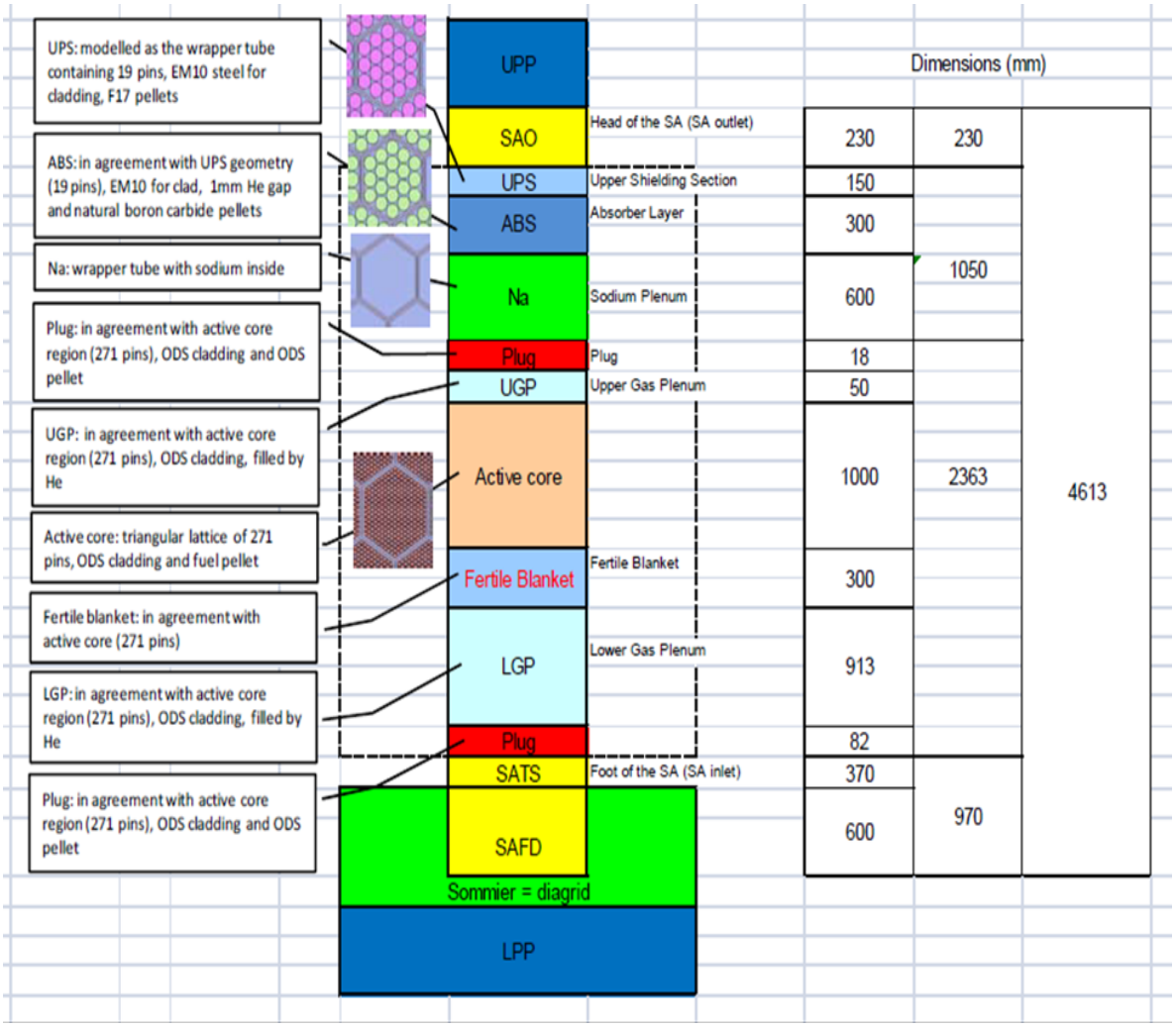

Fig. 3 – CP-ESFR: Inner and outer sub assembly regions

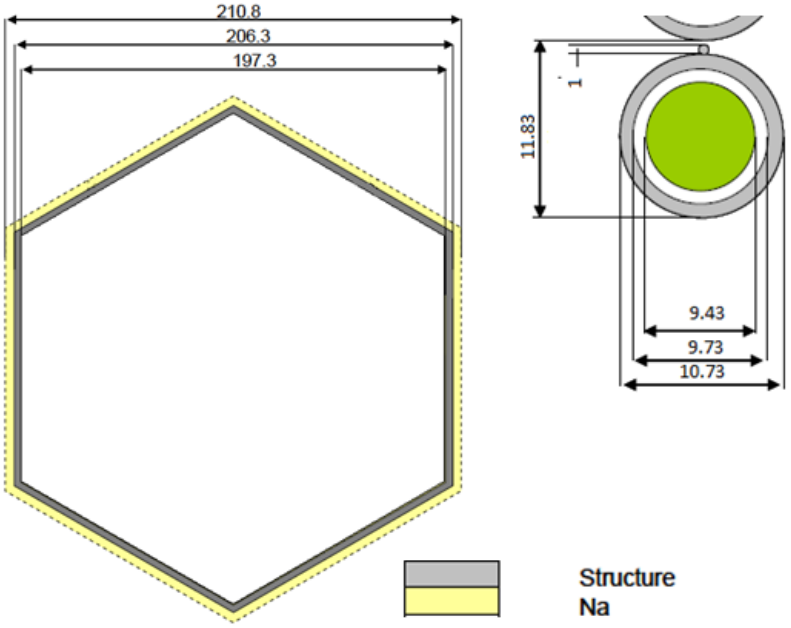

Fig. 4 – CP-ESFR: hexagonal wrapper tube and fuel pin

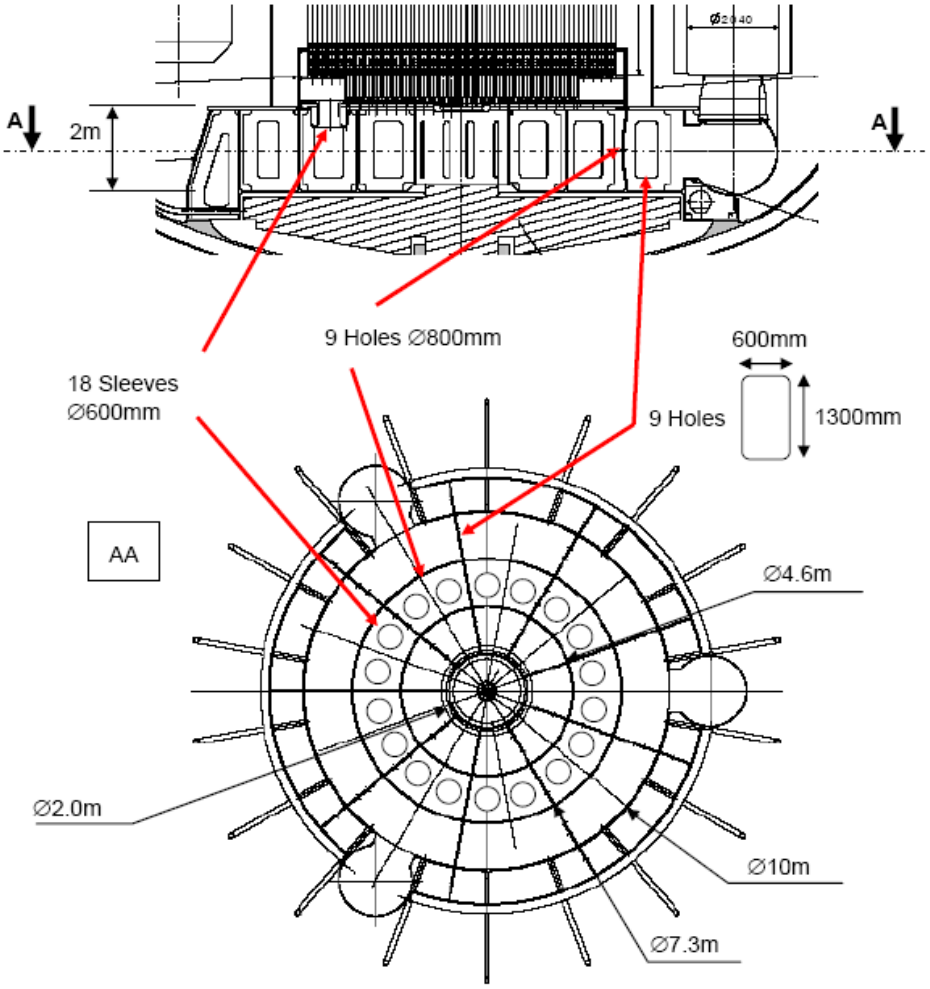

Fig. 5 – CP-ESFR: diagrid strongback and pump radial and axial sections

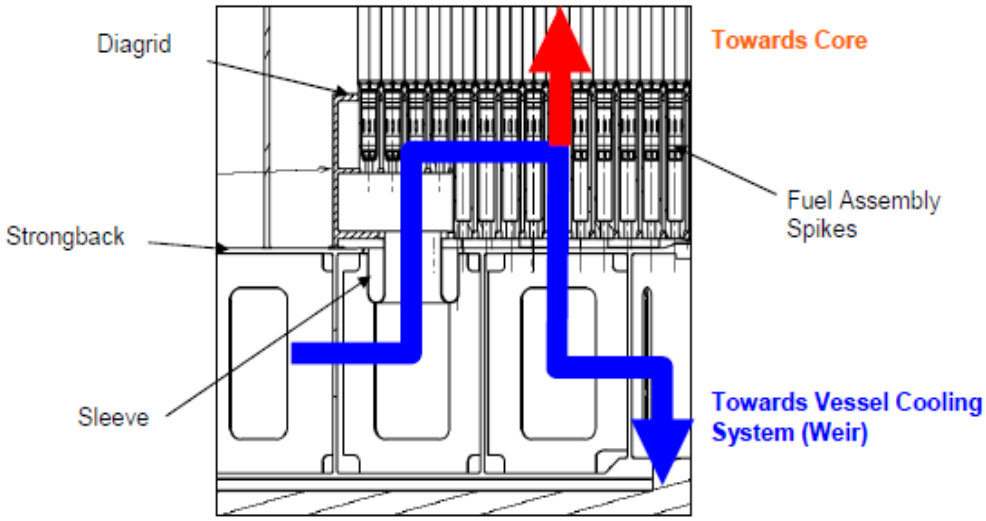

Fig. 6 – CP-ESFR: flow sodium from strongback to diagrid

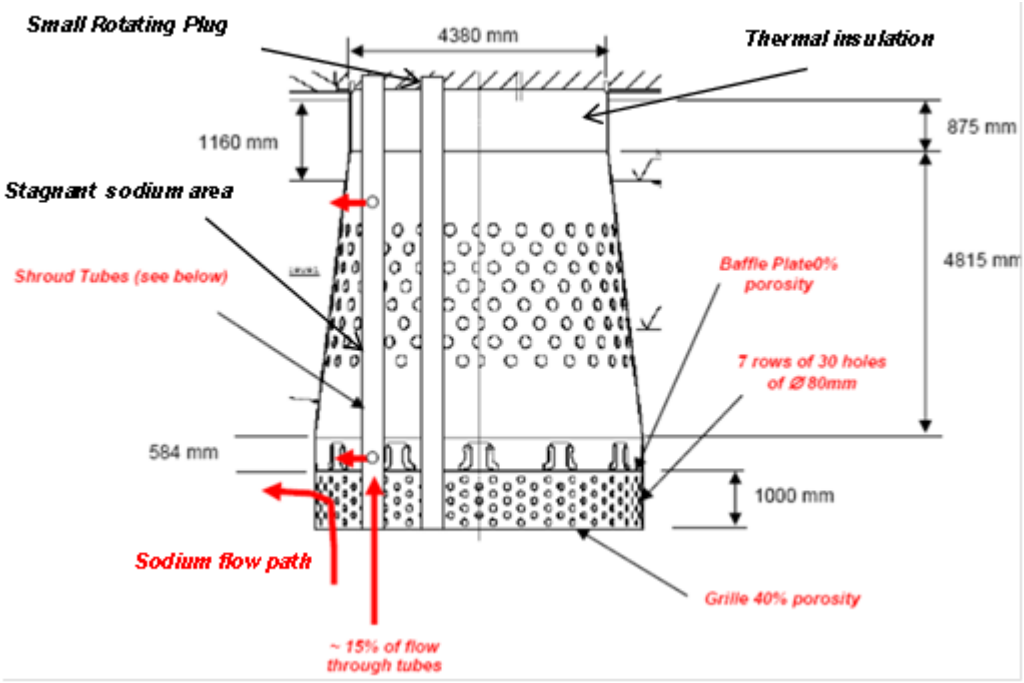

Fig. 7 – CP-ESFR: Above Core Structure

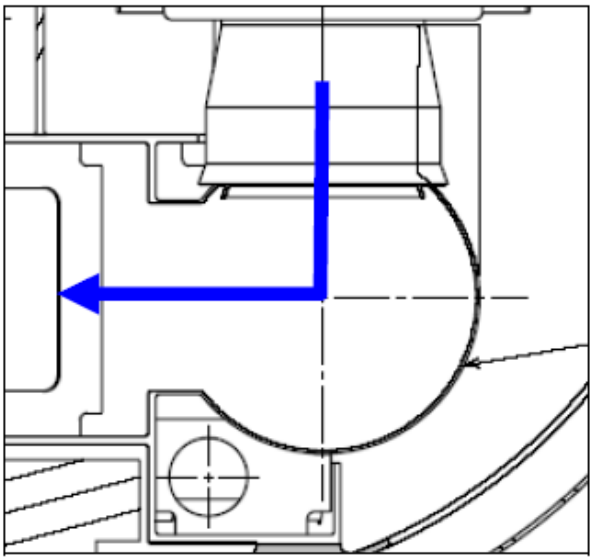

Fig. 8 – CP-ESFR: Pump connection to stongback by sphere

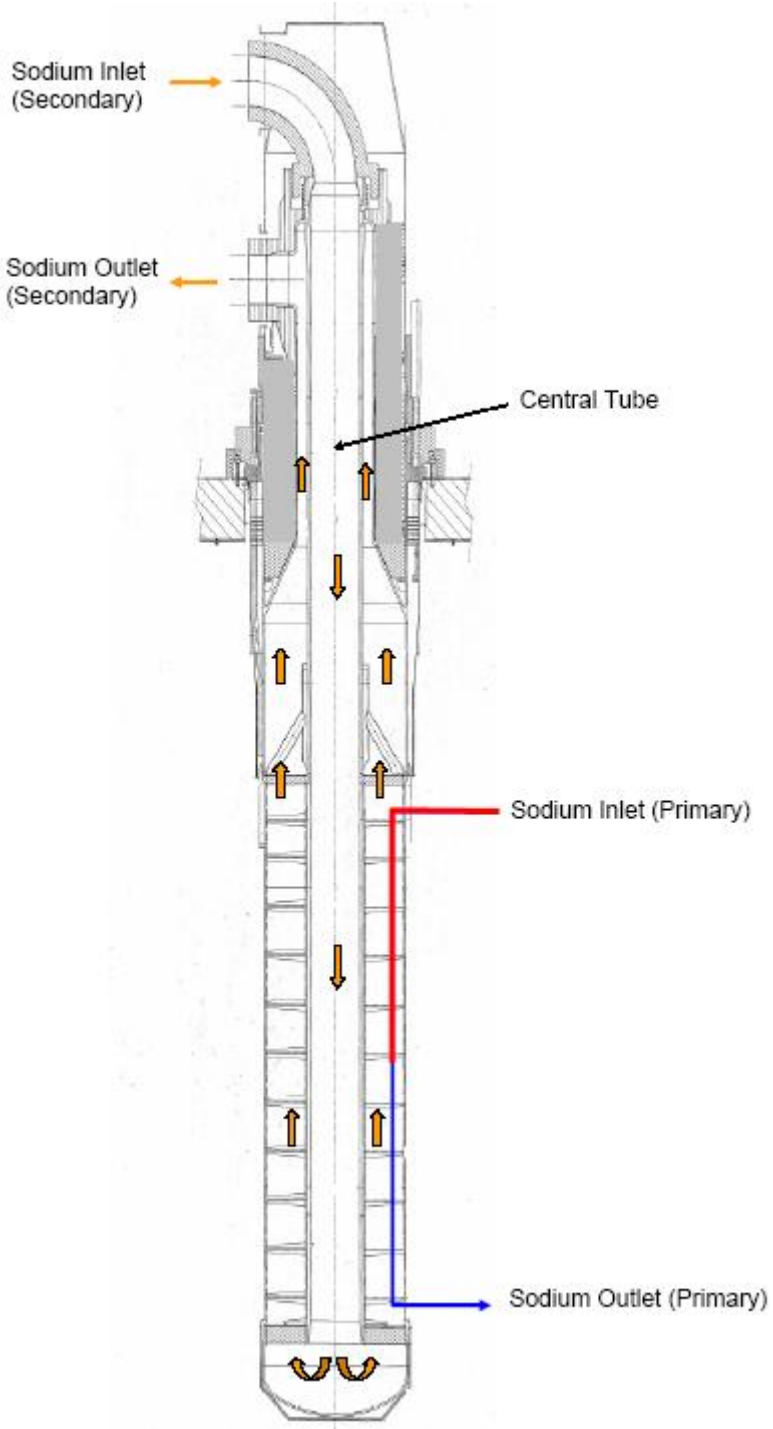

Fig. 9 – CP-ESFR: IHX

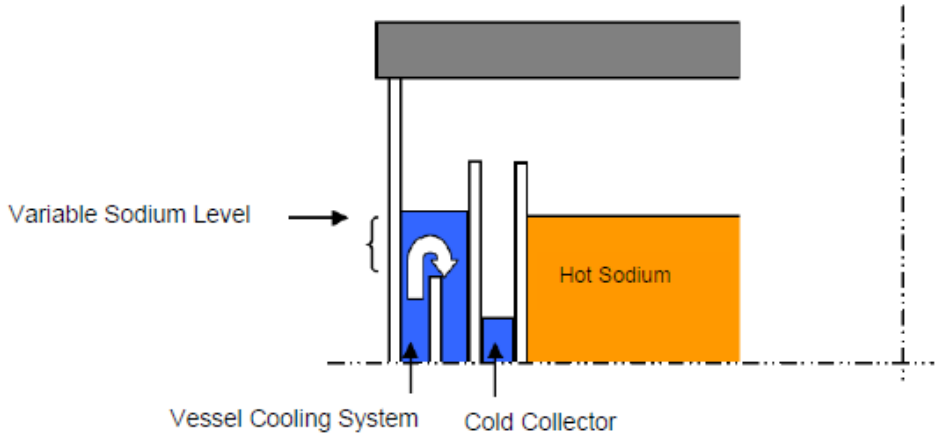

Fig. 10 – CP-ESFR: Weir system

1.2 Nodalization description

RELAP5-3D© nodalization of CP-ESF models the primary and the secondary systems. The primary system is assembled using 1D components (Fig. 11). It is divided into the following main parts:

1. the core region,
2. the hot pool region,
3. the ACS,
4. the IHX primary side,
5. the cold pool region,
6. the pump,
7. the strongback and diagrid regions, and
8. the vessel cooling bypass

The **core region** is divided into 8 separate PIPE components according with the following rationale. Component 100 (CV100) represents the central dummy assembly, which is a reflector. RELAP5-3D© pipe CV101 is equivalent to 3FA. These are the power peak FA, indeed the symmetry of the reactor is of 120°. According with the design of the core, the maximum power FA can be located either in the inner and in the outer zones of driver zone, depending upon the irradiation history. The 1D schematization of the nodalization neglects this difference, because in any case the hot FA are modeled separately. The inner and outer core zones are nodalized with a PIPE components equivalent to 222 and 228 FA, respectively (i.e CV 104 and CV326). The peripheral core region is modeled separating the 84 reflector subassembly channels and the 456 reflector blind channels. One PIPE component represents the CR subassemblies (CV557). The fuel assembly channels are subdivided into 25 hydraulic volumes connected to the lower volumes of the strongback. Exception is the core bypass zone fed by the top volumes modeling the strongback, which are 22 hydraulic volumes. Heat structures are implemented in the input deck, accounting for both active and passive structures. Each equivalent fuel assembly box is connected from the thermal point of view with the RELAP5-3D© component representing the core bypass (CV590).

The **hot pool region** is schematized with two stacks of pipes connected with cross junctions, representing the inner and the outer zones. PIPES and BRANCH components from CV630 to CV 635 model the volume between the core barrel (lower part of inner vessel) and the core region. Radial connections allow the flow between the inner part of this zone and the core bypass PIPE (above). Similar approach is used to represent the upper part, including the conical shaped zone of the inner vessel (from CV 640 to CV 652). On the top, three BRANCH components initialized with inert gas, model the reactor zone above the sodium level free surface. The passive heat structures of the hot pool region are accounted for. The overall mass of metal is

preserved and distributed along the vertical direction according with the specifications in Ref. [7]. Some of them exchange energy with other reactor zones (e.g. inner vessel heat structures is a passive structure between the hot and cold pool zone; the coolant in the ACS exchanges energy with the hot pool region through the ACS heat structure; the lower annular dead zone of the hot pool surrounding the core region exchange energy with the coolant flowing through the strongback and the diagrid). Some others are modeled as thermal inertia (i.e. coolant pump housing and upper part of the IHX).

The **ACS** is represented with the same rationale of the hot pool region, thus separating the inner and the outer fluid in order to allow the recirculation of coolant in the zone. The shroud tubes are modeled with two PIPE components, which represent the equivalent number of tubes in the inner and outer zones of the ACS. The tubes are hydraulically connected with their corresponding ACS zone into three places: two in the sodium zone (bottom and middle height) and one in the non-condensable zone (top). Heat exchange from shroud tubes and ACS is also modeled.

Six **IHX** are represented with an equivalent component. The primary side is rather simple and based on two BRANCH components for the inlet and outlet zones and a PIPE component for the tube zone. The IHX is connected upstream and downstream with the hot and cold regions, respectively The secondary system is modeled with: 2 TIME DEPENDENT VOLUME and 1 TIME DEPENDENT JUNCTION components for setting the boundary conditions (i.e. pressure at the outlet and coolant temperature and mass flow rate at the inlet); and 2 PIPES components having 26 sub-volumes each representing the descending tube and the ascending tubes. Suitable thermal coupling is implemented to calculate the heat exchange primary to secondary systems as well as the thermal losses between the IHX

The **cold pool region** is schematized with the same approach used in the hot pool region. The volume is divided into two concentric zones (i.e. inner and outer). The two parallel stacks of PIPE and BRANCH components is used. The hydraulic zone is extended from the bottom of the main vessel up to the top of the gas line where it is connected with the hot zone and the bypass zones through the gas plenum on the top of the vessel. The cold pool zone connects the IHX component with the suction of MCPs. The passive heat structures are modeled according with the CP-ESFR design.

The six **pumps** are modeled with an equivalent PUMP component of RELAP5. The main data of the pump model (i.e. the homologous curves) and the MCP coastdown versus time are reported in Tab. 3 and Tab. 4, respectively. They have been set up on the basis of the data available in Ref. [6].

The **strongback** and **diagrid** regions are represented connecting PIPE and BRANCH components according with the rationale hereafter discussed. The annular region connected with the PUMP outlet is vertically oriented. The region is connected with the diagrid zone, which is located below the core region. It is modeled separating the annular region feeding the blanket zone from the central part connected with the inner and outer driver. A connection link the top blind zone of the diagrid represented with a single BRANCH component with the core bypass. On the contrary, the FA are fed from the bottom of the diagrid zone. The second bypass is modeled connecting the central lower part of the diagrid, in downward direction, with the central part of the strongback zone (PIPE component in RELAP5). The coolant flows downward towards the vessel cooling system. The heat structures of the zone are geometrically complicate and detailed data of the geometry are not always available. However, Refs. [6] and [7] provide integral data of the metal volumes in the reactor. Therefore, passive heat structures have been implemented in RELAP5 nodalization preserving the overall heat capacity and as much as possible, the flow areas. These are uniformly distributed in the RELAP5 hydraulic regions according with the CP-ESFR design available data, if no details are available.

The **vessel cooling bypass** is considered in the nodalization. It connects the lower part of the vessel below the strongback with the gas zone on the top of the reactor and the cold pool. This hydraulic region is connected with the heat structure modeling the reactor primary vessel, with an adiabatic boundary condition on the external wall (i.e. left boundary condition). On the other side, the hydraulic component is connected with the hot and the cold zone of the nodalization.

The main features of the RELAP5-3D© model are reported hereafter.

- The elevations of the different parts of the plant are maintained in the nodalization.
- A sliced approach is applied at all systems (i.e. primary and secondary systems).
- The node to node ratio is kept uniform, as much as possible, with reference maximum ratio of 1.2 between adjacent sub-volumes.
- The heat transfer correlation used for non-bundle zone relies in a convective heat transfer coefficient function of Pe number and described in Ref. [9].
- The wire wrapped fuel bundle zone relies on a convective heat transfer correlazion by Todreas Carelli [9], which accounts also for the rod diameter and the pitch. This correlation was developed for a range of P/D from 1.1 to 1.4 and Pe number from 10 t0 5000. Moreover, this correlation was assessed on experimental data with different liquid metal fluids using bare rod bundles, but a few used wire-wrapped rods. The correlation gives good results when the P/D is between 1.1. and 1.2 but the Nusselt is under predicted for grater values[9].
- Large volumes, such as the hot and the cold pools are modeled with a stack of parallel pipes cross connected. This trigger 2D flow paths in the zones.
- The roughness is set 5.0e-5m with the exception of the core region and the SG tubes.
- The energy loss coefficients in the junctions are evaluated or estimated on the basis of the system geometry.

Octant	Indipendent Variable	Head	Torque
HAN	v/alpha	h/alpha^2	beta/alpha^2
1	0.0000	1.1946	0.0000
	0.1334	1.1449	0.1527
	0.2668	1.1050	0.2948
	0.4001	1.0851	0.4342
	0.5335	1.0950	0.5842
	0.6669	1.1151	0.7436
	0.8003	1.0751	0.8604
	0.9336	1.0254	0.9574
	1.0670	0.9746	1.0399

Octant	Indipendent Variable	Head	Torque
HVN	alpha/v	h/v^2	beta/v^2
2	0.937	0.856	0.913
	0.833	0.637	0.765
	0.750	0.478	0.637
	0.682	0.348	0.511
	0.625	0.259	0.414
	0.577	0.080	0.138
	0.536	-0.050	-0.093
	0.125	-0.757	-6.055

Octant	Indipendent Variable	Head	Torque
HAD	v/alpha	h/alpha^2	beta/alpha^2
3	-0.9336	1.9014	-1.7753
	-0.8003	1.7521	-1.4021
	-0.6669	1.5928	-1.0622
	-0.5335	1.4236	-0.7595
	-0.4001	1.3639	-0.5457
	-0.2668	1.3042	-0.3479
	-0.1334	1.2444	-0.1660

Octant	Indipendent Variable	Head	Torque
HVD	alpha/v	h/v^2	beta/v^2
4	-0.5355	1.2544	-2.3423
	-0.5767	1.3141	-2.2785
	-0.6248	1.3738	-2.1989
	-0.6816	1.4734	-2.1617
	-0.7498	1.6127	-2.1510
	-0.8331	1.7123	-2.0555
	-0.9372	1.8716	-1.9970

Octant	Indipendent Variable	Head	Torque
HAT	v/alpha	h/alpha^2	beta/alpha^2
5	0.9336	1.0157	5.9584
	0.8003	1.0746	5.4034
	0.6669	1.1250	4.7140
	0.5335	1.0950	3.6707
	0.4001	1.0746	2.7017
	0.2668	1.0955	1.8362
	0.1334	1.1548	0.9678
	0.0000	1.0955	0.0000

Octant	Indipendent Variable	Head	Torque
HVT	alpha/v	h/v^2	beta/v^2
6	0.4686	-0.3383	-4.5359
	0.4998	-0.1792	-2.2526
	0.5355	-0.0398	-0.4669
	0.5767	0.1193	1.2996
	0.6248	0.2591	2.6051
	0.6816	0.3584	3.3039
	0.7498	0.4779	4.0048
	0.8331	0.6268	4.7273
	0.9372	0.8461	5.6727

Octant	Indipendent Variable	Head	Torque
HAR	v/alpha	h/alpha^2	beta/alpha^2
7	-0.1334	1.4712	-1.2329
	-0.2668	1.6086	-2.6962
	-0.4001	1.7749	-4.4622

Octant	Indipendent Variable	Head	Torque
HVR	alpha/v	h/v^2	beta/v^2
8			

Tab. 3 – CP-ESFR, : RELAP5-3D© pump model, single phase homologous courves.

PUMP COAST-DOWN				
t (s)	**Q(kg/s)**	**rpm% Q%**	**rpm**	**rad/s**
0	7.49750	100	550.000	57.5959
10	3.74875	50	275.000	28.7979
15	2.99900	40	220.000	23.0383
23	2.24925	30	165.000	17.2788
40	1.49950	20	110.000	11.5192
90	0.74975	10	55.000	5.7596
190	0.37488	5	27.500	2.8798
323	0.22493	3	16.500	1.7279
490	0.14995	2	11.000	1.1519
990	0.07498	1	5.500	0.5760

Tab. 4 – CP-ESFR, : RELAP5-3D© pump model, coastdown vs time.

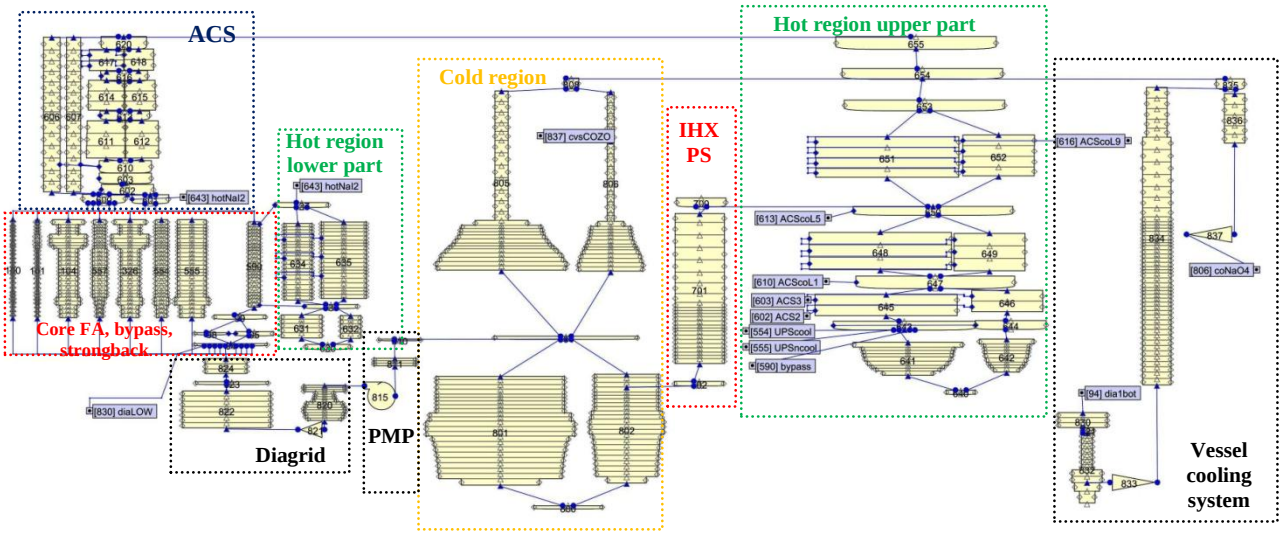

Fig. 11 – CP-ESFR: RELAP5-3D© nodalization sketch of primary system

1.3 Nodalization qualification and preliminary results

Preliminary tests have been performed to investigate the hydraulic performances of the nodalization in terms of mass flow paths in the primary system as well as pressures distribution, the implementation of the pump and its characteristic curves, the calculation of the FA performances based on axial uniform power distribution. These tests are devoted to assess the performances of different parts of the nodalization. Steady state results representative of the CP-ESFR design conditions will be addressed when the neutronic data and the FA power distributions will be received (in the framework of AdP2012 LP2 Task A3).
The assessment is limited to:

- geometrical verification, i.e. comparisons between geometry of design and nodalization features,
- the evaluation of the pressure drop in the wire wrapped fuel assembly as function of Re, see Fig. 14,
- the verification of the heat transfer performance of the FA at different power levels (uniform linear power is imposed), Fig. 12 and Fig. 13,
- pressure drop along the loop in isothermal conditions (or steady state conditions),
- mass flow distributions in primary system, see Tab. 5,

- performances of the heat exchange in the IHX at different operating modes,
- pumps performances verification.

The verification of steady state results at nominal conditions will be performed when the model will be updated with the neutronic data. Then, it will be applied to the investigation of TH core safety parameters with different fuel prototypes and the simulation of postulated accidents :

	No.	design [kg/s]	R5-3D [kg/s]	error [kg/s]	error %
Dummy central FA	**1**	1.3	5.9	4.6	342.5
Power peak FA	**3**	121.9	122.7	0.8	0.7
Inner core FA	**222**	9025.3	9052.3	27.0	0.3
Outer core FA	**228**	8197.0	8151.5	-45.5	-0.6
Reflector assembly	**84**	112.0	115.1	3.1	2.8
Blind reflector assembly	**246**	0.0	0.0	0.0	0.0
CR	**33**	646.0	629.3	-16.7	-2.6
Low press bypass	--	830.0	844.1	14.1	1.7
Core bypass	--	600.0	617.4	17.4	2.9
Total pump	--	19536.0	19538.4	2.4	0.0

Tab. 5 – CP-ESFR nodalization. Mass flow distribution in primary system: design data vs. code results

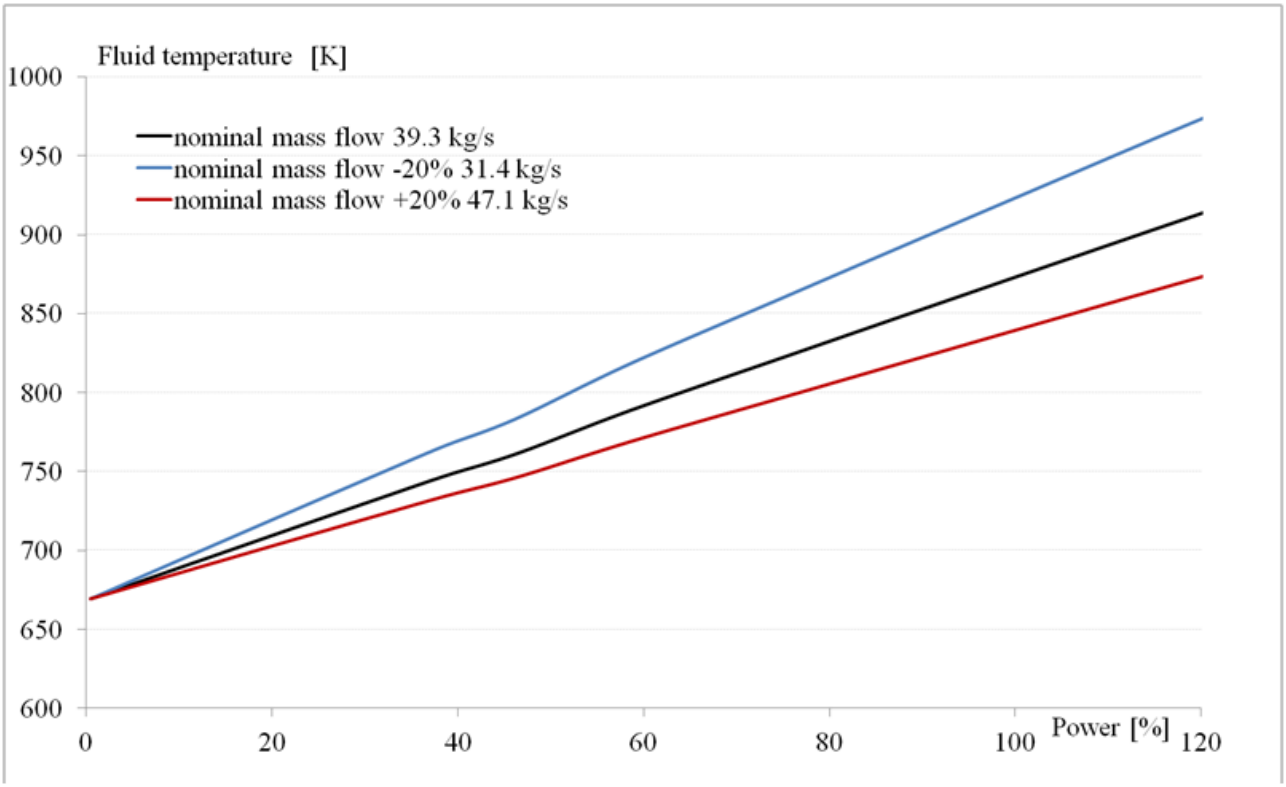

Fig. 12 – CP-ESFR fuel assembly performances: sodium temperature vs. power at core outlet

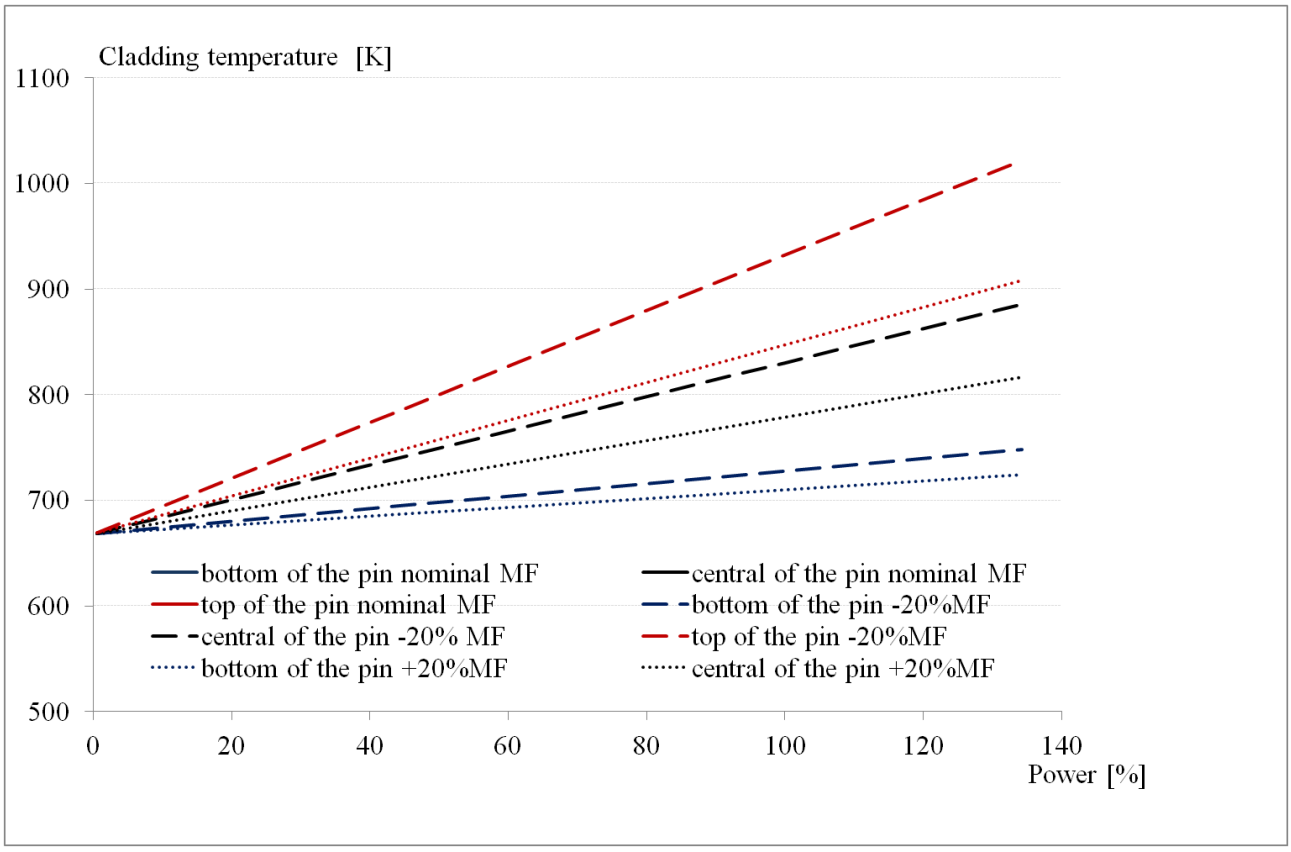

Fig. 13 – CP-ESFR fuel assembly performances: cladding temperature vs. power at core outlet

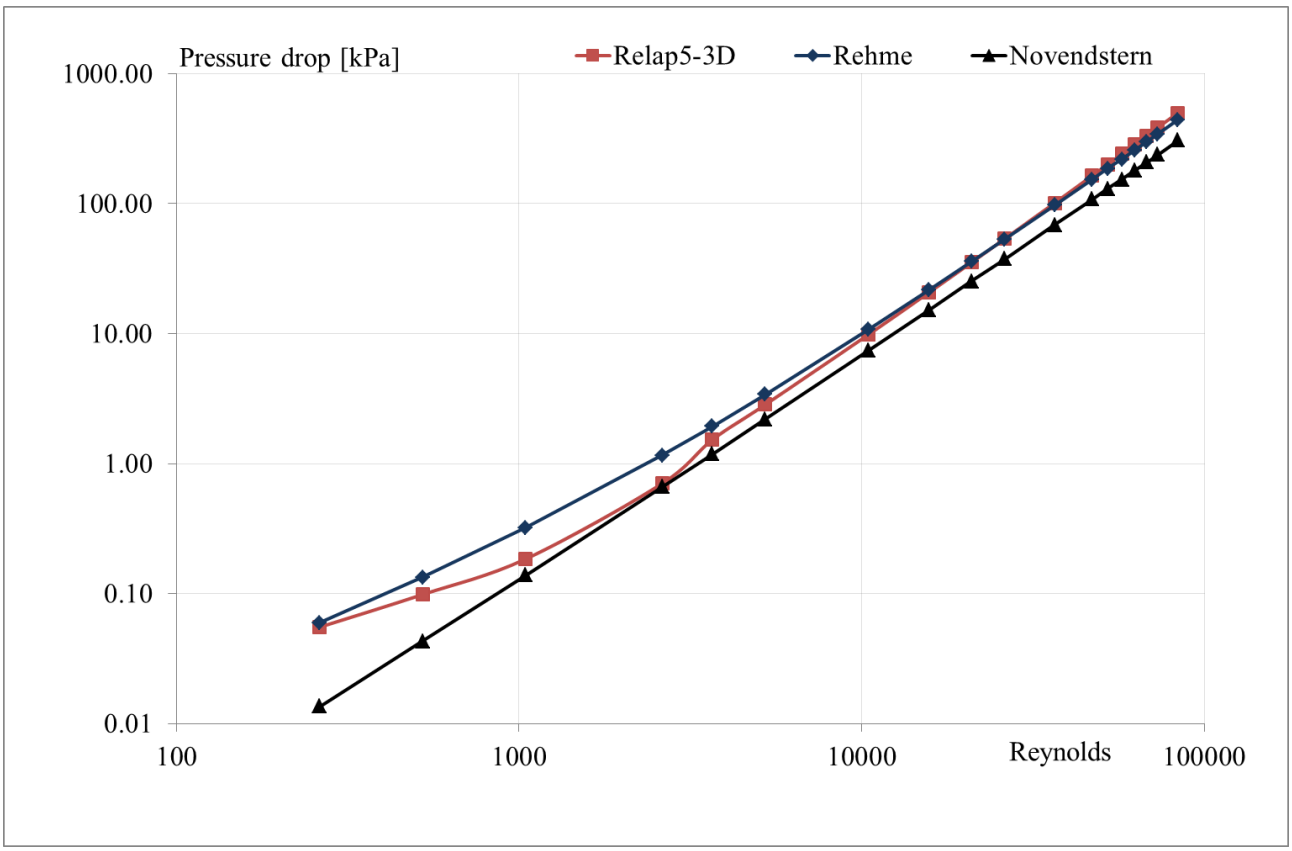

Fig. 14 – CP-ESFR fuel assembly performances: friction losses in wire wrapped fuel assembly vs. experimental based empirical correlations.

1.4 Conclusive remarks and follow up

A RELAP5-3D© nodalization of pool type sodium cooled fast reactor, CP-ESR, has been developed and set up. The hydraulic performances of the nodalizations in terms of flow and pressure distributions are satisfactory. The implementation of the pump model and of the homologous curves for the head and torque for single phase operation is carried out.

Tests on the modeling of the FA performances have been completed. Friction pressure losses in the wire wrapped fuel assembly zone have been compared with correlations available in literature. The heat exchange performances have been tested with constant linear power in the active zone and setting Todreas Carelli correlation.

The nodalization will be completed implementing the neutronic data and the power distribution calculated in the framework of the LP2 A3 task of the AdP2012. Then, it will be applied to investigate specific accident scenarios for providing input data to 1) a full core thermal-hydraulic model of CP-SFR and 2) to a fuel pin performances code.

1.5 References

[1] *Fiorini, G.L., 2009. The Collaborative Project on European Sodium Fast Reactor (CP ESFR), FISA 2009, 22-24 June, Prague, Czech Republic*

[2] *G.L. Fiorini, A. Vasile, D. Blanchet et al, "ESFR 'Working Horses' Core Concept Definition", CEA Cadarache, 2009*

[3] *B. Vezzoni, A. Rineiski, F. Gabrielli, W. Maschek, M. Marchetti, Optimized ESFR core with Minor ctinides, KIT, Karlsruhe, January 2012*

[4] *J. Krepel (PSI), K. Mikityuk (PSI), O. Huml (PSI),H. Tsige-Tamirat (JRC.IE), L. Ammirabile (JRC.IE),D. Blanchet (CEA), F. Polidoro (RSE), "Working horses" ESFR core concepts: neutronic and thermal-hydraulic characteristics, PSI Villigen, November 2010*

[5] *R. Sunderland, V. Sheth, L Buiron, P. Tetart, S. Massara, H. Tsige-Tamirat, A. Rineiski, B.Vezzoni, F. Gabrielli, M. Marchetti, D. Zhang, M. Flad, W. Maschek, J. Krepel, K. Sun, K. Mikityuk, R. Ochoa, N. García- Herranz, D. Cuervo, C. Ahnert, ESFR Cores with Optimised Characteristics – Final Report, AMEC , November 2012*

[6] *GENOT Jean-Sebastien, ESFR Working Horse Pool Concept Description, AREVA, July 2009*

[7] *CP-ESFR-OC-Vademecum.xls*

[8] *Rineiski, B. Vezzoni, F.Gabrielli, W. Maschek, M. Marchetti, A. Omenetto, X.-N. Chen, D. Zhang, H. Tsige-Tamirat, K.Sun, J. Krepel, K. Mikityuk, D. Rochman, A.J. Koning, D.F. DaCruz, F. Polidoro, Synthesis of options to optimize feedback coefficients, Final Report, KIT, Karlsruhe, February 2012*

[9] *The RELAP5-3D©Code Development Team, RELAP5-3D© Code Manual Volume IV: Models and Correlations, INEEL-EXT-98-00834, Revision 4.0 June 2012*

2 DEVELOPMENT AND SET UP OF EBR-II NODALIZATION BY RELAP5-3D©V4.0.3 CODE

2.1 Framework

The activity discussed in the present section is connected with the international CRP "Benchmark Analyses of an EBR-II Shutdown Heat Removal Test" promoted by IAEA [3].

The CRP addresses Shutdown Heat Removal Tests (SHRT) performed at the Experimental fast Breeder Reactor EBR-II within the framework of the US Integral Fast Reactor development and demonstration programme. The CRP is aimed at improving the participants' simulation capabilities in the various fields of research and design of sodium cooled fast reactors through data and codes validation and qualification. The scope of the CRP is twofold: firstly, validation of the state-of-art liquid metal cooled fast reactor codes and data used in neutronics, thermal hydraulics and safety analyses, and, secondly, training of the next generation of fast reactor analysts through international benchmark exercises.

The report presents the TH nodalization developed and set up by REALP5-3D© code.

2.1.1 EBR-II plant overview

The EBR-II plant is located in Idaho and was designed and operated by Argonne National Laboratory for the US Department of Energy. Operation began in 1964 and continued until 1994. EBR-II was rated for a thermal power of 62.5 MW_t with an electric output of approximately 20MW_e.

EBR-II is a sodium-cooled reactor with three loops, characterized by the following mass flow rates:

- Primary sodium: 485 kg/s
- Intermediate sodium: 315 kg/s
- Secondary steam: 32 kg/s

All primary system components were submerged in the primary tank, which contained approximately 340 m^3 of liquid sodium at 371°C. An argon cover gas was maintained over the surface of the sodium in the primary vessel to minimize the opportunity for air to contact the sodium.[2] Fig. 15 shows the primary tank and the other components The primary cooling system consisted of two mechanical centrifugal pumps operated in parallel and pumping a total of 485 kg/s of sodium.[2] The two pumps drew sodium from this pool and provided sodium to the two inlet plena for the core. Subassemblies in the inner core and the extended core regions received sodium from the high-pressure inlet plenum, accounting for approximately 85% of the total primary flow. The blanket and the reflector subassemblies in the outer blanket region received sodium from the low-pressure inlet plenum.

Hot sodium exited the subassemblies into a common upper plenum where it mixed before passing through the outlet pipe into the intermediate heat exchanger (IHX). The pipe feeding sodium to the IHX is referred to as "Z-pipe". Sodium then exited the IHX back into the primary sodium tank before entering the primary sodium pumps again.

Sodium in the intermediate loop traveled from the IHX to the steam generator where its heat was transferred to the balance-of plant (BOP). The colder sodium intermediate loop then traveled through a similar length of piping back to the IHX. The steam generator consisted of two parallel superheaters and seven parallel evaporators. Fig. 16 shows a simple schematic of the primary, intermediate and steam systems. Note that th power, flow and temperature conditions described earlier are for typical EBR-II operation..

The reactor-vessel grid-plenum assembly accommodated 637 hexagonal subassemblies. The subassemblies were segregated into three regions: core, inner blanket (IB) and outer blanket (OB). The central core comprised 61 subassemblies in the first five rows. The inner blanket region was composed of Rows 6 and 7.

Originally these rows were loaded with blanket subassemblies. But for SHRT-17, no blanket subassemblies were loaded in this region. Instead, Row 6 contained the driver-fuel and irradiation subassemblies of the expanded core and Row 7 contained reflector and subassemblies. The outer blanket region comprised the 510 subassemblies in Rows 8-16, which were either blanket or reflector subassemblies.

EBR-II was heavily instrumented to measure mass flow rates, temperatures and pressures throughout the system.

The EBR-II reactor core vessel grid-plenum assembly accommodated 637 hexagonal subassemblies, which were installed in one of three regions: central core, inner blanket (IB) or outer blanket (OB). Fig. 18 illustrates the subassemblies arrangement of the reactor and the subassembly identification convention. Each subassembly position was identified by a unique combination of three parameters: row, sector and position within the sector. Subassembly row identification begins at Row 1 for the subassembly in the core-center and moves outward to Row 16. Row 1 had one subassembly, Row 2 had six subassemblies. From Row 2 outward to Row 14, each row had 6 more subassemblies than the last. Rows 15 and 16 were not complete rows and had 66 and 24 subassemblies, respectively.

Each row was broken up into six sectors A through F. As each row approximated a hexagon, each side of the row was assigned to one of the six sectors. The final parameter needed to identify a subassembly location is the position within the sector. The line of subassemblies dividing sectors A and F were defined as the subassemblies in position 1 of their respective rows within the sector A. The line of subassemblies that divide sector a and B are therefore defined as the subassemblies in position 1 of their respective rows within sector B. This patterns continues for the remaining four sides of the core layout. As an example, the subassembly XX09 is positioned in subassembly location 5D3, where 5 is the row, D is the sector and 3 is the position within the sector.

The central core comprised the 61 subassemblies in the first 5 rows. Two of these positions contained safety-rod subassemblies and eight positions contained control-rod subassemblies. These subassemblies are identified by the letter S and C, respectively, in Fig. 17. Two positions in Row 5 contained the in-core instrument subassemblies (INSAT) XX09 and XX10, and one position in Row 5 contained the in-core instrument test facility (INCOT) XY16. The remaining central core subassemblies were either driver-fuel or experimental-irradiation subassemblies of varying types. For SHRT-17 test only the MARK-II A I type driver subassembly was used.

In Fig. 17, driver subassemblies are denoted by the letter D, instead the letter P indicates a partial driver, which are driver subassemblies where approximately half of the fuel elements are replaced by steel elements. HFD in Fig. 17 refers to a high-flow driver, all of which were located in Row 6. A high flow driver subassembly was the basic driver subassembly with extra inlet flow holed drilled into the subassembly inlet nozzle region to allow higher subassembly coolant flow.

The expanded core region was composed of Rows 6 and 7. This region is also named inner blanket region because originally housed blanket subassemblies. But for SHRT-17 test no blanket subassemblies were loaded in this region. Instead Row 6 contained the driver-fuel and irradiation subassemblies and Row 7 contained reflector subassemblies. The outer blanket region comprised the 545 subassemblies in Rows 8-16, which were either blanket or reflector subassemblies. In Fig. 17 reflector subassemblies are identified with the letter R.

In Fig. 17. those subassemblies whose label begins with letter K were steel subassemblies; The remaining subassemblies are all experimental or driver-irradiation type subassemblies. Fig. 18 illustrates the rest of the core.

The outer configuration of all subassemblies was very similar. The upper adapter was formed to fit the top of the hexagonal outer tube of the central region and the top part of the upper adapter was slotted to adjust the orientation of the subassembly within the reactor grid. The lower surface of the mushroom-shape head on the upper adapter provided a solid surface for grasping during fuel handling with gripper devices.

The center region of each subassembly was surrounded by a hex tube, which created an independent flow channel for each subassembly. Each face of the hexagonal tube contained a spacer button, formed by dimpling the tube wall outward. The buttons served to prevent the subassemblies from touching if bowing were to occur.

The lower adapter positioned the subassembly within the reactor grid and determined the amount of coolant flow through the subassembly. Subassemblies that were to be positioned in Rows 1 through 5 had core-type lower adapters. The core-type adapter was a stainless steel, machined cylindrical nozzle. The upper portion had a rounded shoulder, which sat in the hole of the upper grid plate in the core region. The core region lower adapters had four sets of coolant flow holes. Depending on the row in which the subassembly was position, a different number of flow holes were covered by the various step sizes of the lower grid plate.

The expanded core-type lower adapter was used for driver fuel in Row 6 and irradiation subassemblies located in Rows 6 or 7 of the reactor. The inner blanket lower adapter with two sets of flow holes was used for the subassemblies, other than driver fuel type, located in Rows 6 or 7. The outer blanket lower adapter was used for subassemblies in Rows 8-16. These adapters fit into stainless steel tubes that interconnected the upper and lower grid of the reactor grid assembly to provide a flow path from the low-pressure plenum. Yet another type of lower adapter was used for the control rod and safety rod subassemblies.

The inner configuration of the center section of subassembly varied depending upon the specific subassembly type. For each subassembly type that include fuel elements Tab. 6 presents the nominal design parameters of the fuel element by type and gives design data for the wire-wrapped cladded fuel elements. Tab. 7 presents the nominal design parameters for the subassembly hexagonal duct wall.

Fig. 19 shows an isometric view of the inner configuration of a MARK-II AI subassembly. The center section of the MARK-II AI subassembly consisted of an upper shield, a core bundle of fuel elements and a lower shield. The MARK-II AI and MARK-II A fuel elements were part of the central core driver and expanded core driver subassembly designs. The MARK-II S element was used in the high worth control rod design.

Each fuel element clad tube contained a single metal fuel slug. U-5Fs is the fissium alloy uniquely developed and fabricated for the Argonne EBR-II reactor. The fuel element were sodium bonded. Above the sodium bond level was a fission gas plenum that was initially filled with an inert gas until fission gas was produced. The inert gas used was Helium with Xenon tracer isotope added for tagging a leaking fuel element.

The EBR-II coolant systems model for the SHRT-17 test includes the major components in the primary sodium circuit and the intermediate side of the intermediate heat exchanger. Beginning at the outlet of the reactor core, the primary sodium circuit includes the upper plenum, reactor outlet piping, auxiliary EM sodium pumps, reactor inlet piping and high- and low-pressure inlet plena. The inlet ad outlet of the intermediate side of the heat exchanger are boundary conditions for the model.
Fig. 20 illustrates the major components in the EBR-II primary sodium circuit. Sodium discharged from the two pumps into the reactor outlet piping, which is known as the ‘Z-Pipe’. The shape of the pipe accommodates thermal expansion. The top of the Z-Pipe contained the auxiliary EM pump, with rated to provide up the 0.5% of the nominal pump head.

Sodium exited the Z-Pipe and entered the shell side of the intermediate heat exchanger. Cold sodium was the discharged into the primary sodium tank. The two primary sodium pumps took suction from the primary sodium tank and provided sodium to the reactor inlet piping. Fig. 20 [2] shows the two primary sodium pumps and their inlet piping. Both sets of inlet piping provided sodium to the high-pressure and low-pressure inlet plena. The high pressure inlet plenum provided sodium to the subassemblies in the first 7 rows; while the low-pressure inlet plenum provided sodium to Rows 8-16.

The primary tank is the outer boundary of the primary sodium circuit and is modeled as a vertically oriented cylinder. It encompasses all of the major primary sodium components. The reactor vessel, intermediate

exchanger and two primary sodium pumps are modeled as vertically oriented cylinders. Sodium piping is modeled as a series of straight pipes connected by pipe bends that, unless otherwise stated, have a bend radius equal to the pipe radius. The reactor vessel, IHX, pumps and sodium piping are assumed to be the only components that displaced sodium in the primary tank. The main characteristics of the all components are given in the following sections.

The cylindrical primary sodium tank, illustrated in Fig. 21 contains two vessel walls with the space between the inner and outer vessel walls filled with argon gas. Outside of the inner vessel wall is the argon layer; outside of the argon gas layer is the outer vessel wall. Both vessel walls are composed of Type 304 stainless steel

The total volume of sodium in the primary system is approximately 340.69 m^3 at an average nominal temperatures of 644.26 K. This volumes of sodium includes all sodium in the major components, piping, reactor subassemblies and primary tank sodium is occupied by argon gas. The core support structure below the reactor vessel is assumed to displace a negligible amount of the sodium.

The EBR-II reactor vessel and its internal components are illustrated in Fig. 22. Sodium discharged from the primary sodium pumps entered the low-pressure inlet plenum from the two inlet pipes or the high-pressure inlet plenum. Sodium from these two inlet plena was provided to the reactor subassemblies and then discharged into the common upper, or outer plenum. Sodium exited the upper plenum through the Z-Pipe.

The neutron shielding surrounded the reactor, upper plenum and lower plena with sections removed from the inlet and outlet piping. Other than the grid plates that separated the lower plena, there was no significant shielding below the reactor. Above the upper plenum sat the reactors cover, through which control rod drive shafts and instrumentation leads entered the reactor vessel.

Fig. 23 below illustrates the EBR-II high- and low-pressure inlet plena.
The lower plenum received coolant from the two low-pressure inlet pipes. Sodium passed through a vertically oriented baffle plate with 50 baffle flow holes, then passes through a horizontally oriented baffle plate with 592 baffle holes and into the low-pressure inlet plenum Sodium enters one of the 510 outer blanket stainless steel tubes that feed the outer blanket region subassemblies (Rows 8-16), which are identified in Fig. 23. All structure in the inlet plena is composed of Type 304 stainless steel.
The upper inlet plenum received sodium from the two high-pressure inlet pipes. Sodium then passed through a vertical baffle plate, around the stainless steel tubes connecting the low-pressure plenum with the core, and into the high-pressure inlet plenum. In the high-pressure inlet plenum, sodium was distributed to the subassemblies in Rows 1-7.

The central core region of the high-pressure inlet plenum contains a series of seven concentric hexagonal steps. Each step has an aperture for each subassembly in the row in which the bottom of each subassembly is inserted. As the lower adapter of each subassembly in Rows 1-7 has a series of sodium inlet flow holes, these steps have varying heights to block off certain holes depending on the desired amount of sodium flow through the subassembly.

The actual EBR-II upper plenum contained a baffle plate to mix the outlet sodium flow. Not enough detail is available, it assumed that the sodium leaving the upper plenum is fully mixed when it enters the reactor outlet pipe.
The upper plenum consists of two regions: a cylindrical region directly above the reactor subassemblies and an annular region surrounding the cylindrical region. Sodium leaves the upper plenum through the reactor outlet pipe and into the Z-Pipe.

The primary sodium circuit has three pumps: two main and one electromagnetic pump. The two main primary pumps lay opposite each other at a radius of 3.251 meters from the center of the core. Primary sodium pump #1 was located 120° counter-clockwise from the IHX, while the primary sodium pump #2 was located 60° clockwise from the IHX. The electromagnetic pump was located around part of the Z-Pipe. Both types of pumps are assumed to constructed of Type 304 stainless steel.

Two sets of sodium piping were installed in the primary sodium circuit: the reactor outlet and the reactor inlet piping. The reactor outlet pipe, or Z-Pipe, began at the reactor outlet plenum and ended at the intermediate exchanger. It was constructed in a Z-shape to account for thermal expansion during periods of elevated outlet and cold pool sodium temperatures. The reactor inlet piping was two identical sets of piping from both the primary sodium pumps to the inlet plena. Both sets of piping were constructed of Type 304 stainless steel. In the following piping descriptions, the x-axis is assumed to be on the line between the axial centerlines of the reactor core and IHX.

Because the sodium in the reactor outlet pipe is at higher temperature than the bulk sodium surrounding it, the Z-Pipe is a double-walled structure. The annular region between the two pipe walls is filled with static sodium. In the upper section of the Z-Pipe resides the auxiliary EM pump.
The intermediate heat exchanger transfers heat from the radioactive primary system to the intermediate system and isolates the primary system from the water inventory in the steam plant. The heat exchanger is a tube-and shell design with single-wall straight tubes and is operated in the counter flow mode.

The heat exchanger consists of three modules or components, all composed of Type 304 stainless steel. The well casing is a cylindrical annulus with its major axis oriented vertically and it hangs from the primary tank cover from a lip at the upper end of the well casing and continues downward to an elevation of 1.559 meters above the bottom of the active core. It consists of four concentric steel cylinders with stagnant sodium between each layer. The lower end of the casing is terminated by a hemispherical head. Welded to the top of the tube bundle is the shield plug. Once the tube bundle and shield plug are lowered as a unit into the well casing, a cover is placed over the open end of the well casing and welded shut.

Heat transfer from primary to intermediate sodium takes place in the lower half of the intermediate exchanger where the tube bundle is located. The primary coolant is admitted on the shell side through a horizontal inlet pipe (i.e. the outlet of the Z-Pipe) that penetrates the well casing wall 4.939 meters above the bottom of the active core. The fluid exits the inlet pipe and enters the upper region of the tube bundle, where it is distributed horizontally by baffles. The upper end of the tube bundle (above the inlet pipe) is terminated by the upper tube sheet, resulting in the primary sodium being directed downward parallel to the tubes. The primary sodium travels down the length of the tubes and exits the well casing horizontally just above the lower tube sheet through an annular opening in the well casing.

The intermediate sodium enters the intermediate heat exchanger through a vertical pipe that penetrates the well casing cover. This pipe extends down the length of the well casing to the hemispherical region defined by the lower tube sheet and the well casing lower hand. A set of hemispherical baffles redirect the fluid 180° so that it flows upward. The fluid then enters the bottom of the tubes at the lower tube sheet. The fluid flows up the length of the tubes and then exits the tubes into another hemispherical-shaped region defined on its bottom by the upper tube sheet and on its upper side by a hemispherical-shaped spun from metal. An exit pipe is welded to the hemispherical cap. The exit pipe travels the length of the upper-half of the well casing up to the well casing cover, where it exits the intermediate heat exchanger through a penetration the well casing cover.
The collection of internals in the upper half of the well casing is known as the shield plug. The shield plug contains the inlet and the outlet intermediate side pipes, while the remaining space is occupied by various thermal and radiation shields. The shield plug represents a large thermal connections to both the primary and intermediate flow paths are rather weak, with time scales on the order of seconds or minutes. The areas available for heat transfer and the radius of the shield plug are such that the heat transfer rates are small compared to the energy storage capability of the shield material.
Fig. 24 illustrates the intermediate heat exchanger.

PIN GEOMETRY	MARK-II AI	MARK-II A	MARK-IIS	XX09	XX10	Outer Blanket
Number of pins	91	91	61	59	18	19
Number of elements				61		
Fuel alloy	U-5Fs	U-5Fs	U-5Fs	U-5Fs	Stainless Steel	Depleted U
Fuel -slug lenght [m]	0.3429	0.34290	0.3429	0.3429	N/A	1.397
Fuel-slug diameter [m]	0.0336	0.0336	0.0336	0.0336	N/A	0.01109
Cladding-wall thickness [m]	0.00032	0.00032	0.00032	0.00032	Solid rod	0.000457
Cladding-wall OD [m]	0.00441	0.00441	0.00441	0.00441	0.00881	0.01252
Element lenght [m]	0.6108	0.6362	0.5334	0.6108	0.6108	1.575
Restrainer height above fuel [m]	0.0127	0.0127	0.0127		None	N/A
Sodium level above fuel [m]	0.03175	0.00635	0.00635	0.03175	N/A	0.03048
Plenum gas	Inert gas	Inert gas	Inert gas	Inert gas	N/A	Inert gas
Cladding Material	316	316	316	316	316	304
Spacer-wire diameter [m]	0.00124	0.00124	0.00124	0.00124	0.00124	None
Spacer-wire material	316	316	316	316	316	N/A
Spacer-wire pitch [m]	0.15240	0.15240	0.15240	0.15240	0.15240	None

Tab. 6 - EBR-II design parameters (nominal) of subassembly fuel elements.

	MARK-II AI MARK-II A	XX09 XX10	Safety HWCR	Reflector Uranium Blanket
Pitch center to center [m]	0.05893	0.05893	0.05893	0.05893
OUTER HEX TUBE				
Flat to flat outside [m]	0.05817	0.05817	0.05817	0.05817
Flat to flat inside[m]	0.0561	0.0561	0.0561	0.0561
Material	316SS	304SS	304SS	304SS
INNER HEX TUBE				
Flat to flat outside [m]		0.0484	0.0484	
Flta to flat inside [m]		0.0464	0.0464	
Material		304SS	304SS	
Upper Adapter/Fixture	304SS		304SS	304SS
Upper Axial Shield	304SS		304SS	
Lower Axial Shield	304SS		304SS	
Lower Adapter	304SS		304SS	304SS

Tab. 7 - EBR-II design parameters (nominanl) for subassembly structure.

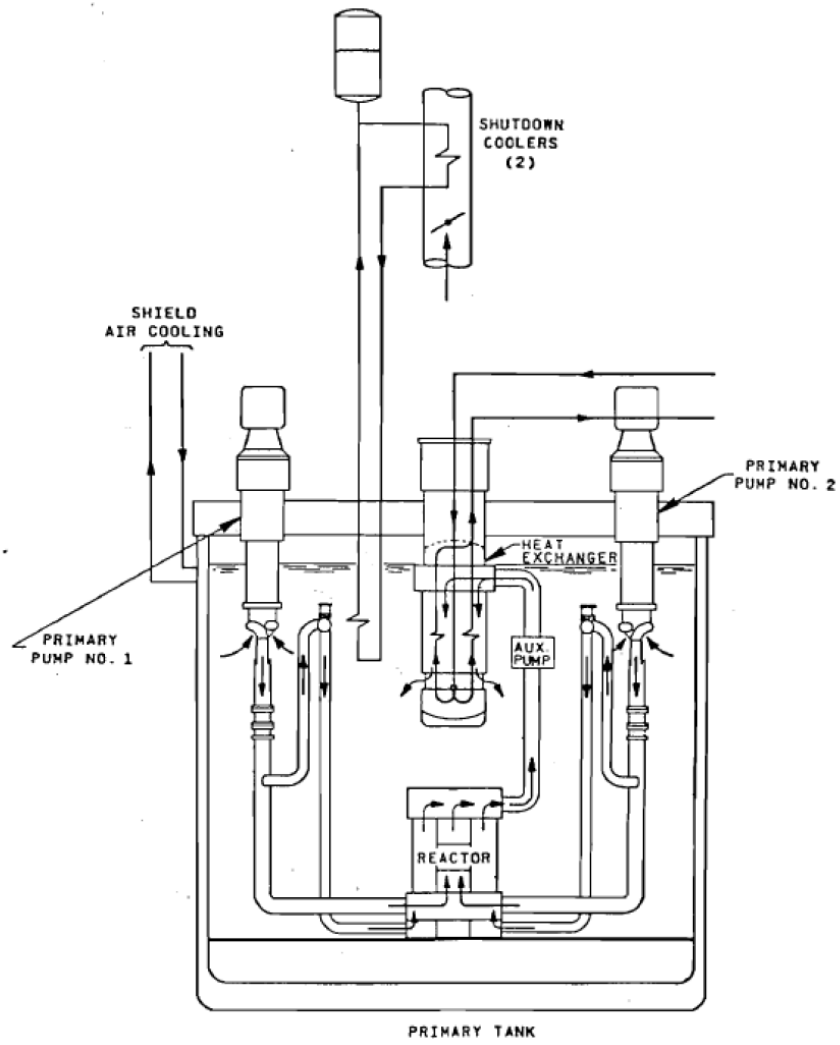

Fig. 15 - EBR-II Primary Tank Sodium Flow Paths.

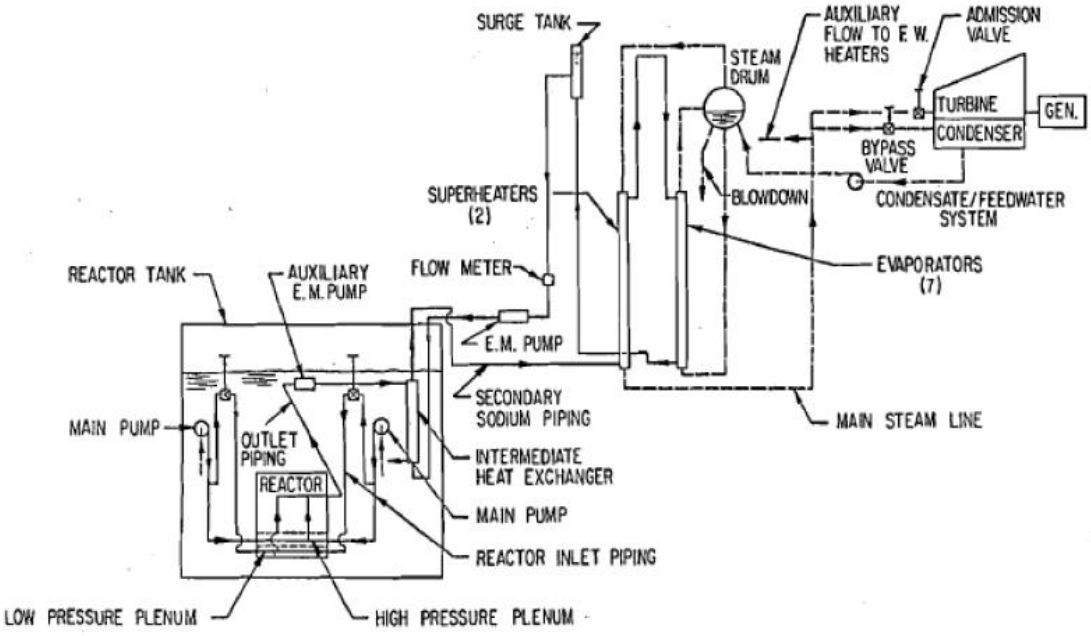

Fig. 16 - EBR-II Plant Schematic.

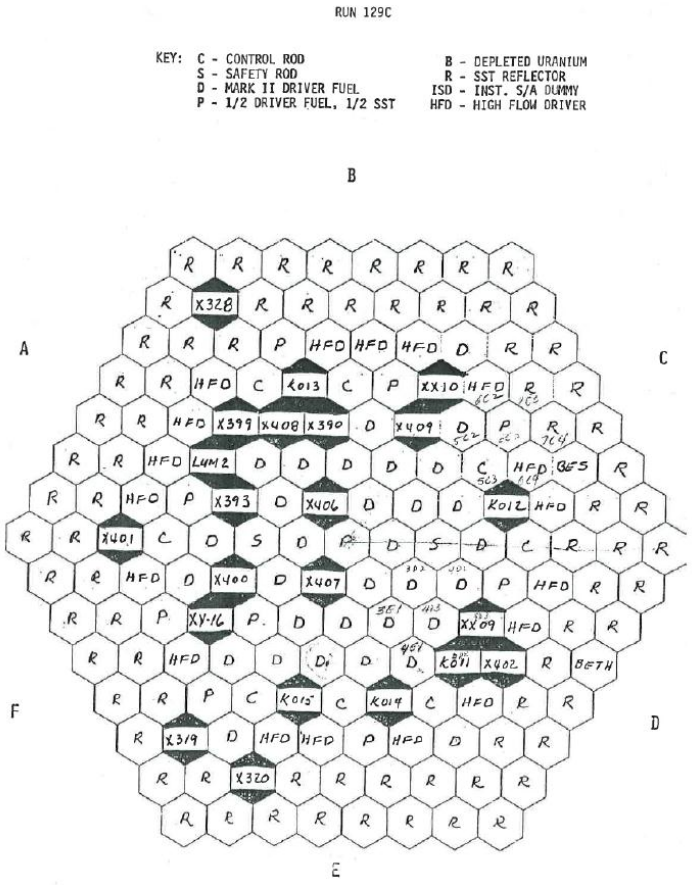

Fig. 17 - EBR-II SHRT-17 Core Loading Pattern (First 8 Rows)

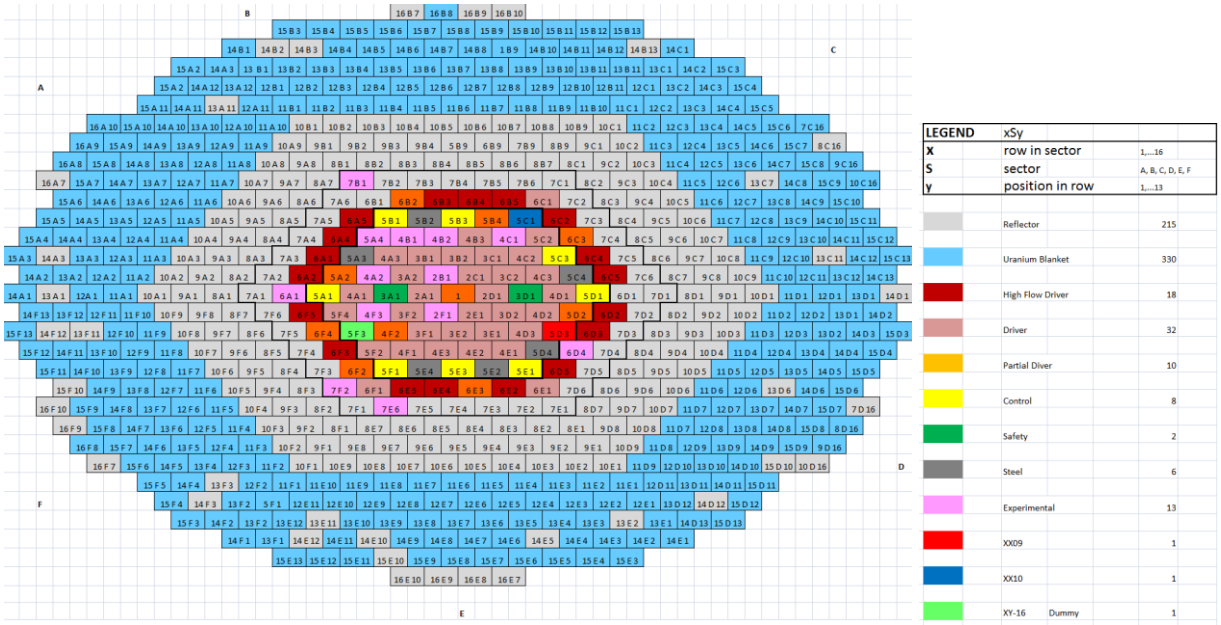

Fig. 18 - EBR-II Core Layout

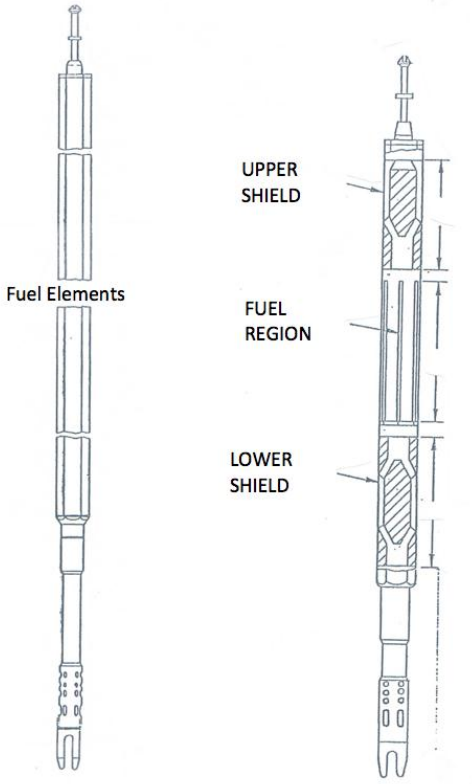

Fig. 19 - EBR-II MARK-II AI Subassembly Configuration.

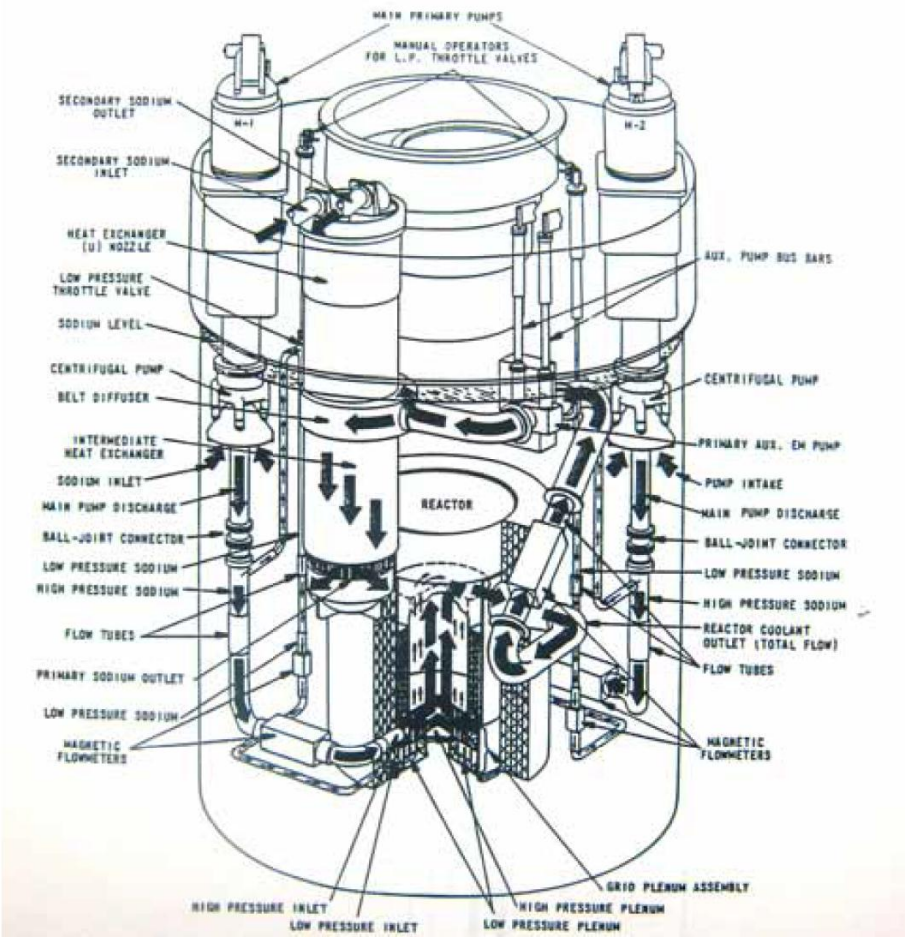

Fig. 20 - EBR-II Primary Tank Layout.

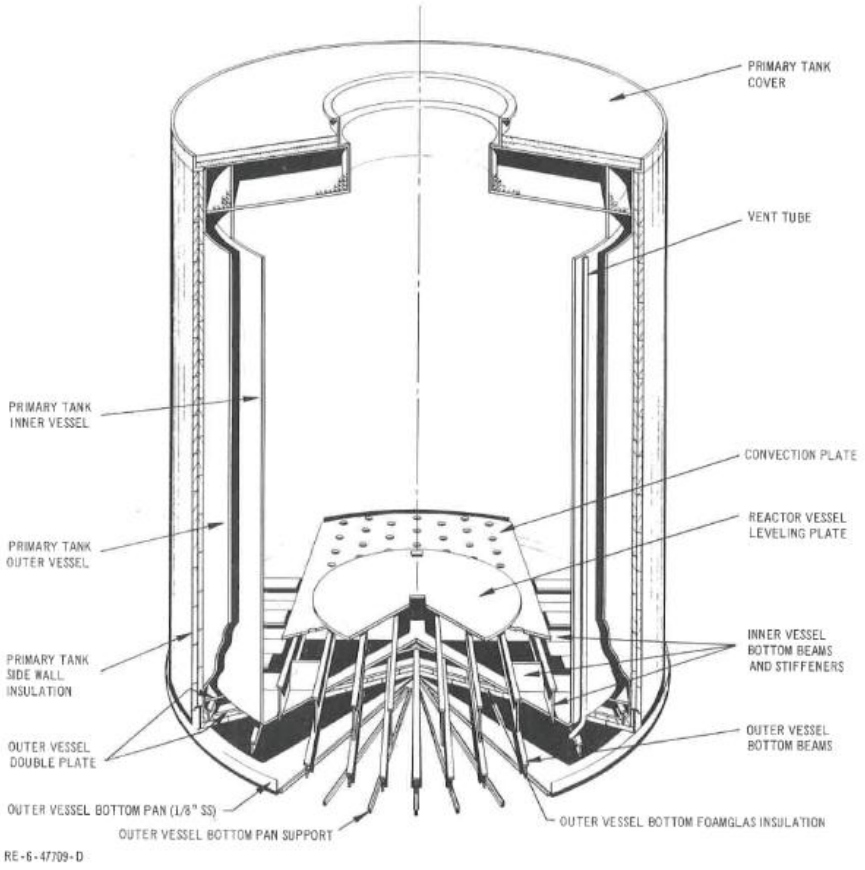

Fig. 21 - EBR-II Primary Tank Vessel.

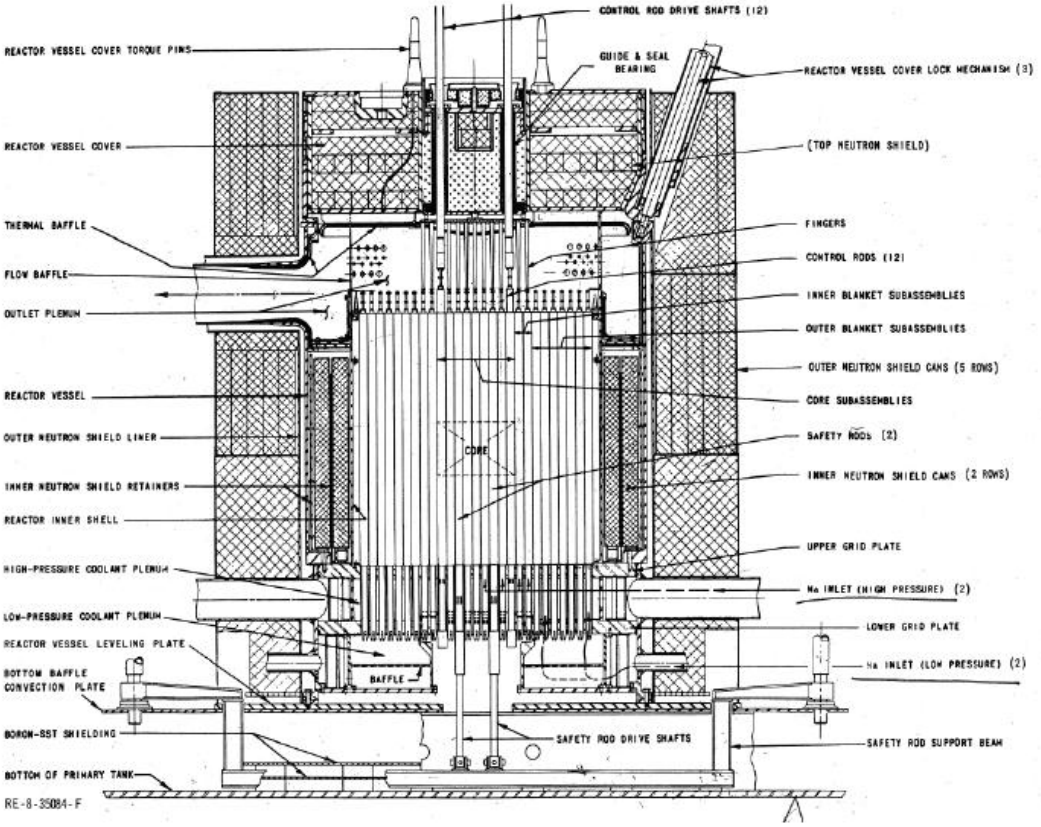

Fig. 22 - EBR-II Reactor Vessel.

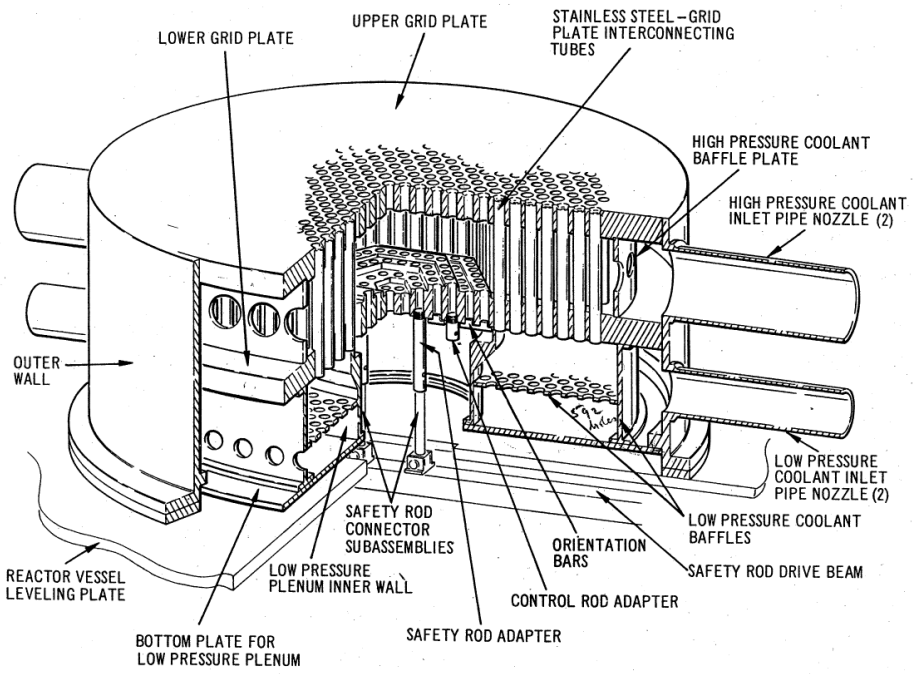

Fig. 23 – EBR-II High and Low Pressure Inlet Plena.

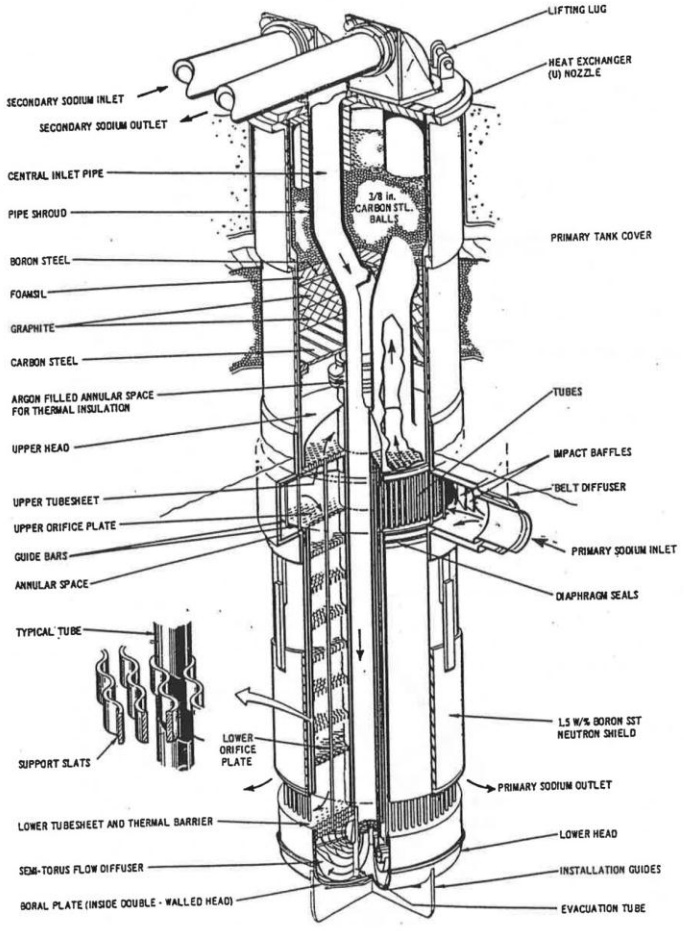

Fig. 24 - EBR-II Intermediate Heat Exchanger.

2.2 Nodalization description

RELAP5-3D© nodalization of EBR-II reactor represent the primary and the secondary systems. The primary system is modeled with a 3D component, with the exception of

1. the low and high pressure pipelines, connecting the pool system with the reactor zone Fig. 27,
2. the "Z-pipe" from the outlet of the reactor zone towards the IHX and, then to the reactor pool (Fig. 28),
3. the core channels: blanket and driver assemblies.

Fig. 25 shows the representation of the of the MULTID component in r, Z coordinates. The 3D component has: 6 radial, 12 azimuthal and 23 axial subdivisions (see also Fig. 26). Starting from the bottom, the death zone of the reactor is modeled as bypass, where at the center is located the safety rod drive shaft. The second and the third layers models the annular pool system, the low and the high pressure coolant plena. The core bypass is connected with the high pressure coolant plenum in the bottom and the upper plenum on the top. It is thermally coupled with the FA, through the wrappers and the pool system through the netronic shield. Besides, the top of the neutronic shield only the sodium pool is modeled, with its cover gas on the top. It must been stressed that each component in the pool is positioned as in the real 3D geometry.

The reactor core is divided into two main parts:

1. the driver FA, fed by the high flow plenum, which are modeled one by one as in EBR-II reactor.
2. the peripheral zone, where blanket and reflector assemblies, are represented as 24 equivalent PIPE components.

The fuel and driver channels represntations are rather detailed for representing all relevant positions, such as: change of geometry , BAF, TAF, and positions of the thermocouples. Each type of channel, as described in Ref. [1], is modeled in the nodalization: i.e. reflector, blanket high flow driver, driver, partial driver, control, safety, steel, experimental, XX09, XX10 and XY-16. Sample representation of MARK-II driver channel is depicted in Fig. 29.

The **IHX** primary side (Fig. 28) is connected upstream with the Z-pipe and downstream with the pool system. This is represented with a PIPE component of RELAP5. Suitable thermal coupling is implemented to calculate the heat exchange primary to secondary systems as well as the thermal losses between the IHX.

The secondary system (Fig. 28) is modeled with:

- 2 TIME DEPENDENT VOLUME and 1 TIME DEPENDENT JUNCTION components for setting the boundary conditions according with the reactor design (i.e. pressure at the outlet and coolant temperature and mass flow rate at the inlet).
    - The secondary sodium temperature is imposed with the TIME DEPENDENT VOLUME component at the inlet.
    - The system pressure is imposed with a TIME DEPENDENT VOLUME component at the outlet.
    - The mass flow rate is regulated with a PI controller connected with a TMDPJUN component.
- 2 PIPES connected by a BRANCH component modeling the central tube of the IHX, where the sodium flows downwards, the tube bundle, where the largest part of the core power is removed from primary system, and the lower plenum connecting the pipe with the tube bundle. The heat exchange with the primary system is modeled with a thermal structure. This REALP5 component exchange energy in concurrent direction (i.e. primary system and central tube) and counter-current direction (i.e. primary system and tube bundle).

The main features of the RELAP5-3D© model are reported hereafter.

- The elevations of the different parts of the plant are maintained in the nodalization.
- A sliced approach is applied at all systems (i.e. primary and secondary systems).
- The node to node ratio is kept uniform, as much as possible, with reference maximum ratio of 1.2 between adjacent sub-volumes.
- The heat transfer correlation used for non-bundle zone relies in a convective heat transfer coefficient function of Pe number and described in Ref. [9].
- The wire wrapped fuel bundle zone relies on a convective heat transfer correlazion by Todreas Carelli [9], which accounts also for the rod diameter and the pitch. This correlation was developed for a range of P/D from 1.1 to 1.4 and Pe number from 10 t0 5000. Moreover, this correlation was assessed on experimental data with different liquid metal fluids using bare rod bundles, but a few used wire-wrapped rods. The correlation gives good results when the P/D is between 1.1. and 1.2 but the Nusselt is under predicted for grater values[9].
- The roughness is set 5.0e-5m with the exception of the core region and the SG tubes.
- The energy loss coefficients in the junctions are evaluated or estimated on the basis of the system geometry.

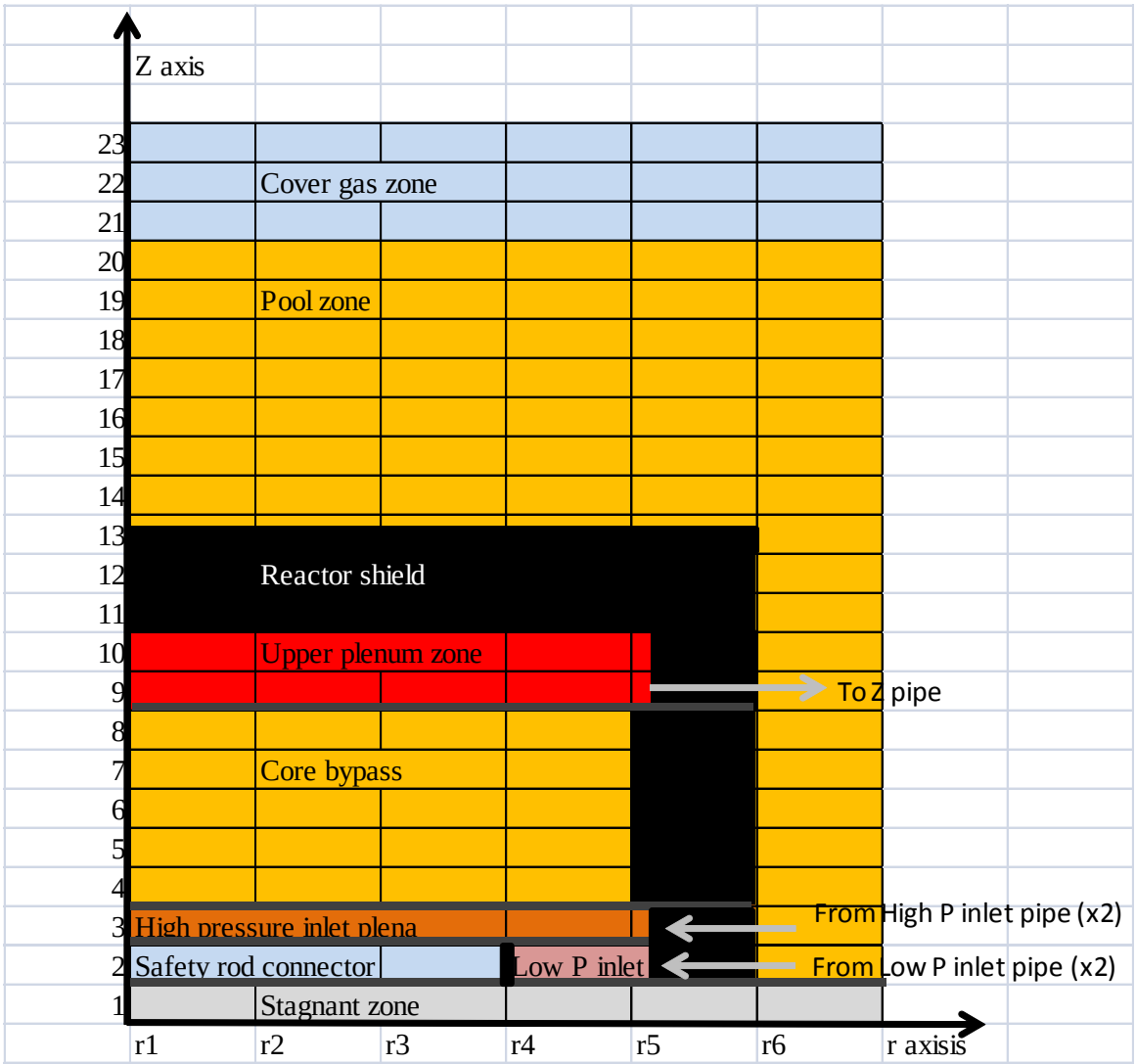

Fig. 25 - EBR-II nodalization: schematizzation of 3D component in the plane R, Z.

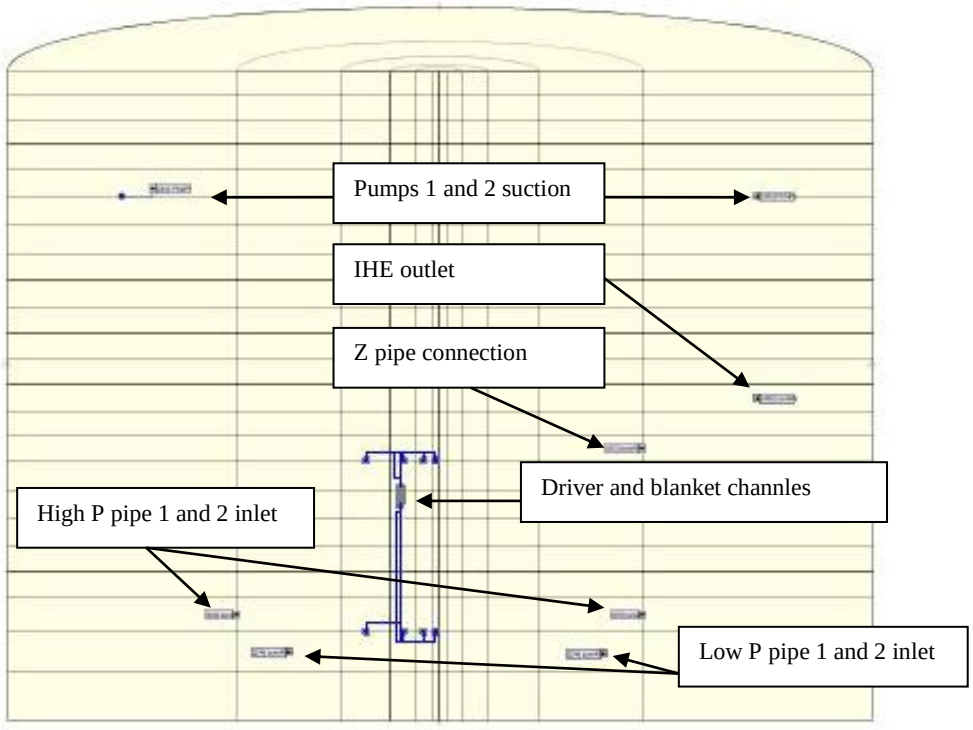

Fig. 26 - EBR-II nodalization: schematization of the 3D component with the 1D componenet connections.

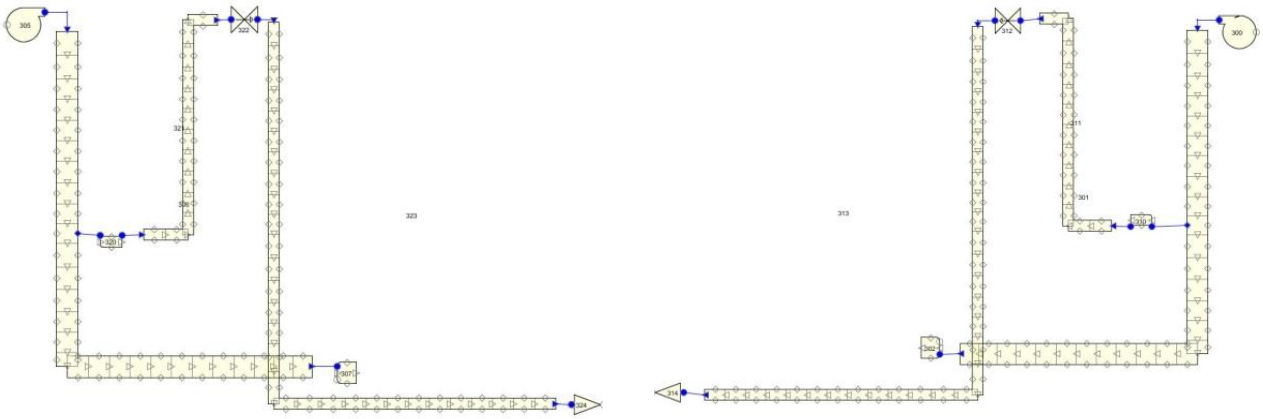

(a) pump 1 and high and low pressure lines 1 *(b) pump 2 and high and low pressure lines 2*

Fig. 27 - EBR-II nodalization: schematization from pumps connctions to high and low pressure reactor inlet plena.

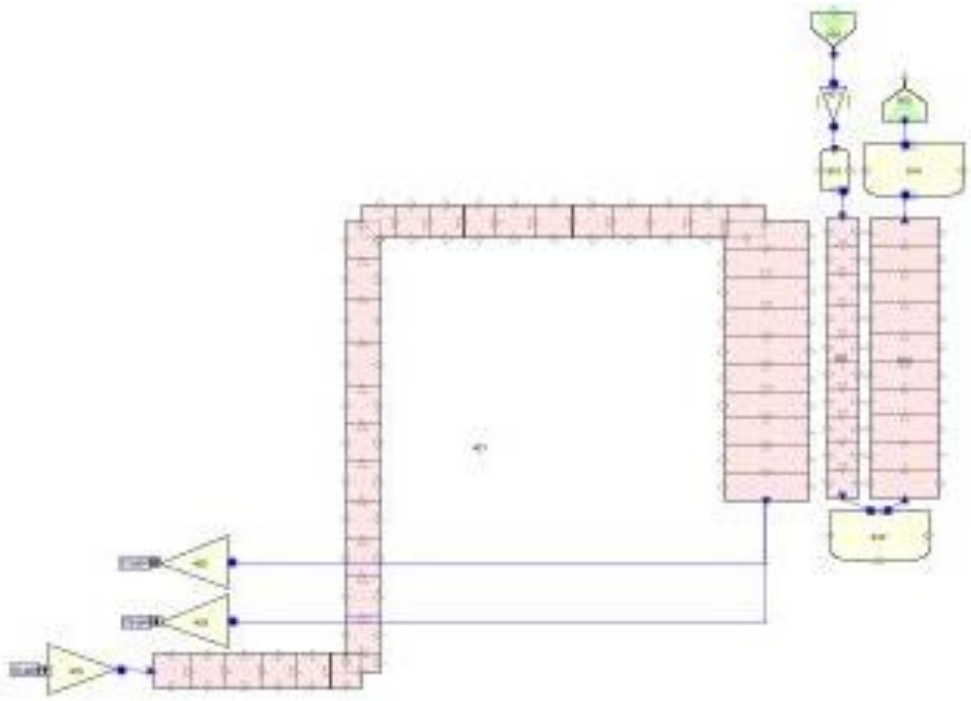

Fig. 28 - EBR-II nodalization: schematization of Z pipe, IHE primary and secondary sides.

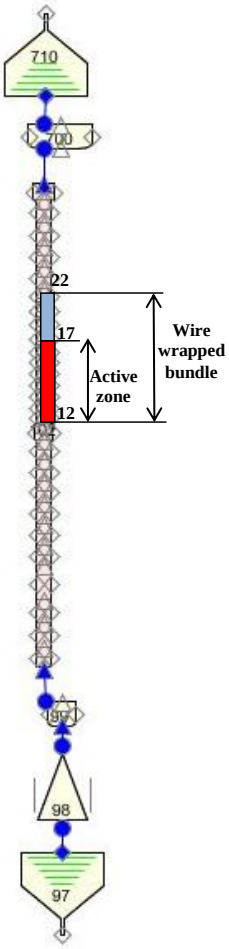

Fig. 29 – EBR-II nodalization: MARK-IIA fuel assembly

2.3 Nodalization qualification and preliminary results

Preliminary tests have been performed to investigate the hydraulic performances of the nodalization in terms of mass flow paths in the primary system as well as pressures distribution, the implementation of the pump and its characteristic curves, the calculation of the FA performances based on axial uniform power distribution. These tests are devoted to assess the performances of different parts of the nodalization. Steady state results representative of the EBR-II test SHRT17 will be addressed, when the nodalization will be completed with the neutronic data and the axial power profile in the fuel bundle.
The assessment is limited to the following steps.

- Geometrical verification, i.e. comparisons between geometry of design and nodalization features.
- The evaluation of the pressure drop in the wire wrapped fuel assembly as function of Re (Fig. 30), calculated for the MARK-II FA with the boundary conditions reported in Tab. 8 and Tab. 9.
- The verification of the heat transfer performance of the FA at different power levels (uniform linear power is imposed), considering two different fuel assemblies of EBR-II test SHRT-17, i.e. minimum and the maximum mass flow rates (see Tab. 10). The single FA calculation is set imposing a constant bypass coolant temperature (see Fig. 31 and Fig. 32).
- pressure drop along the loop in isothermal conditions,
- mass flow distributions in fuel channels, see Tab. 11,

The EBR-II have still to be finalized, in particular the following actions are to be implemented:

- set up of the pumps homologous curves,
- set up of the reactor bypasses, according with Ref. [1],
- improvement of the mass flow distributions in the FA channels,
- development of the point kinetic model (currently the power is imposed by means of a table)
- implementation of the reactivity feedback in the point kinetic model,
- achievement of steady state conditions,
- simulations of the tests SHRT17 and 45.

INITIAL CONDITIONS	
Power	0 [MW]
Core inlet temperature	700 [K]
Upper plenum pressure	1.953e+05 [Pa]
Rated mass flow rate	3.6194 [kg/s]

Tab. 8 – EBR-II nodalization. MARK II pressure drop test: initial conditions

Mass flow rate [kg/s]	% Mflow	ΔP [Pa]	Core inlet pressure [Pa]
0.18097	5%	111.733	2.136E+05
0.36194	10%	448.863	2.145E+05
0.72388	20%	1468.55	2.176E+05
1.0858	30%	2968.09	2.224E+05
1.4478	40%	4910.28	2.290E+05
1.8097	50%	7272.84	2.372E+05
2.1716	60%	10040.4	2.471E+05
2.5336	70%	13201.8	2.587E+05
2.8955	80%	16748	2.719E+05
3.2575	90%	20672.1	2.868E+05
3.6194	100%	24968.2	3.032E+05
3.9813	110%	29631.5	3.213E+05
4.3433	120%	34657.8	3.411E+05
4.7052	130%	40043.5	3.624E+05
5.0672	140%	45785.6	3.853E+05
5.4291	150%	51881.2	4.098E+05
5.791	160%	58328	4.359E+05
6.153	170%	65123.7	4.637E+05
6.4787	179%	71538	4.900E+05
6.8388	189%	78951.6	5.205E+05
7.2007	199%	86747.2	5.529E+05
7.5626	209%	94885.2	5.868E+05
7.9246	219%	103364	6.223E+05
8.3246	230%	113131	6.633E+05

Tab. 9 – EBR-II nodalization. MARK II pressure drop test: RELAP5-3D results

INITIAL CONDITIONS		
	Low mass flow rate	**High mass flow rate**
Core Rated Power	57.3 [MW]	57.3 [MW]
Fuel assembly rated power	0.534 [MW]	0.892 [MW]
Core inlet temperature	700 [K]	700 [K]
Upper plenum pressure	1.953e+05 [Pa]	1.953e+05 [Pa]
Mass flow rate	3.6194 [kg/s]	7.8861 [kg/s]

Tab. 10 – EBR-II nodalization. MARK II heat exchange tests: initial conditions

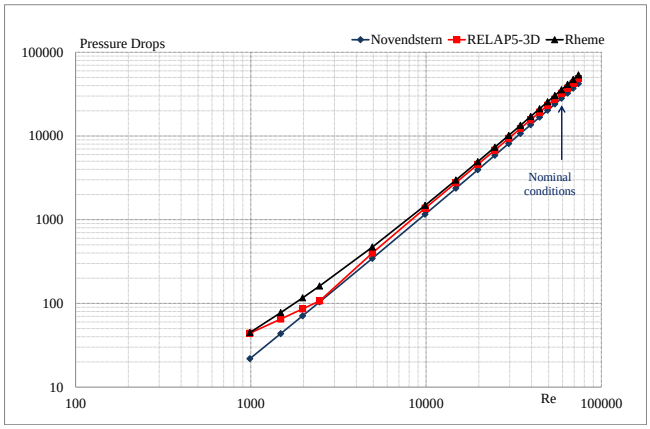

(a) DP vs. Re

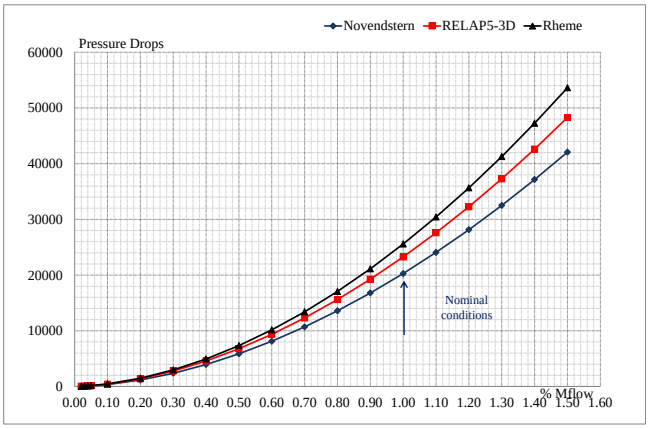

(b) DP vs. dimensionless mass flow

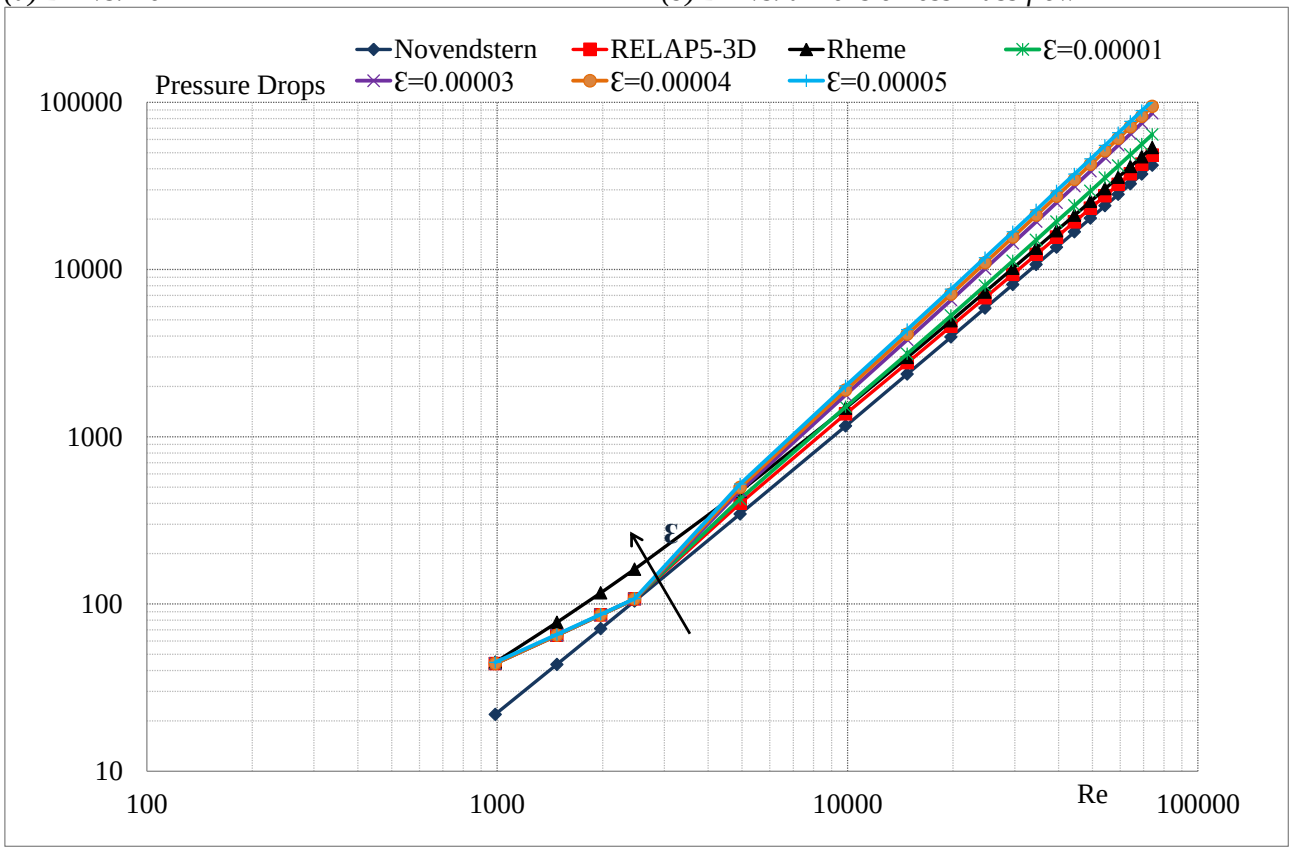

(a) DP vs. Re at different roughness

Fig. 30 – EBR-II nodalization. MARK II dynamic pressure drop in wire wrapped fuel bundle

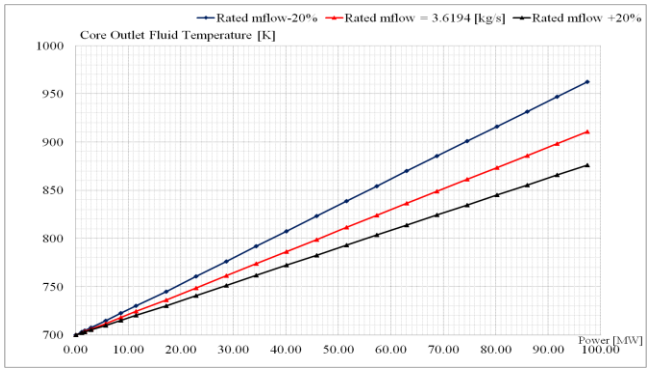

(a) Coolant temperature vs power at different mass flow rate

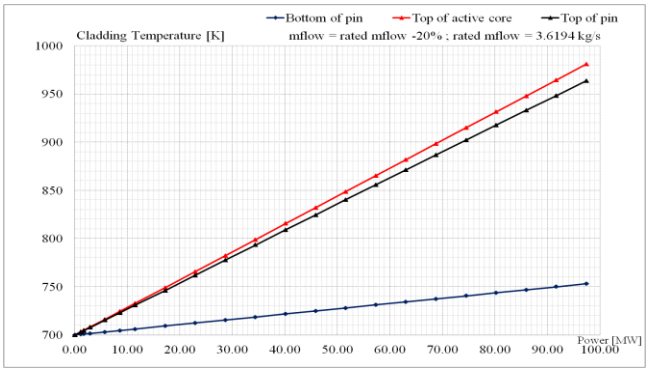

(b) Cladding temperature at different elevations vs power at nominal mass flow rate minus 20%

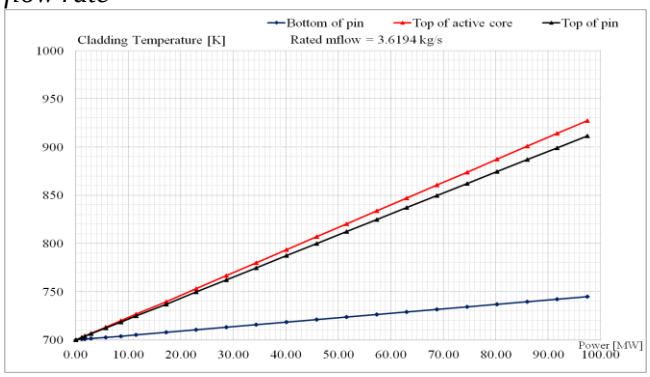

(c) Cladding temperature at different elevations vs power at nominal mass flow rate

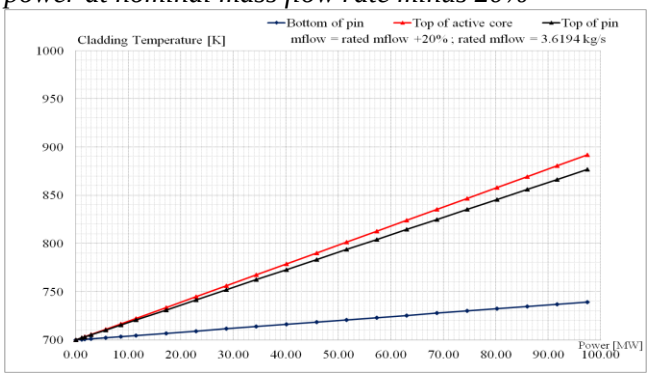

(d) Cladding temperature at different elevations vs power at nominal mass flow rate plus 20%

Fig. 31 – EBR-II nodalization. MARK II heat exchange tests: low mass flow rate tests

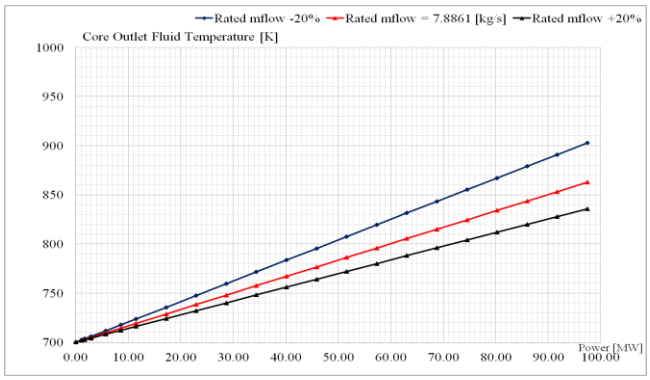

(a) Coolant temperature vs power at different mass flow rate

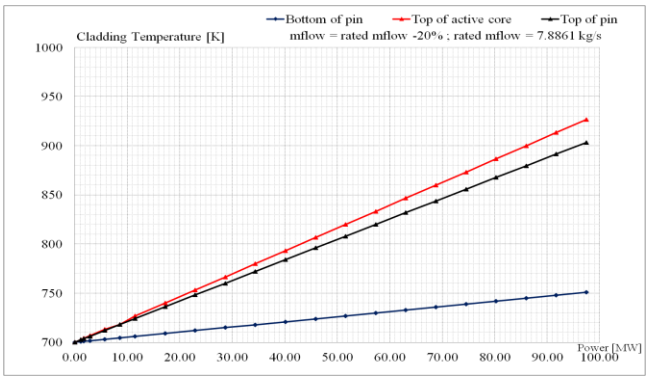

(b) Cladding temperature at different elevations vs power at nominal mass flow rate minus 20%

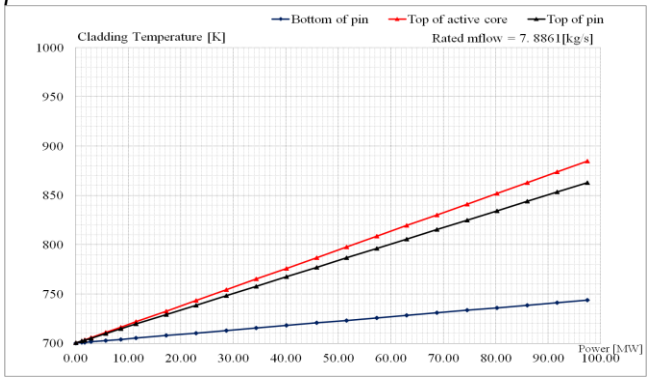

(c) Cladding temperature at different elevations vs power at nominal mass flow rate

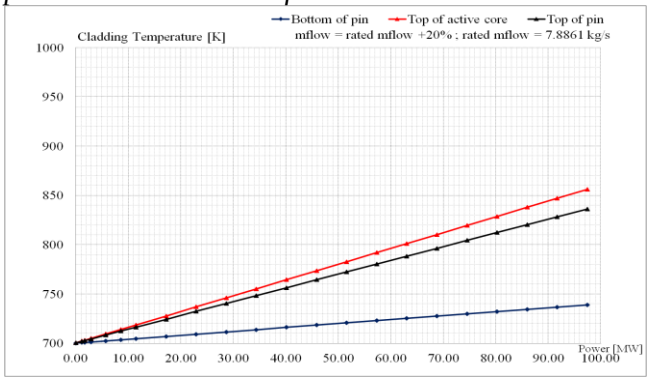

(d) Cladding temperature at different elevations vs power at nominal mass flow rate plus 20%

Fig. 32 – EBR-II nodalization. MARK II heat exchange tests: high mass flow rate tests

EBR-II - ring	Type	No FA	Mass flow	
			EBR-II	R5-3D
	Reflector	12	1.98	**1.80**
	Blanket	12	3.63	**3.53**
Ring 7 - Tot. FA 36	Reflector	33	0.17	**0.17**
	Exp	3	0.69	**0.70**
Ring 6 - Tot. FA 30	Reflector	2	0.17	**0.17**
	Exp	2	3.94	**4.11**
	Driver	3	3.62	**3.65**
	Partial D	5	2.66	**2.74**
	High flow	18	3.94	**4.12**
Ring 5 - Tot. FA 24	Exp	1	4.45	**4.64**
	Driver	3	4.45	**4.61**
	Partial D	3	3.11	**2.87**
	CR	8	3.35	**3.23**
	SS FA	6	0.72	**0.78**
	XX09	1	2.73	**2.87**
	XX10	1	0.34	**0.65**
	Dummy	1	0.65	**0.86**
Ring 4 - Tot. FA 18	Exp	5	5.15	**5.72**
	Driver	12	5.15	**5.41**
	Partial D	1	3.34	**3.79**
Ring 3 - Tot. FA 12	Driver	10	6.7	**6.47**
	Safety	2	5.14	**4.71**
Ring 2 - Tot. FA 6	Exp	2	7.77	**6.72**
	Driver	4	7.78	**6.54**
Ring 1 - Tot. FA	Partial D	1	3.97	**3.70**
	TOTAL FLOW		***459.07***	***455.67***

Tab. 11 – EBR-II nodalization: SHRT-17 boundary conditions: fuel assembly mass flow distribution at steady state

2.4 Conclusive remarks and follow up

A RELAP5-3D© nodalization of EBR-II has been developed and set up. The nodalization models the overall pool system and the reactor zone with a 3D component, and the driver core fuel assemblies, fed by the high flow line, one by one. This is developed and set-up thanks the experimental data provided by the IAEA coordinated research project (CRP) on EBR-II Shutdown Heat Removal Tests (SHRT). The report describes the framework of the activities , the nodalization and the first steps of qualification.

Tests on the FA performances modeling have been completed. Friction pressure losses in the wire wrapped fuel assembly zone have been compared with correlations available in literature. The heat exchange performances have been tested with constant linear power in the active zone and setting the Todreas Carelli correlation.

The EBR-II nodalization have still to be finalized, in particular the following actions will be implemented:

- set up of the pumps homologous curves,

- set up of the reactor bypasses, according with Ref. [1],
- improvement of the mass flow distributions in the FA channels,
- development of the point kinetic model (currently the power is imposed by means of a table)
- implementation of the reactivity feedback in the point kinetic model,
- achievement of steady state conditions,
- simulations of the tests SHRT17 and 45.

2.5 References

[1] T. Sumner and T.Y.C. Wei, Benchmark Specifications and data Requirements for EBR-II Shutdown Heat Removal tests SHRT-17 and SHRT-45R, ANL-ARC-226 (rev 1), May 31, 2012.

[2] IAEA. Status of Fast Reactor Research and Technology Development. IAEA-TECDOC-1691, Vienna, 2012.

[3] http://www.iaea.org/NuclearPower/Technology/CRP/index.html

PART B: REVIEWING THE TH-SYS CODES CAPABILITIES AND LIMITATIONS IN SAFETY ANALYSES OF GEN. IV POOL TYPE LIQUID METAL FAST REACTOR

3 QUALIFICA DI CODICI DI CALCOLO DEDICATI ALLE ANALISI DI SISTEMA AVANZATI QUANDO APPLICATI NELLA SIMULAZIONE DI IMPIANTI A METALLO LIQUIDO

CIRTEN

Consorzio **I**nteruniversitario per la **R**icerca **TE**cnologica **N**ucleare

UNIVERSITÀ DEGLI STUDI DI PALERMO

DIPARTIMENTO DI ENERGIA, INGEGNERIA DELL'INFORMAZIONE, E MODELLI MATEMATICI

Qualifica di codici di calcolo dedicati alle analisi di sistema avanzati quando applicati nella simulazione di impianti a metallo

Autori

F. Castiglia, M. Giardina

CERSE-UNIPA RL 1220/2013

Palermo, Agosto 2013

Lavoro svolto in esecuzione dell'Attività LP2.a.3_d
AdP MSE-ENEA sulla Ricerca di Sistema Elettrico - Piano Annuale di Realizzazione 2012
Progetto B.3.1 "Sviluppo competenze scientifiche nel campo della sicurezza nucleare e collaborazione ai programmi internazionali per il nucleare di IV generazione

Indice

SOMMARIO

L'attività di ricerca svolta nell'ambito della linea progettuale LP2.a.3-d ha riguardato lo studio delle capacità di alcuni modelli impiegati nel codice Relap5/mod3.2β di simulare le fenomenologie caratteristiche della termoidraulica degli impianti di tipo LFR.

INTRODUZIONE

L'attività di ricerca svolta dal nostro gruppo di lavoro nell'ambito della linea progettuale LP2.a.3-d del PAR 2012-13 ha visto lo studio delle capacità di alcuni modelli, impiegati nel codice Relap5/mod3.2β, di simulare alcune fenomenologie della termoidraulica dell'impianto ELFR (European Lead Fast Reactor).

Per quanto riguarda la fase di implementazione delle caratteristiche dei metalli pesanti, il codice è stato modificato nel passato da alcuni ricercatori dell'Ansaldo che hanno inserito fluidi come il piombo e la lega eutettica piombo-bismuto.

Nella presente relazione tecnica viene descritta la successiva attività di modifica operata dal nostro gruppo che ha riguardato lo scambio termico e le perdite di carico i presenza di metalli liquidi e le fenomenologie termofluidodinamiche coinvolte in alcuni sistemi come lo scambiatore di calore di tipo elicoidale e quello a baionetta che si intendono utilizzare nell'impianto ELFR ed nel prototipo sperimentale ALFRED.

Inoltre, nell'appendice A viene effettuata una presentazione delle correlazioni presenti in letteratura per lo scambio termico in presenza di metalli liquidi e vengono descritte alcune delle correlazioni impiegate nel codice Relap5/mod3.2β e nella versione tridimensionale RELAP5-3D, mentre nell'appendice B viene discussa la qualifica di alcuni modelli del codice RELAP5-3D per la simulazione della tecnologia a piombo.

CAPITOLO 1

IL PROGETTO EUROPEAN LEAD FAST REACTOR (ELFR)

1.1 Introduzione

La tecnologia dei reattori veloci refrigerati con il piombo sembra possedere un grande potenziale per soddisfare tutti i principali obiettivi stabiliti dal "Generation IV International Forum" (GIF) e tra i vari progetti messi a punto negli ultimi dieci anni dalla comunità scientifica italiana ed internazionale si trovano diverse soluzioni [1, 2] come il progetto ELSY (European Lead-cooled System).

Le attività di ricerca riguardanti l'impianto Elsy sono iniziate nel 2006, sotto il coordinamento dell'Ansaldo Nucleare con la collaborazione tecnico-scientifica di alcuni enti italiani come ENEA, CIRTEN e CESI. Successivamente, dopo una profonda analisi dei punti critici e l'individuazione dei principali problemi relativi al layout dell'impianto, si è pensato di far confluire tutte le scelte progettuali innovative ed i possibili miglioramenti in una configurazione denominata ELFR.

In questo ambito, è in fase di sviluppo il progetto di un prototipo sperimentale denominato LEADER (Lead-cooled European Advanced DEmonstration Reactor) con l'obiettivo di dimostrare la fattibilità di alcune delle scelte progettuali a supporto di un reattore commercialmente ELFR per la produzione di energia elettrica su larga scala.

Il progetto ELFR ha caratteristiche alquanto avanzate ed innovative per le scelte tecnologiche, tra queste l'impiego di un circuito primario compatto e l'eliminazione del circuito di raffreddamento intermedio sono destinate a garantire la competitività tecnica nel panorama della futura generazione di reattori nucleari.

Dal punto di vista della sicurezza, il progetto prevede l'uso di due sistemi ridondanti e diversificati per la rimozione del calore di decadimento (Decay Heat Removal, DHR), realizzati anche facendo ricorso a dispositivi di intervento di tipo passivo.

Il maggiore punto di forza è l'adozione di criteri come la sicurezza intrinseca connessa al piombo che consente un più elevato grado di affidabilità del sistema nel suo complesso (alto valore della temperatura del punto di ebollizione pari a 1745 °C, assenza di reazioni esotermiche con aria o acqua, effetto buoyancy derivante dall'alta densità del piombo, bassa produzione di Polonio).

Il piombo fuso ha l'elevata capacità di intrappolare prodotti di fissione e schermare la radiazione gamma garantendo la riduzione della dose che può essere assorbita dal personale, in caso di condizioni incidentali particolarmente gravose. Inoltre, nonostante l'alta densità del piombo, le cadute di pressione nel circuito primario possono essere ridotte in quanto le basse perdite di energia dei neutroni consentono di utilizzare passi tra gli elementi di combustibile più grandi. Infine, in presenza di incidenti gravi con fusione del nocciolo, il piombo favorisce la dispersione del combustibile fuso (densità del piombo leggermente

superiore a quella del combustibile), riducendo la probabilità di formazione di massa critica con successivi eventi di criticità.

Di contro, tra le maggiori criticità troviamo il valore elevato del punto di fusione del piombo (327.4 °C), che richiede nuove strategie ingegneristiche per evitare fenomeni di solidificazione del refrigerante, soprattutto in caso di spegnimento del reattore per refueling, e il problema dell'elevata corrosività nei confronti dei materiali strutturali, soprattutto alle alte temperature. Quest'ultimo aspetto comporta la necessità di un attento controllo della purezza del piombo e un'oculata scelta dei materiali da impiegare nel sistema.

In Tabella 1 vengono sintetizzati alcuni punti chiave più importanti per lo sviluppo tecnologico degli impianti LFR.

Tabella 1: Riassunto dei punti chiave e strategie proposte nell'ambito della ricerca e sviluppo degli impianti LFR

Tecnologia del piombo	Pre-purificazione	Capacità dell'industria di produrre piombo ad elevate purezza
	Purificazione durante la fase operativa	Tecnologie per la purificazione di elevate quantità di piombo
	Controllo dell'ossigeno	Estensione della tecnologia di controllo della concentrazione di ossigeno disciolto nel metallo liquido per i reattori piscina.
Materiali resistenti alla corrosione del piombo.	Corrosione dei materiali ad alte temperature.	Selezione di una temperatura di uscita dal noccio bassa per la progettazione del reattore Sviluppo di nuovi materiali resistenti fino a temperature di 650°C
	Corrosione del vessel del reattore	Temperatura di progetto del vessel almeno fino a 400°C.
	Materiali degli interni di reattori	Protezione dei materiali mediante il controllo dell'ossigeno (formazione di ossidi di ferro superficiali negli acciai strutturali, evitandone la corrosione)
	rivestimento del combustibile	Uso di materiali di acciaio ferritico and austenitico per ritardare processi di ossidazione della guaina
Funzioni di sicurezza principali	Sistemi DHR ridondanti e diversificati	Uso di fluidi differenziati come l'aria atmosferica e l'acqua
	Sistema di spegnimento affidabili e diversificati	Necessità di scegliere soluzioni diversificate.

1.2 Configurazione del circuito primario dell'impianto ELFR

L'impianto ELFR è un sistema, refrigerato a piombo, che prevede la produzione di una potenza di 600 MW_e, con molte delle caratteristiche progettuali inizialmente selezionate per l'impianto Elsy. Uno scheda del circuito primario viene mostrato in Fig. 1.

La progettazione del core comporterà, nei prossimi anni, studi attenti sulla tipologia del combustibile da impiegare, sulla neutronica, sui problemi termo-meccanici ed opportuni calcoli dei fenomeni termo-fluidodinamici che possono interessare l'impianto sia durante le varie fasi di normale funzionamento, sia in condizioni incidentali.

La temperatura del refrigerante all'ingresso del core è stata imposta al valore di 400 °C, sia per consentire un margine sufficiente rispetto alla temperatura di solidificazione del piombo, sia per evitare l'infragilimento degli acciai martensitici/ferritici. Inoltre, per rispettare il limite di temperatura di 550 °C, oltre cui la corrosione dei rivestimenti diventerebbe significativa, si è deciso di fissare la temperatura del refrigerante in uscita dal core al valore di 480 °C. Un ulteriore problema per i rivestimenti è anche l'erosione da parte della portata di piombo, per cui è necessario limitare la velocità massima, che nel caso dell'impianto ELFR è pari a 2 m/s.

Per quanto riguarda il core, in Fig. 2 viene mostrato lo schema dell'elemento di combustibile (FA, Fuel Assembly) costituto da un fascio di barre in geometria esagonale con elemento inscatolato, in cui le singole barrette hanno un diametro esterno di 10.5 mm, distribuite secondo un passo reticolare pari a 15 mm. Si pensa di utilizzare in alternativa una diversa configurazione costituita da un reticolo quadrato con griglie spaziatrici e senza scatola esterna, tuttavia su questo tema sono ancora in fase di svolgimento studi di verifica e fattibilità.

I canali esagonali rivestono le seguenti funzioni:

- convogliare il flusso del refrigerante verso le barre di combustibile evitando la formazione di flussi trasversali tra i diversi fasci;
- fornire un supporto strutturale per agganciare le barrette del fascio, migliorando la stabilità del core;
- creare una barriera contro la potenziale propagazione del combustibile in presenza della fusione delle barre del fascio durante condizioni incidentali.

I FA si estendono oltre il livello di copertura del gas, ben al di sopra della superficie del piombo fuso (Fig. 1), per facilitare la gestione e movimentazione degli elementi durante la vita dell'impianto. Nonostante l'estensione oltre lo spazio di copertura del gas, i FA sono spinti dal piombo verso l'alto (spinta di galleggiamento) per cui viene utilizzata una zavorra di tungsteno per aumentare la stabilità dell'elemento, soprattutto durante le operazioni di refuelling. Inoltre, molle precaricate vengono inserite nella parte superiore "diagrid" sia per controbilanciare l'effetto di risucchio dovuto all'aspirazione delle pompe primarie, sia per consentire le dilatazioni termiche degli elementi. Il refrigerante primario, all'uscita del core, attraversa alcune restrizioni (funnel) e fori, posti nella regione alta del canale, che consentono di dirigere la portata verso le pompe primarie (Fig. 3).

Gli altri componenti principali del sistema primario sono: vessel interno (Reactor Vessel, RV), vessel esterno di sicurezza (Safety Vessel, SV), generatori di vapore (Steam Generator System, SGS) e pompe primarie di tipo assiale.

Per quanto riguarda gli SG, si pensa di utilizzare la tipologia prevista nell'impianto Elsy, dato che questi componenti sono caratterizzati da scelte progettuali di tipo innovativo, basate anche su concetti di sicurezza di tipo intrinseca e passiva.

La potenza termica del fluido refrigerante primario viene rimossa da otto SG verticali, alla pressione di 180 bar (temperatura dell'acqua di ingresso 335 °C, temperatura di uscita 450°C in condizione di surriscaldamento), con fasci di tubi a spirale.

Gli SG sono posizionati nella regione superiore del vessel, all'interno della sezione anulare tra il core e la parete del RV (Fig. 1), e ancorati al tetto del reattore tramite una flangia. Come già detto, questa configurazione consente di sfruttare la circolazione naturale per la rimozione del calore residuo, in caso di malfunzionamento delle pompe. Inoltre, l'eliminazione del sistema di raffreddamento intermedio consente di contenere tutto il refrigerante primario all'interno del reattore, evitando i problemi legati alla circolazione del refrigerante all'esterno del vessel.

Il fascio di tubi a spirale sono disposti nella regione inferiore tra due pareti cilindriche forate che separano la regione interna, che ospita la pompa di alimentazione, e la regione esterna del collettore freddo del circuito primario (Fig. 4a).

L'ingresso e l'uscita di ogni tubo del fascio sono collegati al collettore dell'acqua di alimentazione e al collettore del vapore, entrambi installati sopra il tetto del RV (fig. 4b). L'acqua di alimentazione circola all'interno del tubo a spirale più esterno ed esce dal tubo a spirale più interno (fig. 4c), per cui la configurazione dello scambio termico tra primario e secondario segue uno schema "counter-current".

Le due pareti principali forate permettono il passaggio della portata del piombo che entra dal fondo del SG, attraversa radialmente il fascio tubiero ed, infine, esce dalla parete esterna del SG (fig. 4a). Questa configurazione assicura che il refrigerante fluisca sempre verso i fascio tubiero dello scambiatore, anche in caso di riduzione del livello dovuto alla perdita di refrigerante dal vessel.

La presenza delle due pareti nel SG consente di ridurre eventuali ripercussioni negative sul core dovute a rotture del fascio tubiero (Steam Generator Tube Rupture, SGTR). In caso di SGTR, la posizione dei fori nelle pareti principali è realizzata in modo tale che il passaggio della portata di piombo sia inibita con l'intervento di uno speciale meccanismo completamente passivo.

La pompa primaria, situata nella regione interna del SG (Fig. 4a), è una pompa assiale, a velocità costante, con aspirazione nella gamba calda. Essa fornisce la prevalenza necessaria per forzare il fluido primario caldo ad entrare dal fondo dei SG, attraversare in direzione radiale la regione anulare in cui sono posizionati i fasci di tubi a spirale, e lambire gli elementi di combustile del core.

Le caratteristiche della girante sono state determinate tenendo presenti i limiti di velocità del flusso del piombo ed i problemi di corrosione del corpo e della girante. Infatti, l'inevitabile alta velocità del piombo fuso, soprattutto all'ingresso della pompa e nelle pale, insieme all'elevata temperatura, renderebbe significativa la corrosione del materiale.

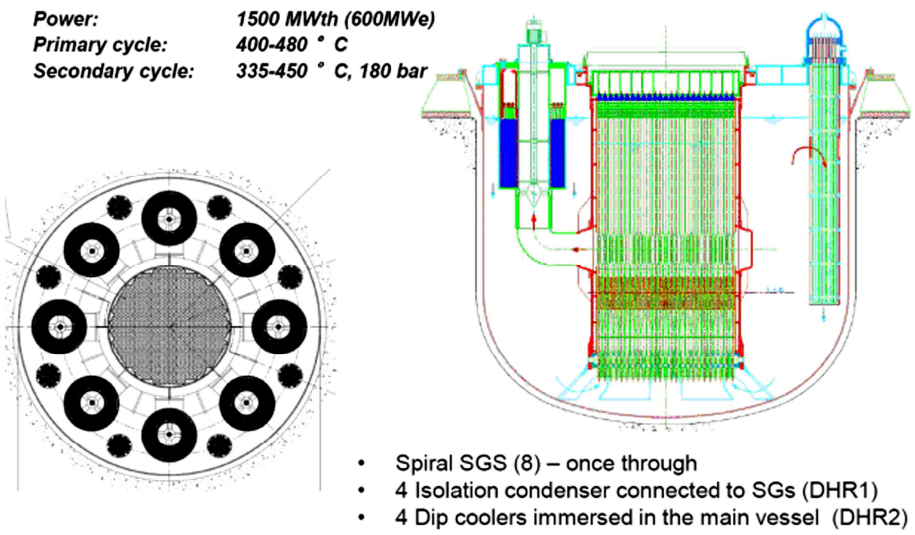

Fig. 1- Sezione trasversale del vessel e schema del circuito primario dell'impianto ELFR

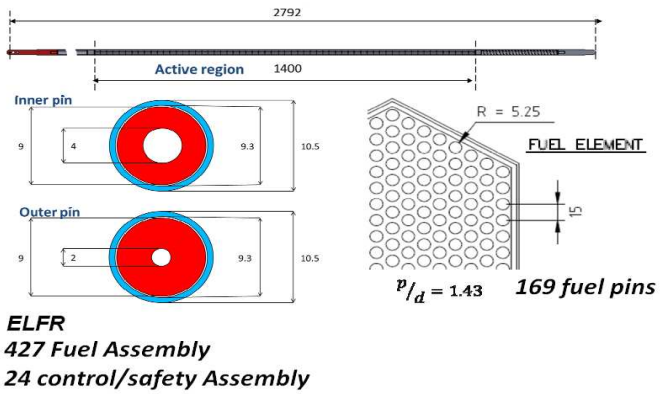

Fig. 2 - Schema del FA nell'impianto ELFR.

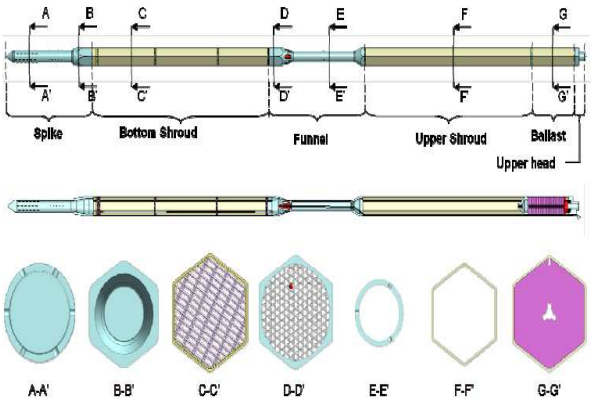

Fig. 3 - Elementi dell'assemblaggio distribuiti lungo l'altezza del FA previsti nell'impianto ELFR.

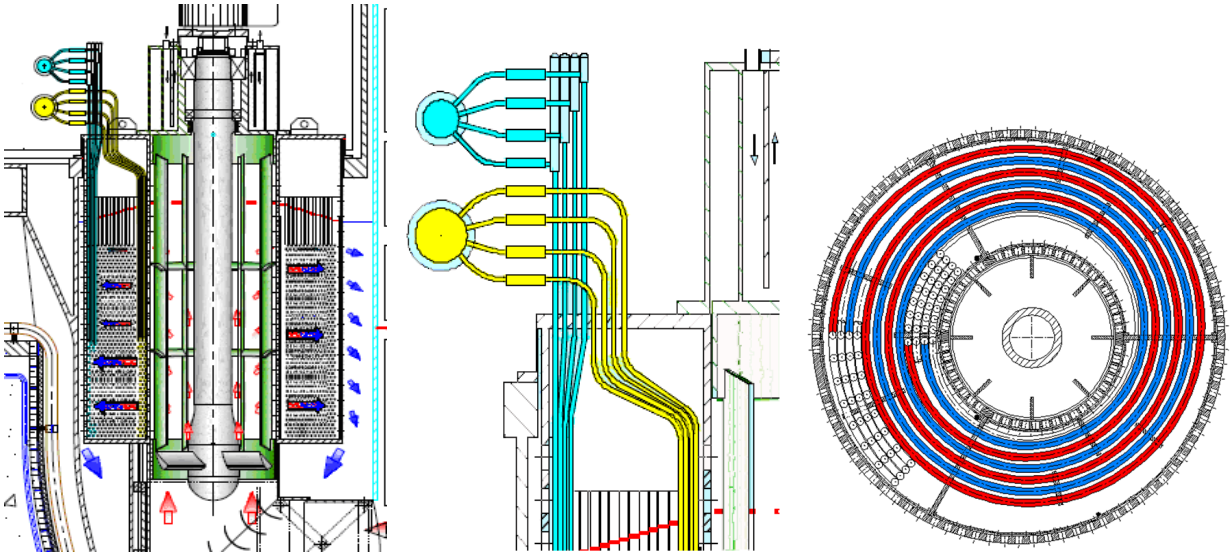

(a) (b) (c)

Figura 4. - Schema dello scambiatore di calore in cui sono alloggiati i tubi a spirale e dei collettori di ingresso ed uscita dell'acqua di refrigerazione.

1.2.1 Descrizione del sistema Decay Heat Removal

Dopo l'arresto del reattore, il calore di decadimento prodotto nel core deve essere rimosso da opportuni sistemi con caratteristiche di elevata affidabilità. Per soddisfare questo requisito sono stati progettati due dispostitivi indipendenti e ridondanti, il sistema DHR1 (Decay Heat Removal, DHR) composto da quattro Isolation Condenser systems (ICs), collegati a 4 degli 8 SG (Fig. 1), ed il sistema DHR2 costituito da quattro unità immerse nel circuito primario all'interno del RV. Tre su quattro IC sono sufficienti per asportare il calore di decadimento, eliminando le possibili condizioni di rotture singole, che possono inibire l'intero sistema.

È necessario sottolineare che questi sistemi si trovano in una fase preliminare di progettazione, pertanto, possono essere soggetti a modifiche e miglioramenti sulla base dei risultati ottenuti nell'ambito delle valutazioni riguardanti la sicurezza.

Il primo DHR è pronto a funzionare dopo lo scram del reattore, in caso di indisponibilità del normale percorso di intervento dei dispositivi di sicurezza. La logica di azionamento garantisce prima il funzionamento del DHR1, successivamente l'intervento del DHR2 in caso di guasto del primo sistema. Il numero totale dei sistemi chiamati ad operare non deve mai superare le tre unità, al fine di evitare un eccessivo raffreddamento del refrigerante primario.

Ciascuno dei quattro IC è costituito da (Fig. 5):

- scambiatore di calore con fascio tubiero verticale e collettori inferiore e superiore orizzontali,

- piscina, riempita con acqua, in cui è immerso l'IC (la quantità di acqua contenuta nella piscina è sufficiente per garantire 3 giorni di funzionamento),
- valvola di isolamento del condensato (questa funzione deve essere eseguita da almeno due valvole parallele per eliminare problemi di guasti singoli),
- serbatoio di stoccaggio per l'acqua posto all'uscita della valvola di isolamento.

La linea di uscita del collettore caldo del SG viene collegata con l'IC, mentre la linea inferiore dell'IC è connessa alla linea principale di alimentazione dell'acqua dello SG. Come già detto, questa connessione comprende una valvola di isolamento del condensato ed un serbatoio (volume di 4,5 m^3) che mantiene l'acqua alla temperatura di ingresso dell'acqua di alimento del SG.

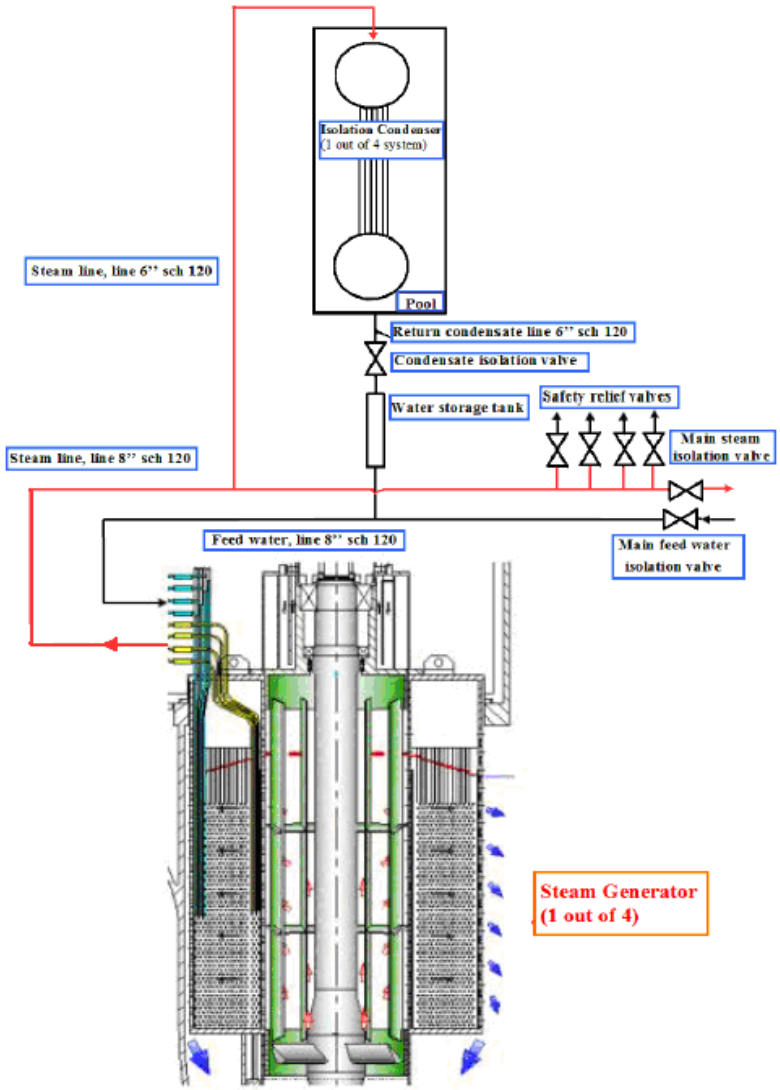

Figura 5. - Schema di funzionamento del sistema IC.

A seguito del segnale di scram del reattore, la valvola di isolamento del condensato, che si trova sulla linea di ritorno della condensa dell'IC, connette tale linea con quella di alimentazione del SG. Il serbatoio che si trova a valle della valvola si riempie di acqua mantenuta alla temperatura dell'acqua di alimento del SG. La funzione di questo serbatoio è di minimizzare il transitorio termico nel generatore di vapore, quando il sistema è chiamato ad operare.

Il vapore prodotto viene inviato ai sistemi di sfiato rilasciando il vapore in atmosfera (opzione ancora da esaminare).

1.3 L'impianto dimostrativo ALFRED

Nell'ambito del Framework Programme VII dell'Unione Europea riguardante il progetto LEADER (Lead-cooler European Advanced Demonstrator Reactor) si sta sviluppando una attività di ricerca riguardante l'impianto nucleare dimostrativo ALFRED (reattore di 300 di MW_{th} raffreddato a piombo).

Molte delle scelte progettuali saranno basate sull'impianto ELFR, descritto nei paragrafi precedenti, con alcune differenze che verranno sinteticamente descritte di seguito.

La configurazione che si pensa di impiegare per il core è composta da 171 elementi esagonali inscatolati, ciascuno elemento può alloggiate 127 barrette di combustibile (pellet forate), 12 barre di controllo (CR) e 4 barre di sicurezza (SR). Al fine di migliorare la circolazione naturale, l'altezza attiva è più bassa rispetto a quella prevista per l'impianto ELFR.

Per quanto riguarda gli scambiatori di calore, si pensa di adottare fasci di tubi a baionetta immersi nella piscina del RV.

Lo scambiatore è costituito da tre cilindri coassiali come mostrato in Fig. 6 e la regione anulare esterna contiene un gas inerte (elio). Il piombo entra dall'alto nella regione anulare del RV e lambisce la superfice esterna dello scambiatore, trasferendo la potenza, precedentemente asportata dal core, all'elio e poi all'acqua che risale controcorrente nella shell cilindrica intermedia.

L'acqua entra dall'alto, fluisce attraverso il guscio cilindrico interno e, in basso, risale, fluendo attraverso il gap anulare che viene a formarsi fra il guscio cilindrico più interno e quello più esterno in cui si trova l'elio. Il gap riempito di elio garantisce il monitoraggio di eventuali perdite nel circuito dovuto ad rotture dei tubi e separa fisicamente il fluido primario e secondario, costituendo anche una via di scarico in caso di rottura del tubo esterno o del tubo intermedio.

Tra le scelte progettuali, ancora in studio, vi è l'opzione di saldare nella superficie interna del guscio cilindrico intermedio, in cui risale l'acqua, una spirale metallica che, forzando il fluido a ruotare, induce una componente trasversale che, sovrapponendosi a quella assiale, aumenta la risultante della velocità e produce un moto elicoidale. Ne segue che il moto risulta simile a quello che si ha all'interno di un condotto elicoidale, con una sezione che, in prima approssimazione, è rettangolare. In più, la spira elicoidale ha

l'effetto di indurre una certa rugosità, influenzando la distribuzione di velocità, il livello di turbolenza e l'attrito alla parete.

In Tabella 2 viene mostrato il confronto tra le opzioni progettuali adottate nel reattore ELFR e quelle previste nell'impianto dimostrativo ALFRED.

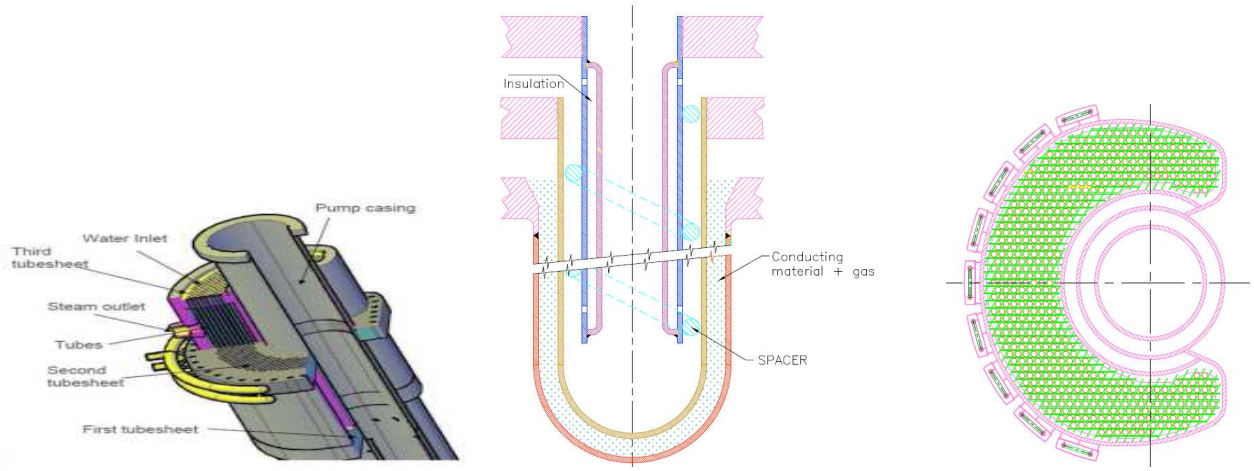

(a) (b) (c)

Figura 6. - Schema dello scambiatore di calore di tipo a baionetta che si pensa di utilizzare nell'impianto dimostrativo ALFRED.

Tabella 2. Confronto tra le opzioni progettuali adottate nel reattore ELFR e quelle previste nell'impianto dimostrativo ALFRED.

Items	ALFRED Options	LFR Options
Fuel Clad Material	T91 (coated)	T91 (coated)
Maximum Clad Neutron Damage (dpa)	100	100
Maximum Clad Temperature in Normal Operation (°C)	550	550
Maximum core pressure drop (MPa)	0.1 (30 min grace time for ULOF)	0.1
Control/Shutdown System	2 diverse and redundant systems of the same concept derived from CDT	2 diverse and redundant systems of the same concept derived from CDT
1st System for Shutdown	Pneumatic Inserted Absorber Rods: shutdown system passively inserted by pneumatic (by depressurization) from the top of core	Pneumatic Inserted Absorber Rods: shutdown system passively inserted by pneumatic (by depressurization) from the top of core.
2nd System for Shutdown	Buoyancy Absorbers Rods: control/shutdown system passively inserted by buoyancy from the bottom of the core.	Buoyancy Absorbers Rods: control/shutdown system passively inserted by buoyancy from the bottom of the core.
Refuelling System	No refuelling machine stored inside the Reactor Vessel	No refuelling machine stored inside the Reactor Vessel
DHR System	2 diverse and redundant systems (actively actuated, Passively operated)	2 diverse and redundant systems (actively actuated, Passively operated)
DHR1	Options are under investigation (Isolation Condenser connected to the Steam Generator: 4 units provided on 4 out of 8 SGs 1 out 4 redundancy)	Alternate solution to ELSY DHR should be exploited
DHR2	Isolation Condenser connected to the other 4 Steam Generator (1 out 4 redundancy)	Isolation Condenser connected to the Steam Generator: 4 units provided on 4 out of 8 SGs
Seismic Dumping Devices	2D isolator below reactor building	2D isolator below reactor building

CAPITOLO 2

MODELLI DEL CODICE DI CALCOLO RALAP5/mod3.2.β UTILIZZABILI PER LA SIMULAZIONE DI FENOMENOLOGIE TERMOFLUIDODINAMICHE CARATTERISTICHE DELL'IMPIANTO ELFR

2.1 Il codice RELAP5/MOD3

Come è noto, il codice di calcolo RELAP5/MOD3 [3] è stato sviluppato per effettuare analisi termoidrauliche *best-estimate*, inizialmente limitate a reattori nucleari ad acqua leggera, durante condizioni operative normali e nel corso di situazioni incidentali. Esso consente, tuttavia, di simulare un'ampia varietà di sistemi termoidraulici, sia nucleari che convenzionali.

Tale codice incorpora un modello idrodinamico monodimensionale atto a descrivere fenomenologie transitorie riguardanti miscele acqua–vapore, nelle quali inoltre è possibile contemplare la presenza di componenti non condensabili nella fase vapore, nonché solubili nella fase liquida. I vari modelli e le varie funzioni di supporto sono oggetto di *subroutines* separate.

La modellazione di un sistema termoidraulico è essenzialmente basata sulla sua nodalizzazione mediante l'utilizzo di componenti propri del codice, che comprendono sia volumi idraulici (quali pipe, branch, annulus) che giunzioni (singole, multiple o tempo-dipendenti) oppure valvole, pompe, etc., in grado di simulare gli effettivi componenti del circuito.

Per ciascun nodo, il codice risolve otto equazioni di bilancio alle derivate parziali (conservazione della massa e dell'energia nei volumi, conservazione del momento nelle giunzioni, nonché per entrambe le fasi due equazioni di trasporto riferite all'incondensabile ed al soluto eventualmente presenti) in cui è possibile utilizzare sia un modello omogeneo di equilibrio del processo di flusso bifase, sia un modello non-omogeneo di non-equilibrio per la fase liquida e per la fase vapore. I fenomeni che dipendono da gradienti in direzione trasversale, rispetto a quella di efflusso, utilizzano per l'attrito e lo scambio termico modelli costitutivi basati su correlazioni semi-empiriche. Il sistema delle equazioni, mediato sui volumi di competenza e discretizzato alle differenze finite, viene risolto tramite un efficiente schema numerico parzialmente implicito, che permette calcoli abbastanza veloci di transitori termofluidodinamici.

Le proprietà scalari del fluido, come la pressione, l'energia, la densità e la frazione di vuoto sono rappresentate dallo stato medio del fluido e sono calcolate al centro del volume di controllo. Le proprietà vettoriali del fluido, come le velocità, sono invece calcolate nelle giunzioni tra un volume e l'altro e sono associate con il flusso di massa ed energia tra i volumi di controllo.

I percorsi dei flussi di calore sono descritti da un modello monodimensionale rappresentato dalla struttura termica connessa con i volumi di controllo idrodinamici per simulare le pareti delle tubature, gli elementi riscaldanti, le barrette di combustibile nucleare e le superfici degli scambiatori di calore.

2.1.1 Modelli Costitutivi

Per descrivere il comportamento dei volumi che costituiscono il sistema termoidraulico vengono impiegati modelli costitutivi. La procedura consiste nel determinare il regime di moto e successivamente nell'identificare le leggi costitutive più adatte, all'interno di un insieme di correlazioni che dipendono dal regime individuato.

Un esempio è il caso di fluido bifase per il quale i modelli costitutivi permettono la valutazione di alcuni parametri necessari per la risoluzione dell'equazione di bilancio, ed in particolare:

- lo scambio termico all'interfaccia e lo scambio termico alla parete,
- l'attrito all'interfaccia e l'attrito alla parete,
- la pressione e la velocità all'interfaccia.

Il termine di attrito all'interfaccia è valutato dalla differenza tra le velocità delle due fasi e da un fattore di attrito determinato sulla base di diverse correlazioni in funzione del regime di moto. Il modello di attrito alla parete si basa sull'approccio proposto da Chisolm, facente uso di un moltiplicatore bifase, calcolato ricorrendo alla correlazione Heat Transfer and Fluid Flow Service (HTFS) [4].

2.1.2 Modelli di scambio termico

Lo scambio termico viene valutato come scambio termico tra ciascuna delle due fasi e l'interfaccia, che contempla il trasporto di calore nella massa dovuto alla differenza tra la temperatura all'interfaccia e la temperatura media della fase, e lo scambio termico alla parete schematizzata mediante strutture termiche connesse ai volumi idrodinamici.

Le possibilità di simulazione sono ampie e comprendono barrette di combustibile, riscaldatori in geometria piana o cilindrica, trasmissione del calore attraverso i tubi del generatore di vapore e dalle pareti del vessel. Le conducibilità termiche e le capacità termiche volumetriche, dipendenti dalla temperatura, sono fornite da tabelle e funzioni. Per la soluzione della conduzione di calore si usa una tecnica alle differenze finite in cui ciascun intervallo di *mesh* può avere una spaziatura diversa ed un materiale diverso. La dipendenza dal tempo della sorgente di calore interna, può essere ottenuta dal modello di cinetica del reattore, da tabelle che danno la potenza in funzione del tempo o da una variabile di controllo. Sono permesse condizioni iniziali di simmetria o di parete isolata e tabelle di temperatura superficiale, flusso di calore, coefficiente di trasmissione termica, in funzione del tempo.

Il codice fa uso di una curva di ebollizione per la valutazione dei regimi di scambio termico (pre-CHF, post-CHF e condensazione). Per quanto riguarda i regimi in pre-CHF, vengono presi in esame il regime liquido

monofase, ebollizione nucleata sottoraffreddata e satura. I regimi di post-CHF comprendono la regione *Transition Boiling*, *Film Boiling* e convezione con solo vapore.

Quindi, in relazione alla soluzione termica, il codice permette di simulare il trasferimento di calore tra fluido e superfici solide, prendendo in considerazione tutti i processi di trasferimento del calore, cioè:

- convenzione naturale e forzata con liquido sia in regime laminare che turbolento;
- convenzione naturale e forzata con gas sia in regime laminare che turbolento;
- ebollizione nucleata sotto-raffreddata e saturata con criterio di previsione del fenomeno di DNB (Departure from Nucleate Boiling) e della generazione di vapore;
- flusso termico critico (CHF);
- criterio di previsione del fenomeno di dry-out;
- temperatura di ribagnamento (rewetting temperature);
- ebollizione a film per moti anulari inversi;
- condensazione a film, anche in presenza di gas non condensabili.

2.2 Descrizione del modello idrodinamico adottato dal codice RELAP5/MOD3.2

In questa versione del codice sono stati aggiunti nuovi modelli e delle semplificazioni d'uso per l'utilizzatore.

I nuovi modelli includono:

- correlazione di Bankoff per il counter-current flow limiting (CCFL);
- componente ECCMIX utilizzato per schematizzare il mescolamento del liquido sottoraffredato di alimentazione dei sistemi di refrigerazione di emergenza del core ECCS (Emergy Core Cooling System) e il conseguente fenomeno di condensazione all'interfaccia;
- modello per la reazione Zirconio-acqua per descrivere la produzione di energia esotermica sulla superficie dell'incamiciatura delle barrette ad alta temperatura;
- modello per lo scambio termico per irraggiamento tra superficie e superficie con diverse geometrie definibili dall'utilizzatore nell'input;
- modello di rilevamento del livello;
- modello per la stratificazione termica.

2.3 Modifiche apportate al codice RELAP5/mod3.2β per la simulazione di sistemi con tecnologia LFR

Le modifiche, apportate presso l'Ansaldo–Divisione Nucleare di Genova, hanno interessato sia le sezioni del codice concernenti il dimensionamento e l'inizializzazione dei parametri, sia quelle più direttamente dedicate al calcolo delle proprietà fisiche e termodinamiche dei fluidi [5, 6].

Per quanto riguarda il primo aspetto, sono stati ridimensionati e nuovamente inizializzati alcuni parametri di lavoro necessari per consentire la predisposizione del codice a riconoscere e a processare fluidi diversi

rispetto a quelli considerati nella versione originale; in particolare, nella subroutine di inizializzazione, sono state fatte le assegnazioni di stringa necessarie per il riconoscimento e l'indirizzamento dei modelli verso le tabelle contenenti le proprietà termodinamiche dei nuovi fluidi, mentre in una successiva subroutine sono state inserite le istruzioni necessarie per la loro effettiva utilizzazione.

Per quanto riguarda le modifiche introdotte per il calcolo delle proprietà fisiche del Pb e del Pb-Bi, esse hanno interessato le subroutine di indirizzamento alla sezione relativa alla nuova tipologia di fluidi. Sono state, poi, introdotte apposite correlazioni rispettivamente per la conducibilità termica, la tensione superficiale e la viscosità dei suddetti fluidi.

Le modifiche del codice, effettuate dal nostro gruppo di ricerca dell'ex Dipartimento di Ingegneria Nucleare, attuale Dipartimento DEIM (Dipartimento di Energia, Ingegneria dell'informazione, e Modelli Matematici), dell'Università di Palermo, hanno riguardato l'introduzione di un pacchetto di nuove procedure adatte alla valutazione dello scambio di calore e delle perdite di carico in tubi elicoidali verticali ed orizzontali, sia in condizione monofase che bifase, e lo scambio termico all'interno di fasci di barre refrigerate con il piombo.

Per quanto riguarda lo scambio termico, il codice RELAP5 contiene diversi pacchetti relativi al trasferimento del calore tra la superficie di una parete ed un fluido confinante (o viceversa). Essi consentono di studiare le fenomenologie di scambio termico in convezione forzata, per ebollizione nucleata, ebollizione a film, condensazione etc.

La maggior parte delle costruzioni logiche necessarie per la selezione dell'opportuno pacchetto da utilizzare nei calcoli di scambio termico, sulla base delle condizioni termofluidodinamiche riscontrate nel sistema in esame, viene effettuata nella subroutine HTRC1, in cui i coefficienti di scambio termico sono determinati mediante l'uso di una delle seguenti cinque *subroutines*: DITTUS, PREDNB, PREBUN, PSTDNB, e CONDEN.

Per quanto riguarda la subroutine DITTUS, essa viene utilizzata per il calcolo dei coefficienti di scambio termico in convezione forzata per deflussi monofase o per miscele gas-liquido o vapore-liquido e contiene correlazioni per il regime laminare, il regime turbolento e la convezione naturale.

In Figura 7 viene riportato il diagramma di flusso utilizzato per l'applicazione dei vari modelli di scambio termico contenuti nel pacchetto relativo al trasferimento di calore alla parete.

Le procedure implementate nel codice hanno riguardato anche il pacchetto relativo alla lettura e memorizzazione dei dati geometrici dell'elica (diametro ed inclinazione) necessari per la formulazione dell'input. Ciò al fine di rendere disponibile all'utente una nuova *flag* per l'applicazione del pacchetto valido per la geometria elicoidale, qualora fosse necessario.

La modifica ha riguardato la subroutine RPIPE in cui vengono processati sia i dati geometri del componente pipe o annulus, sia le opzioni contenute nelle *flags* indicate come jefvcahs, utilizzate nelle carte CCC1101÷CCC1199. Il digit corrispondente alle flag j (non utilizzato dal codice) viene adesso correlato all'opzione di uso o no del nuovo pacchetto sui tubi elicoidali (j = 1: il pacchetto viene utilizzato, j = 0 o non specificato: il pacchetto non viene utilizzato).

Inoltre, poiché le carte relative alla descrizione geometrica del componente pipe non prevedono l'inserimento del diametro dell'elica, necessario per l'applicazione dei modelli di scambio termico e delle perdite di carico contenute nel nuovo pacchetto, si è provveduto ad utilizzare la prima parola (W1) delle carte CCC1401÷CCC1499, in cui è possibile specificare il diametro idraulico della giunzione del condotto. Nella nuova versione, quando si verifica la condizione j = 1 in fase di processamento dei dati di input (effettuata solo una volta e all'inizio del calcolo), il diametro idraulico viene posto uguale al diametro valutato dall'area della sezione del volume inserita dall'utente nella prima parola (W1) delle carte CCC0101÷CCC0199, mentre il diametro dell'elica viene posto uguale al valore inserito nelle carte CCC1401÷CCC1499.

Queste modifiche consentono, ad esempio, di schematizzare in modo dettagliato un fascio tubiero di tipo elicoidale concentrico, che altrimenti dovrebbe essere rappresentato ricorrendo ad un unico volume equivalente.

Per quanto riguarda il calcolo del coefficiente dello scambio termico, nella DITTUS, quando j = 1 e il deflusso è monofase, viene chiamata una ulteriore subroutine, denominata HTCOIL, che valuta alcuni parametri fisici del fluido alla temperatura di parete, necessari per la valutazione della correlazione del numero di Nusselt riportata nell'Eq. (1) (vedi paragrafo 2.3.1).

Si noti che, la versione del codice cos' modificata consente di trattare solo lo scambio termico in ebollizione nucleata. Successivi lavori hanno riguardato i regimi di scambio termico dryout e post-dryout su cui sono in fase di svolgimento i lavori di validazione.

Per quanto riguarda le perdite di carico, il codice utilizza alcune procedure contenute nella subroutine FWDRAG, dove i coefficienti di perdita per le due fasi (vapore e liquido) vengono valutati sulla base di correlazioni valide per flussi in regime laminare o turbolento. Tali coefficienti vengono poi impiegati nel pacchetto relativo alla soluzione della equazione della quantità di moto.

Nella nuova versione del codice, in FWDRAG, quando si richiede l'applicazione del pacchetto relativo alla geometria elicoidale in deflusso monofase o bifase, si procede con la valutazione del coefficiente di attrito di Fanning sulla base delle correlazioni di Ito o di Xin, come descritto nei successivi paragrafi.

E' da notare che nel caso di deflusso monofase le correlazioni utilizzate approssimano molto bene i dati sperimentali anche per numeri di Reynolds al di fuori del campo di validità dichiarato dagli autori. Tuttavia, nella regione di transizione dal regime laminare a quello turbolento, la discontinuità del modello può portare a errori di valutazione non trascurabili.

Per tenere in considerazione questo aspetto, nella subroutine FWDRAG, quando si procede con l'applicazione delle correlazioni valide per deflusso monofase, si è fatto ricorso ad una procedura di interpolazione che in prima approssimazione consente di eliminare la discontinuità nella regione di transizione.

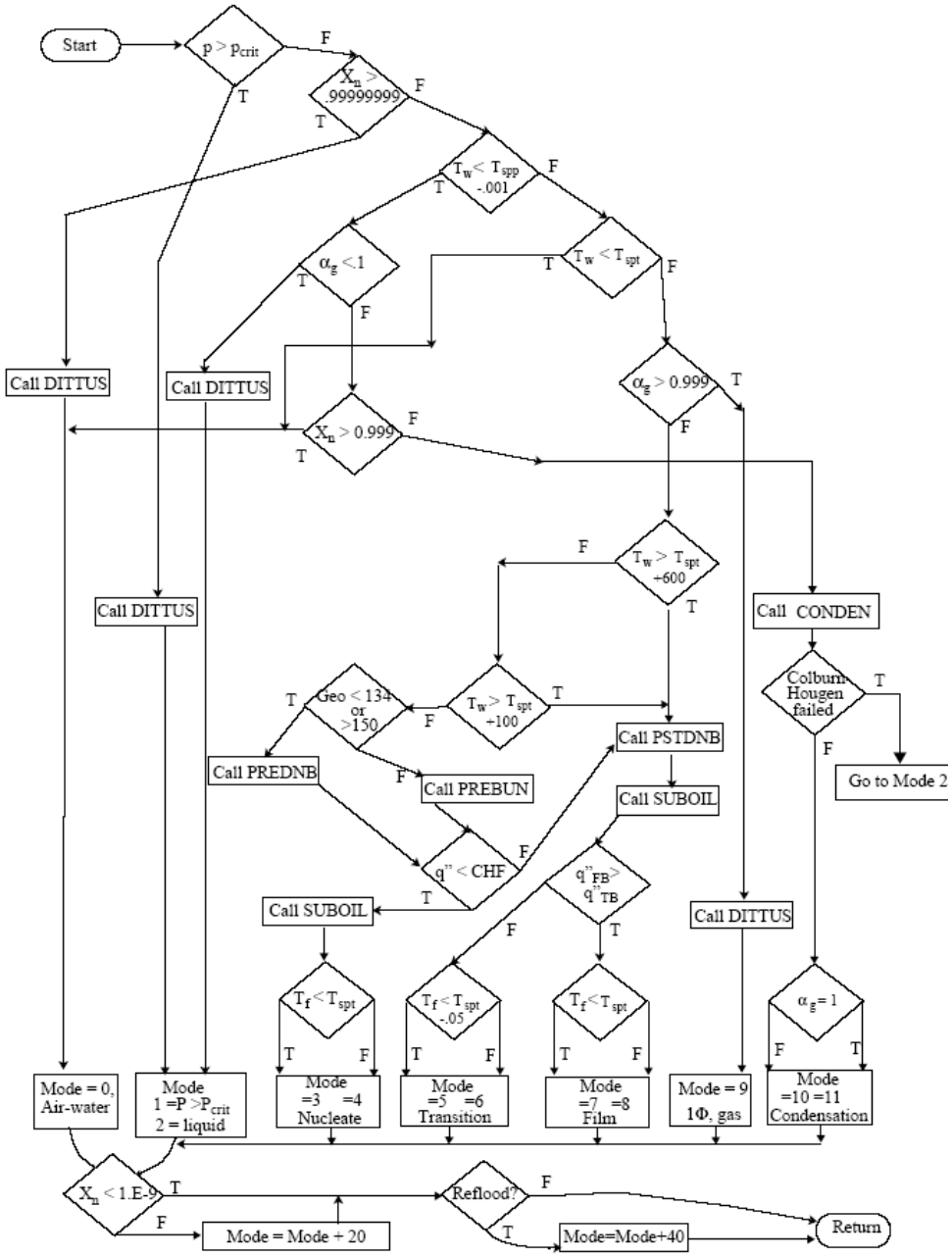

Figura 7. - Diagramma di flusso del pacchetto di trasferimento di calore alla parete utilizzato dal codice RELAP5.

Ciò ha consentito di migliorare le prestazioni del codice nella simulazione delle perdite di calcolo per un ampio intervallo del valore della portata del fluido e quindi del numero di Reynolds.

Relativamente alle perdite di carico in deflusso bifase, il codice RELAP5 ricorre ai modelli basati sui moltiplicatori bifase di Lockart-Martinelli.

Per il pacchetto elicoidale, invece, sono state utilizzate le correlazioni Lockart-Martinelli modificate da Xin et Al.. Queste correlazioni sono valide sia per tubi elicoidali verticali che orizzontali per cui viene esteso il campo di applicabilità del codice modificato a condizioni operative e geometrie differenti.

2.3.1 Simulazione dello scambio termico e perdite di carico in tubi elicoidali interessati da deflusso monofase

Nell'ambito degli studi dello scambio termico e delle perdite di carico in tubi elicoidali, sono state svolte svariate attività di ricerca riguardanti l'uso del codice di calcolo termoidraulico avanzato RELAP5/mod3.2.β, opportunamente modificato per l'analisi di transitori operativi ed incidentali in reattori nucleari di tipo ADS (Accelerator Driven System), come ad esempio l'impianto LBE-XADS (LBE-eXperimental Accelerator Driven System) e l'impianto EFIT (European Facility for Industrial Transmutation), facility europea per la realizzazione della trasmutazione su scala industriale.

Varie attività sperimentali sono state svolte a supporto di questi impianti con lo scopo di investigare il comportamento termoidraulico dei componenti, e tra queste quelle realizzate nell'impianto sperimentale MEGAPIE (MEGAwatt Pilot Experiment) [7] condotte nell'ambito di una collaborazione fra centri di ricerca europei e giapponesi. Le molte campagne sperimentali hanno riguardato anche lo studio delle capacità di scambio termico dello scambiatore THX (Target Heat eXchanger), realizzato presso il Paul Scherrer Institute (PSI) in Svizzera con la finalità di dimostrare la fattibilità di produrre una sorgente di neutroni di elevata energia da impiegare in vari settori della ricerca, ed in particolare, per il bruciamento dei rifiuti radioattivi. Questo sistema è costituito da un assemblaggio di dodici cooling pins a baionatta inseriti all'interno di dodici canali nel lato primario per asportare la potenza prodotta nel processo di spallazione e mantenere il bersaglio al disotto delle temperature limiti imposte. Per migliorare le prestazioni di scambio termico di ogni unità, è stato saldato nel lato secondario dello scambiatore di calore un filamento metallico elicoidale, in modo da creare un percorso del flusso anulare a spirale intorno al diametro del pin (Fig. 8).

Nel corso di una collaborazione tra il nostro gruppo di ricerca e l'ENEA di Bologna sono state svolte diverse attività di validazione della versione del codice RELAP/Mod3.2β modificato rispetto alla sua capacità di simulare alcuni aspetti della termofluidodinamica dei metalli liquidi [8-10]. Per far ciò ci si è serviti di una serie di test eseguiti presso il centro di ricerca ENEA di Brasiamone, effettuati facendo uso di una configurazione dell'impianto CHEOPE (CHEmical OPErational transient), che ha consentito di simulare il comportamento di uno dei 12 elementi di scambio termico a baionetta previsti per MEGAPIE [11].

Per lo studio dello scambio termico si è pensato di utilizzare fra le correlazioni disponibili in letteratura quella di Gnielinski [12], unitamente alle espressioni per il calcolo del coefficiente di attrito proposte da Ito [13].

La correlazione di Gnielinski, dapprima ottenuta per tubi dritti, è stata successivamente estesa a tubi curvi. L'espressione è:

$$Nu = \frac{(f_c/2)\,\mathrm{Re}\,\mathrm{Pr}}{1+12.7\sqrt{f_c/2}\left(\mathrm{Pr}^{2/3}-1\right)}\left(\frac{\mathrm{Pr}}{\mathrm{Pr}_w}\right)^{0.14} \qquad (1)$$

dove Nu, Re e Pr sono, nell'ordine, i numeri di Nusselt, Reynolds e Prandtl; Pr_w è il numero di Pr valutato alla temperature di parete, ed, infine, f_c è il fattore d'attrito di Fanning valutato secondo le seguenti correlazioni:

$$f_c = \frac{16}{\mathrm{Re}} \qquad \mathrm{Re} < 13.5(\mathrm{D}/\mathrm{d})^{-0.5} \qquad (2)$$

$$f_c = \frac{344(\mathrm{D}/\mathrm{d})^{-0.5}}{\left\{1.56+\log_{10}\left[\mathrm{Re}(\mathrm{D}/\mathrm{d})^{-0.5}\right]\right\}^{5.73}} \qquad 13.5(D/d)0.5<Re<2000[1+13.2(D/d)-0.6] \qquad (3)$$

$$f_c = 0.076\,\mathrm{Re}^{-0.25} + 0.0075\cdot\left(\frac{\mathrm{D}}{\mathrm{d}}\right)^{-0.5} \qquad \mathrm{Re} > 1500 \qquad (4)$$

essendo d il diametro del tubo e D il diametro dell'elica.

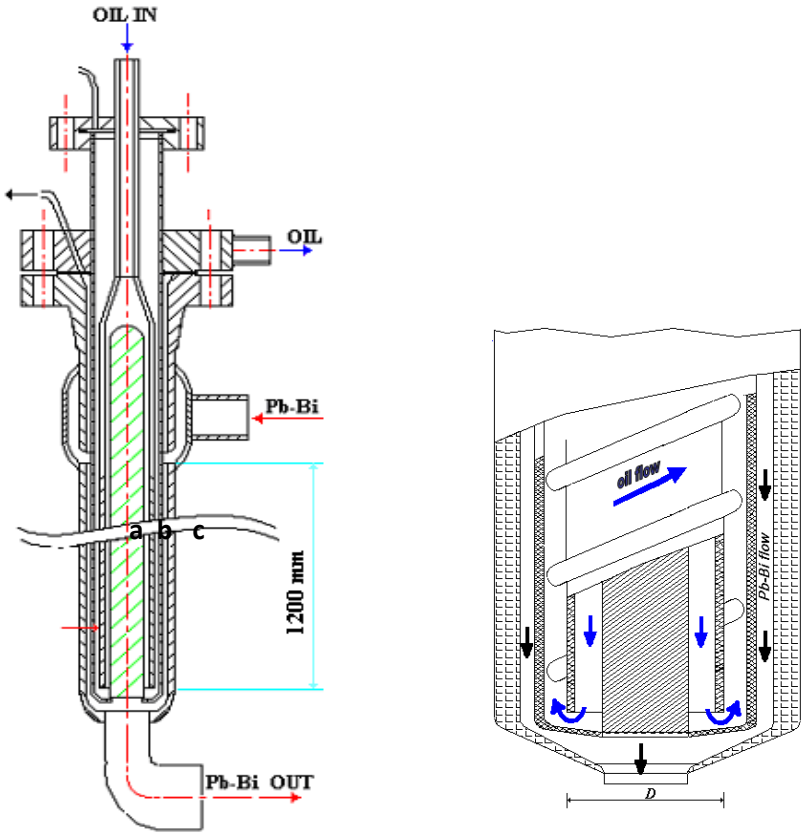

Figura 8. - Schema del Cooling pin dell'impianto sperimentale CHEOPE

Il codice è stato utilizzato per la simulazione dei dati sperimentali riguardanti gli elementi di scambio termico utilizzati negli impianti sperimentali CHEOPE e MEGAPIE e ciò ha comportato un lavoro volto all'adattamento dei modelli di scambio termico, validi per tubi elicoidali, alla geometria presa in esame, come descritto in [14]. In particolare, le ipotesi assunte per l'applicazione dell'eq. (1) sono state supportate anche dal confronto con i risultati ottenuti dal CRS4 Institution [15] utilizzando il codice 3Dym STAR-CD.
I risultati ottenuti nell'ambito del lavoro di validazione in termini di scambio termico e perdite di carico in condotti elicoidali per varie geometrie e condizioni operative hanno consentito di mostrare le buone capacità del codice nella simulazione delle fenomenologie termofluidodinamiche coinvolte sia per i casi con impiego di tubi a baionatta, come descritto prima, sia per i casi in cui si utilizzano scambiatori nucleari elicoidali [16-19].

2.3.2 Simulazione delle perdite di carico e dello scambio termico in tubi elicoidali interessati da deflussi bifase

Per la valutazione delle perdite di carico in deflusso bifase, il metodo di calcolo impiegato nella maggior parte delle procedure in uso è basato sulle correlazioni di Lockhart-Martinelli che fanno ricorso al parametro di similitudine χ^2, definito come il rapporto tra i gradienti di pressione del liquido e del gas che si stabilirebbero se le due fasi fluissero da sole nel condotto, e che consente di trovare la relazione tra le perdite di carico bifase e quelle monofase:

$$\chi^2 = \frac{\phi_G^2}{\phi_L^2} = \frac{\left(\frac{dP}{dz}\right)_{L,f}}{\left(\frac{dP}{dz}\right)_{G,f}} \qquad (5)$$

dove per tubi dritti in geometria cilindrica si ha:

$$\phi_L^2 = 1 + \frac{C}{\chi} + \frac{1}{\chi^2} \qquad (6)$$

$$\phi_G^2 = 1 + C\chi + \chi^2 \qquad (7)$$

Alcuni lavori sul tema reperibili in letteratura hanno messo in evidenza che la maggior parte dei dati sperimentali riguardanti i tubi elicoidali possono essere interpretati in modo soddisfacente utilizzando le correlazioni Lockhart-Martinelli opportunamente modificate. In questo ambito, Xin et al. [20, 21], utilizzando i loro studi sperimenti realizzanti con condotti elicoidali aventi geometria caratterizzata da rapporti D/d (diametro elica/diametro tubo) nell'intervallo 26÷50 ed elica orizzontale ed verticale, hanno individuato la seguente correlazione per il moltiplicatore bifase della fase liquida, ϕ_L:

$$\phi_L = [1 + K \quad \chi \quad F_d{}^n](1 + \frac{20}{\chi} + \frac{1}{\chi^2})^{1/2} \tag{8}$$

dove

$$F_d = Fr_L \left(\frac{d}{D}\right)^{1/2} (1 + \tan\beta)^{0.2} \tag{9}$$

con Fr_L il numero di Froude valutato per la fase liquida.

I valori consigliati per le costanti che compaiono nella Eq. (8) sono riportati in Tabella 3.

Tabella 3 - Valori dei parametri costanti in Eq. (9)

Fd	< 1	> 1
K	0.01528	0.0023
n	-0.6	-1.7

Sulla base delle equazioni sopra riportate si ottiene la seguente relazione:

$$\frac{\phi_G^2}{\phi_L^2} = \frac{\left(\frac{dP}{dz}\right)_{G,f}}{\left(\frac{dP}{dz}\right)_{L,f}} = \frac{1 + C\chi + \chi^2}{[1 + K \quad \chi \quad F_d{}^n]^2 (1 + \frac{C}{\chi} + \frac{1}{\chi^2})} = \frac{\chi^2}{[1 + K \quad \chi \quad F_d{}^n]^2} \tag{10}$$

Le modifiche del codice RELAP5 hanno riguardato l'introduzione di un pacchetto di nuove procedure adatte alla valutazione delle perdite di carico in tubi elicoidali interessati da deflusso bifase sulla base delle correlazioni di Lockhart-Martinelli, modificate secondo le eq.s (8)-(10). Si noti che il codice è stato modificato anche per lo studio delle geometrie riguardanti l'elica orizzontale sempre sulla base degli studi condotti da Xin che, per questa geometria, consiglia di utilizzare nell'eq. (6) C=10.25.

Utilizzando il codice modificato, sono stati svolti vari lavori di validazione riguardanti diversi condizioni operative e geometria dell'elica come descritto in [22-24].

Per quanto riguarda lo studio del processo di scambio termico di un fluido bollente in convezione forzata, il codice usa le correlazioni di Chen [25] che, sulla base del principio di sovrapposizione degli effetti, determina il coefficiente di scambio termico convettivo bifase come somma di due componenti: il coefficiente di scambio termico legato alla sola convezione monofase h_{mac} (coefficiente di scambio termico macroscopico) e quello legato invece alla sola ebollizione nucleata, h_{mic} (coefficiente di scambio termico microscopico):

$$h_{TP} = h_{mac} F + h_{mic} S \qquad \text{con} \quad F > 1 \quad \text{e} \quad S < 1 \tag{11}$$

Nell' eq. (11), Chen sceglie per il calcolato del termine h_{mic} la correlazione di Forster-Zuber (1955) valida per l'ebollizione nucleata.

Esplicitando i vari termini, si ottiene la seguente relazione:

$$h_{TP} = \left(\frac{k}{d}\right) 0.023\, Re_L^{0.85}\, Pr_L^{0.4}\, F + 0.00122\ \Omega\ \Delta T_w^{0.24} \Delta P_{sat}^{0.75} S \tag{13}$$

con

$$\begin{cases} F = \begin{cases} 1 & \chi_{tt}^{-1} \le 0.1 \\ 2.35\left(\chi_{tt}^{-1} + 0.213\right)^{0.736} & \chi_{tt}^{-1} > 0.1 \end{cases} \\ \Omega = \left(\dfrac{k_L^{0.79} c_{pL}^{0.45} \rho_L^{0.49} g_c^{0.25}}{\sigma^{0.5} \mu_L^{0.29} h_{LG}^{0.24} \rho_G^{0.24}} \right) \\ S = \dfrac{1}{1 + 2.5310^{-6} \left(F^{1.25}\, Re_L\right)^{1.17}} \end{cases} \tag{14}$$

Successivi studi condotti da Seban e Mclaughlin riguardanti i tubi elicoidali [26] hanno comportato la modifica dell' equazione (13) come segue:

$$h_{TP} = \left(\frac{k}{d}\right) (1-x)^{0.8}\, 0.023\, Re_L^{0.85}\, Pr_L^{0.4} \left(\frac{d}{D}\right)^{0.1} F + 0.00122\, \Omega\, \Delta T_{sat}^{0.24} \Delta P_{sat}^{0.75} S \tag{15}$$

con

$$F = 2.35\left(\chi_{tt}^{-1} + 0.213\right)^{0.736} \tag{16}$$

$$S = \begin{cases} \left(1 + 0.12\, Re_{tp}\right)^{-1.14} & Re_{tp} < 32.5 \\ \left(1 + 0.42\, Re_{tp}^{0.48}\right)^{-1} & 32.5 \le Re_{tp} < 70 \\ 0.0797 & Re_{tp} > 70 \end{cases} \tag{17}$$

$$Re_{tp} = 10^{-4} \frac{G_L d}{\mu_L} F^{1.25} \tag{18}$$

La nuova procedura prevede che, per le modalità di trasferimento di calore che comportano lo scambio termico monofase (mode 2), il codice procede con il calcolo delle correlazioni di Gnielinski descritte in precedenza; invece in condizione di ebollizione nucleata e per film, quando la subroutine PSTDNB chiama la subroutine DITTUS, il codice procede con la valutazione delle Eq.s 15÷18.

Inoltre, per la modalità di scambio mode 9 (convezione monofase vapore o convezione bifase supercritica) e per condizioni di scambio termico mode 2 che prevedono α_g> 0.1si procede con il calcolo della correlazione di Mori and Nakayama [27] valida per tubi elicoidali, secondo le seguenti espressioni:

$$h = \begin{cases} \dfrac{1}{26.2}\left(\dfrac{k_G}{d}\right)\dfrac{Pr_G}{\left(Pr_G^{\,2/3}-0.074\right)}Re_G^{\,4/5}\left(\dfrac{d}{D}\right)^{1/10}\left\{1+\dfrac{0.098}{\left[(Re_G)(d/D)^2\right]^{1/5}}\right\} & \text{per il gas} \quad (19) \\ \dfrac{1}{41.0}\left(\dfrac{k_L}{d}\right)Pr_L^{5/6}\,Re_L^{\,4/5}\left(\dfrac{d}{D}\right)^{1/12}\left\{1+\dfrac{0.061}{\left[(Re_L)(d/D)^{2.5}\right]^{1/6}}\right\} & \text{per il liquido} \quad (20) \end{cases}$$

Il lavoro di validazione riguardante queste ultime modifiche saranno oggetto di future attività di ricerca volte alla verifica dell'applicabilità del codice per varie condizioni operative e geometrie.

2.3.3 Scambio termico per l'analisi di circuiti refrigerati a piombo liquido

Il codice RELAP5/mod3.2.β nell'ambito dei lavori svolti dai ricercatori dell'Ansaldo, descritti nel paragrafo 2.3, è stato modificato per la simulazione dello scambio termico con i metalli liquidi ricorrendo alla correlazione di Subbotin secondo l'eq. (a3) (vedi Appendice A).

Successivamente, per lo studio dello scambio termico in presenza di un fascio di tubi, il nostro gruppo ha implementato due ulteriori correlazioni eq.s (a14) e (a11), la prima applicata per rapporti P/D nell'intervallo 1<P/D<1.2 e la seconda per rapporti P/D nell'intervalli 1.2<P/D<1.6, per tenere in considerazione che l'eq. (a14), rispetto agli altri modelli e correlazioni riportate in letteratura, non consente di ottenere valutazioni accurate dei dati sperimentali riguardanti rapporti P/D maggiori di circa 1.2, come descritto nel paragrafo B.1 dell'Appendice B.

Tuttavia è da tenere in considerazione che le due correlazioni riguadano geometrie del fascio del tipo quadrato e triangolare, per cui sarebbe opportuno un approfondimento sulla loro applicabilità nel campo di interesse della presente relazione.

CONCLUSIONI

Dato il crescente interesse nei confronti di sistemi nucleari innovativi raffreddati con il piombo liquido e la necessità di indagare la capacità dei codici di sistema utilizzati nel settore nucleare di simulare con una certa accuratezza le fenomenologie termofluidodinamiche coinvolte in questi sistemi, nell'ambito della linea progettuale LP2 del PAR 2012-13 è stato svolto uno studio relativo alle capacità di alcuni dei modelli impiegati nel codice Relap5/mod3.2β di simulare la termoidraulica dell'impianto ELFR, oggetto della presente relazione

Recenti modifiche effettuate dal nostro gruppo di lavoro, in aggiunta alle attività svolte da alcuni ricercatori dell'Ansaldo nucleare, hanno reso questo codice in grado di trattare diverse tipologie di fluido e capace di simulare la termoidraulica di alcuni dei componenti che verranno impiegati negli impianti ELFR ed Alfred.

In particolare, sono stati implementati modelli per lo studio dello scambio termico all'interno di un fascio tubiero attraversato da un refrigerante a metallo liquido e procedure per la simulazione delle perdite di carico e dello scambio termico monofase e bifase dei condotti elicoidali verticali ed orizzontali, di cui si è discusso nel presente rapporto, che potrebbero essere impiegati per la simulazione dei generatori di vapore previsti nell'impianto ELFR. Inoltre, il codice è stato opportunamente modificato e validato per la simulazione degli scambiatori di calore di tipo a baionetta, in cui si pensa di inserire una spirale per agevolare fenomeni di turbolenza e di scambio di calore.

Per le procedure riguardanti lo scambio termico bifase in un condotto elicoidale che coinvolge diversi regimi di moto sono in corso ulteriori lavori di validazione, anche sulla base di eventuali risultati di attività sperimentali condotte presso l'ENEA di Brasimone.

BIBLIOGRAFIA

1. S. Monti, Overview of IAEA activities in support of fast reactors development and deployment & objectives of the meeting, Technical Meeting To Identify Innovative Fast Neutron Systems Development Gaps, IAEA, Vienna, Austria, 29 February 2012 – 02 march 2012.
2. M. Tarantino, L. Cinotti, D. Rozzia, Lead-cooled fast reactor (LFR) development gaps, Technical Meeting To Identify Innovative Fast Neutron Systems Development Gaps, IAEA, Vienna, Austria, 29 February 2012 – 02 march 2012.
3. C. D. Fletcher, R.R. Scuhltz, RELAP5/MOD3 Code manual, NUREG/CR–5535, INEL–95/174, Idaho National Engineering Laboratory, June 1995.
4. K. T. Claxton, J. G. Collier, and J. A. Ward, H.T.F.S. Correlation for Two-Phase Pressure Drop and Void Fraction in Tubes, HTFS Proprietary Report HTFS-DR-28, AERE-R7162, November 1972.
5. R. Lobello, A. Alemberti, Technical report – Relap5 code Modifications for ADS Demonstration Facility Simulation, ADS 1 TRIX 0243, Ansaldo Nucleare, 31/03/2000.
6. P. Meloni, Attività di supporto lo sviluppo di un modello numerico per la simulazione del comportamento termoidraulico di un reattore raffreddato a piombo utilizzando il codice RELAP5, prot. ENEA/2006/71178/FPN-FIS-NUC, 22 ottobre 2007.
7. G. S. Bauer, M. Salvators, G. Heusener, MEGAPIE a 1 MW pilot experiment for a liquid metal spallatio target, Journal of Nuclear Materials, 296 (2001), 17-33.
8. P. Meloni, Heat Transfer Prediction of the THX Exchanger in MEGAPIE Facility by Using RELAP5 Code Suitably Modified to Deal with Helical Channel, FPN-P9EH-010, Centro Ricerche ENEA Bologna, 2007.
9. P. Meloni, Sviluppo di un modello numerico per la simulazione del comportamento termoidraulico di un reattore raffreddato a piombo utilizzando il codice RELAP (Parte I), FPN-P9EH-008, Centro Ricerche ENEA Bologna, 2007.
10. P. Meloni, Sviluppo di un modello numerico per la simulazione del comportamento termoidraulico di un reattore raffreddato a piombo utilizzando il codice RELAP (Parte II), FPN-P9EH-0I2, Centro Ricerche ENEA Bologna, 2008.
11. P. Agostini, Observation resulting from MEGAPIE cooling pin tests in Brasimone, Derivable 22A MEGAPIE – TEST, EU Project No. FIKW-CT-2001- 00159 (PU).
12. V. Gnielinski, Helically coiled tubes of circular cross sections, Hemisphere Publishing Corporation, 1987.
13. H. Ito, Friction factors for turbulent flow in curved pipes, Journal of Basic Engineering, Trans. Amer. Soc. Mech. Engrs., Vol. D81, 1959, pp 123-134.

14. M. Casamirra, F. Castiglia, M. Giardina, P. Meloni, RELAP5 Modification for CHEOPE Simulations, International Conference Nuclear Energy for New Europe 2005, Bled, Slovenia, September 5-8, 2005. ISBN/ISSN: 961-6207-25-3, Editors Borut Mavko,Ivo Kljenak (Slovenia).
15. S. Buono, L. Maciocco, V. Moreau, L. Sorrentino, Optimisation of the pin cooler design for the Megapie Target using full 3D numerical simulations, CRS4-Technical Report DRAFTv1.22.
16. M. Casamirra, F. Castiglia, M. Giardina, C. Lombardo, Modifing RELAP5 code to deal with helical coiled ducts, XXIV Congresso Nazionale Sulla Trasmissione Del Calore, U.I.T., Napoli, Italy - 21- 23 June 2006.
17. M. Casamirra, F. Castiglia, M. Giardina, C. Lombardo, P. Meloni, P. Agostini, Prediction of the heat exchange in MEGAPIE facility by using RELAP5 code, XXVI Congresso Nazionale UIT sulla Trasmissione del Calore, Palermo, 23-25 Giugno 2008, ISBN 978-884672217-1.
18. P. Meloni, P. Agostani, M. Giardina, M. Casamirra, F. C., Calogera Lombardo, Verification of the RELAP5 code against the MEGAPIE irradiation experiment, The Tenth OECD Nuclear Energy Agency Information Exchange Meeting on Actinide and Fission Product Partitioning and Transmutation, Mito, Japan 6-10 October 2008.
19. Caronia, M. Casamirra, F. Castiglia, P. Chiovaro, M. Ciofalo, P.A. Di Maio, I. Di Piazza, M. Giardina, C. Lombardo, E. Oliveri, S. Puleo, G. Vella, Studio con il codice RELAP5 dello scambio termico e delle perdite di carico in generatori di vapore a tubi elicoidali, Rapporto tecnico CERSE-UNIPA RL-1201/2008, Palermo, Dicembre 2008.
20. R.C. Xin, A. Awwad, Z. Dong, M.A. Ebadian, H.M. Soliman, An Investigation and Comparative Study of the Pressure Drop in Air-Water Two-Phase Flow in Vertical Helicoidal pipes, Int. J. Heat and Mass Transf., vol. 39, pp.735-743, 1996.
21. R.C. Xin, A. Awwad, Z. Dong, M.A. Ebadian, An experimental study of single-phase and two-phase flow pressure drop in anular helicoidal pipes, Int. J. Heat and Fluid Flow, 18, pp. 482-488, 1997.
22. F. Castiglia, P. Chiovaro, M. Ciofalo, M. Di Liberto, P.A. Di Maio, I. Di Piazza, M. Giardina, F. Mascari, G. Morana, G. Vella, Modifiche del codice RELAP5 per lo studio delle perdite di carico in generatori di vapore a tubi elicoidali interessati da flussi bifase, CERSE-UNIPA RL-1204/2009, Maggio 2010.
23. F. Castiglia, P. Chiovaro, M. Ciofalo, P.A. Di Maio, M. Giardina, F. Mascari, G. Morana, G. Vella, Modifiche del codice RELAP5/MOD3.2.b per lo studio delle perdite di carico e dello scambio termico in condotti elicoidali interessati da deflussi bifase: validazione attraverso gli esperimenti effettuati dal Politecnco di Milano presso l'impianto SIET di Piacenza, CERSE-UNIPA RL 1209/2011, Luglio 2011.
24. Castiglia F., Giardina M., Morana G., De Salve M., Panella B., Analyses of single- and two-phase flow pressure drops in helical pipes using a modified RELAP5 code, Nuclear Engineering and Design,

Volume 250, September 2012, Pages 585–591, DOI: 10.1016/j.nucengdes.2012.06.008Document, 2012. Indice scopus eid=2-s2.0-84862742411.

25. J. C. Chen, A correlation for boiling heat transfer to saturated fluids in convective flow, ASME Paper 63-HT-34. 6th International Heat Transfer Conf., Boston, MA (1963).
26. Seban, R.A., Mclaughlin, E.F., 1963. Heat transfer in tube coils with laminar and turbulent flow. Int. J. Heat Mass Trans., 1963, 6, pp. 387–395.
27. Mori, Y., Nakayama, W., 1967. Study on forced convective heat transfer in curved pipes (second report, turbulent region). Int. J. Heat Mass Trans. 10 (1), 37–59.

APPENDICE A

MODELLI DI SCAMBIO TERMICO PER I METALLI LIQUIDI

A.1 Introduzione

Nei reattori raffreddati a metallo liquido la geometria dei canali causa una distribuzione di temperatura non uniforme attorno alle barre di combustibile che porta sforzi termici aggiuntivi, surriscaldamenti locali e possibili effetti negativi sull'integrità della barretta.

La maggior parte dei lavori sperimentali riguardanti la misurazione dei parametri dello scambio termico all'interno di un reticolo regolare di tubi cilindrici attraversato da fluidi a metallo liquido sono stati condotti durante la metà del secolo scorso, e negli ultimi anni tali esperimenti sono stati riesaminati in vista dello studio del nocciolo e degli scambiatori di calore che si pensa di impiegare nei reattori nucleari avanzati LFR. I maggiori requisiti di sicurezza e affidabilità richiesti per il progetto di questi sistemi hanno portato anche alla necessità di avere simulazioni numeriche dei processi e delle fenomenologie di trasferimento di calore che si svolgono nel core e nel circuito termoidraulico primario quanto più possibile attendibili.

Rispetto al trasferimento di calore in acqua, le fenomenologie di scambio termico nei metalli liquidi differiscono significativamente essendo questi fluidi caratterizzati da un numero di Prandtl (Pr) molto basso. Come è noto, il numero di Pr ha un preciso significato fisico per lo sviluppo degli strati limite (termico e dinamico) a contatto con una superficie, fornendo una misura della predominanza degli effetti della perturbazione termica rispetto a quella fluidodinamica. In particolare, nella regione di temperature 200÷800°C, il numero Pr varia nell'intervallo 0.01÷0.005 per il sodio e nell'intervallo 0.03÷0.005 per l'eutettico piombo-bismuto, mentre per l'acqua esso varia nell'intervallo 1÷6, nella stessa regione di intervallo della temperatura. Quindi, il contributo dovuto al trasferimento di calore totale per conducibilità termica (rispetto al contributo dovuto alla convezione) è molto superiore per il caso di metallo liquido rispetto all'acqua.

Sperimentalmente è stato rilevato che il trasferimento di calore per il metallo liquido può essere correlato al numero di Nusselt (Nu) ricorrendo ad espressioni del tipo:

$$Nu = a + b*Pe^{c} \qquad (a1)$$

dove a, b e c sono costanti e Pe è il numero di Peclet (prodotto dei numeri di Reynolds e Prandtl).

Il primo e secondo termine in eq. (a1) descrivono, rispettivamente, i contributi dalla conducibilità termica e dalla convezione. Sperimentalmente, la costante c è abbastanza vicino al valore 0.8, mentre, a, e, b, dipendono dalla geometria della sezione di scambio termico (tubo circolare, corona circolare, fascio tubiero, ecc..).

Di seguito verranno trattate le correlazioni disponibili in letteratura per lo studio dello scambio termico riguardante i metalli liquidi, per diverse configurazioni e geometrie dei tubi.

Buona parte delle correlazioni che verranno presentate in questa appendice sono state sviluppate considerando un flusso termico costante oppure la temperatura assiale costante, per cui è importante tenere presente che la loro applicabilità per la simulazione dello scambio termico nelle barre di combustibile di un reattore nucleare di tipo LFR deve essere attentamente rivalutata.

Alcuni ricercatori hanno trovato che per profili cosinusoidali della distribuzione assiale della potenza Nu cambia tra ingresso ed uscita in modo sostanziale (nella parte bassa del core i valori sono più elevati, mentre nella parte alta sono più bassi). Tuttavia non è chiaro se in queste ricerche sono stati considerati gli effetti della diminuzione assiale del numero di Pe dovuto al riscaldamento.

La variazione assiale di Nu dovrebbe, quindi, essere ulteriormente investigata per consentire l'esame di eventuali ripercussioni sui valori massimi della temperatura del combustibile e della guaina.

Sulla base del lavoro bibliografico descritto in [A1], in questa appendice viene ulteriormente approfondito l'argomento ed evidenziato quali correlazioni vengono impiegate in alcuni codici di calcolo di sistema utilizzati per analisi termofluidodinamiche riguardanti gli impianti LFR, con particolare riferimento al codice RELAP5-3D [A2].

A.2 Modelli di scambio termico per i metalli liquidi

Come è noto, le modalità microscopiche di trasmissione dell'energia nella convezione e nella conduzione sono le medesime, la sostanziale differenza sta nel fatto che, essendo il fluido in moto, al trasporto di energia dovuto alle interazioni molecolari si somma il moto di materia che veicola tale energia nello spazio e nel tempo.

Quindi, nel meccanismo del trasporto di energia per convezione hanno grande importanza sia i fenomeni di trasporto del calore per conduzione sia il trasporto di materia. Poiché la conducibilità termica dei fluidi, tranne che per i metalli liquidi, è abbastanza piccola, la velocità del trasporto di energia dipende principalmente dal moto di mescolamento del fluido. Di conseguenza, per trasmettere una certa potenza termica per convezione attraverso un fluido è richiesto un gradiente di temperatura più grande in una regione a bassa velocità rispetto a quello necessario in una regione ad alta velocità. Quindi, in corrispondenza dello strato limite dinamico si viene a generare anche uno strato limite termico.

Se il fluido è caratterizzato da moto laminare lo scambio termico in direzione perpendicolare al moto del fluido avviene unicamente per conduzione (molecular diffusion). Nello strato di fluido aderente alla parete il calore può fluire soltanto per conduzione, conseguentemente in questo strato si ha di solito una significativa variazione di temperatura. Una situazione diversa, invece, è quella relativa al moto turbolento. In questo caso il meccanismo di conduzione del calore da particella a particella è potenziato dall'instaurarsi di innumerevoli vortici che favoriscono lo scambio di energia interna tra le diverse zone di fluido attraverso

la diffusione turbolenta (eddy diffusion). In questo caso allontanandosi dalla parete, il movimento del fluido facilita il trasporto di energia ed il gradiente di temperatura sarà meno significativo, annullandosi infine nella corrente principale.

Rispetto ai fluidi convenzionali, il meccanismo del trasferimento di calore in un metallo liquido (con basso Pr) si caratterizza per l'elevato contributo della diffusione molecolare e, quindi, della conduzione. Ciò comporta che la resistenza termica è distribuita su tutta la sezione trasversale del flusso, per cui condizioni di scambio termico con flusso di calore costante o con temperatura alla parte costante producono profili di temperatura differenti a causa delle diverse condizioni al contorno; come conseguenza le correlazioni di scambio termico sono caratterizzate da differenze significative.

A.3 Correlazioni di scambio termico valide per tubo cilindrico

I primi studi teorici riguardanti il trasferimento di calore nei metalli liquidi fu affrontata da Martinelli, il quale riconobbe che per questi fluidi la conduzione molecolare del calore nel cuore turbolento prevale sugli effetti dovuti alla "eddy diffusion", notando che il rapporto delle "eddy diffusivities" del calore e del momento non necessariamente dovevano essere uguali ad uno, come assunto nella precedente teoria basata sul concetto "heat transfer analogy". Su queste basi, in [A3] Martinelli ha calcolato il coefficiente di scambio termico, ricorrendo al principio del "momentum transfer analogy" in cui si tengono in considerazione gli effetti significativi della conducibilità molecolare.

Seguendo la teoria di Martinelli, Lyon ha dimostrato [A4, A5] che i risultati teorici per il calcolo di Nu possono essere rappresentati da una funzione del tipo eq. (a1), ricavando un'equazione semi-empirica valida per i metalli liquidi come riportato di seguito:

$$\mathrm{Nu} = 7.0 + 0.025(\psi \mathrm{Pe})^{0.8} \qquad \text{(a2)}$$

essendo $\Psi = \varepsilon_{H/} \varepsilon_M$, rapporto tra la "eddy diffusivity" del calore (ε_H) e la "eddy diffusivity" della quantità di moto (ε_M). L'eq. (a2) è valida per flusso di calore costante alla parete. Se il parametro Ψ è uguale ad 1, l'eq. (a2) viene detta equazione Martinelli-Lyon. Questa correlazione si basa su dati sperimentali ottenuti con flusso termico imposto.

Tuttavia, è stato trovato sperimentalmente che Nu, soprattutto per il caso di metalli liquidi pesanti, generalmente è più basso del 20-30% del valore calcolato tramite l'eq. (a2) [A6]. Per indagare le discrepanze tra teoria e sperimentazione, alcune attività di ricerca sono state rivolte allo studio degli effetti locali della resistenza termica nella superficie di contatto. I risultati hanno mostrato che l'effetto della resistenza nella superficie è troppo piccola per giustificare le discrepanze descritte prima [A7].

Seban e Shimazaki pubblicarono nel 1951 [A8], per flusso turbolento e scambio termico con temperatura di parete costante, una correlazione molto simile alla eq. (a2):

$$Nu = 5.0 + 0.025Pe^{0.8} \qquad \text{(a3)}$$

La stessa relazione è stata trovata da Subbotin et al. [A9] per descrivere le loro misure sperimentali riguardanti tubi circolari, con sodio come fluido di lavoro, nell'intervallo del numero di Peclet 40≤Pe≤1150, ottenendo una accuratezza per la predizione dei dati sperimentali del 10%. Tuttavia, successivamente, Subbotin, nell'ambito di collaborazioni con i ricercatori dell'istituto IPPE (Physics and Power Institute, Obninsk), pubblicò altre correlazioni valide per fasci di tubi bagnati longitudinalmente con reticolo triangolare [A10, A11], come verrà descritto nel paragrafo successivo. Quindi, l'applicazione delle correlazioni del numero di Nu ottenute da Subbotin è condizionata dalla qualifica sperimentale basata su condizioni geometriche differenti.

A.4 Correlazioni di scambio termico valide per un fascio di barre disposte secondo un reticolo triangolare

I primi lavori riguardanti lo scambio termico di un fascio di tubi in geometria triangolare vengono svolti da Dwyer e Tu, nel 1960 [A12] e da Friedland e Bonilla nel 1961 [A13], ottenendo, rispettivamente, le seguenti relazioni basate sul calcolo di Nu in funzione del numero di Peclet e del rapporto passo/diametro (x=P/D):

$$Nu = 0.93 + 10.81x - 2.01x^2 + 0.0252x^{0.273}\ (\psi Pe)^{0.8} \qquad \text{(a4)}$$

$$Nu = 7.0 + 3.8\left(\frac{P}{D}\right)^{1.52} + 0.027\left(\frac{P}{D}\right)^{0.27}(\Psi \cdot Pe)^{0.8} \qquad \text{(a5)}$$

Le due relazioni sono state ottenute utilizzando dati sperimentali realizzati con flusso di calore costante. L'eq. (a5) è valida per i seguenti intervalli: 10 ≤ Pe ≤ 100000 e 1.375 ≤ P/D ≤ 10.

Il numero di Pe viene corretto con il fattore Ψ descritto nel paragrafo precedente.

Sulla base delle indagini sperimentali eseguite nei laboratori nazionali di Brookhaven per la studio del trasferimento di calore in un fascio di 13 pins, diametro esterno 13 mm, raffreddati con mercurio [A14], ed in un fascio di 19 pins, raffreddati con una lega di sodio-potassio NaK [A15], usando per entrambi i casi un rapporto P/D=1.75, è stata valutata la seguente relazione semi-empirica, in cui la dipendenza dal rapporto P/D è stata ottenuta anche ricorrendo ad un approccio teorico:

$$Nu = 6.66 + 3.126\frac{P}{D} + 1.184\left(\frac{P}{D}\right)^2 + 0.0155(\Psi \cdot Pe)^{0.86} \qquad \text{(a6)}$$

dove il parametro Ψ viene calcolato mediante la seguente correlazione empirica:

$$\Psi = 1 - \frac{1.82}{\mathrm{Pr}\cdot\left(\frac{\varepsilon_M}{\nu}\right)_{max}^{1.4}} \qquad \text{(a7)}$$

L'Eq. (a6) viene considerata valida per i seguenti intervalli: 70 ≤ Pe ≤ 10000 e 1.3 ≤ P/D ≤ 3.

Per il calcolo del rapporto $(\varepsilon_M/\nu)_{max}$ si può utilizzare la seguente approssimazione [A16]:

$$\ln\left(\frac{\varepsilon_M}{\nu}\right)_{max} = 0.864\cdot\ln(\mathrm{Re}) - 0.24\frac{P}{D} - 2.12 \qquad \text{(a8)}$$

Nel 1965, sempre per un reticolo di barre triangolare, Subbotin ha proposto le seguente correlatione valida per rapporti 1.1<P/D<1.5 e Pe 80<Pe<4000 [A10]:

$$Nu = 0.58\left(\frac{d_h}{d}\right)^{0.55} Pe^{0.45} \qquad \text{(a9)}$$

dove d_h e d sono, rispettivamente, il diametro idraulico e il diametro del tubo.

Questa relazione fu utilizzata per calcoli di scambio termico in reattori refrigerati con Pb-Bi, ed i risultati ottenuti portarono ad una sottostima del coefficiente di scambio termico per valori del numero di Pe bassi.

Sebbene l'eq. (a9) sia stata derivata per geometria triangolare, essa può essere applicata anche per studi riguardanti reticoli quadrati utilizzando la seguente espressione:

$$Nu = 0.58\left(\frac{4}{\pi}x^2 - 1\right)^{0.55} Pe^{0.45} \qquad \text{(a10)}$$

Nel 1969, Borishanskii et al. [A17] hanno pubblicato i risultati ottenuti per 7 pins, diametro 22 mm e lunghezza riscaldata del tubo di prova pari a 800 mm, caratterizzati da 1.1 ≤ P/D ≤ 1.5, utilizzando refrigeranti con numeri di Prandtl pari a 0.007 (sodio) e 0.03 (mercurio). Le temperature del fluido furono fatte variare tra 206<T<236 °C.

Le correlazioni ottenute per descrivere i dati sperimentali presi in esame, estesa anche alle misure effettuate dall'IPPE (Pr ≈ 0.024), sono state valutate in modo da trattare calcoli validi per Pe≤2200:

$$\mathrm{Nu}_{lam} = 24.12\log_{10}\left(-8.12 + 12.76\frac{P}{D} - 3.65\left(\frac{P}{D}\right)^2\right)$$

$$\mathrm{Nu}_{turb} = 0.0174\left(1.0 - e^{-6.0\left(\frac{P}{D}-1.0\right)}\right) B^{0.9}$$

$\mathrm{Nu} = \mathrm{Nu}_{lam}$ B=1 Pe ≤ 200

$\mathrm{Nu} = \mathrm{Nu}_{lam} + \mathrm{Nu}_{turb}$ B=Pe-200 200 ≤ Pe ≤ 2200

(a11)

Nel 1972, tre serie di dati sperimentali sono stati realizzati da Gräber e Rieger con sezioni di prova costituiti da 31 tubi, diametro esterno 12 mm, disposti secondo fasci triangolari equilateri con rapporti P/D=1.25, 1.6 e 1.95. Il fluido di lavoro è stato NaK (44% Na e 56% K), con temperature nell'intervallo 100<T<425 °C. Il numero di Pr varia con la temperatura nell'intervallo $0.011 \leq Pr \leq 0.024$. Un totale di 246 dati sperimentali in termini di Nu in funzione di Pe sono stati pubblicati in [A18].

Sulla base delle loro attività sperimentali, gli autori propongono la segunete correlazione:

$$Nu = 0.25 + 6.2\frac{P}{D} + \left(-0.007 + 0.032\frac{P}{D}\right) Pe^{\left(0.8 - 0.024\frac{P}{D}\right)} \qquad \text{(a12)}$$

con intervalli di validità pari a: $110 \leq Pe \leq 4300$, $1.2 \leq P/D \leq 2.0$

Per valori $P/D \leq 1.0$, alcune ricerche sperimentali e analitiche suggeriscono una correlazione più complessa che copre un ampio spettro di parametri e consente di ottenere valutazioni con un accuratezza del 15%. Tale correlazione è stata presentata da Subbotin et al. nel 1973 [A11] e successivamente discussa anche da Ushakov et al. [A19]:

$$Nu = Nu_{lam} + \frac{3.67}{90\left(\frac{P}{D}\right)^2}\left(1 - \frac{1}{\frac{1}{6}\left(\left(\frac{P}{D}\right)^{30} - 1\right) + \sqrt{1.15 + 1.24\varepsilon}}\right) Pe^{0.56 + 0.19\frac{P}{D} - 0.1\left(\frac{P}{D}\right)^{-80}} \qquad \text{(a13)}$$

dove Nu_{lam} è calcolato come segue:

$$Nu_{lam} = \left(7.55\frac{P}{D} - 6.3\left(\frac{P}{D}\right)^{-17\frac{P}{D}\left(\frac{P}{D} - 0.81\right)}\right)\left(1 - \frac{3.6\frac{P}{D}}{\left(\frac{P}{D}\right)^{20}\left(1 + 2.5\varepsilon^{0.86}\right) + 3.2}\right) \qquad \text{(a13')}$$

Gli intervalli di validità sono i seguenti: $1 \leq Pe \leq 4000$, $1.0 \leq P/D \leq 2.0$, $0.01 < \varepsilon < \infty$.

Il parametro ε dipende dal numero e dalla geometria delle barretta, dalla disposizione geometrica (triangolare oppure quadrata) e dalla conduttività termica del combustibile, della guaina e del refrigerante [A20]. E' difficile comprendere perché Nu dovrebbe dipendere sia dai dati geometrici che termici del combustibile e della guaina se la correlazione deve essere usata nei codici di calcolo per valutare il trasferimento di calore tra la superficie esterna del rivestimento ed il refrigerante. Si raccomanda, quindi, di utilizzare l'equazione per ε indipendente dalla disposizione delle barre di combustibile e pari al rapporto tra la conduttività termica del refrigerante e della guaina.

Per (P/D) ≥ 1.2, poiché la dipendenza dal parametro ε è trascurabile, si può utilizzare la seguente correlazione con uno scostamento dall'eq. (13') inferiore al 5%:

$$\mathrm{Nu} = 7.55\frac{\mathrm{P}}{\mathrm{D}} - 20\left(\frac{\mathrm{P}}{\mathrm{D}}\right)^{-13} + \frac{0.041}{\left(\frac{\mathrm{P}}{\mathrm{D}}\right)^{2}}\mathrm{Pe}^{\left(0.56+0.19\frac{\mathrm{P}}{\mathrm{D}}\right)} \qquad \text{(a13'')}$$

Gli intervalli di validità dell'eq. (13'') sono: 1 ≤ Pe ≤ 4000, 1.2 ≤ P/D ≤ 2.0

Kazimi e Carelli suggeriscono una correlazione messa a punto in seguito alle molte campagne sperimentali effettuate utilizzando Na, Hg e NaK come refrigeranti [A21]. In base ai lavori svolti da Waltar riportati in [A22], questa correlazione è stata utilizzata per analisi del Fast Flux Text Facility (FFTF) e del Clinch River Breeder Reactor (CRBR), caratterizzati da rapporti P/D pari a 1.2 e 1.3, rispettivamente:

$$\mathrm{Nu} = 4 + 0.16\left(\frac{\mathrm{P}}{\mathrm{D}}\right)^{5} + 0.33\left(\frac{\mathrm{P}}{\mathrm{D}}\right)^{3.8}\left(\frac{\mathrm{Pe}}{100}\right)^{0.86} \qquad \text{(a14)}$$

Gli intervalli di validità sono: 10 ≤ Pe ≤ 5000, 1.1 ≤ P/D ≤ 1.4.

La maggior parte degli esperimenti sono stati condotti utilizzando fasci di barre nude, ma un numero limitato di prove ha riguardato barrette con filo distanziatore. La correlazione risulta essere in buon accordo con i dati sperimentali per 1.1 <P/D <1.15, ma sottostima Nu per P/D>1.15 [A23].

Il codice di calcolo ATHENA usa, per lo studio dello scambio termico con i refrigerati a metallo liquido in convezione forzata, l'eq. (a3). Questa versione è stata modificata inserendo anche l'eq. (a14) per la simulazione dello scambio termico in fasci di barre [A24]. La stessa procedura viene impiegata anche dalla versione 3D del codice RELAP5, come vedremo nell'Appendice B.

Nel rapporto [A25], riguardante il reattore veloce a piombo BREST, si raccomanda, per disposizioni triangolare delle barrette, una correlazione che risulta dalla combinazione di due differenti equazioni. La parte laminare è presa dall'eq. (a19) (vedi paragrafo successivo), valida per fasci di tubi in geometria quadrata, e la parte turbolenta dall'eq. (a13''):

$$\mathrm{Nu} = 7.55\frac{\mathrm{P}}{\mathrm{D}} - 14\left(\frac{\mathrm{P}}{\mathrm{D}}\right)^{-5} + \frac{0.041}{\left(\frac{\mathrm{P}}{\mathrm{D}}\right)^{2}}\mathrm{Pe}^{\left(0.56+0.19\frac{\mathrm{P}}{\mathrm{D}}\right)} \qquad \text{(a15)}$$

Non vien fornito nessun l'intervallo di validità, né è disponibile una qualifica sperimentale.

Mikityuk in [A26] effettua una revisione delle principali correlazioni e dei dati sperimetali presenti in letteratura, e vengono utilizzati i dati sperimentali riportati in [A14, A17, A18, A27] per valutare la seguente nuova correlazione, ottenuta con il miglior adattamento sui 658 punti sperimentali presi in esame:

$$\mathrm{Nu} = 0.047\left(1 - \mathrm{e}^{-3.8\left(\frac{\mathrm{P}}{\mathrm{D}}-1\right)}\right)\left(\mathrm{Pe}^{0.77} + 250\right) \qquad \text{(a16)}$$

Gli intervalli di validità sono: $30 \le Pe \le 5000$, $1.1 \le P/D \le 1.95$.

L'uso dei dati di Zhukov [A27], ottenuti per geometria quadrata, si giustifica per il fatto che essi ha un intervallo di validità simile a quello valutato per la geometria triangolare. Inoltre, in [A27] viene messo in evidenza che anche le eqs. (a13'') e (a12), tra le correlazioni descritte nell'articolo, consentono di ottene una buona rappresentazione dei dati sperimentali esaminati.

A.4.1 Confronto di alcune correlazioni di scambio termico valide per fascio di barre in geometria triangolare

Nelle Figure a1 e a2 vengono confrontate alcune correlazioni di scambio termico ottenute per tubi cilindrici e per fascio di barre in geometria triangolare utilizzando il rapporto P/D=1.324, valido per il progetto Elsy.

In Figura a1 si può notare che l'eq. (a2) valuta valori di Nu superiori anche al 30% rispetto all'eq (a3). Si ricorda che le due relazioni sono state valutate, rispettivamente, per flusso di calore e temperatura alla parete costanti.

L'eq. (a7') approssima le eq.s (a11), (a12) e (a13'') per valori di Pe>1000, mentre sottostima Nu per valori di Pe inferiori. Molto prossime tra loro sono le predizioni di Nu fornite dalle eq.s (a2) e (a15) e dalle eq.s (a12) e (a13'').

In Figura a2 vengono messe a confronto le eqs. (a11), (a12), (a13''), (a14), (a15) e (a16) e, come si può vedere dal grafico, le correlazioni eqs. (a11), (a12), (a13''), e (a16) predicono valori del numero di Nu molto vicini tra loro, con una leggera sovrastima e sottostima di Nu da parte dell'eq. (a11) per Pe> 1300.

È da notare che la correlazione di Mikityuk eq. (a16) è stata ottenuta estendendo la sua applicazione ad un numero significativo di dati sperimentali. Ciò giustifica il suggerimento dello stesso autore di impiegare questa correlazione in quei codici di calcolo utilizzati per la simulazione del comportamento termoidraultico del reattore refrigerato a piombo ELSY.

In sintesi si può affermare che la correlazione di Subbotin/Ushakov eq. (a13'') e di Mikityuk eq. (a16) sembrano avere la migliore qualificazione dal punto di vista sperimentale.

Nello stesso grafico viene, infine, riportata l'eq. (a14) che, rispetto a tutte le altre correlazioni, sottostima fortemente Nu. Tuttavia questa correlazione è stata già impiegata per studi sui reattori come il Fast Flux

Text Facility (FFTF), il Clinch River Breeder Reactor (CRBR) e il reattore veloce a piombo BREST, inoltre viene utilizzata, come già detto, da codici di calcolo qualificati come ATHENA e RELAP5-3D.

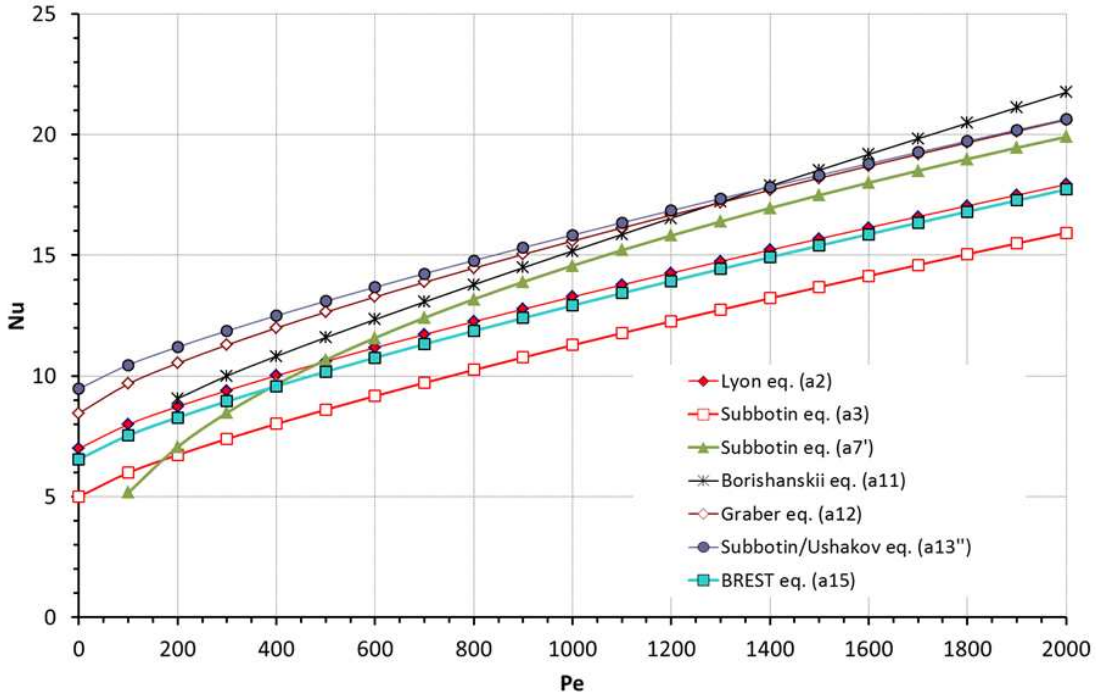

Figura a1. Rappresentazione delle correlazioni ottenute per tubi cilindrici e per fasci di tubi in geometria triangolare, valide per l'impianto Elsy.

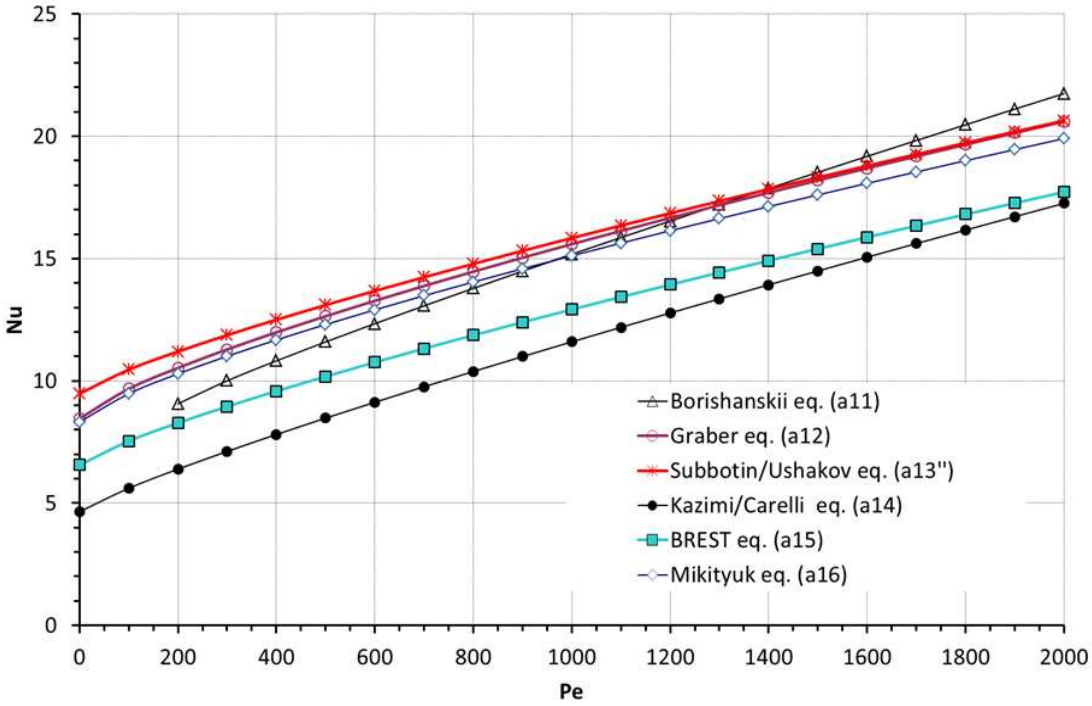

Figura a2. Rappresentazione di alcune correlazioni ottenute per fasci di tubi in geometria triangolare, valide per l'impianti Elsy.

A.5 Correlazioni di scambio termico valide per un fascio di barre disposte secondo un reticolo quadrato

In [A28] Kirillov et al. propongono la seguente correlazione valida per fasci di tubi quadrati con rapporto x=P/D>1.2 e Pr<0.05:

$$Nu = (0.3 + 8.6x)(1 + 10^{-3} Pe^{0.87}) \tag{a17}$$

Questa correlazione è applicabile per valori di ε_{k0}, detto parametro di similitudine, maggiore di 10^{-2}:

$$\varepsilon_{k0} = \frac{k_w}{k_f}\left[1 - \frac{k_w - k_o}{k_w + k_o}\left(\frac{R_1}{R_2}\right)^{12}\right]\left[1 + \frac{k_w - k_o}{k_w + k_o}\left(\frac{R_1}{R_2}\right)^{12}\right]^{-1} \tag{a18}$$

dove k_w, k_f e k_o sono la conducibilità termica del cladding, del fluido termovettore e del combustibile, rispettivamente, mentre R_1 e R_2 sono il raggio interno (solo combustibile) e il raggio esterno (cladding compreso) della barretta.

Nel rapporto BREST [A25] per barre in geometria quadrata si raccomanda l'uso di una correlazione simile all'eq. (a15), valida per geometria triangolare, che tuttavia predice valori di Nu più bassi:

$$\mathrm{Nu} = 7.55\frac{\mathrm{P}}{\mathrm{D}} - 20\left(\frac{\mathrm{P}}{\mathrm{D}}\right)^{-5} + \frac{0.0354}{\left(\frac{\mathrm{P}}{\mathrm{D}}\right)^{2}}\mathrm{Pe}^{\left(0.56+0.204\frac{\mathrm{P}}{\mathrm{D}}\right)} \tag{a19}$$

Gli intervalli di validità sono: 100 ≤ Pe ≤ 1600, 1.28 ≤ P/D ≤ 1.46.

Tra i pochi studi sperimentali disponibili per i reticoli quadrati, troviamo quelli realizzati in Russia utilizzando un fascio di 25 barre refrigerate con NaK. I risultati, validi per P/D=1.28 e P/D=1.46, sono stati presentati nel 1994 da Zhukov et al. [A29].

Successivamente, è stato pubblicato un report più dettagliato [A27] in cui sono stati inclusi i risultati validi per P/D=1.25 e P/D=1.0, nonchè indagini sull'influenza della griglia distanziatrice con ostruzioni della sezione trasversale del flusso (ε) rispettivamente del 10% e del 20%.

Gli esperimenti con griglia distanziatrice sono stati realizzati con P/D=1.46.

Le correlazioni proposte per descrivere i dati sperimentali presi in esame sono le seguenti:

$$\mathrm{Nu} = 7.55\frac{\mathrm{P}}{\mathrm{D}} - 14\left(\frac{\mathrm{P}}{\mathrm{D}}\right)^{-5} + \mathrm{A}\cdot\mathrm{Pe}^{\left(0.64+0.246\frac{\mathrm{P}}{\mathrm{D}}\right)} \tag{a20}$$

in cui la costante A può essere posta uguale ai seguenti valori:

A=0.007 per barre senza distanziatori (a20')

A=0.010 ε =10% (a20'')

A=0.009 ε =20% (a20''')

Una correlazione valida sempre per reticoli quadrati viene presentata da Dwyer [A30]:

$$Nu = 6.66 + 3.36x + 1.368x^2 + 0.0155(\overline{\psi}Pe)^{0.86} \quad \text{(a21)}$$

con

$$\overline{\psi} = 1 - \frac{1.013x^{1.4}}{Pr(Re/10^3)^{1.281}} \quad \text{(a22)}$$

Questa relazione è valida per valori P/D> 1.35.

Infine, riportiamo la correlazione di Calamai [A31] che non fa distinzione tra geometria triangolare e quadrata:

$$Nu = 4 + 16x^{-5} + 0.33x^{3.8}\left(\frac{Pe}{100}\right)^{0.86} \quad \text{(a23)}$$

A.5.1 Confronto di alcune correlazioni di scambio termico valide per fascio di barre in geometria quadrata

Anche le correlazioni che vengono mostrate nelle Figure a3 e a4, valide per fascio di barre in geometria quadrata, vengono valutate utilizzando il rapporto P/D dell'impianto Elsy.

Le eq.s (a11), (a14) e (a15), valide per geometria triangolare, vengono riportate a titolo di confronto.

Le eq.s (a20'') e (a20'''), valutate con presenza di distanziatori, sono prossime tra loro, mentre la correlazione eq. (a20'), senza distanziatori, risulta essere molto vicina alle curve ottenute utilizzando le eq.s (a15) e (a19). Tra l'eq. (a15) e l'eq. (a20') si valuta una differenza di circa il 10%.

L'eq. (a11) approssima l'eq. (a23) per Pe inferiore a circa 1200 mentre coincide con l'eq (a20'') per valori di Pe superiori.

E' da notare da parte dell'eq. (a17), rispetto a tutte le altre correlazioni presentate in Figura a3, la sovrastima di Nu fino a Pe pari a circa 1400.

In Figura a4, in cui vengono riportate le eq.s (a14), (a15), (a19) e (a20'), le varie correlazioni predicono valori di Nu al variare di Pe molto vicini, con scostamenti che non superano il 30%. Quindi sembrerebbe per questi casi poco influente il tipo di geometria.

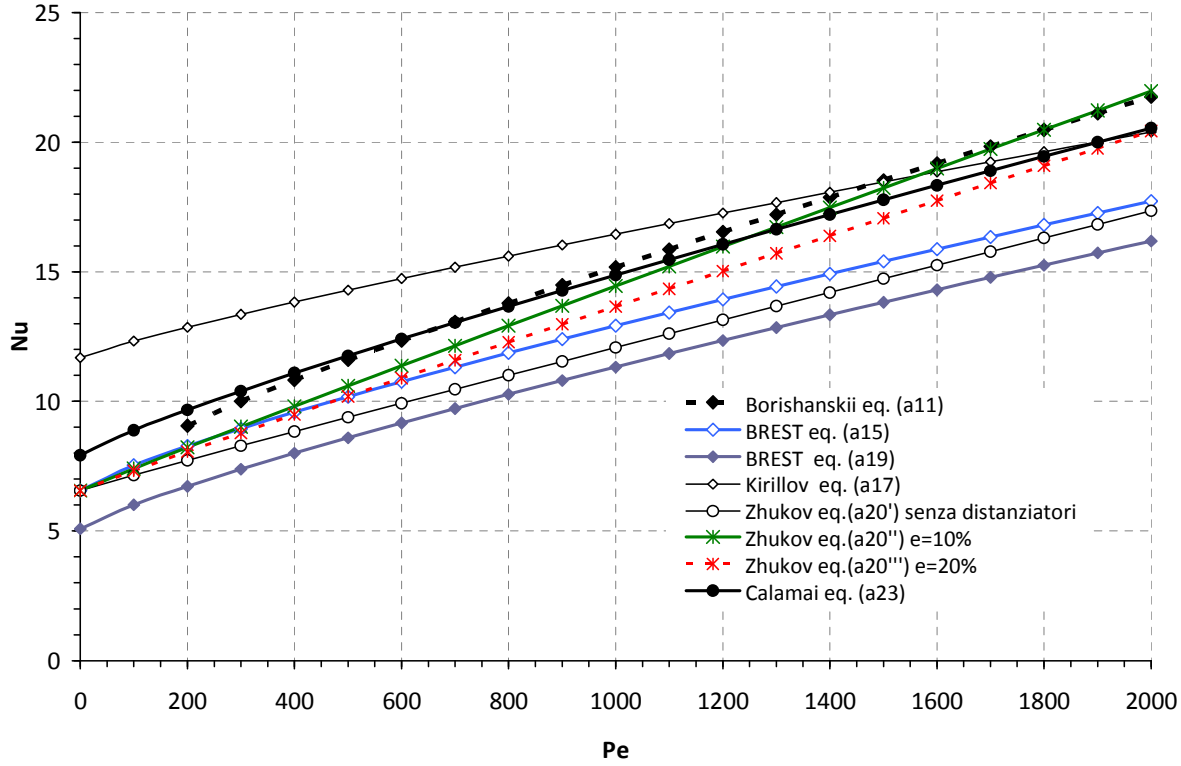

Figura a3. Rappresentazione delle correlazioni ottenute per fasci di tubi in geometria quadrata.

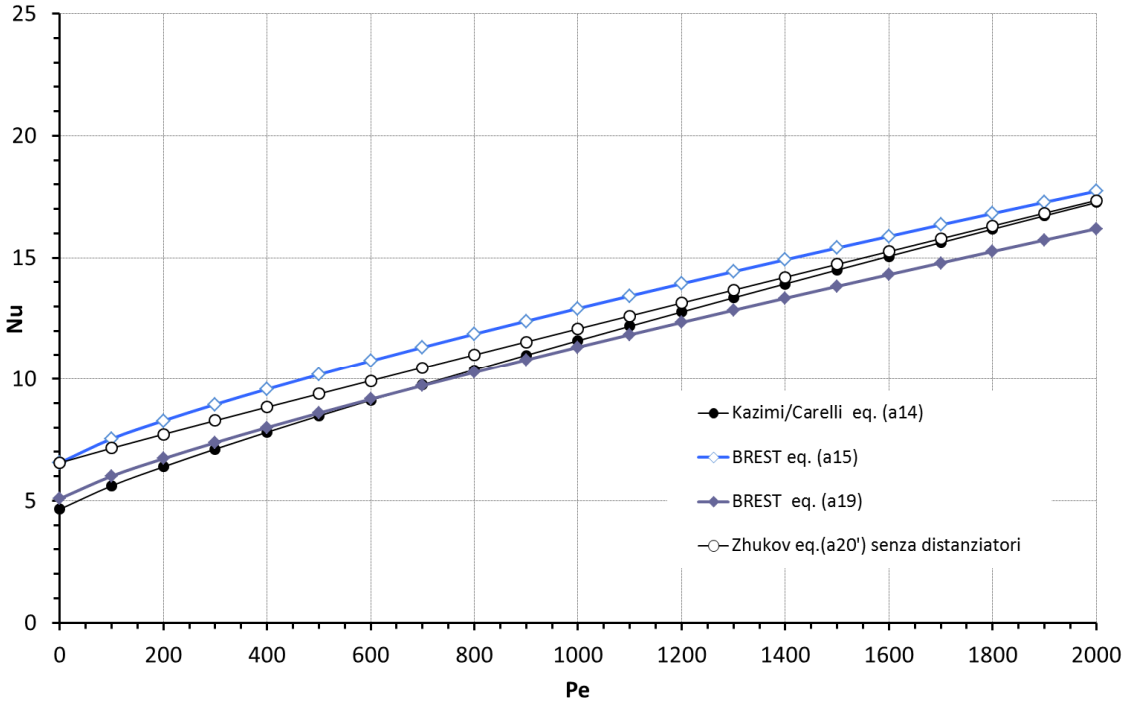

Figura a4. Rappresentazione di alcune correlazioni ottenute per fasci di tubi in geometria quadrata e confronto cone le correlazioni valide per geometria triangolare.

Dal confronto dei risultati è evidente l'importanza della griglia distanziatrice.

Nella maggior parte delle pubblicazioni o campagne sperimentali effettuate sullo scambio termico con fluidi di lavoro a metallo liquido non viene specificato l'uso di distanziatori o, se utilizzati, non viene chiarita la tipologia.

In [A18], in cui viene presentata l'eq. (a12) valida per geometria triangolare, si vede la presenza di alcune griglie distanziatrici, tuttavia nella Figura a2 del paragrafo A2.2.1, la presenza delle grigie sembrebbe poco influente, essendo l'eq. (a12) molto vicina alle curve ottenute utilizzando dati sperimetali effettuati senza distanziatori. Questo risultato è però in contrasto con quello ottenuto da Zhukov et al. che indicano, in presenza di distanziatori, un incremento di Nu, anche del 30%, per Pe pari a circa 2000. Questa differenza potrebbe essere anche più elevata in quanto gli autori hanno sviluppato le loro correlazioni mediando sull'altezza della regione stabilizzata.

Si può concludere che nei calcoli dei codici di calcolo utilizzati per l'analisi termica del core del reattore di un impianto LFR potrebbe essere importante tenere in considerazione l'influenza di eventuali fili distanziatori presenti nel fascio tubiero, anche se i risultati sopra riportati risultano essere non sempre coerenti tra loro.

BIBLIOGRAFIA

A1. Pfrang, W., Struwe, D., Assessment of Correlations for Heat Transfer to the Coolant for Heavy Liquid Metal Cooled Core Designs, FZKA 7352.Forschungszentrum Karlsruhe GmbH, Karlsruhe, October 2007.

A2. RELAP5-3D, Code Manual, Models and Correlations, Volume IV, INEEL-EXT-98-00834 Revision 2.4, June 2005.

A3. Martinelli, R.C., 1947. Heat transfer to molten metals. Trans. ASME 69, 47–59.

A4. Lyon R. N., Heat transfer at high fluxes in confined spaces, PhD thesis, University of Michigan, Ann Arbor, Mich., 1949.

A5. Lyon R.N., 1951. Liquid metal heat transfer coefficients. Chem. Eng. Progr., 47, 75–79.

A6. Lubarsky B., Kaufman S J., Review of experimental investigations of liquid-metal heat transfer, NACA R-1270 (1956).

A7. MscDonald W. C., Quittentom R. C., A critical analysis of metal wetting and gas entrainment in heat transfer to molten metals, Chem. Engng. Prog. Symp. Ser. 50(9), 59-67 (1954).

A8. Seban R. A., Shimazaki T. T., Heat transfer to a fluid flowing turbulently in a smooth pipe with walls at constant temperature, Transactions of the ASME, Vol. 73, May 1951, pp. 803-809.

A9. Subbotin V. I., Papovyants A. K., Kirillov P. L., Ivanowskii N. N., A study of heat transfer to molten sodium in tubes, Soviet Atomic Energy, Vol. 13, 1962, pp. 991-994; translated from Atomnaya Énergiya, Vol. 13, No. 4, 1962, pp. 380-382

A10. Subbotin, V.I., Ushakov, P.A., Kirillov, P.L., Ibragimov, M.H., Ivanovski, M.N.,Nomofilov, E.M., Ovechkin, D.M., Sorokin, L.N., Sorokin, V.P., 1965. Heat transfer from fuel elements of liquid meta-cooled reactors. Proceedings of the 3rd International Conference on Peaceful Use of Nuclear Energy, 8, NY, pp. 192–203.

A11. Subbotin V. I., Ushakov P. A., Zhukov A. V., Matyukhin N. M., Yur'ev Yu. S., Kudryavtseva L. K., Heat transfer in cores and blankets of fast breeder reactors, Proceedings of Second Symposium of Member Nations of Council for Mutual Economic Aid "State and Prospects of Work on the Construction of Atomic Power Stations with Fast Neutron Reactors", October 1973, Obninsk, Vol. 2 (1975).

A12. Dwyer, O.E., Tu, P.S., 1960. Analytical Study of Heat Transfer Rates for Parallel Flow of Liquid Metals Through Tube Bundles, Part I. Chemical Engineering Progress Symposium Series 56 (30), 183–193.

A13. Friedland A. F., Bonilla C. F., Analytical study of heat transfer rates for parallel flow of liquid metals through tube bundles, A.I.Ch.E. Journal Vol. 7, No. 1, March 1961, pp. 107-112.

A14. Maresca, M. W., Dwyer O. E., Heat transfer to mercury flowing in-line through a bundle of circular rods, Transactions of the ASME series C. Journal of Heat Transfer Vol. 86, May 1964, pp. 180-186.

A15. Kalish S. , Dwyer O. E., Heat transfer to NaK flowing through unbaffled rod bundles, International Journal of Heat and Mass Transfer, Vol. 10, 1967, pp. 1533-1558.

A16. Zhukov A. V., Sorokin A. P., Titov P. A., Ushakov P. A., Thermohydraulic problems in lead-cooled reactors, Soviet Atomic Energy, Vol. 72, 1992, pp. 138-147; translated from Atomnaya Énergiya, Vol. 72, No. 2, 1992, pp. 142-151.

A17. Borishanskii V. M., Gotovski M. A., Firsova É. V., "Heat transfer to liquid metals in longitudinally wetted bundles of rods" Soviet Atomic Energy, Vol. 27, 1969, pp. 1347-1350; translated from Atomnaya Énergiya, Vol. 27, No. 6, 1969, pp. 549-552.

A18. Gräber H., Rieger M., "Experimentelle Untersuchung des Wärmeübergangs an Flüssigmetall (NaK) in parallel durchströmten Rohrbündeln bei konstanter und exponentieller Wärmefluss-dichteverteilung", Atomkernenergie Vol. 19, 1972, pp. 23-40

A19. Ushakov P.A., Zhukov A.V., Matyukhin N.M., "Heat transfer to liquid metals in regular arrays of fuel elements" High Temperature, Vol. 15, 1977, pp 868-873; translated from Teplofizika Vysokikh Temperatur, Vol. 15, No. 5, 1977, pp. 1027-1033

A20. Kirillov P.L., Ushakov P.A., "Liquid-metal heat transfer in rod bundles" Thermal Engineering, Vol.48, No. 2, 2001, pp 127-133; translated from Teploenergetika

A21. Kazimi M.S., Carelli M.D., "Clinch River Breeder Reactor Plant heat transfer correlation for analysis of CRBRP assemblies" Westinghouse, CRBRP-ARD-0034, 1976.

A22. Waltar A.E., Reynolds A.B., "Fast breeder reactors" Pergamon Press, N.Y. 1981, p. 340

A23. Todreas, N. E. and M. S. Kazimi, 1990, Nuclear Systems I Thermal Hydraulic Fundamentals, Hemisphere Publishing Corporation, New York.

A24. Davis C. B., Shieh A. S., Overview of the Use of ATHENA for Thermal-Hydraulic Analysis of Systems with Lead-Bismuth Coolant, April 2, 2000 – April 6, 2000, 8th International Conference on Nuclear Engineering, INEEL/CON-2000-00127.

A25. Adamov E.O., Orlov V.V., "Naturally safe lead-cooled fast reactor for large-scale nuclear power" Dollezhal RDIPE, Moscow, 2001

A26. Mikityuk K., "Heat transfer to liquid metal: review of data and correlations for tube bundles", Nuclear Engineering and Design 239 (2009) 680–687

A27. Zhukov A.V., et al., "An experimental study of heat transfer in the core of a BREST-OD-300 reactor with lead cooling on models" Thermal Engineering, Vol.49, No.3, 2002, pp. 175-184; translated from Teploenergetika.

A28. Kirillov P.L., Yuriev Y. S., Bobkov V.P., Heat transfer in liquid metals, Report No 3 on the contract 98/59-00867-73, Enea.

A29. Zhukov A.V., Sorokin A.P., Smirnov V.P., Papandin M.V., “Heat transfer in lead-cooled in fast reactors (LCFR)” Advanced Reactor Safety: Proceedings of the International Topic Meeting, Pittsburgh, PA, April 17-21, 1994, American Nuclear Society, vol.1, pp.66-69.

A30. Dwyer O. E., Recent developments in liquid metal heat transfer, Atomic Energy Review, 4, pp.3-92, 1966.

A31. Calamai G. J., et.al, Steady State Thermal and Hydraulic Characteristics of the FFTF Fuel Assemblies, ARD-FRT,1582, June 1974.

APPENDICE B

QUALIFICA DI ALCUNI MODELLI DEL CODICE RELAP5-3D PER LA SIMULAZIONE DELLA TECNOLOGIA A PIOMBO

B.1 Correlazioni di scambio termico utilizzate dal codice RELAP5-3D per la simulazione dei sistemi LFR

Per la valutazione del trasferimento di calore nei metalli liquidi il codice RELAP5-3D usa l'eq. (a3), riportata in Appendice A, come correlazione di default (geometria 100 e 101 nell'input Relap). Tuttavia in [B1] viene consigliata l'eq. (a2) come correlazione più appropriata per lo studio del core del reattore ABTR (Advanced Burner Test Reactor). In questo impianto, infatti, ci si aspetta un profilo di potenza con andamento relativamente piatto per cui l'assunzione di flusso termico costante risulta essere più appropriata rispetto all'ipotesi di temperatura costante. Se si esaminano le condizioni di scambio termico per l'impianto EBR-II (Experimental Breeder Reactor) in condizioni operative normali si valuta che l'eq. (a2) porta ad una predizione del numero di Nusselt superiore di circa il 30% rispetto ai calcoli effettuati facendo ricorso all'eq. (a3).

In alternativa all'opzione di default, per valutazioni di scambio termico in un fascio di tubi (geometria 110 relativa a "vertical Bundle" nell'input Relap), il codice usa l'eq. (a14).

Todreas e Kazimi [B2] hanno verificato che quest'ultima correlazione consente valutazioni accurate dei dati sperimentali caratterizzati da valori del rapporto P/D=1.15, ma sottostima Nu per P/D=1.3. Sulla base di questi risultati gli autori riferiscono che nella simulazione dello scambio termico nel core del reattore EBR-II è prevedibile una sottostima di Nu da parte dell'eq. (a14) di circa il 30%

Sempre in [B2] si riporta una correlazione alternativa messa a punto da Borishanskii et al., come descritto nel paragrafo 2.3 con l'eq. (a11), che consente buone predizioni dei dati sperimentali caratterizzati da più elevati valori del rapporto P/D.

Sulla base delle loro analisi gli autori suggeriscono di modificare il codice Relap5-3D utilizzando quest'ultima correlazione per lo scambio termico in un fascio tubiero.

B.2 Correlazioni per la valutazione delle perdite di carico utilizzate dal codice RELAP5-3D per la simulazione dei sistemi LFR

Per quanto riguarda la valutazione del coefficiente di attrito alla parete, in [B1] vengono messe a confronto i modelli utilizzati dal codice Relap5-3D per lo studio delle perdite di carico e le correlazioni empiriche messe a punto da Cheng e Todreas [B3] per fasci di barre con filo distanziatore.

Le correlazioni del fattore di attrito di Darcy, ottenute da Cheng e Todreas, sono fornite per caratterizzare regimi di moto laminare, turbolento e transizioni secondo le seguenti relazioni:

$\mathrm{Re} < \mathrm{Re}_L$ for the laminar regime where $\mathrm{Re}_L = 10^{1.7(P/D-1)+\log_{10}300}$ and

$Re > Re_T$ for the turbulent regime where $Re_T = 10^{0.7(P/D-1)+4}$ and

$Re_L < Re < Re_T$ for transition regime.

$f_L = C_{fL}/Re$ for the laminar regime

$f_T = C_{fT}/Re^{0.18}$ for the turbulent regime and

$f = f_L(1-\psi)^{1/3} + f_T\psi^{1/3}$ for the transition regime, where

$$C_{fL} = \left\{-974.6 + 1612(P/D) - 598.5(P/D)^2\right\}(H/D)^{0.06-0.085(P/D)}$$

$$C_{fT} = \left\{0.8063 - 0.9022\log_{10}(H/D) + 0.3526(\log_{10}(H/D))^2\right\}(P/D)^{9.7}(H/D)^{1.78-2.0(P/D)} \quad \text{(b1)}$$

$$\psi = \log_{10}(Re/Re_L)/\log_{10}(Re_T/Re_L),$$

Il numero di Reynols tiene in considerazione gli effetti della geometria dei distanziatori attraverso i parametri P/D e H/D, essendo H l'altezza di un avvolgimento dell'elica.

Il modello per la valutazione del coefficiente di attrito impiegato dal codice Relap5-3D contiene correlazioni valide per regime laminare, turbolento, e di transizione, analoghe a quelle utilizzate nelle versioni monodimensionali Relap5/mod3.3 e Relap5/mod3.2.

Per il regime laminare il codice si avvale della soluzione esatta per flusso completamente sviluppato in un tubo di sezione circolare e superficie liscia:

$$f_L = \frac{64}{Re\phi} \quad \text{(b2)}$$

dove ϕ è il fattore di forma che permette all'utente di prendere in esame geometrie diverse dal tubo circolare.

Per il regime turbolento il codice usa la correlazione di Zigrang-Sylvester [B4] che si basa sugli studi di Colebrook-White [B5]:

$$\frac{1}{\sqrt{f_T}} = -2\log_{10}\left(\frac{\varepsilon/D_{hy}}{3.7} + \frac{2.51}{Re}\left(1.14 - 2\log_{10}\left(\frac{\varepsilon}{D_{hy}} + \frac{21.25}{Re^{0.9}}\right)\right)\right) \quad \text{(b3)}$$

Per la regione di transizione si presuppone che essa si verifichi tra i numeri di Reynolds 2200 e 3000, per cui viene impiegata una procedura di interpolazione tra questi due valori secondo la seguente relazione:

$$f = \left(3.75 - \frac{8250}{Re}\right)\left(f_{T,3000} - f_{L,2200}\right) + f_{L,2200} \qquad \text{(b4)}$$

Il modello Relap5-3D, che impiega le eq.s (b2), (b3) e (b4), viene confrontato con le correlazioni di Cheng e Todreas per P/D = 1,3 e H/D = 30, come mostrato in Figura b1.

Il fattore di attrito ricavato con i modelli impiegati nel Relap5-3D coincidono con quelli calcolati con Cheng e Todreas tranne nella regione di transizione, in cui si ha una sottostima di circa il 40% per Re uguale a circa 2200.

Sulla base di questi risultati, in [B1] si sottolinea che i modelli impiegati nel codice RELAP5-3D non hanno la necessità di essere ulteriormente modificati, ritenendoli adatti per la simulazione dei reattori nucleari veloci refrigerati con i metalli liquidi.

Queste considerazioni possono essere estese alle versioni monodimensionali del codice, poiché come già detto utilizzano le stesse correlazioni per la valutazione delle perdite di carico.

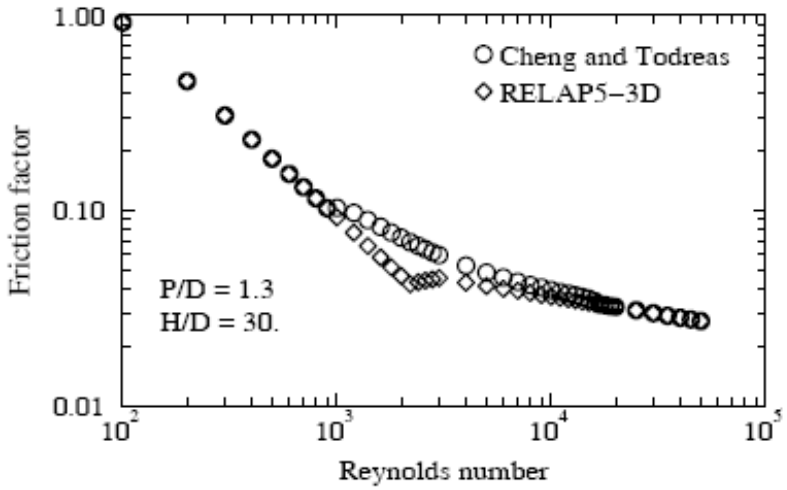

Figura b1. Confronto tra i modelli utilizzati da codice Relap5 per la valutazione del fattore di attrito e le correlazioni empiriche di Cheng e Todreas

B.3 La conduzione nel fluido

Il codice Relap5-3D trascura per l'acqua il fenomeno della conduzione assiale, essendo la conducibilità termica di questo fluido relativamente bassa.

Nel caso di metalli liquidi la conduttività termica è molto maggiore (per il sodio è circa 100 volte più grande), per cui il trasferimento di calore in direzione assiale può assumere un ruolo importante [B6].

Kays and Crawford presentano una regola empirica abbastanza semplice per stabilire se la conduzione assiale può influenzare il trasferimento di calore: cioè la conduzione assiale può essere trascurata se il numero di Peclet è inferiore a 100 [B6].

Il numero medio di Peclet nel core dell'impianto EBR-II durante fasi operative normali è circa 100, mentre in caso di test riguardanti *loss of primary flow* diminuisce di circa un fattore 20. Di contro, gli effetti di conduzione assiale potrebbero essere significativi nelle analisi dell'impianto ABTR, specialmente durante transitori con riduzione della portata, sicché in [B1] viene suggerita la necessità di modificare il codice per lo studio termofluidodinamico del core di questo reattore.

B.4 Stratificazione termica

La stratificazione e miscelazione termica all'interno di un reattore può influenzare significativamente la temperatura di ingresso del fluido e di conseguenza la temperatura della guaina del combustibile durante i transitori di lunga durata [A38]. Questi processi vengono governati da fenomenologie multidimensionali e, sebbene Relap5-3D ha equazioni del momento di tipo tridimensionale, esse non includono il termini viscosi di secondo ordine che determinano il mescolamento turbolento. Ne consegue che il codice non può eseguire calcoli accurati riguardanti processi di miscelazione.

In alcune analisi riportate in [B6], gli effetti di miscelazione e stratificazione termica sono stati trattati attraverso opportuni studi di nodalizzazione, oppure il codice è stato opportunamente accoppiato con calcoli effettuati ricorrendo a codici CFD.

BIBLIOGRAFIA

B1. Davis C. B., Applicability of RELAP5-3D for Thermal-Hydraulic Analyses of a Sodium-Cooled Actinide Burner Test Reactor, Idaho National Laboratory, July 2006, INL/EXT-06-11518.

B2. Todreas, N. E. and M. S. Kazimi, 1990, Nuclear Systems I Thermal Hydraulic Fundamentals, Hemisphere Publishing Corporation, New York.

B3. Cheng, S. K. and N. E. Todreas, 1986, "Hydrodynamic Models and Correlations for Bare and Wire-Wrapped Hexagonal Rod Bundles – Bundle Friction Factors, Subchannel Friction Factors and Mixing Parameters," Nuclear Engineering and Design, 92 (1986), pp. 227 – 251.

B4. Zigrang, D. J. and N. D. Sylvester, 1985, "A Review of Explicit Friction Factor Equations," Transactions of ASME, Journal of Energy Resources Technology, 107, pp. 280-283.

B5. Colebrook, C. F., 1939 "Turbulent Flow in Pipes with Particular Reference to the Transition Region Between Smooth and Rough Pipe Laws," Journal of Institute of Civil Engineers, 11, pp. 133-156.

B6. Kays, W. M. and M. E. Crawford, 1980, Convective Heat and Mass Transfer, Second Edition, McGraw-Hill Book Company, New York.

B7. Mohr, D., L. K. Chang, E. E. Feldman, P. R. Betten, and H. P. Planchon, 1987, "Loss-of-Primary-Flow Without-Scram Tests: Pretest Predictions and Preliminary Results," Nuclear Engineering and Design, 101, pp. 45-56.

APPENDICE C

PUBBLICAZIONI RIGUARDANTI I RISULTATI OTTENUTI NELL'AMBITO DEL LAVORO DI VALIDAZIONE DI ALCUNI MODELLI IMPLEMENTATI NEL CODICE RELAP5/mod3.2β

In questa appendice vengono raccolte alcune pubblicazioni del gruppo di ricerca del DEIM, in cui si riportano parte dei risultati ottenuti nell'ambito del lavoro di validazione del codice RELAP5/mode3.2β, modificato come descritto nel capitolo 2, e che costituiscono parte integrante del presente rapporto.

International Conference
Nuclear Energy for New Europe 2005
Bled, Slovenia, September 5-8, 2005

RELAP5 Modification for CHEOPE Simulations

Maddalena Casamirra, Francesco Castiglia, Mariarosa Giardina
Department of Nuclear Engineering, University of Palermo
V.le delle Scienze, 90128, Palermo, Italy
castiglia@din.unipa.it

Paride Meloni
ENEA, Research Centre "E. Clementel"
Via Martiri di Montesole 4, 40129, Bologna, Italy
paride.meloni@bologna.enea.it

ABSTRACT

Nowadays, an extensive R&D program is in progress in order to maximize the safety of the Lead-Bismuth Eutectic alloy (LBE) ADS plants and optimise their layout. Recently, in the framework of the collaboration between the Department of Nuclear Engineering of the University of Palermo and the ENEA "E. Clementel" Research Centre in Bologna, validation works on the LBE RELAP5mod3.2.2β code, were carried out. The validation was based on the experimental tests performed on the CHEOPE (CHEmical OPErational transient) facility, an experimental rig built up to evaluate the heat transfer performances between the LBE and a diathermic oil secondary fluid, in support to the MEGAPIE (MEGAwatt PIlot Experiment) project, aimed at testing the LBE spallation target technology at 1 MW proton-beam power. As expected, the comparison between the experimental results and post test calculations highlighted not fully satisfactory RELAP5 evaluations of the oil-side heat transfer coefficient, due to RELAP5 code inadequacies in predicting the 3D effects induced in the oil bulk by the facility peculiar geometry, about which is referred in the following. In the present paper we have suitably modified the RELAP5 heat transfer model, to take into account the consequent improved heat transfer conditions. The obtained results show very good performance of the so modified RELAP5 code.

1 INTRODUCTION

The Accelerator Driven Systems (ADSs) seem to supply an adequate answer to the problem of the closure of the nuclear fuel cycle [1]. These systems couple a proton accelerator and a subcritical fission core by means of a spallation target, where the additional neutrons necessary for the criticality are produced. Among the alternatives proposed to the international attention, it is worth to mention the one consisting in a LBE (Lead-Bismuth Eutectic) cooled ADS concept. An example is the XADS (eXperimental Accelerator Driven System) project, an 80 MW_{th} prototype experimental facility in which the LBE circulation is enhanced by resorting to the gas-lift principle [2].

An extensive R&D program is in progress in order to maximize the safety of the LBE ADS plants and to optimise their layout. So, several facilities have been built up in the world,

to support preliminary experimental plant designs and various experimental programs are in progress to investigate different component concepts. Among the most important research initiatives, it is worth to mention the MEGAPIE one, set up in the framework of an international collaboration, aimed at testing the LBE spallation target technology at 1 MW proton-beam power [3].

Recently in the framework of the collaboration between the Department of Nuclear Engineering of the University of Palermo and the ENEA "E. Clementel" Research Centre in Bologna, validation works on the RELAP5mod3.2.2β code [4] (the *best estimate* nuclear code modified to deal with the fluids used in LBE-ADS) were carried out. Among other, this activity was based on the experimental tests performed, in support to the MEGAPIE studies, on the CHEOPE facility, an experimental rig built up to carry out measurements on the heat transfer performances between the lead-bismuth eutectic alloy and a suitable diathermic oil. Indeed this facility was modified to be nothing but a heat exchanger, moreover, to improve the above mentioned performances, a spiral has been welded in the secondary side of the heat exchange element, so as to induce 3D effects in the bulk of the oil.

Due to RELAP5 code inadequacies in making previsions for such effects, it was decided to modify the code heat transfer models so as to take into account the improved heat transfer situation.

In the present paper we refer on the work carried out for the implementation of such model in the code, as well, on the activities performed for the validation of the model by experimental data obtained by CHEOPE [5].

2 THE CHEOPE FACILITY

In the framework of the international agreement with PSI (Paul Scherrer Institut) and other European research organizations about the research program on ADS, it was agreed to design, build and manage a device that could provide thermal fluid dynamic data on the LBE in support to MEGAPIE project. To the aim, new equipment was set up employing some components of CHEOPE device, just working inside the reactor PEC (Prove Elementi Combustibile) area of the ENEA Centre in Brasimone. The device was recently operated to check the heat transfer and thermal stability performance on a prototype of heat exchanger between oil and LBE, similar to one of the 12 heat exchangers to be used in the MEGAPIE experiment.

The CHEOPE experimental equipment consists of two circuits inside of which the organic oil and the LBE separately flow exchanging heat in a heat transfer element (the cooling pin) whose performances have to be tested.

The cooling pin is a bayonet type heat exchanger with three coaxial cylinders (see Figure 1). The Pb-Bi enters the top and, flowing down along the external cylindrical shell (region a, in Figure 1), transfers the power absorbed from the heater to the oil, swimming against the tide in the intermediate shell (region b). Finally, goes out from the bottom coming back to the pump. On the other hand, the oil comes in from the top, flows along the heat exchanger internal shell (region c) and, at the bottom, goes back up flowing through the intermediate annular gap between the internal and the external cylindrical shields. After removing the heat from the Pb-Bi, the oil goes out through a suitable collector and is directed to a areotherm system where it transfers the absorbed heat to the environment. It is worth to note that two organic oils were candidates as secondary coolant: Dowtherm A and Diphyl THT. The first one is endowed with better heat transfer properties, but poorer behaviour under irradiation, vice versa the second. Preliminary numerical simulations [6] showed, that it is possible to use the second one, provided that its heat transfer characteristics were improved, promoting turbulence inside of it. As previously said, to this aim a metallic wire was helicoidally welded

on the external surface of the most internal cylinder (rising oil side). This, forces the flow to rotate while rising, so producing a helical flow superimposed to the axial one, then increasing the main flow velocity. It follows that the oil path become similar to that inside a helical duct, with an almost rectangular section. What's more, the helical wire behaves like roughness elements which affect the velocity distribution, the turbulence level and the turbulent wall shear.

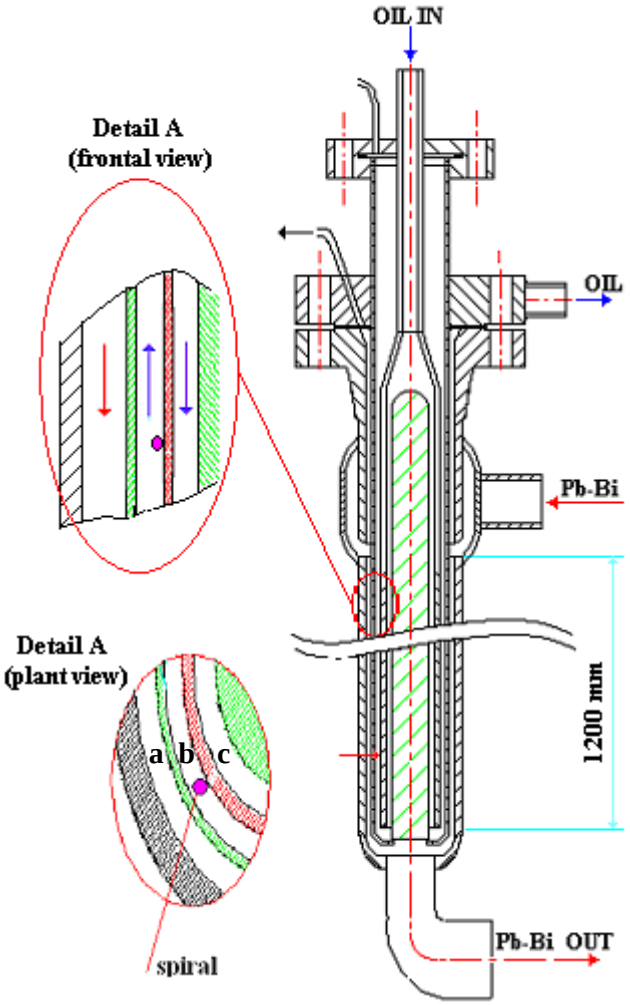

Fig. 1: Cooling pin

Table 1 reports the facility nominal conditions and the main pin cooling geometrical parameters.

Table 1: CHEOPE facility nominal conditions and main pin cooling geometrical parameters.

LBE mass flow rate	0.33 l/s	Heat exchanger height	1200 mm
Oil mass flow rate	0.83 l/s	Spiral diameter	1.5 mm
LBE inlet temperature	623.15 K	Oil annulus internal diameter	47 mm
Oil inlet temperature	413.15 K	Oil annulus width	2.1 mm
LBE Reynolds number	40660	Steel wall width	1.5 mm
Oil Reynolds number	6386	PbBi annulus width	4.25 mm

The test section has been equipped with 18 suitably located thermocouples, in order to gather temperatures. Flow meters and differential pressure meters have been inserted to check the parameter involved in the heat transfer phenomena.

3 RELAP5 CODE MODIFICATION

As it is known, the RELAP5Mod3.2.2β code, as it is, does not include the peculiar geometry nor the thermalfluidynamics to deal with the matter at hand. Therefore, it does not allow to take into account the improved heat transfer situation. So, we have decided to supplement the code with a suitable model which, traduced in FORTRAN subroutines, could allow to evaluate a heat transfer coefficient able to simulate the thermal exchange situation.

The thermal-hydraulic behavior of fluids along helical pipes is not yet well understood. In any case, collecting experimental results, various authors [7-9] suggested many correlations (unfortunately not always in agreement to one another) to be used to calculate heat transfer and friction factors in curved tubes.

Among the correlations available in literature we thought to utilize, as given also in [10], the Gnielinski correlation [11] for the heat transfer, together with the Ito's proposals [12] for friction factors.

Indeed, an equation developed by Gnielinski especially for technical proposal has been used. Such an equation, at first obtained for straight tubes [13], subsequently has been extensively tested also for curved ducts and, provided suitable friction factors are employed together it, good performances in foreseen the Nusselt number, also in this case, has been found. The formula is:

$$Nu = \frac{(f_c/2)\,Re\,Pr}{1+12.7\sqrt{f_c/2}\left(Pr^{2/3}-1\right)}\left(\frac{Pr}{Pr_w}\right)^{0.14} \qquad (1)$$

where Nu, Re and Pr are, in the order, the Nusselt, Reynolds and the Prandtl number; Pr_w is the Pr evaluated at wall temperature and, finally, f_c is the Fanning friction factor.
The Fanning friction factor losses from Ito's proposals are shown in Table 3 at different Reynolds number intervals.

Table 3: Fanning friction factor losses from Ito's proposals.

$f_c = \frac{16}{Re}$	$Re < 13.5(D/d)^{-0.5}$
$f_c = \frac{344(D/d)^{-0.5}}{\left\{1.56+\log_{10}\left[Re(D/d)^{-0.5}\right]\right\}^{5.73}}$	$13.5(D/d)^{-0.5} < Re < 2000\left[1+13.2(D/d)^{-0.6}\right]$
$f_c = 0.076Re^{-0.25}+0.0075\left(\frac{D}{d}\right)^{-0.5}$	$Re > 15000$

In Table 3 *D* is the effective helically coiled tube diameter and *d* the internal duct one.

As above said, since in CHEOPE the spiral in the oil cylindrical channel induces a horizontal component of velocity to the oil rising axially the annular gap, the oil path results similar to that inside a helical duct, where the *D* is the internal diameter of the intermediate shell (region b in Figure 1), and *d* is the hydraulic equivalent diameter of the oil cross section, in helical flow (see Figure 2).

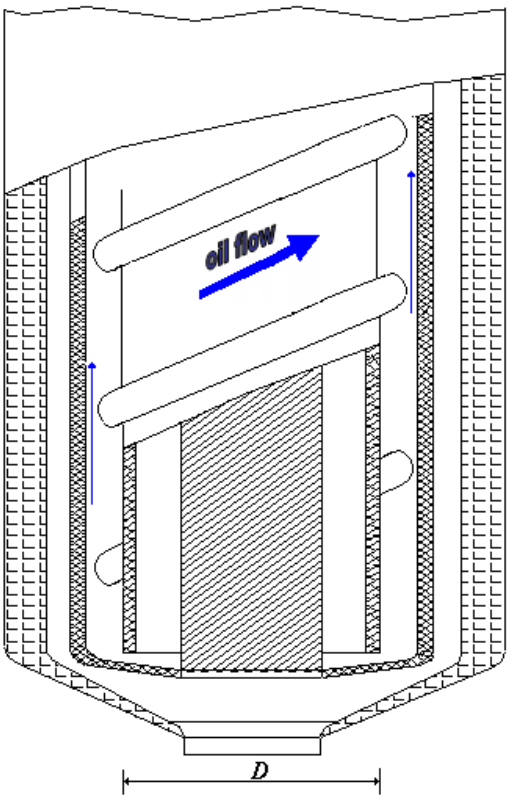

Fig. 2: sketch of the cooling pin

It is to be remarked that, so doing, the resulting geometry simulates the effective flow situation only approximately. In fact, as there is a tolerance between the spiral and the oil shell, it there will be some very small vertical out flow whose effects will not be accounted for. Owing to the foreseeable poor extent of such effects, for the moment we decided to pass by this aspect.

4 RELAP5 NODALIZATION

Figure 3 shows the nodalization used for the Relap5Mod3.2.2β analyses.

The cooling pin has been schematized by tree vertical annuli, respectively numbered as 520, 530, 460 , each one subdivided in 21 sub-volumes, the first one 0.078 m length and all the others 0.0561 m length. As the analyzed experiments are performed in steady state conditions, during the test the LBE and oil mass flow rates keep constant values, therefore no pumps have been schematized and the constant mass flows are assured by the two time dependent junctions 105 and 345, for LBE and oil, respectively.

To simulate the power absorbed by LBE in the heater the heat structure 1410 has been used. Moreover, to better simulate the heat transfer inside the cooling pin, several heat structures have been introduced. In particular, in the central zone, the heat structure 1520, subdivided in 21 sub-structures on the base of the vertical subdivision of the above mentioned annuli, simulates the exchanged power between the flowing down oil and the one rising the intermediate cylindrical shell, whereas the heat structure 1530, also this subdivided in 21 sub-volumes, allows to represent the heat transfer surface between oil and LBE.

In the annulus 530, which schematizes the region where the spiral welded is located, we have imposed a flag for the application of the Gnielinski heat transfer correlation.

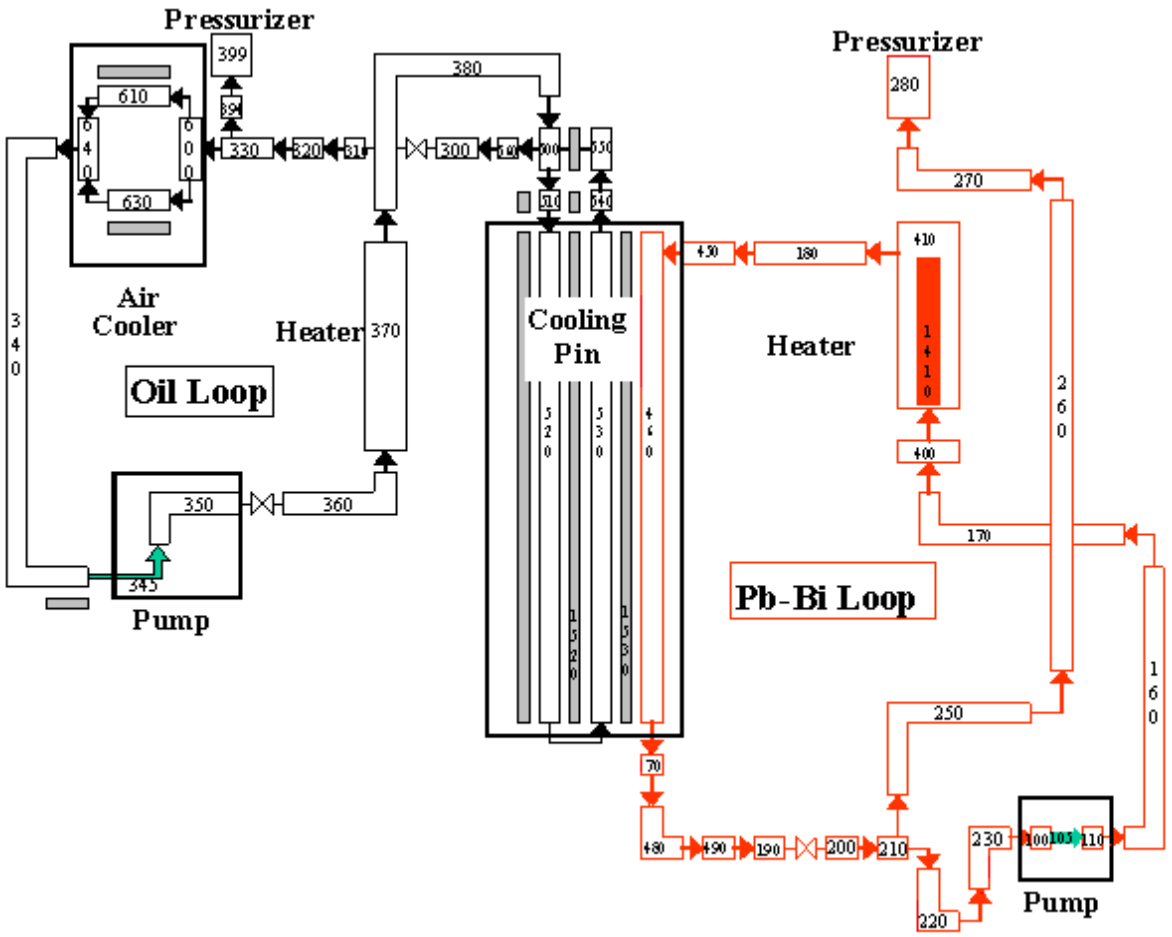

Fig. 3: RELAP5 nodalization

5 RELAP5 ANALYSES

For these analyses it was referred to a couple of test conditions termed E1 and E2, as well to the relevant experimental data supplied by the ENEA Centre in Brasimone [5]. Table 3 shows the test imposed conditions and the main experimental results.

Table 3: RELAP5 imposed conditions relevant the E1 and E2 tests

	E1	E2
Power [W]	27430	21590
LBE mass flow [l/s]	0.147	0.155
Oil mass flow [l/s]	0.563	0.556
LBE inlet T [K]	579.05	537.25
Oil inlet T [K]	410.15	409.35
LBE outlet T [K]	455.95	445.85
Oil outlet T [K]	436.65	430.25
Pressure in the LBE pressurizer (MPa)	1.1E5	1.1E5
Pressure in the Oil pressurizer (MPa)	1.1E5	1.1E5

Table 4 reports, in terms of oil and LBE inlet and outlet temperatures, the comparison between the experimental data and the results obtained in the simulation by modified RELAP5 code. As a reference, also reported in Table 4 are the results obtained by using the

not modified code. The input data are the LBE and oil mass flows, the power absorbed by LBE in the heater and the oil inlet temperature.

The results obtained by using the modified RELAP5 code show very good agreement between experimental data and calculated results, the percent error being around 1% only in one case whereas in the others cases is of an order of magnitude lower.

Table 4: Comparison between the experimental data and the RELAP5 simulations

	E1			E2		
	experim.	unmodified	modified	experim.	unmodified	modified
Power [W]	27430			21590		
Oil inlet T [K]	410.15			409.35		
Oil outlet T [K]	436.65	436.90	436.90	430.25	430.79	430.8
LBE inlet T [K]	579.05	592.31	579.94	537.25	550.82	535.33
LBE outlet T [K]	455.95	473.19	461.38	445.85	462.64	447.71

Table 5 reports the logarithmic mean temperature difference, LMTD, defined as:

$$LMTD = \frac{(T_{finlet} - T_{winlet}) - (T_{fout} - T_{wout})}{\ln \frac{T_{finlet} - T_{winlet}}{T_{fout} - T_{wout}}} \quad (2)$$

where T_{finlet} and T_{winlet} are, respectively, the fluid (LBE or Oil) and the wall temperatures at the inlet and T_{fout} and T_{wout} the corresponding ones at the outlet (one of the components of the global heat exchange capability) whose percent errors result 4.7% and 0.4% for E1 and E2 cases respectively, however collapsing from 20% and 25% relevant the not modified case.

It should be noted that the results obtained by using the not modified RELAP5 code, whereas reproduce in good way the oil outlet temperatures, show, as it was expected, not so negligible overestimate of the Pb-Bi inlet and outlet temperatures. Such overestimate has obviously to be charged to the code underestimate of the global heat transfer coefficient, which just induced us to add a different heat transfer model in the code. Table 5 reports the global heat exchange evaluation, together with the relevant error, performed by using the code temperature results in conjunction with LMTD method.

Table 5: LMTD, and global heat exchange coefficient

	E1			E2		
	experim.	unmodified	modified	experim.	unmodified	modified
LMTD	85.16	102.37	89.16	65.55	82.19	65.81
Percent error		20.21%	4.7%		25.39%	0.4%
H global W/(m^2K)]	1790.04	1407.2	1596.68	1831.14	1368.57	1714.52
Percent error		21.4%	10.8%		25.3%	6.4%

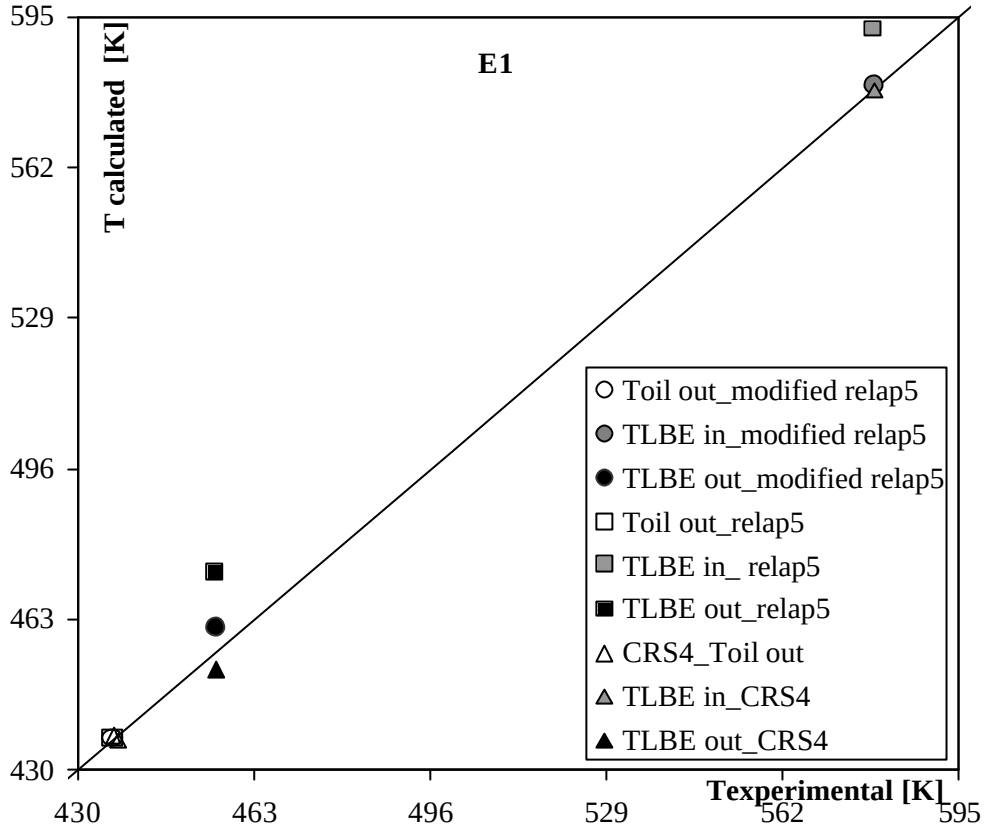

Figure 4 : inlet and outlet calculated temperatures against experimental ones, for E1 test

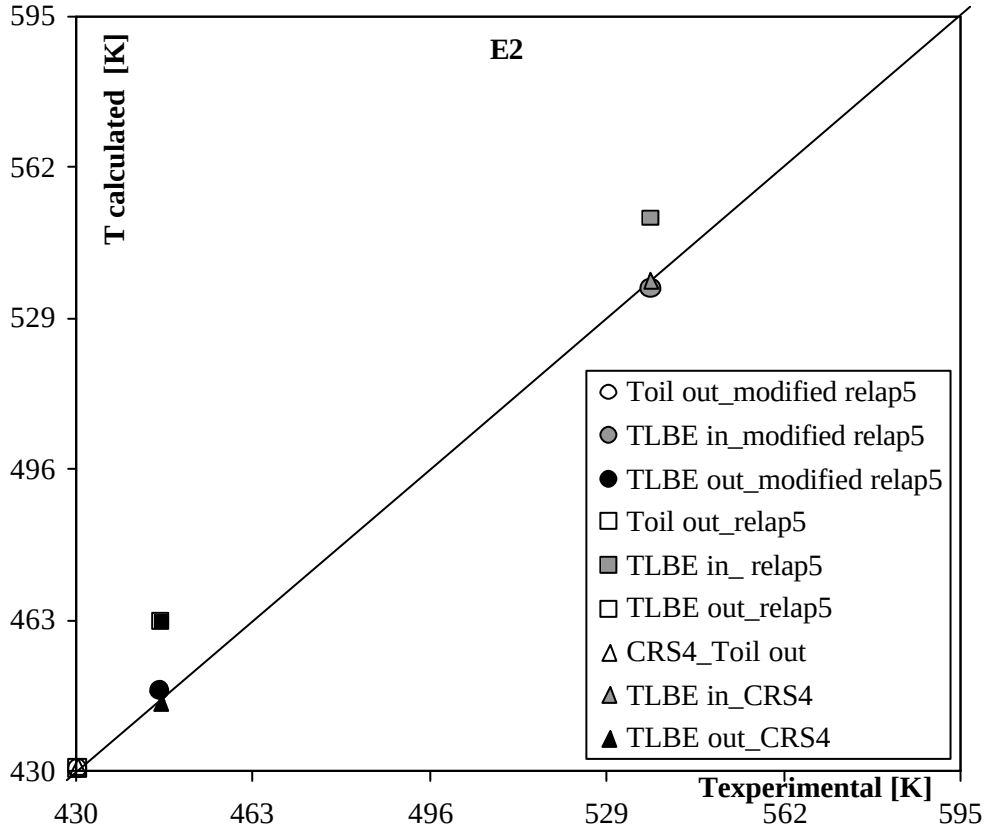

Figure 5: inlet and outlet calculated temperatures against experimental ones, for E2 test

In order to have an independent confirmation of the results, a comparison has been made with data computed by CRS4 Institution [6] using the STAR-CD 3Dym code with a very accurate meshing, as one can see in Figures 4 and 5 where the inlet and outlet temperatures of the both fluids are reported, for the two cases E1 and E2, respectively.

6 CONCLUSIONS

The present paper dealt with the validation works of the RELAP5mod3.2.2β code, the well known nuclear *best estimate* code, modified to deal with the fluids used in LBE-ADS plants, that have been carried out in the framework of a collaboration between the Department of Nuclear Engineering of the University of Palermo and the ENEA "E. Clementel" Research Centre in Bologna.

This validation has been performed by using the experimental data supplied by ENEA Research Centre in Brasimone, in the framework of XADS and MEGAPIE projects. The experimental tests have been carried out by using the CHEOPE facility, an experimental rig already working for research activities in the area of the Italian fast reactor PEC, suitable fitted to check the heat transfer performances of 1 of the 12 heat exchangers foreseen in the MEGAPIE demonstration facility.

It is worth to note that a metallic spiral has been welded on the surface of the oil rising shell, in order to improve the oil turbulence and then enhance the heat transfer.

As the RELAP5 thermalhydraulical models are not able to deal with the peculiar geometry of the so modified region, we have thought to add an additional heat transfer model in the code, to take into account the improved heat transfer conditions and to test at which extent it was possible to better approach the experimental results by using a one-dimensional code.

To the purpose, we have introduced some new subroutines which allowed the code to evaluate the heat transfer situation by using the Gnielinski correlation [11] oil side. In fact, the spiral there induces a helical flow component.

The performed simulations produced very good agreement between the experimental data and code calculations.

In order to have an independent confirmation of the results obtained by us, a comparison has been made with data computed by CRS4 using a 3Dym code.

This comparison resulted quite satisfactory.

Finally, a more refined modellization ought to be adopted in order to account for the effect of a slight vertical flow, due to the tolerance between the spiral and the oil shell, and this with minor effort. However, given the obtained results, this could be the subject of further deepening, if is the case.

ACKNOWLEDGMENTS

We would like to tank the ENEA research Centre in Brasimone for supplying the experimental data.

Work supported by the Ministero della Istruzione dell'Università e della Ricerca (MIUR): PRIN 2004, and by ENEA funds: contract November 2003, n° FIS/2003/3980.

REFERENCES

[1] C. Rubbia, J.A. Rubio, S. Buono, F. Carminati, N. Fiétier, J. Galvez, C. Gelès, Y. Kadi, R. Klapisch, P. Mandrillon, J.P. Revol and Ch. Roche, Conceptual Design of a Fast Neutron Operated Hugh Power Energy Amplifier, European Organisation for Nuclear Research, CERN/AT/95-44 (ET), Geneva, 29th September, 1995.

[2] L. Cinotti and G. Gherardi, The Pb-Bi Cooled XADS Status of Development, Proceedings of the II International OECD Workshop on Materials for Hybrid Reactors and Related Technologies, Brasimone, Italy, April 18-21, 2001.

[3] G.S. Bauer1, M. Salvatores, and G. Heusener: MEGAPIE, a 1 MW pilot experiment for a liquid metal spallation target, Journal of Nuclear Materials, Vol. 296, pp17-33, 2001.

[4] C.D. Fletcher, R.R. Scuhltz, RELAP5/MOD3 Code manual, NUREG/CR–5535, INEL–95/174, Idaho National Engineering Laboratory, June 1995.

[5] P. Agostini, Observation resulting from MEGAPIE cooling pin tests in Brasimone, Derivable 22A MEGAPIE – TEST, EU Project No. FIKW-CT-2001-00159 (PU).

[6] S. Buono, L. Maciocco, V. Moreau, L. Sorrentino, Optimisation of the Pin Cooler design for the Megapie Target using full 3D numerical simulations, CRS4-Technical Report DRAFT v1.22, January 18th 2002

[7] P.Kumar, R. L. Judd, Heat Transfer with Coiled Wire Turbulence Promoters, The Canadian Journal of Chemical Engineering, 48, 1970, pp. 378-383.

[8] R. Sethumadhavan, M. Raja Rao, Turbulent Flow Heat Transfer and Fluid Friction in Helical-wire-Coil-Inserted Tubes, International Journal of Heat and Mass Transfer, Vol. 26, 1983, pp. 1833-1845.

[9] Vicari, K. F. F. & Möller, S. V., Characteristics of the Turbulent Flow in Pipes with Helical Turbulence Promoters, Proceedings of the llth Symposium on Turbulent Shear Flows, Grenoble, France, 1997 vol. 2, P2-49 - P2-54.

[10] R. Bongiorni, Thermal hydraulic features of helical coil ducts and pressure drop experiments in turbulent and laminar flow for several geometries, Degree Thesis, Politecnico of Milano, Italy, 2003.

[11] V. Gnielinski, Helically coiled tubes of circular cross sections, Hemisphere Publishing Corporation, 1987.

[12] H. Ito, Friction factors for turbulent flow in curved pipes, Journal of Basic Engineering, Trans. Amer. Soc. Mech. Engrs., Vol. D81, 1959, pp123-134.

[13] V. Gnielinski, New Equations for Heat and Mass Transfer in Turbulent Pipe and Channel Flow, International Chemical Engineering, Vol. 16, 1976, pp. 359-368.

RELAP5 SIMULATIONS FOR CHEOPE EXPERIMENTS

Francesco Castiglia [1]
Department of Nuclear Engineering, University of Palermo, V.le delle Scienze, 90128, Palermo, Italy
Phone: +39 091 232 252, Fax: +39 091 232 215, e-mail: castiglia@din.unipa.it

Maddalena Casamirra, Mariarosa Giardina
Department of Nuclear Engineering, University of Palermo, V.le delle Scienze, 90128, Palermo, Italy
mdcasamirra@din.unipa.it, mgiardina@din.unipa.it

Paride Meloni, Giuseppe Morana
ENEA, Research Center "E. Clementel",Via Martiri di Montesole 4, 40129, Bologna, Italy
paride.meloni@bologna.enea.it

ABSTRACT

Nowadays, an extensive R&D program is in progress in order to maximize the safety of the Lead-Bismuth Eutectic alloy (LBE) ADS plants and optimise their layout. Recently, in the framework of a collaboration between the Department of nuclear engineering of the Palermo University and the ENEA "E. Clementel" Research Centre of Bologna, validation works on the RELAP5mod3.2.2β, a *best estimate* nuclear code, modified to deal with the fluids used in LBE-ADS, were carried out. This validation was based on the experimental tests performed on the CHEOPE (CHEmical OPErational transient) facility, an experimental rig built up to evaluate the heat transfer performances between the LBE and a diathermic oil secondary fluid, in the framework of the MEGAPIE (MEGAwatt PIlot Experiment) project, aimed at testing the LBE spallation target technology at 1 MW proton-beam power. The comparison between the experimental results and post test calculations highlighted not fully satisfactory evaluations of the oil-side heat transfer coefficient, due to RELAP5mod3.2.2β code inadequacies in predicting the 3Dym. effects induced in the oil bulk by the facility peculiar geometry. In the present paper we have stressed the RELAP5 heat transfer models to test at which extent it was possible to better approach the experimental results.

KEYWORDS

ADS, LBE, heat transfer.

1. INTRODUCTION

The Accelerator Driven Systems (ADSs) seem to supply an adequate answer to the problem of the closure of the nuclear fuel cycle (Rubbia *et al.*, 1995). These systems couple a proton accelerator and a subcritical fission core by means of a spallation target, where the additional neutrons necessary for the criticality are produced. Among the alternatives proposed to the international attention, it is worth to mention the one consisting in a LBE (Lead-Bismuth Eutectic) cooled ADS concept. An example is the Ansaldo XADS (eXperimental Accelerator Driven System) project, an $80MW_{th}$ prototype experimental facility in which the LBE circulation is enhanced by resorting to the gas-lift principle (Cinotti and Gherardi, 2001).

An extensive R&D program is in progress in order to maximize the safety of the LBE ADS plants

[1] Corresponding author

and to optimise their layout. In this framework, a lot of facilities have been built up in the world, to support preliminary experimental plant designs and several experimental programs are in progress to investigate different component concepts. Among the most important research initiatives, we mention the MEGAPIE one, set up in the framework of a collaboration between European and Japanese research centres, aimed at testing the LBE spallation target technology at 1 MW proton-beam power (Agostini, 2001).

Recently in the framework of a collaboration between the Department of nuclear engineering of the Palermo University and the ENEA "E. Clementel" Research Centre of Bologna, validation works on the RELAP5mod3.2.2β (Fletcher and Scuhltz, 1995), the *best estimate* nuclear code modified to deal with the fluids used in LBE-ADS, were carried out. This validation was based on the experimental tests performed on the CHEOPE facility, an experimental rig built up to measure the thermal exchange characteristics between the lead-bismuth eutectic alloy and a diathermic oil secondary fluid. The comparison between experimental results (Agostini, 2001) and post test calculations highlighted not fully satisfactory evaluations of the oil-side heat transfer coefficient, due to RELAP5mod3.2.2β code inadequacies in making previsions for the 3Dym. effects induced in the oil bulk by a suitable spiral welded in the secondary side of the heat exchange element with the aim to improve the heat transfer. Before to resort to 3 Dym. analyses we want to continue to use the RELAP5 code, by stressing its heat transfer models, as it will shown in the following.

2. THE CHEOPE FACILITY

In the framework of the research program on ADS, and of the international agreement with PSI (Paul Scherrer Institut) and other European research organizations, it was agreed to design, build and manage a device that could furnish thermal fluid dynamic data on LBE. To the aim a new equipment was set up employing some components of CHEOPE device, just working inside the reactor PEC (Prove Elementi Combustibile) area of the ENEA Centre of Brasimone. The device was recently employed to check the thermal exchange and thermal stability performance on a prototype of heat exchanger (cooling pin) between oil and LBE, analogous to the devices to be employed in the MEGAPIE experiment.

The CHEOPE experimental equipment (Figure 1) consists of two circuits inside of which the organic oil and the LBE separately flow, and of a heat exchanger (the cooling pin) whose performance have to be tested. The thermal power generated by spallation reactions in MEGAPIE has to be suitably removed by a diathermic oil inside suitable heat exchangers. The cooling pin just reproduces one of the 12 heat exchangers foreseen in MEGAPIE, the two circuits reproducing the boundary conditions.

The cooling pin is a bayonet type heat exchanger with three coaxial cylinders (see Figure 2). The Pb-Bi enters the top and, flowing down along the external cylindrical shell, transfers to the oil, swimming against the tide in the intermediate shell, the power absorbed from the heater and, finally, goes out from the bottom coming back to the pump.

The oil comes in from the top, flows along the heat exchanger internal shell and, at the bottom, goes back up flowing through the intermediate annular gap between the internal and the external cylindrical shields. After removing the power from the Pb-Bi, the oil goes out through a suitable collector and is directed to a system of areotherms to transfer the absorbed power to the environment. It is worth to note that, on the basis of preliminary heat transfer considerations, a metallic spiral has been welded on the external surface of the most internal cylinder (rising oil side) with the aim to improve the turbulence of the oil rising the annular gap.

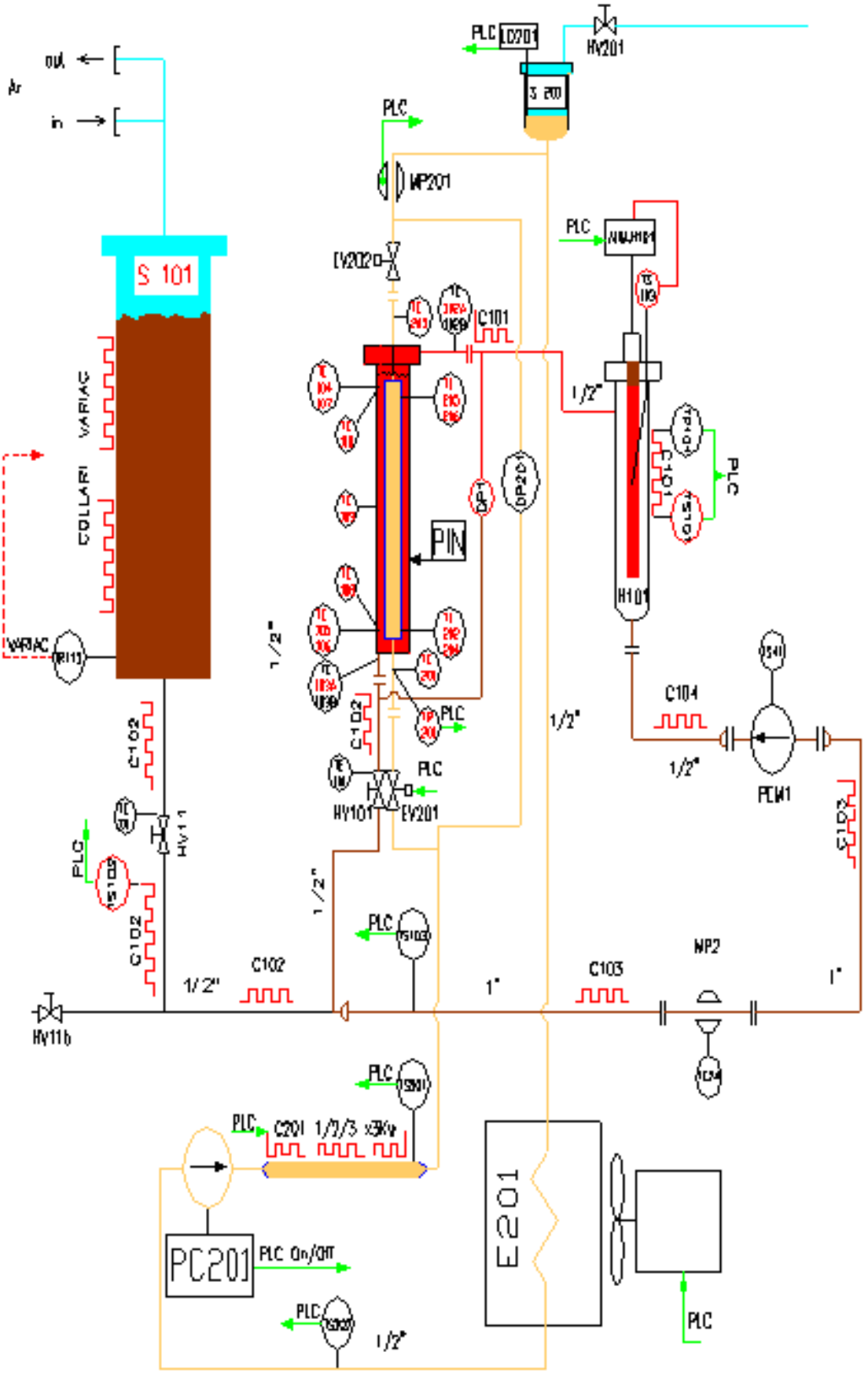

Fig. 1: CHEOPE facility flow plan

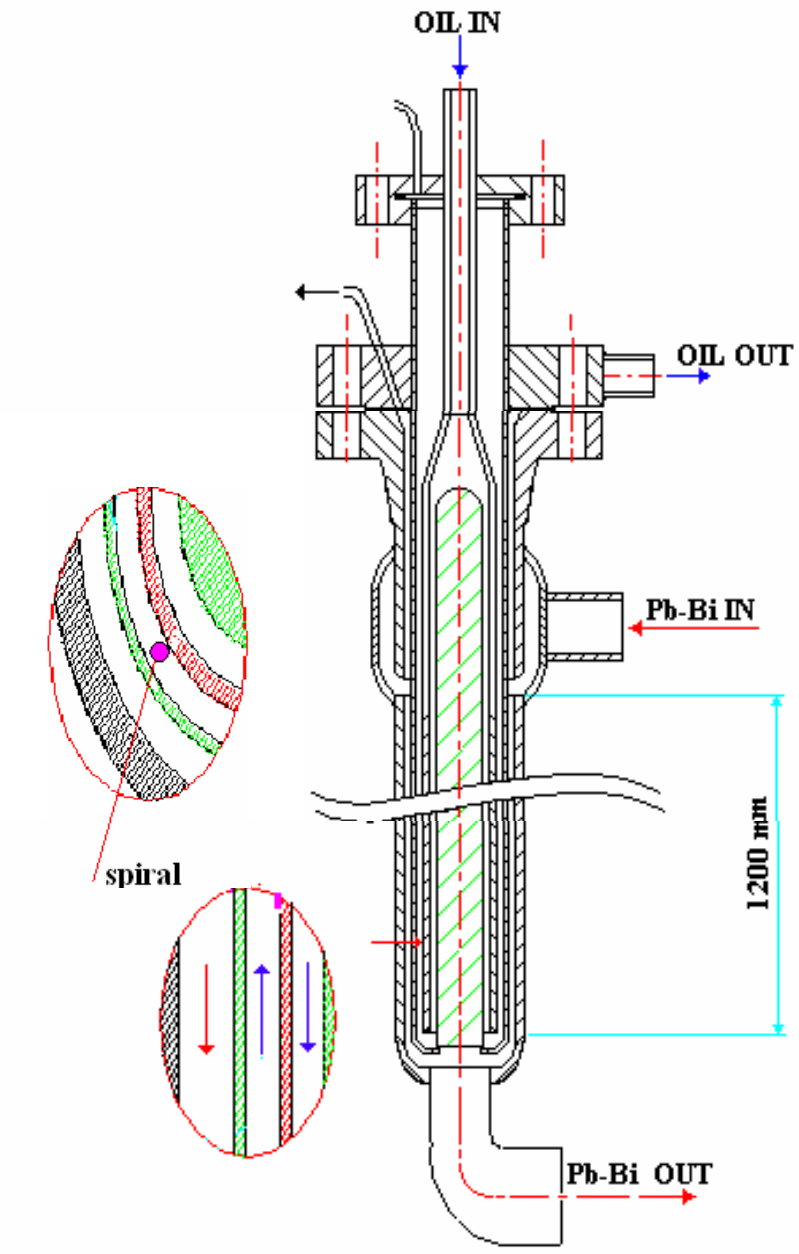

Fig. 2: cooling pin

In Table 1 the facility nominal conditions are reported.

LBE mass flow rate	0.33 l/s
Oil mass flow rate	0.83 l/s
LBE inlet temperature	350°C
Oil inlet temperature	140°C
LBE Reynolds number	40660
Oil Reynolds number	6386

Table 1

Table 2 shows the main pin cooling geometrical parameters.

Heat exchanger high	1200 mm
Spiral diameter	1.5 mm
Oil annulus internal diameter	47 mm
Oil annulus width	2.1 mm
Steel wall width	1.5 mm
PbBi annulus width	4.25 mm

Table 2

In order to gather the temperatures, the test section has been equipped with 18 suitably located thermocouples. Moreover, flow and differential pressure meters have been inserted with the aim to check the parameter involved in the heat transfer phenomena.

3. RELAP5 NODALIZATION

Figure 3 shows the nodalization used for the Relap5 Mod3.2.2β analyses.

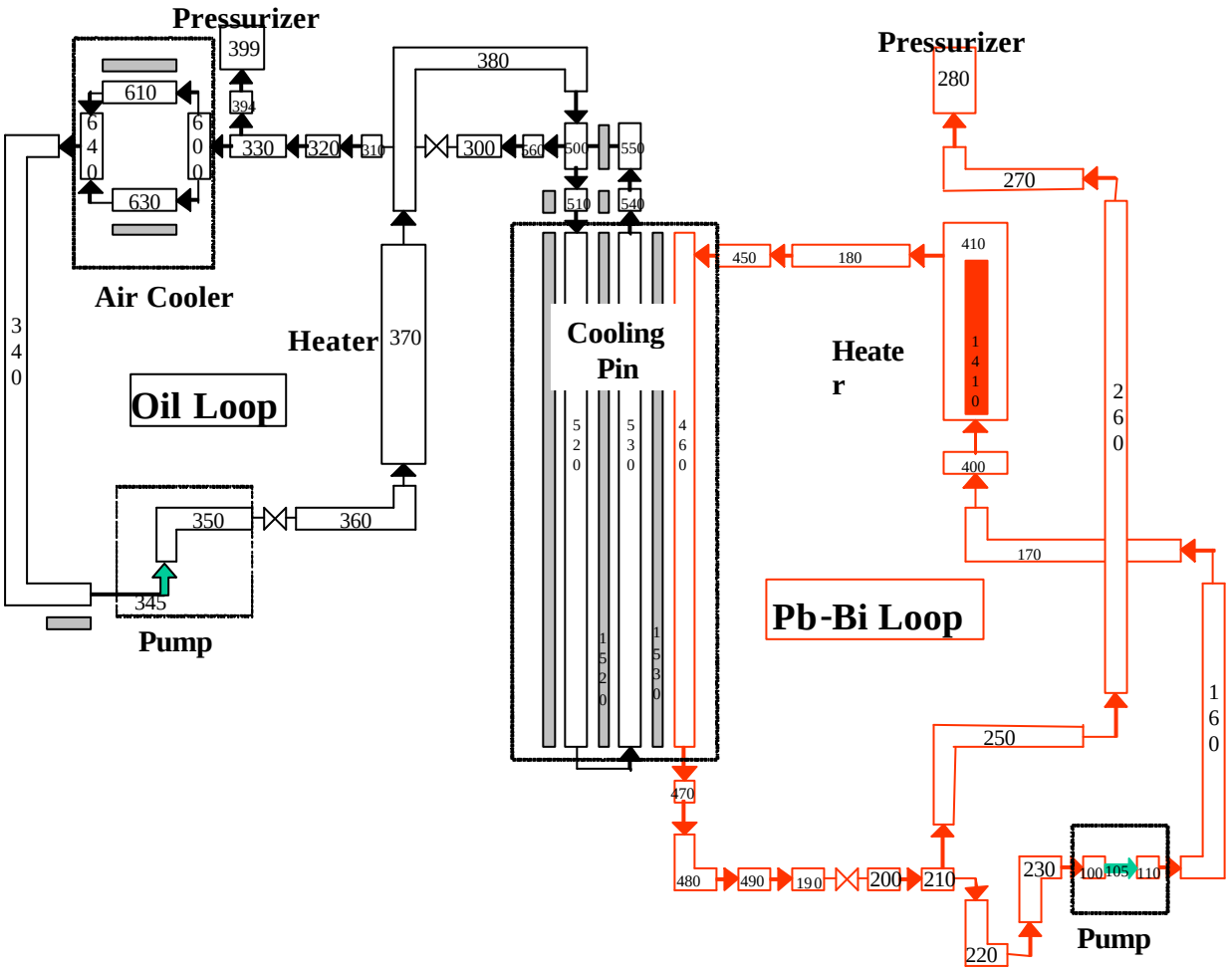

Fig. 3: RELAP nodalization

The cooling pin has been schematized by the tree annulus (520, 530 460). Because during the test the LBE and oil mass flow rates keep constant values, no pumps have been schematized and the mass flow is granted by the two time dependent junction 105 and 345, for LBE and oil respectively.

To simulate the power absorbed by LBE in the heater the heat structure 1410has been used. Moreover, to simulate the heat exchange inside the cooling pin several heat structures have been introduced. In particular, in the central zone, the heat structure 1520 simulates the power exchange between the flowing down oil and the one rising the intermediate cylindrical shell, whereas the heat structure 1530 allows to reproduce the heat transfer between oil and LBE.

4. RELAP5 ANALYSES

For these analyses it was referred to a couple of test conditions termed E1 and E2, together with the relevant experimental data supplied, as previously said, by the ENEA Centre of Brasimone (Agostini, 2001). Table 3 shows the main test imposed conditions and experimental results.

	E1	E2
Power [W]	27430	21590
LBE mass flow [l/s]	0.147	0.155
Oil mass flow [l/s]	0.563	0.556
LBE inlet T [K]	579.05	537.25
Oil inlet T [K]	410.15	409.35
LBE outlet T [K]	455.95	445.85
Oil outlet T [K]	436.65	430.25

Table 3

In Table 4 the comparison between the experimental data and the results obtained in the RELAP5Mod.3.2.2β simulations are reported. As in the experiments, the LBE and oil mass flow, the power and the oil inlet temperature have been imposed as input data.

	E1		E2	
	experim.	RELAP	experim.	RELAP
Power [W]	27430		21590	
LBE inlet T [K]	579.05	592.31	537.25	550.82
Oil inlet T [K]	410.15		409.35	
LBE outlet T [K]	455.95	473.19	445.85	462.64
Oil outlet T [K]	436.65	436.90	430.25	430.79

Table 4

These results whereas reproduce in excellent way the oil outlet temperatures, show a code overestimate of the Pb-Bi inlet and outlet temperatures, however with maximum percent error less than 4%. Such overestimate has obviously to be charged to the code underestimate of the total heat transfer coefficient. In fact, the evaluation of it, performed by using the code temperature results in conjunction with logarithmic mean temperature difference method, confirms this assumpion as shown in Table 5.

	E1		E2	
	experim.	RELAP5	experim.	RELAP5
H global [W/(m^{2}K)]	1790,04	1407,2	1831,14	1368,57

Table 5

Indeed, as it is known, the RELAP5Mod.3.2.2β is a one-dimensional code and, as such, it doesn't allow to simulate the oil side 3Dym. effects brought about by the spiral introduction.

Therefore, the study of the resulting geometric configuration should be done by using 3Dym models. Nevertheless, also in consideration of the excellent results for the oil outlet temperatures and of the not so striking percent error as for the LBE temperatures, it was thought, for the moment, to test at which extent, suitably modifying appropriate parameters in code input, it was possible to better approach the experimental results.

In particular, it was chosen to perform a sensitivity analysis on the equivalent hydraulic diameter (D_h) of the oil rising annular gap.

By the light of the above considerations, after the first analyses, carried out with the above said equivalent hydraulic diameter equal to the nominal one, a further series of analyses were carried out reducing D_h between 80% up to 20% of its nominal value.

These analyses show that, for a value of equivalent hydraulic diameter equal to 30% of the nominal one, a good agreement between the calculated and the experimental data is found, both for the two tests E1 and E2, as shown in Table 6.

D_h 30%	E1		E2	
	experim.	RELAP5	experim.	RELAP5
Power [W]	27430		21590	
LBE inlet T [K]	579.05	578.76	537.25	539.71
Oil inlet T [K]	410.15		409.35	
LBE outlet T [K]	455.95	460.25	445.85	451.91
Oil outlet T [K]	436.65	436.92	430.25	430.82

Table 6

In particular, in Table 6 one can see that the LBE inlet and outlet temperatures are a few far from the experimental values with a percent error as low as nearly 1%. In Figure 4 the code temperatures are reported, against the experimental ones, in the whole for the two tests E1 and E2. It was believed not suitable to further reduce the Dh parameter.

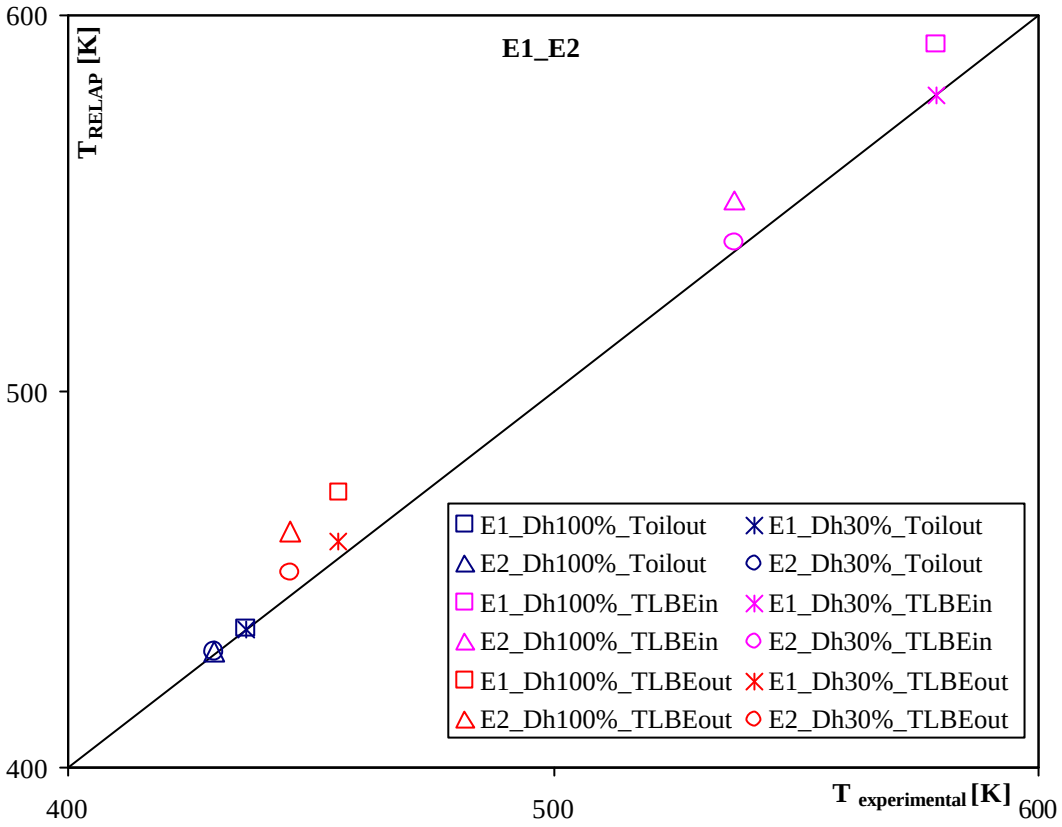

Fig. 4

Finally, Table 7 shows the comparison between the global heat transfer coefficient values, evaluated as just above said, for the modified situation taken in consideration.

D_h 30%	E1		E2	
	experim.	RELAP5	experim.	RELAP5
H global [W/(m^{2}K)]	1790,04	1674,08	1831,14	1568,17

Table 7

5. CONCLUSIONS

The present paper dealt with the validation works of the RELAP5mod3.2.2β code, the well known nuclear *best estimate* code, modified to deal with the fluids used in LBE-ADS plants, that have been carried out in the framework of a collaboration between the Department of nuclear engineering of the University of Palermo and the ENEA "E. Clementel" Research Centre of Bologna.

This validation has been performed with the aid of the experimental data supplied by ENEA Research Centre of Brasimone, in the framework of XADS and MEGAPIE projects. The experimental tests have been carried out by using the CHEOPE facility, an experimental rig already working at ENEA of Brasimone for research activities in the area of the Italian fast reactor PEC, suitable fitted with the aim to test the heat transfer characteristics between the lead-bismuth eutectic alloy and a diathermic oil. The test allowed to check the heat transfer performance of one of the 12 heat exchange elements (cooling pin) designed for the MEGAPIE demonstration facility.

It is worth to note that a metallic spiral has been welded on the surface of the oil rising shell, in order to improve the oil turbulence.

The obtained results suffer for the inadequacies of the RELAP5 models in taking into account the thermalhydraulic phenomenologies involved by the peculiar geometry of this region which, due to the undergone geometric modifications, should be investigated by means of 3Dym heat transfer models. Before to do this, we thought to stress the code as it is performances, by changing the equivalent hydraulic diameter of the rising oil shell in the code input, with the aim to test the extent at which the code can furnish better predictions, rather to reproduce the physical phenomenology.

The obtained results seem to be quite satisfactory.

ACKNOWLEDGEMENTS

We would like to tank the ENEA research Center of Brasimone for supplying the experimental data.

Work supported by the Ministero della Istruzione dell'Università e della Ricerca (MIUR): PRIN 2004, and by ENEA funds: contract November 2003, n° FIS/2003/3980.

REFERENCES AND CITATIONS

P. Agostini, *Observation resulting from MEGAPIE cooling pin tests in Brasimone*, Derivable 22A MEGAPIE – TEST, EU Project No. FIKW-CT-2001-00159 (PU)

L. Cinotti and G. Gherardi, *The Pb-Bi Cooled XADS Status of Development*, Proceedings of the II International OECD Workshop on Materials for Hybrid Reactors and Related Technologies, Brasimone, Italy, April 18-21, 2001.

C.D. Fletcher, R.R. Scuhltz, *RELAP5/MOD3 Code manual, NUREG/CR–5535, INEL–95/174*, Idaho National Engineering Laboratory, Giugno 1995.

C. Rubbia, J.A. Rubio, S. Buono, F. Carminati, N. Fiétier, J. Galvez, C. Gelès, Y. Kadi, R. Klapisch, P. Mandrillon, J.P. Revol and Ch. Roche, *Conceptual Design of a Fast Neutron Operated Hugh Power Energy Amplifier*, European Organisation for Nuclear Research, CERN/AT/95-44 (ET), Geneva, 29th September, 1995.

Proceedings of ICONE19
19th International Conference on Nuclear Engineering
May 16-19, 2011, Chiba, Japan

ICONE19-43144

RELAP5 SIMULATION OF TWO-PHASE FLOW EXPERIMENTS IN VERTICAL HELICAL TUBES

F. Castiglia
Department of Nuclear Engineering of the University of Palermo
Viale delle Scienze, 90128 Palermo, Italy
Phone : +399123208,
Fax :+3991232215
castiglia@din.unipa.it

M. Giardina
Department of Nuclear Engineering of the University of Palermo
Viale delle Scienze, 90128 Palermo, Italy
Phone : +3991224,
Fax :+3991232215
mgiardina@din.unipa.it

G. Morana
Department of Nuclear Engineering of the University of Palermo
Viale delle Scienze, 90128 Palermo, Italy
Phone : +3991224,
Fax :+3991232215
gmorana@din.unipa.it

M. De Salve
Department of Energetics of Politecnico of Torino Corso Duca degli Abruzzi, 24, 10129 Torino Italy
mario.desalve@polito.it

B. Panella
Department of Energetics of Politecnico of Torino Corso Duca degli Abruzzi, 24, 10129 Torino Italy
bruno.panella@polito.it

Keywords: Helical tube, two-phase flow, pressure drop, Relap5, IRIS.

ABSTRACT

In the framework of the investigation on the thermal-fluid dynamics phenomena in helical pipes of the innovative nuclear power reactor steam generator, at the Department of Nuclear Engineering at the University of Palermo, various research activities were performed relating to validations works of the models implemented in RELAP5/MOD3.2β thermal-hydraulic advanced code in order to simulate two phase flow phenomena taking place in these systems, though the one-dimensional nature of it.

In this paper it is shown that the results obtained by the analyses of the experiments performed in different international laboratories and related to various helical pipes geometries, allows to prove the good performance of the so modified RELAP5 code.

1. INTRODUCTION

The widespread use of the helical pipe in heat exchangers for air conditioning and refrigeration systems, chemical and nuclear power reactors is due to high efficiency in heat transfer and compactness in volume.

Depending on specific applications of these components, for adequate design purposes, it is important to dispose a thorough knowledge of heat transfer and pressure drop characteristics, both in single-phase and in two-phase flow conditions, this because, due to centrifugal force in the cross section of the helical pipe, the secondary flow is a significant factor affecting the flow phenomena.

Recently, in these topics, the Department of Nuclear Engineering of the University of Palermo (Italy) dealt with validation works on RELAP5/mod3.2.2β code [1-4] in simulating two-phase flow vertical helical tubes relevant to experiments carried out at various national as well international research laboratories [5-11].

This has been performed taking into consideration that the code, based on one-dimensional thermal-hydraulic relationships, has limitations in modelling complicated geometries and thermal-fluid dynamics phenomena such as those involved in these systems. So, to overcome these difficulties, the code was improved with Lockhart-Martinelli frictional pressure drop correlations valid for two-phase flow helical pipes, as modified by Xin et Al.

In this paper we report the results obtained by using the modified RELAP5 code in the simulation of a lot of experiments carried out at the Department of Energetics of Politecnico of Torino (Italy) to investigate the fluid dynamics aspects in the helical pipes of innovative power reactor steam generator (Generation III and IV). Several test sections with different helical tube diameter were tested in order to study the effect of the centrifugal forces on the flow pattern. The measured experimental data were the pressure drops along the pipe as well the void fractions at various water and air mass flow rate conditions.

It will be show that the so modified RELAP5 code allows to represent fairly well the experimental data taken into consideration.

2. TWO-PHASE FLOW PRESSURE DROPS CORRELATION

As well known, the total pressure gradient in two-phase flow $(dP/dz)_{TP}$ can be expressed by three terms:

$$\left(\frac{dP}{dz}\right)_{TP} = \left(\frac{dP}{dz}\right)_{TP,f} + \left(\frac{dP}{dz}\right)_{TP,g} + \left(\frac{dP}{dz}\right)_{TP,a} \quad (1)$$

where $(dP/dz)_{TP,f}$ is the frictional pressure gradient, $(dP/dz)_{TP,g}$ the gravitational pressure gradient, and $(dP/dz)_{TP,a}$ the acceleration pressure gradient. In case of to no phase change the last term can be ignored.

For two-phase flow in vertical coils, the gravitational pressure gradient is determined from the void fraction data using the following equation:

$$\left(\frac{dP}{dz}\right)_{TP,g} \approx (1-\alpha)\rho_l \, g \sin\beta \quad (2)$$

with α void fraction, ρ_l liquid density, g gravitational acceleration and β helix angle.

The frictional pressure gradient can be determined from the total pressure gradient, that is measured in the experiment, and the gravitational pressure gradient, that is calculated in accordance with Eq. (2), by using the following expression:

$$\left(\frac{dP}{dz}\right)_{TP,f} = \left(\frac{dP}{dz}\right)_{TP} - \left(\frac{dP}{dz}\right)_{TP,g} \quad (3)$$

It is to be noted that the fluid properties, especially the gas ones, were determined using the average value of inlet and outlet pressures as a reference.

The frictional pressure drop data can be correlated by the pressure drop multipliers ϕ_L and ϕ_G versus Lockhart-Martinelli parameter χ, which are defined as follows:

$$\phi_L^2 = \frac{\left(\frac{dP}{dz}\right)_{TP,f}}{\left(\frac{dP}{dz}\right)_{L,f}}, \quad \phi_G^2 = \frac{\left(\frac{dP}{dz}\right)_{TP,f}}{\left(\frac{dP}{dz}\right)_{G,f}} \quad (4)$$

$$\chi^2 = \frac{\phi_G^2}{\phi_L^2} = \frac{(dP/dz)_{L,f}}{(dP/dz)_{G,f}} \quad (5)$$

The pressure drop multipliers, in case of straight pipes, are represented in terms of the Lockhart-Martinelli parameters by using the following correlations:

$$\phi_L^2 = 1 + \frac{C}{\chi} + \frac{1}{\chi^2} \quad (6)$$

$$\phi_G^2 = 1 + C\chi + \chi^2 \quad (7)$$

where the constant C changes from 5 to 20, depending on the laminar or turbulent flow that takes place in the pipe.

Concerning the two phase flow in helical pipes, three forces affect the flow pattern and pressure drops: inertial force; liquid gravity; and centrifugal force. Inertial force enhances the mixing of the two phases; whereas liquid gravity and centrifugal forces tend to separate the two phases, due to the large density difference between the liquid and gas phases. However, when the flow direction changes, the net effect can be the separation or the mixing of the phases.

The effects of these forces can be represented in terms of Froude number, Fr ($Fr = u^2/gd$, with, u, the phase velocity and, d, the tube diameter), ratio of pipe diameter to helical one, d/D, and helix angle, β.

Various authors [12, 13] indicate that most of the two-phase flow pressure drop data in helical coils can be satisfactorily predicted by the above quoted Lockhart-Martinelli correlations Eq. (4), with however a specific definition of the Lockhart-Martinelli parameter Eq. (5) based on the single-phase flow frictional pressure drop in helical pipes.

Furthermore, Xin et al. [10, 11] obtained extensive data on the pressure drop of two-phase flow in vertical and horizontal helical pipes, respectively, and in [10] correlated the frictional pressure drop multipliers as a function of Fr, d/D, β parameters.

In particular, they propose the following relationship to evaluate the pressure drop multiplier, ϕ_L, to deal with helical geometry:

$$\phi_L = [1 + K \cdot \chi \cdot F_d{}^n](1 + \frac{C}{\chi} + \frac{1}{\chi^2})^{1/2} \quad (8)$$

with C equal to 20.0 and the parameter F_d defined as:

$$F_d = Fr_L \left(\frac{d}{D}\right)^{1/2} (1 + \tan\beta)^{0.2} \quad (9)$$

where Fr_L is the liquid phase Froude number.

The values of the other parameters in Eq. (8) are reported in Table 1.

Table 1 – Values of the parameter in Eq. (8)

F_d	≤ 1	≥ 1
K	0.01528	0.0023
n	-0.6	-1.7

With this, the liquid phase influence is taken into account by the liquid Fr number, whereas the influence of the gas phase is accounted by the Lockhart-Martinelli parameter χ.

The above relationships are valid in the range of D/d = 26 through 50. The maximum deviation between the prediction of Eq. (8) and the experimental data of the pressure drops multiplier ϕ_L was evaluated by Xin about $\pm$ 35 %.

To evaluate the two-phase flow pressure drops, Eq.s (4), (5) and (8), (9) were used. Moreover, to calculate the friction factor in single-phase pressure gradients, $(dP/dz)_L$ and $(dP/dz)_G$, in the above mentioned equations, Ito correlations [14] as described in Eq.s (10)-(12) were used:

$$f_c = \frac{16}{\mathrm{Re}} \qquad \mathrm{Re} < 13.5(D/d)^{-0.5} \qquad (10)$$

$$f_c = \frac{344(D/d)^{-0.5}}{\left\{1.56 + \log_{10}\left[\mathrm{Re}\left(\frac{D}{d}\right)^{-0.5}\right]\right\}^{5.73}}$$

$$13.5\left(\frac{D}{d}\right)^{0.5} < \mathrm{Re} < 2000\left[1+13.2\left(\frac{D}{d}\right)^{-0.6}\right] \qquad (11)$$

$$f_c = 0.076\mathrm{Re}^{-0.25} + 0.0075\cdot\left(\frac{D}{d}\right)^{-0.5} \qquad \mathrm{Re} > 15000 \qquad (12)$$

where, Re, is the Reynolds number, D and d as above quoted.

The RELAP5/mod3.2.2β code, modified by using the correlations above described, was tested versus a lot of two-phase flow vertical helical tubes experimental data carried out in various international research laboratories. In the following only some samples of the simulations of experiments performed at Department of Energetics of Politecnico of Torino obtained results are shown.

3. ANALISYS OF EXPERIMENTAL DATA CARRIED OUT AT THE DEPARTMENT OF ENERGETICS OF POLITECNICO OF TORINO

For more details, we refer to [8, 9], whereas here only a brief description of the test sections and the associated instrumentation are described.

The experimental facility consists of an air/water flow loop in which two different helical test sections are inserted. These are made of plexiglass pipes, 12 mm inner diameter, that are wrapped in two different helical coils: the first one with 1 m coil diameter and a helix pitch of 0.79 m; the second one with 0.64 m coil diameter and a helix pitch of 0.485 m.

Some of geometric characteristics are reported in Table 2.

Two different pumps were used to supply water flows in the ranges from 200 to 400 l/h, and from 400 to 800 l/h, respectively. For each water flow rate the air flow was varied from 0.043 g/s to 0.26 g/s.

The pressure inner the tests section was less than 3 bar.

The directly measured quantities were flow rate, pressure drops and mass of water. The air and water flow were measured by high precision rotameters, whereas the pressure drops were measured by nine pressure taps disposed along the coiled tube and eight differential pressure transducers which connect the pressure taps.

Table 3 reports the various positions of the instruments to measure the pressure drop between the first tap (named 1) and the subsequent ones (named 2 through 9).

The void fraction was measured by the quick closing valves method which allows to trap the water hold-up in the test section.

On the basis of experimental data performed at Torino Laboratory, the constant C, in Eq. (6), was estimated equal to 36.85 to get best results. Note that these experiments are characterized by ratio D/d of 53 and 83 which are higher than the geometrical conditions used by Xin.

Table 2 - Test sections geometrical data

	Description	**SI**	**Helix 1**	**Helix 2**
D	Helix diameter	m	0.64	1
d	Pipe diameter	m	0.012	0.012
p	Pitch	m	0.485	0.79
β	Helix angle	rad	0.2367	0.2463

Table 3 - Test sections geometrical data

Taps	**Helix D = 0.64 m**		**Helix D = 1 m**	
Pos.	**Δz [m]**	**ΔL [m]**	**Δz [m]**	**ΔL [m]**
1-2	0.98	4.72	0.22	1.183
1-3	1.096	5.2	1.003	4.39
1-4	1.225	5.75	1.192	5.17
1-5	1.342	6.24	1.395	6
1-6	1.462	6.744	1.594	6.82
1-7	1.946	8.78	1.789	7.62
1-8	2.19	9.88	2.185	9.25
1-9	2.44	10.858	2.385	10.07

3.1 RELAP5 analysis

The RELAP5/Mod3.2.2β code was supplemented by suitable FORTRAN subroutines which can allow to simulate the geometrical configuration as well the thermal-hydraulic conditions as suggested by Eq. (8) through (12).

The constant C values of 20 in Eq. (8) and of 36.85 in Eq. (6) have been tested for comparison with the no modified code.

To simulate the experimental data taken into consideration, Relap5 nodalization, shown in Fig. 1, was used.

The time dependent volume components, numbered 500 and 560, were used to specify the inlet and outlet conditions of the helical coil loop.

Through the time dependent junction, named 505 (TMPJUN505), the air and water mixture is sent to volume PIPE 506, which schematizes helical coil inlet condition. By using this junction the air and water flow conditions are changed, according to the simulated experiments.

The helical pipe is represented by the volume PIPE 510, divided into 50 sub-volumes, for a better approximation of pressure taps position along the pipe length.

3.2 Results

The experimental data have been simulated for each coil diameter, by setting the water mass flow and changing the air one. This operation is repeated for all water flow values. In

Table 4 the water and air mass flow rates employed in the experiments taken into consideration are reported.

The same tests have been simulated by the no-modified Relap5 code, which, as expected, underestimates all the measured pressure drops.

Table 4 - Experimental tests conditions

Dhelix = 0,64 m						
Wwater [l/h]	Wair [l/h]					
200	50	100	150	200	250	300
300	50	100	150	200	250	300
400	50	100	150	200	250	300
600	50	100	150	200	250	300
800	50	100	150	200	250	300
Dhelix = 1,0 m						
Wwater [l/h]	Wair [l/h]					
200	50	100	150	200	250	300
300	50	100	150	200	250	300
400	50	100	150	200	250	300
600	50	100	150	200	250	300
800	50	100	150	200	250	300

Fig.s 2 through 6 report the pressure drops along the pipe for the helix diameter equal to 0.64 m, whereas Fig.s 7 through 11 report the ones for the helix diameter equal to 1.0 m. As it can be seen from all figures, the modified code gives a good prediction of the experimental data, with an average relative error (ε) lower then of 13% by using C = 20 and 15.5% by using C = 36.85, respectively. On the contrary, no-modified code simulations give results with an average relative error about 21%. In Table 5 is also shown the average relative errors for D_h=0.64 m and D_h=1.0 m respectively.

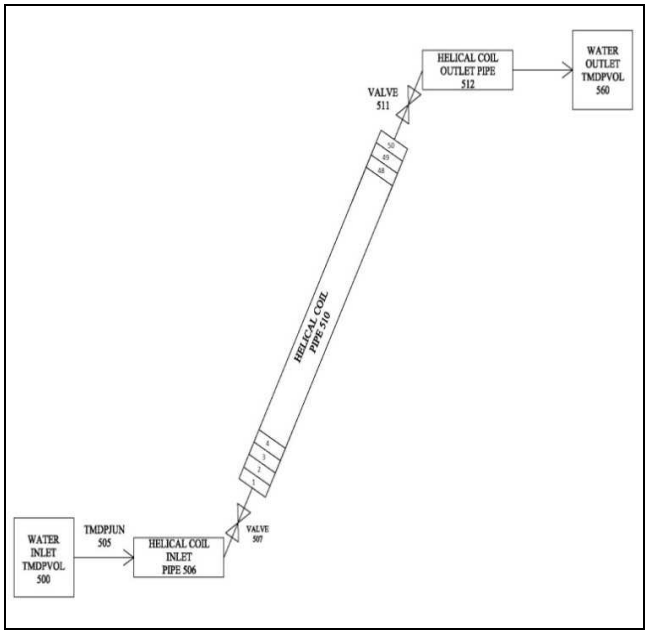

Fig. 1 - Relap5 test section nodalization

In Fig.s 12 through 14 shows simulated versus experimental pressure drops results along the test section, for the no-modified code, the code modified with C=20 and C=36.85, respectively.

For no-modified RELAP the 40% of 430 data point is evaluate within an error of ± 20% and about the 20% of data point within ± 10%. Concerning the modified code with C=20, about 80% of the simulations is calculated with an error of ± 20% and more than 50% within an error of ± 10%.

Finally, for the modified code with C=36.85, we have again about 80% of the simulations within an error of ± 20%, but only the 30% is evaluate within an error of ± 10%. In Table 6 are also shown the obtained values for χ^2 test, for Dh=0.64 m and Dh=1.0 m respectively.

Table 5 – Average relative error values (□)

	No-modified code	**C = 20**	**C = 36.85**
D_h=0.64 m	22.5%	12.8%	12.9%
D_h=1.0 m	19.5%	12.5%	18.2%
Total	21%	12.6%	15.5%

Table 6 – χ^2 values

	No-modified code	**C = 20**	**C = 36.85**
D_h=0.64 m	3.6	1.45	1.75
D_h=1.0 m	2.15	1.10	2.90
Total	5.75	2.55	4.65

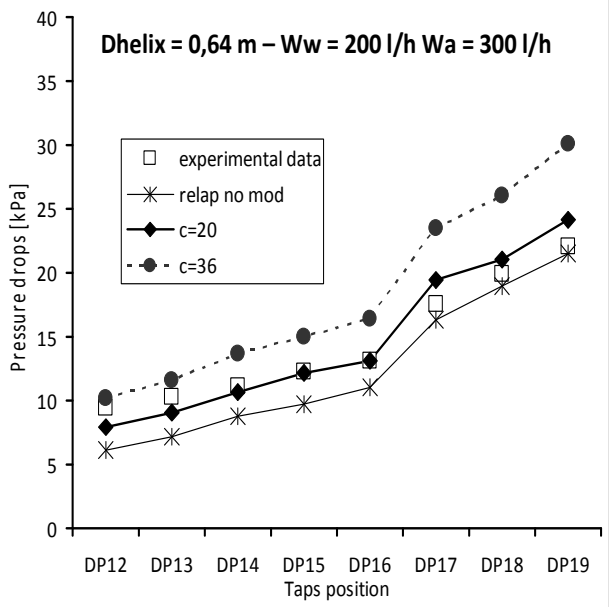

Fig. 2 - Pressure drops along the pipe D = 0.64 m for water mass flow rate of 200 l/h and air mass flow rate of 300 l/h

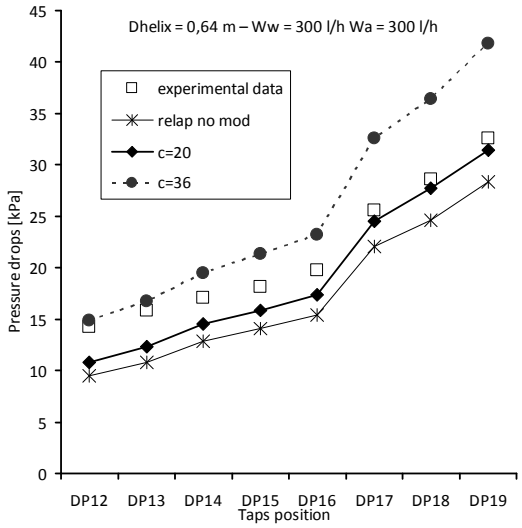

Fig. 3 - Pressure drops along the pipe D = 0.64 m for air and water mass flow rates of 300 l/h

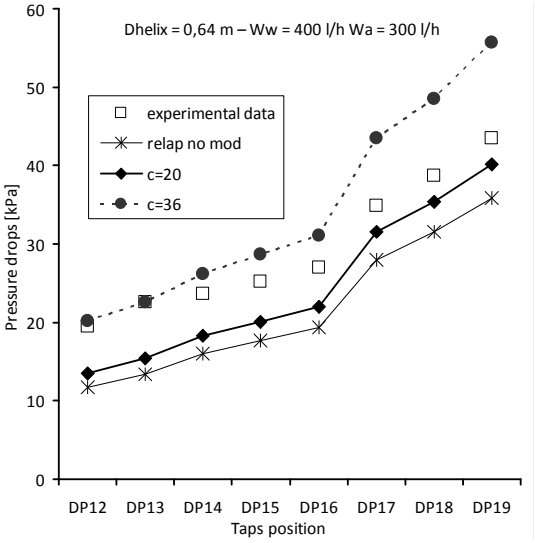

Fig. 4 – Pressure drops along the pipe D = 0.64 m for water mass flow rate of 400 l/h and air mass flow rate of 300 l/h

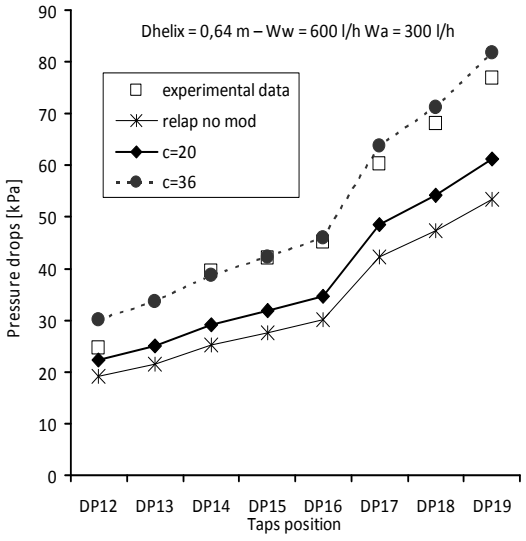

Fig. 5 – Pressure drops along the pipe D = 0.64 m for water mass flow rate of 600 l/h and air mass flow rate of 300 l/h

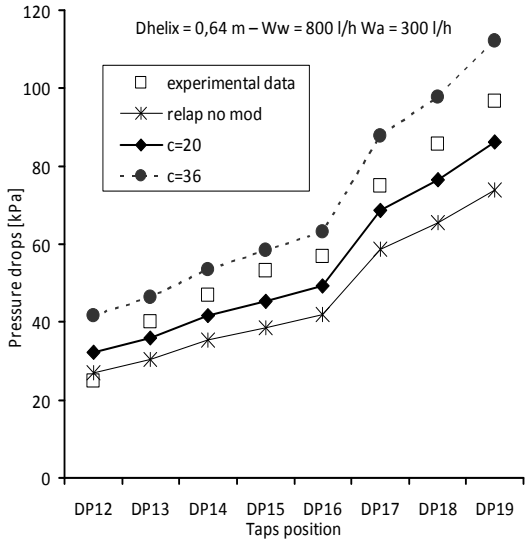

Fig. 6 – Pressure drops along the pipe D = 0.64 m for water mass flow rate of 800 l/h and air mass flow rate of 300 l/h

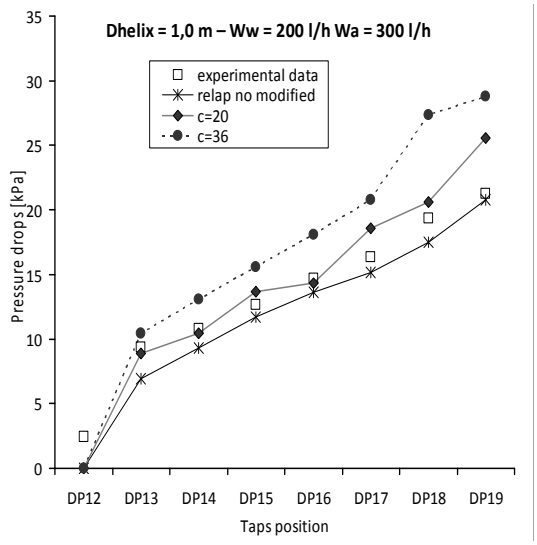

Fig. 7 – Pressure drops along the pipe D = 1,0 m for water mass flow rate of 200 l/h and air mass flow rate of 300 l/h

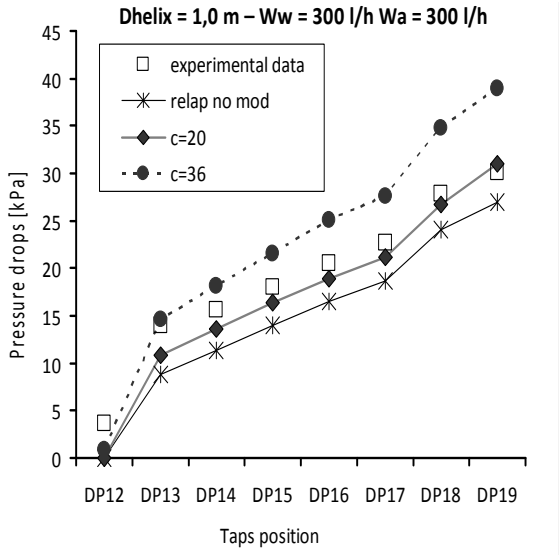

Fig. 8 – Pressure drops along the pipe D = 1,0 m for water mass flow rate of 300 l/h and air mass flow rate of 300 l/h

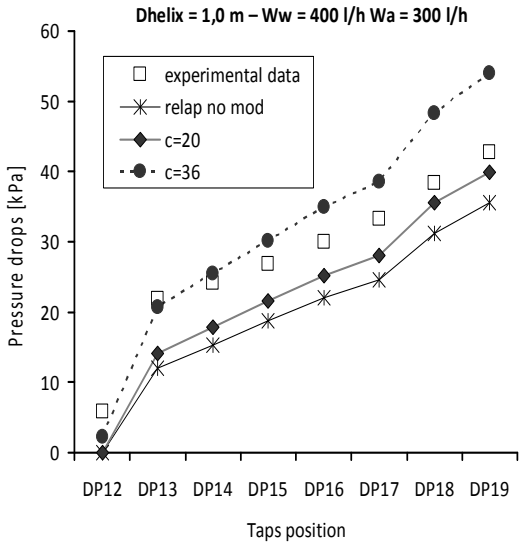

Fig. 9 – Pressure drops along the pipe D = 1,0 m for water mass flow rate of 400 l/h and air mass flow rate of 300 l/h

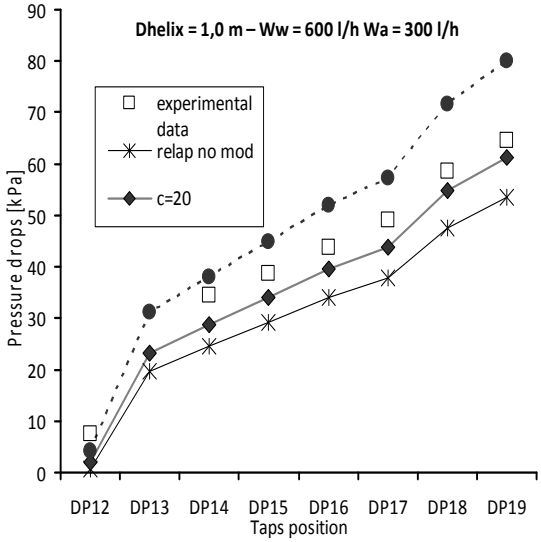

Fig. 10 – Pressure drops along the pipe D = 1,0 m for water mass flow rate of 600 l/h and air mass flow rate of 300 l/h

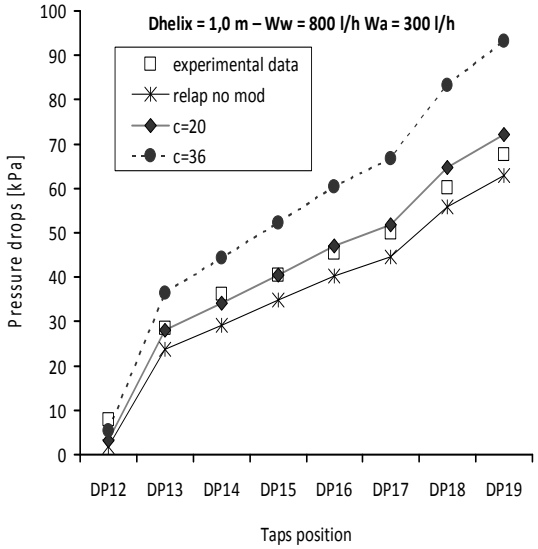

Fig. 11 – Pressure drops along the pipe D = 1,0 m for water mass flow rate of 800 l/h and air mass flow rate of 300 l/h

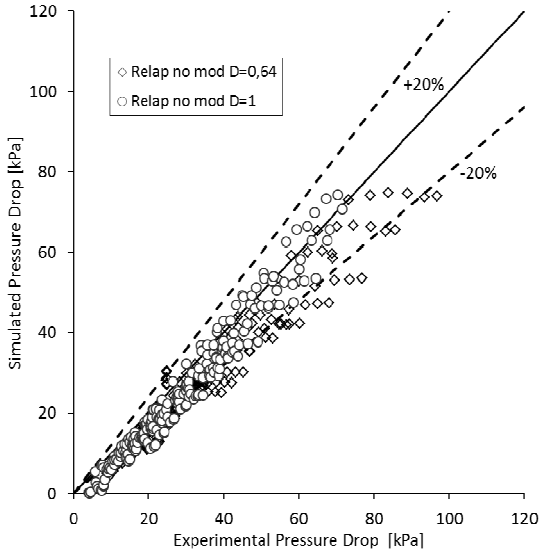

Fig. 12 – Experimental versus simulated two-phase pressure drops by no-modified code

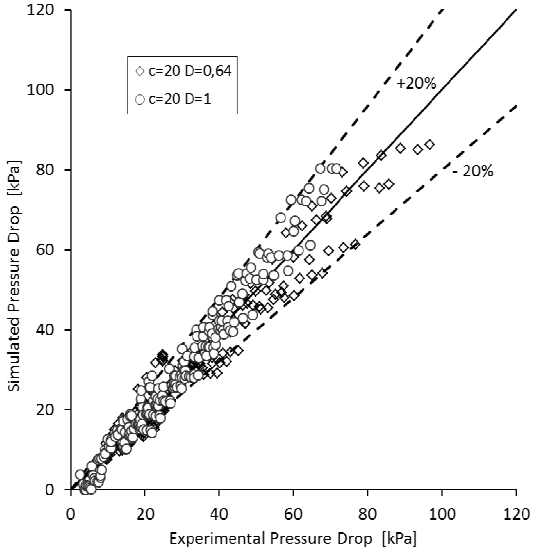

Fig. 13 – Experimental versus simulated two-phase pressure drops by RELAP5 code modified with C = 20

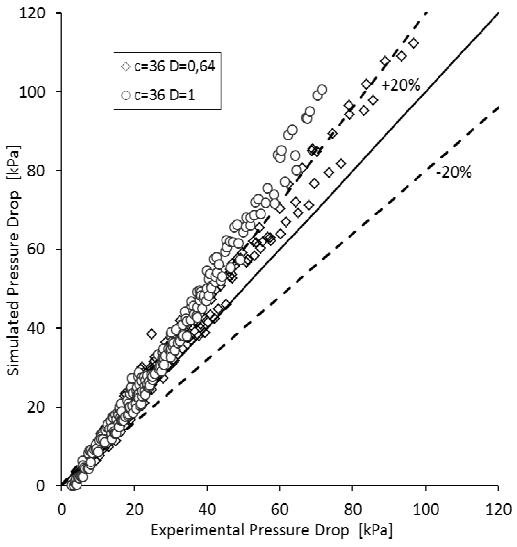

Fig. 14 – Experimental versus simulated two-phase pressure drops by RELAP5 code modified with C = 36.86

4. CONCLUSIONS

In the present study the pressure drops of two-phase flow in vertical helical pipes have been simulated by using Relap5/mod3.2β code suitably improved with Lockhart Martinelli correlations modified as suggested by Xin.

The validation work was performed using experimental data carried out at Department of Energetics of Politecnico of Torino, Italy. The results obtained by no-modified code have been compared with two different modified version of Relap5 code: at first with the implementation of Eq. (8) with C = 20, and then by using Eq. (6) with C = 36.85, as suggest by the studies carried out at Politecnico of Torino.

Both these last code versions give good results compared to the no-modified code version, however the one with C=20 is better than other. In fact, the average relative error goes from 21% (no-mod code) to 12.6% (C=20) and 15.5% (C=36). The χ^2 test also confirms these observations (see Table 6).

5. NOMENCLATURE

C	*constant*	-
D	*coil diameter*	m
d	*tube diameter*	m
f	*Fanning friction factor*	
Fr	*Froude number*	
F_d	*non- dimensional parameter*	
g	*Acceleration of gravity*	m/s^2
h	*hour*	
K	*constant*	-
l	*litre*	
L	*coil length*	m
n	*constant*	-
Re	*Reynolds number based on inside tube diameter*	
u	*fluid velocity*	m/s
W	*flow rate*	l/h
z	*share geodesic*	m

Greek Symbols

ΔP	*pressure drop*	Pa
α	*Void fraction*	-
ρ	*Density*	kg/m^3
β	*Helix angle*	rad
Φ	*Two phase multiplier*	-
χ^2	*Martinelli parameter*	-

Subscripts

a	*air*
c	*coil*
f	*frictional*
G	*gas*
L	*liquid*
w	*water*

REFERENCES

[1] M. Casamirra, F. Castiglia, M. Giardina, P. Meloni, RELAP5 Modification for CHEOPE Simulations, International Conference Nuclear Energy for New Europe, Bled, Slovenia, September 5-8, 2005.

[2] M. Casamirra, F. Castiglia, M. Giardina, C. Lombardo, Modifying RELAP5 code to deal with helical coiled ducts, XXIV Congresso Nazionale sulla trasmissione del calore UIT, Napoli, Italy, 21-23 Giugno 2006, ISBN/ISSN: 88-7741-1569-1. PISA: Edizioni ETS (ITALY).

[3] M. Casamirra, F. Castiglia, M. Giardina, Heat Transfer Prediction of the THX Exchanger in MEGAPIE Facility by Using RELAP5 Code Suitably Modified to Deal with Helical Channel, Rapporto tecnico, FPN-P9EH-010, ENEA di Bologna, 20/12/2007.

[4] M. Casamirra, F. Castiglia, M. Giardina, C. Lombardo, Studio con il codice RELAP5 delle perdite di carico e dello scambio termico in tubi elicoidali interessati da deflussi monofase, XXVII Congresso Nazionale UIT sulla Trasmissione del Calore, Reggio Emilia, 22-24 Giugno 2009, ISBN: 978-88-7488-312-7.

[5] P. Agostini, Observation resulting from MEGAPIE cooling pin tests in Brasimone, Derivable 22A MEGAPIE – TEST, EU Project No. FIKW-CT-2001-00159 (PU).

[6] Shaukat Ali, Pressure drop correlations for flow through regular helical coil tubes, Fluid Dynamics Research, 28 (2001) pp 295–310.

[7] P. Coronel and K.P. Sandeep, Pressure drop and friction factor in helical heat exchangers under nonisothermal and turbulent flow conditions, Journal Of Food Process Engineering 26 (2003) 285-302.

[8] C. Bertani, M. De Salve, M. Malandrone, M. Orio, B. Panella, Studio sperimentale del deflusso bifase aria-acqua in un tubo elicoidale, XXV Congresso Nazionale UIT sulla Trasmissione del Calore, Trieste, 18-20 Giugno 2007.

[9] C. Bertani, M. De Salve, M. Malandrone, M. Orio, B. Panella, Cadute di pressione e grado di vuoto in condotti elicoidali: confronto tra risultati sperimentali e modelli semiempirici, XXVI Congresso Nazionale UIT sulla Trasmissione del Calore, Palermo, 23-25 Giugno 2008.

[10] R.C. Xin, A. Awwad, Z. Dong, M.A. Ebadian, H.M. Soliman, An Investigation and Comparative Study of the Pressure Drop in Air-Water Two-Phase Flow in Vertical Helicoidal pipes, Int. J. Heat and Mass Transf., vol. 39, pp.735-743, 1996.

[11] R.C. Xin, A. Awwad, Z. Dong, M.A. Ebadian, An experimental study of single-phase and two-phase flow pressure drop in anular helicoidal pipes, Int. J. Heat and Fluid Flow, 18, pp. 482-488, 1997.

[12] G. R Rippel, C. R. Eidt, and H. B. Jornan, 1966, Two-phase flow in a coiled tube. Ind. Eng. Chem., 5, 32-39.

[13] S. Banerjee, E. Rhodes, and D. S. Scott, 1969, Studies on concurrent gas-liquid flow in helically coiled tubes. I-Flow patterns, pressure drop, and holdup, Can. J. Chem. Eng., 47, 445-453

[14] H. Ito, 1959, Friction factors for turbulent flow in curved pipes, Trans Series D, J. Basic Engng 81, 123–134.

Nuclear Engineering and Design 250 (2012) 585–591

Contents lists available at SciVerse ScienceDirect

Nuclear Engineering and Design

journal homepage: www.elsevier.com/locate/nucengdes

Analyses of single- and two-phase flow pressure drops in helical pipes using a modified RELAP5 code

F. Castiglia[a,*], M. Giardina[a], G. Morana[a], M. De Salve[b], B. Panella[b]

[a] Department of Energy, University of Palermo, Viale delle Scienze, 90128 Palermo, Italy
[b] Department of Energetics, Polytechnic of Torino, Corso Duca degli Abruzzi, 24, 10129 Torino, Italy

HIGHLIGHTS

- Pressure drops in single and two phase flows in vertical helical pipes are examined.
- Ito single phase and modified Lockhart–Martinelli two-phase correlations were used.
- These correlations were implemented in RELAP5/MOD3.2β thermal–hydraulic code.
- The modified code was used to simulate experiments obtained at several laboratories.
- Lots of experiments performed at different helical geometries are well predicted.

ARTICLE INFO

Article history:
Received 9 November 2011
Received in revised form 25 May 2012
Accepted 5 June 2012

ABSTRACT

Thermal fluid dynamics analyses on single- and two-phase flows in helical pipes of steam generators to be used in Generation III and IV nuclear reactors have been performed. The study concerned with experimental activities as well code simulations carried out in the framework of a collaboration between the Department of Energetics of the Polytechnic of Torino and the Department of Energy of the University of Palermo. The goal was the validation of models implemented in Relap5/Mod3.2β thermal–hydraulic advanced code to simulate the hydrodynamic behaviour of helical pipe components in spite of the one-dimensional nature of the code. It is shown that much of the experimental data obtained at several national and international research laboratories are well predicted by this modified RELAP5 code for the examined helical pipe geometries.

1. Introduction

Helical coiled tubes are of special interest for their many practical advantages, such as compactness, easy manufacture and high efficiency in heat transfer. They have been widely used for compact heat exchanges in boilers, equipment of chemical plants and nuclear power reactors. As far as nuclear power plants are concerned helical tubes have also been recommended for the passive safety heat transfer components. In the past, different nuclear power plants adopted helical-coiled steam generators to drive the turbine, as gas-cooled reactors (Advanced Gas Cooled, AGR, HTGR (IAEA, 2010)), SuperPhénix fast reactor (sodium cooled), as well as water cooled nuclear reactors for ship power propulsion (Otto Hahn). Nowadays, helically coiled steam generators are envisaged for the innovative, more safe and sustainable nuclear reactors, that are likely to be deployed either in near-medium term (IAEA, 2005), or in long term (like Generation IV systems (GIF, 2002)).

An example is the IRIS reactor (Carelli et al., 2004), whereby the safety concept is based on the large utilisation of passive systems able to establish and maintain core cooling and ensure containment integrity following postulated design basis accidents. The IRIS main passive system for core cooling is the so-called emergency heat removal system (EHRS), in which the natural circulation loop includes reactor helical coiled tubes steam generators. Another example is the accelerator driven system (ADS) reactor concept, like the European facility for industrial transmutation (EFIT) facility (Bandini et al., 2008), aimed at demonstrating the feasibility of transmutation process on an industrial scale through the ADS route. The EFIT reactor thermal power is removed in normal operation by height helical coiled tubes steam generators, located in the upper part of the reactor pool to enhance natural circulation in case of loss of flow accidents.

It is evident that, depending on the specific applications of these components, to attain an adequate design, it is important to have a thorough understanding of the heat transfer and pressure drop

* Corresponding author. Tel.: +39 091232252; fax: +39 091232215.
E-mail address: francesco.castiglia@unipa.it (F. Castiglia).

0029-5493/$ – see front matter © 2012 Elsevier B.V. All rights reserved.
http://dx.doi.org/10.1016/j.nucengdes.2012.06.008

Nomenclature

C	constant
D	coil diameter [m]
d	tube diameter [m]
f	Fanning friction factor
Fr	Froude number (u^2/gd)
F_d	non-dimensional parameter
g	gravity acceleration [m/s^2]
h	hour
K	constant
L	coil length [m]
l	liter
n	constant
p	coil pitch [m]
Re	Reynolds number based on inside tube diameter ($\rho ud/\mu$)
u	fluid velocity [m/s]
W	flow rate [l/h]

Greek symbols

β	helix angle
ΔP	pressure drop [Pa]
μ	viscosity [Pa s]
ρ	density [kg/m^3]
ε	relative error

Subscripts

c	coil
G	gas
L	liquid
w	water
a	air

characteristics in both single-phase and two-phase flow conditions because the secondary flow in the cross section of the helical pipe, caused by centrifugal forces, is a significant factor affecting the flow phenomena.

Gou et al. (Gou et al., 2001) performed an interesting experimental investigation on the pressure drop of steam–water two-phase flow in helical coils with a review of previous single and two-phase pressure drops researches.

Recently, in this field, various research activities on thermal fluid dynamics phenomena in the helical pipes of steam generators to be used in Generation III and IV nuclear reactors have been performed in the framework of a collaboration between the Department of Energetics of the Polytechnic of Torino and the Department of Energy of the University of Palermo. The goal of this research has been also to validate models implemented by the authors in RELAP5/MOD3.2β thermal–hydraulic advanced code to simulate both single- and two-phase flow experiments in vertical helical tubes under various operating conditions (Casamirra, 2005, 2006; Casamirra et al., 2007, 2009; Bertani et al., 2007, 2008).

As well known the code, based on one-dimensional thermal–hydraulic relationships, has some drawbacks when using it to model complex geometries and thermal fluid dynamics phenomena such as those involved in these systems, so it has been supplemented with additional friction pressure drop models valid for single- and two-phase flows in helical pipes.

The aim of the experimental data, semi-empirical best-fit correlations and simulations with system code as RELAP5 series is to show the range where an one-dimensional approximation of an helical pipe as an inclined straight pipe is adequate to describe single and two-phase flows in compact heat exchangers helical pipes. Important geometrical parameters are the coil diameter, the helix pitch, the turns and the tube inner diameter.

This paper presents the results of simulations of many experiments performed at several international research laboratories, conducted by using the modified RELAP5 code. In particular, the two-phase flows experiments have been carried out at the Polytechnic of Torino Department of Energetics. The purpose was to investigate the fluid dynamics behaviour of a helically coiled steam generator for use in the IRIS nuclear power reactor design. This system is characterised by 62.85 kg/s secondary coolant flowing inside helical tube bundle of various helical diameter (in the range from 0.64 to 1.59 m) and pitches (in the range from 0.485 to about 1.2 m). So, several test sections with different helical diameters were tested to study the effect of the centrifugal forces on the flow pattern. The measured data were the pressure drops along the pipe and the void fraction for different water-air mass flow rate conditions.

In the following sections, it is shown that the modified RELAP5 code represents the experimental data under consideration fairly well.

2. Pressure drop correlations in helically coiled tubes

As confirmed by experimental results, in both single- and two-phase flows moving across helically coiled tubes, the centrifugal force acting on the fluid is likely to produce a secondary flow field (perpendicular to the axial direction) that increases the pressure drop and, consequently, the heat transfer in comparison with an equivalent straight pipe. Thus, the use of curved tubes in heat exchangers can be highly beneficial in comparison with straight tube heat exchangers.

With respect to the thermal fluid dynamics for flows across helical tubes, three forces affect the flow pattern and the pressure drop: inertial forces, liquid gravity, and centrifugal forces. Inertial forces enhance the mixing of the liquid and gas phases, whereas liquid gravity and centrifugal forces tend to separate them because of their large density differences. In the case of a change in the direction of the flow, the net effect can be the separation or mixing of the phases, depending on which of the forces prevails.

A number of experimental studies on single- and two-phase heat transfer and friction factors in coiled tubes are reported in the literature (Bertani et al., 2007, 2008; Ito, 1959; Xin et al., 1996, 1997; Jeschke, 1925; Dean, 1927; Ritu Gupta Wanchoo and Jafar Ali, 2011; Cioncolini and Santini, 2006; Lockhart and Martinelli, 1949; Rippel et al., 1966; Banerjee et al., 1969; Ali, 2001). However, because of the complexity of the involved mechanisms, the results are difficult to process. Moreover, studies on some types of curved tubes, especially spiral coiled tubes, are limited in number.

On the basis of experimental data, various authors have suggested correlations for predicting the friction factor and the heat transfer in helically coiled tubes that are not always in agreement with each other.

Among the correlations for helical pipes available in the literature, the friction factor given by Ito for single-phase flow (Ito, 1959) has been chosen for this study, and the Lockhart–Martinelli correlations, as modified by Xin et al. (1996, 1997), have been selected for two-phase flow.

2.1. Single-phase flow correlations

The first experimental studies were conducted by Jeschke (1925) for the turbulent flow of air, which led to an empirical formula that was later revised by Merkel and reported in many books. Dean conducted the first theoretical study for fully developed laminar flow (Dean, 1927) and tried to determine the deviation of the

velocity profile from the Poiseille flow pattern using a perturbation method applied to the solution of the Navier–Stokes equation.

Subsequently, by combining his experiments with those reported in the literature, Ito (Ito, 1959) summarised the fluid Fanning friction factor for helical pipes at different Reynolds number as follows:

$$f_c = \frac{344(D/d)^{-0.5}}{\left\{1.56 + \log_{10}\left[Re(D/d)^{-0.5}\right]\right\}^{5.73}} \quad 13.5\left(\frac{D}{d}\right)^{0.5} < Re < 2000\left[1 + 13.2\left(\frac{D}{d}\right)^{-0,6}\right] \tag{1}$$

which is valid for laminar flow, and:

$$f_c = 0.076Re^{-0.25} + 0.0075\left(\frac{D}{d}\right)^{-0.5} \quad Re > 15000 \tag{2}$$

which is valid for turbulent flow.

In these equations, Re is the Reynolds number, D is the helical diameter, and d is the tube diameter.

For a Re number below $0.034(D/d)^2$, in (Ritu Gupta Wanchoo and Jafar Ali, 2011) is shown that the Fanning friction factor for laminar straight tubes can be assumed to be valid, that is:

$$f_c = \frac{16}{Re} \tag{3}$$

The transition from laminar to turbulent flow, according to Ito, is given by a critical Reynolds number which is a function of d/D ratio. Ito verified the validity of the above correlations for $5 < D/d < 20$, which has recently been confirmed by Cioncolini and Santini (2006) through extensive experimental work performed for a wide range of D/d ratio ($7 < D/d < 370$) and Re numbers ($10^3 < \mathrm{Re} < 7 \times 10^4$).

2.2. Two-phase flow correlations

Historically, the most widely used correlation for two-phase frictional pressure drop $(dP/dz)_{TP,f}$ is the Lockhart–Martinelli correlation (Lockhart and Martinelli, 1949), in which the pressure drop multipliers ϕ_L and ϕ_G are defined, respectively, as:

$$\phi_L^2 = \frac{(dP/dz)_{TP,f}}{(dP/dz)_L}, \quad \phi_G^2 = \frac{(dP/dz)_{TP,f}}{(dP/dz)_G} \tag{4}$$

and related to the Lockhart–Martinelli parameter χ^2:

$$\chi^2 = \frac{\phi_G^2}{\phi_L^2} = \frac{(dP/dz)_L}{(dP/dz)_G} \tag{5}$$

where $(dP/dz)_L$ and $(dP/dz)_G$ are the pressure gradients for the liquid phase and the gas phase flowing alone in the channel.

In the case of straight pipes, the same authors presented the above pressure drop multipliers as follows:

$$\phi_L^2 = 1 + \frac{C}{\chi} + \frac{1}{\chi^2} \tag{6}$$

$$\phi_G^2 = 1 + C\chi + \chi^2 \tag{7}$$

The constant C ranges from 5 to 20, depending on whether laminar or turbulent flow occurs in the pipe.

Regarding two-phase flows in helically coiled tubes, previous studies (Rippel et al., 1966; Banerjee et al., 1969) indicated that most of the pressure drop data can be satisfactorily predicted by Eq. (4), based on the friction pressure drop for helical single-phase flow, in conjunction with the Lockhart–Martinelli parameter, Eq. (5). This last has been modified to account for the effects of the inertial force, liquid gravity, and centrifugal force in terms of the Froude number, Fr, the ratio of the pipe diameter to the helical diameter, d/D, and the helix angle β, respectively.

Table 1
Values of the parameters of the liquid pressure drop multiplier, ϕ_L, in Eq. (8).

F_d	≤1	≥1
K	0.01528	0.0023
n	−0.6	−1.7

In particular, Xin et al. (1996, 1997) performed several experiments on the pressure drop in vertical and horizontal helical pipes with two-phase flow and, on the basis of their data (Xin et al., 1997), proposed the following relationship for the pressure drop multiplier, ϕ_L:

$$\phi_L = (1 + K\chi F_d^{\,n})\left(1 + \frac{C}{\chi} + \frac{1}{\chi^2}\right)^{1/2} \tag{8}$$

with $C = 20.0$ and F_d defined as:

$$F_d = \mathrm{Fr}_L\left(\frac{d}{D}\right)^{1/2}(1 + \tan\beta)^{0.2} \tag{9}$$

where Fr_L is the liquid-phase Froude number $(u_l^{\,2}/gd)$ and β is the helix angle.

The values of the other parameters in Eq. (8) are reported in Table 1.

The influence of the liquid phase is therefore accounted for by the liquid Froude number, Fr_L, whereas the influence of the gas phase is accounted for by the Lockhart–Martinelli parameter, χ.

The above relationships are valid in the range $26 < D/d < 50$. The maximum deviation between the prediction of Eq. (8) and the experimental data was found by Xin to be approximately ±35%.

3. Modified RELAP5 code simulations

On the basis of the above considerations, the RELAP5/Mod3.2β code was supplemented by suitable FORTRAN subroutines that allow the simulation of the helical geometry in a single-phase flow configuration, as suggested by Ito's correlations in Eqs. (1) and (2), whereas for $\mathrm{Re} < 13.5(D/d)^{0.5}$, Eq. (3) was used.

To overcome the problem of the friction factor discontinuity, which affects Ito's correlations in the laminar to turbulent transition regime, a procedure based on a linear interpolation method of f_c in Re that is applied between $\mathrm{Re} = 2000[1 + 13.2(D/d)^{-0.6}]$ (Ito's maximum Re value for the laminar range) and Re = 15,000 (Ito's minimum Re value for turbulent flow) has been introduced.

For two-phase flow, Eqs. (4), (5), (8), and (9) have been used, in which $(dP/dz)_L$ and $(dP/dz)_G$ were calculated using Eqs. (1)–(3) for liquid or gas single-phase conditions.

The unmodified and modified versions of the RELAP5 code were tested against the data from many single- and two-phase flow vertical helical tube experiments. Samples of the results are presented in the following sections.

3.1. Single-phase flow analysis of experimental data performed by Ali

The experiments were carried out by using regular helical coils tubes, made by winding thick-walled polyethylene tubing on wooden cylinders of different diameters (Ali, 2001), tangentially extended at their two ends. These straight tube extensions are used to subside fluid disturbances at the entry as well as at the exit of the coil. Pressure-drop data for an equal straight length of the same tubing was obtained and subtracted from the pressure drop data of the coil-straight length combination so as to give the pressure drop data for the coiled portion only. Water at ambient temperature was used as the test fluid.

Table 2
Geometric data of the coils used in the experiments of Ali (2001) for water single-phase flow.

Coil number	d (m)	D (m)	D/d	p (m)	L_c (m)	p/D
1	0.00603	0.116225	19.27	0.05	2.238	0.43
2	0.00603	0.116225	19.27	0.01	2.238	0.086
3	0.00603	0.116225	19.27	0.05	1.123	0.43
4	0.00603	0.116225	19.27	0.01	1.115	0.086
5	0.00464	0.116225	25.05	0.05	2.263	0.43
6	0.00464	0.116225	25.05	0.05	1.132	0.43
7	0.00603	0.22448	37.23	0.01	4.26	0.045
8	0.00603	0.22448	37.23	0.01	2.13	0.045

The pressure drop versus water flow rate data were experimentally obtained for a set of eight thick-walled polyethylene helical coils. The geometrical data of the coils are reported in Table 2, where L_c and p are the coil length and the pitch. The dimensions are such that D/d varies from 19.27 to 37.23, and p/D varies from 0.045 to 0.43.

The nodalization used for the RELAP5 system code consists in an inclined pipe subdivided in sub-volumes, which schematizes the helical coil tubes test section, with length, tube diameter and helical diameter equal to the ones used in the various experiments (in the RELAP5 input a new flag allows one to specify these geometrical parameters). Moreover two horizontal pipes, which are connected with inlet and outlet coil pipes, are used to simulate the straight tube extensions. As the experiments are performed in steady state conditions, with constant values of the water mass flow rate, no pumps have been schematized and the constant mass flow rates are assured by two time-dependent junctions which supply the test section water flow rate of the analysed tests.

In Figs. 1–4 some experiments, reported as log–log plots of $Eu = \Delta P/(2\rho V^2)$ (Euler number) versus the Re number, together with the corresponding unmodified and modified RELAP5 code results, are shown. Moreover, in Figs. 1 and 2 the ±10% error bars relative to each experimental data are also reported.

By using the modified RELAP5 code, fairly good results are obtained with an error below 3% for the runs nos. 1 and 3 (Figs. 1), and a pressure-drop overprediction of approximately 5% for the runs nos. 5 and 6 (Fig. 2). For run no. 8 (Fig. 2), this overprediction reaches approximately 10% for log(Re) above 3.7 (Re number of about 5000), probably because the experiments were performed with a low helix pitch value (nearly-horizontal tube), for which it could be necessary to use other correlations that would be more valid for this geometry, here not treated. Nevertheless, the low errors indicate that Ito's correlations seem to be appropriate for this configuration as well.

On the contrary, when using the unmodified RELAP5 code, the experimental data are underestimated by up to 40% for all tests at every Re number (see, for example, Figs. 3 and 4), Finally, the comparison among Figs. 1 and 2 with Figs. 3 and 4 highlights the effectiveness of the interpolation procedure that was cited in the previous section.

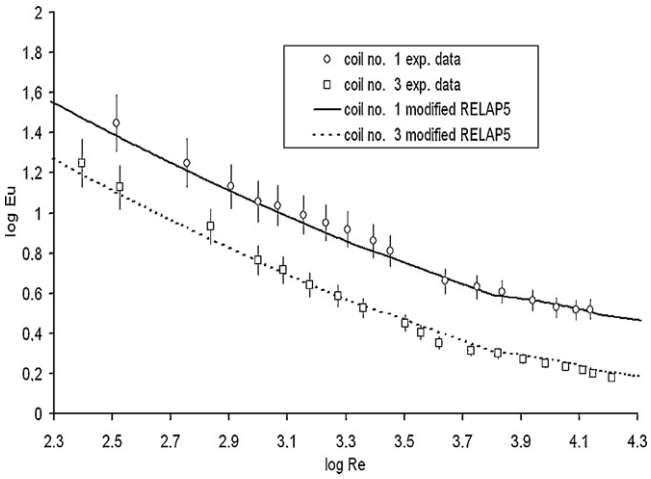

Fig. 1. Ali's (2001) experiments relevant to log Euler numbers for coil no. 1 and coil no. 3: effect of modified RELAP5 smoothing procedure. The bars represent ±10% errors.

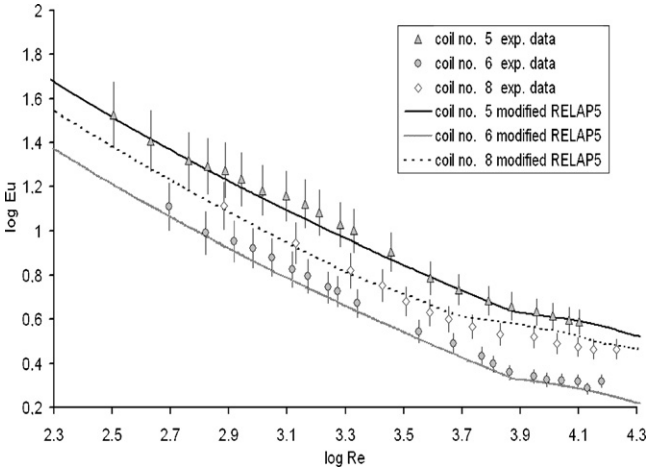

Fig. 2. Ali's (2001) experiments relevant to log Euler numbers for coil no. 5, coil no. 6 and coil no. 8: effect of modified RELAP5 smoothing procedure. The bars represent ±10% errors.

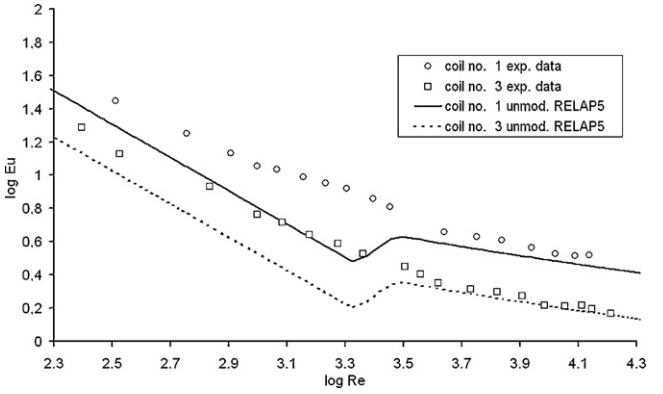

Fig. 3. Ali's (2001) experiments relevant to log Euler numbers for coil no. 1 and coil no. 3 and results obtained by using the unmodified RELAP5 code.

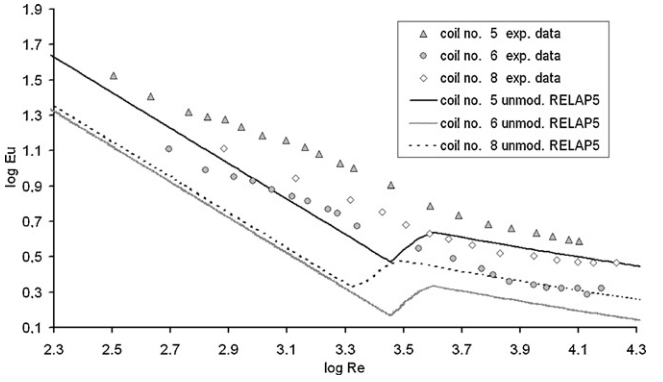

Fig. 4. Ali's (2001) experiments relevant to log Euler numbers for coil no. 5, no. 6 and no. 8 and results obtained by using the unmodified RELAP5 code.

Table 3
Geometric data of the test sections used in the experiments performed at the Polytechnic of Torino laboratory (Bertani et al., 2007, 2008).

	Description	SI	Helix 1	Helix 2
D	Helix diameter	m	0.64	1
d	Pipe diameter	m	0.012	0.012
D/d	–		53.33	83.33
p	Pitch	m	0.485	0.79
p/D	–		0.758	0.79
L_c	Coil length	m	10.25	10.07

3.2. Experimental data performed at the Polytechnic of Torino laboratory

For these experiments (Bertani et al., 2007, 2008), the test sections helical tubes were made of plexiglass to visualize the flow patterns. The test section consists of two tubes with inner and outer diameters of 0.012 m and of 0.018 m, respectively, and a helix angle of 14.12°. The tube named "Helix 1" is characterized by a coil diameter of 0.64 m, a length of 10.25 m, and a pitch of 0.485 m; whereas the tube named "Helix 2" is characterized by a coil diameter of 1 m, a length of 10.07 m, and a pitch of 0.79 m. Some of the geometric characteristics are reported in Table 3.

The parameters directly measured are the flow rates, the pressure drops and the water mass. Both air and water flow rates were measured by rotameter-type flow meters with an accuracy of ±5%. The pressure drops were measured by Rosemount pressure transducers with an accuracy of ±0.5%. The loop absolute pressure is measured at the test section inlet by means of an absolute calibrated pressure transducer, with a maximum uncertainty of 0.1% read values.

The pressure difference was measured by nine differential pressure transducers placed along the pipe at different heights, in correspondence of several taps, and the pressure differences between the first tap (named 1) and the subsequent tap (named 2 through 9) have been reported as ΔP_{12} through ΔP_{19}, at different water mass flow rates. Table 4 reports the location of the taps connected to the pressure transducers.

The void fraction was measured by a quick closing valves method, which was achieved by mounting two solenoid valves at the ends of the test section. The water trapped in the test section is the water hold-up which is purged out and weighed by a calibrated electronical scale.

A schematic representation of the experimental facility is shown in Fig. 5.

The nodalization performed for the RELAP5 analyses consists of the time dependent volume components used to specify the inlet and outlet conditions of the helical coil tubes loop.

Through time-dependent junctions, the air and water flow mixture is sent to a pipe, which schematizes the helical test section, divided into 50 sub-volumes for a better approximation of the pressure taps position along the helical pipe length. In this pipe the "helical flag" is used as explained in the previous section. By using these junctions the air and water flow conditions are changed, according to the simulated experiments.

Table 4
Geometric data of the test sections taps position used in the experiments performed at the Polytechnic of Torino laboratory (Bertani et al., 2007, 2008).

Taps position	Helix 1		Helix 2	
	Δz (m)	ΔL (m)	Δz (m)	ΔL (m)
L12	0.98	4.72	0.22	1.183
L13	1.096	5.2	1.003	4.39
L14	1.225	5.75	1.192	5.17
L15	1.342	6.24	1.395	6.01
L16	1.462	6.744	1.594	6.82
L17	1.946	8.78	1.789	7.62
L18	2.19	9.88	2.185	9.25
L19	2.44	10.25	2.385	10.07

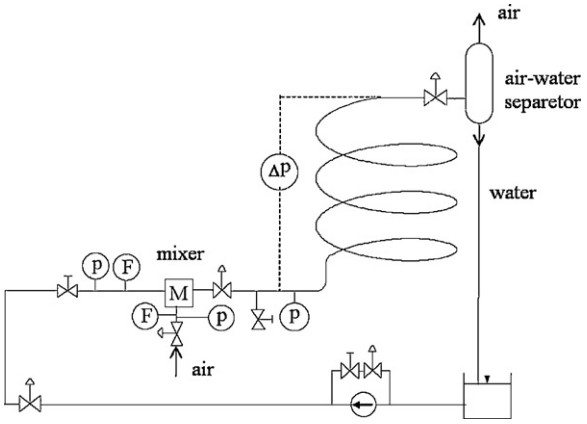

Fig. 5. Schematic of the experimental facility at the Polytechnic of Torino laboratory (Bertani et al., 2007, 2008).

3.2.1. Single-phase flow analysis

Experiments of water single-phase flow rates, in the range from 0.056 to 0.22 kg/s (5500 < Re < 22,650), flowing in the "Helix 2" test section have been performed.

Fig. 6 shows some of the results in term of pressure drops along the test section obtained using the modified and unmodified RELAP5 code together with the corresponding experimental data. With the unmodified code, the data are underestimated, with errors by up to 30% at higher mass flow rates; but for ΔP_{12} for which the prediction can be considered satisfactory.

However, when the simulations are performed with the modified code, the error of the prediction is maintained below 5%.

The analysis of the results highlights the good performance of the modified RELAP5 code.

3.2.2. Two-phase flow analysis

Two different pumps were used to supply water at flow rates of 200–400 l/h and 400– 800 l/h. For each water flow rate, the air flow was varied from 0.043 to 0.26 g/s.

The test data have been simulated for each coil diameter by fixing the water flow rate and changing the air flow rate. This procedure is repeated for each water flow rate value. Table 5 presents the water and air mass flow rates for each helix diameter.

Table 5
Test conditions matrix used in the experiments performed at the Polytechnic of Torino laboratory for air–water two-phase flow (Bertani et al., 2007, 2008).

W_{water} [l/h]	W_{air}[a] [l/h]					
$D_{helix} = 0.64\,m$						
200	50	100	150	200	250	300
300	50	100	150	200	250	300
400	50	100	150	200	250	300
600	50	100	150	200	250	300
800	50	100	150	200	250	300
$D_{helix} = 1.0\,m$						
200	50	100	150	200	250	300
300	50	100	150	200	250	300
400	50	100	150	200	250	300
600	50	100	150	200	250	300
800	50	100	150	200	250	300

[a]The effective volumetric air flow rate in normal l/h is given by the table values times 2.45.

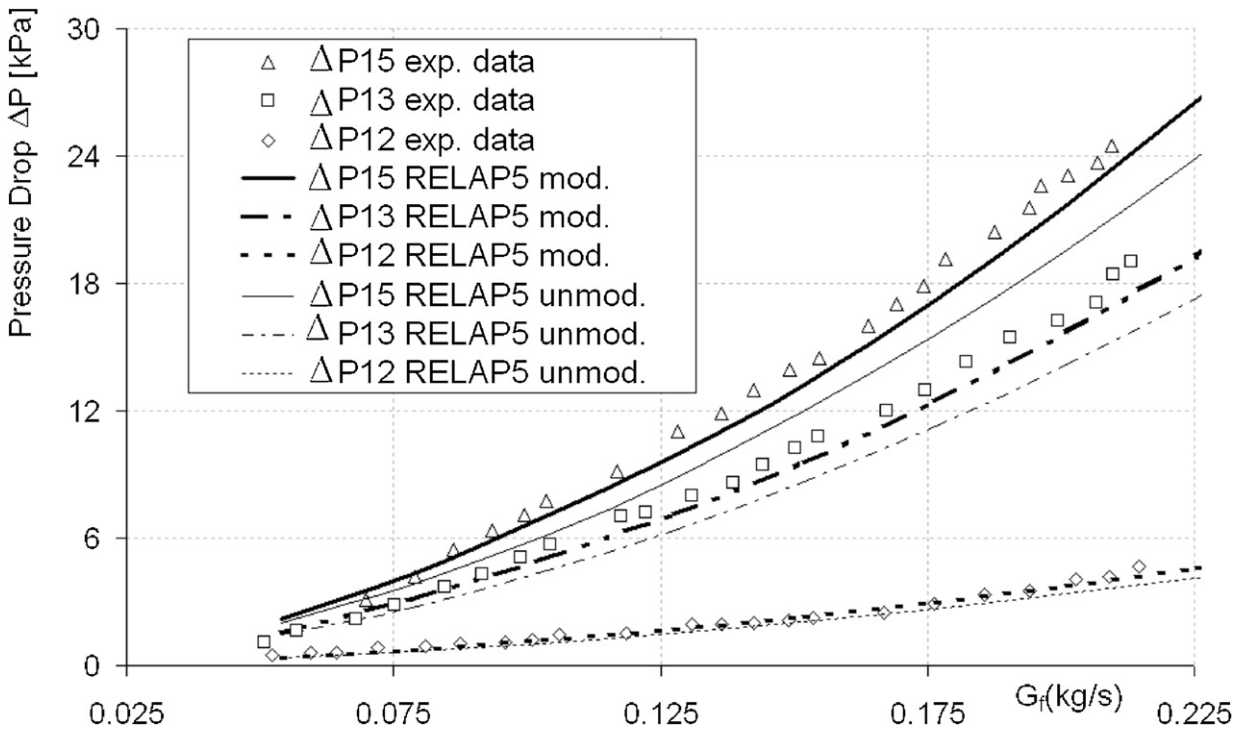

Fig. 6. Comparison of experimental two-phase flow pressure drops ΔP_{12} through ΔP_{15} (Bertani et al., 2007, 2008) with the results obtained by the modified and unmodified RELAP5 code.

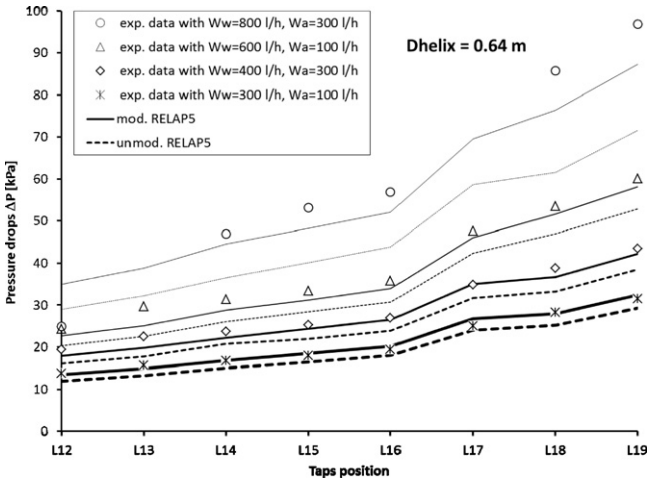

Fig. 7. Comparison of two-phase flow pressure-drops along the helical pipe for the experiments characterized by coil diameter $D = 0.64$ m (Bertani et al., 2007, 2008) with the unmodified (dotted curve) and modified RELAP5 code (continuous curve) simulations.

Some examples of the simulated experimental data are shown in Figs. 7 and 8. In particular, Fig. 7 reports the pressure drops along the pipe (L12 through L19, in Table 4) for the test section with helix diameter of 0.64 m, and Fig. 8 shows the experimental data performed in the test section with helix diameter of 1.0 m.

Table 6
Chi-square test values (χ^2) of the pressure drop experimental data simulations by using unmodified and modified RELAP5 code.

	Unmodified code	Modified code
$D = 0.64$ m	2.8	1.2
$D = 1.0$ m	1.7	1.05

In Table 6 the chi-square test values, which are frequently used to compare the observed test data with the predictions (goodness of fit), are also shown for $D = 0.64$ m and $D = 1.0$ m.

Figs. 9 and 10 show the experimental versus predicted pressure drop results along the test section for unmodified and modified code, respectively.

For the unmodified RELAP5 code, 60% of the 437 data points are evaluated within an error of ±15%, and approximately 94% of the data points are within an error of ±30%, with a substantial tendency towards underprediction. On the other hand, for the modified RELAP5 code, as much as 80% of the predicted values are calculated with an error well below ±15% and about all data are predicted within an error of ±20%.

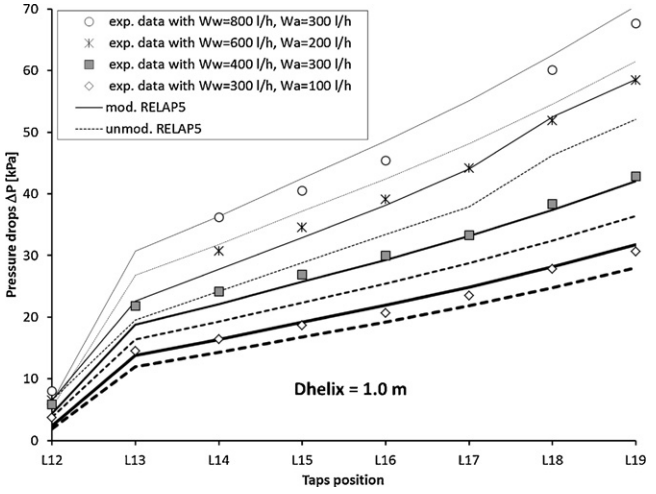

Fig. 8. Comparison of two-phase flow pressure-drops along the helical pipe for the experiments characterized by coil diameter $D = 1$ m (Bertani et al., 2007, 2008) with the unmodified (dotted curve) and modified RELAP5 (continuous curve) code simulations.

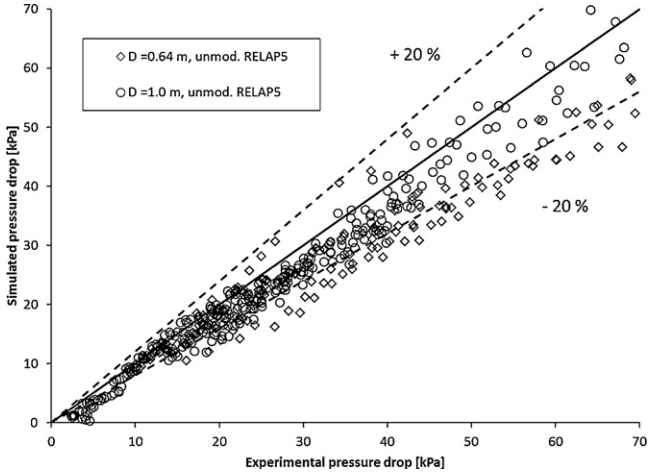

Fig. 9. Air–water two-phase flow pressure-drop predicted by the unmodified RELAP5 code versus experimental values (Bertani et al., 2007, 2008).

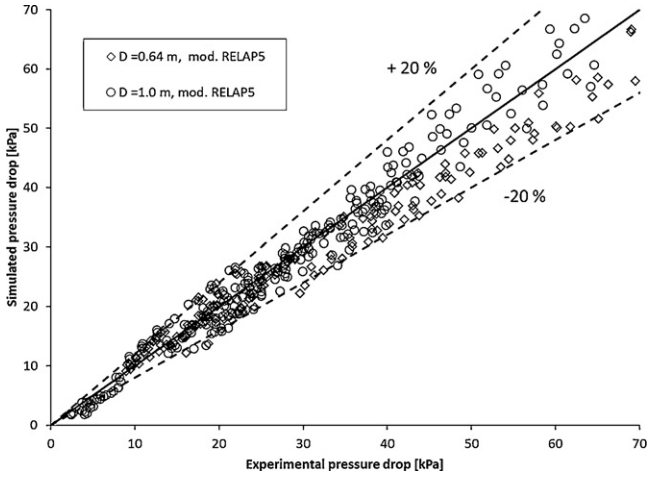

Fig. 10. Air–water two-phase flow pressure-drop predicted by the modified RELAP5 code versus experimental values (Bertani et al., 2007, 2008).

4. Conclusion

In the present study, the pressure drops for single and two-phase flow in vertical helical pipes have been predicted by means of the RELAP5/mod3.2β code that was suitably improved with correlations set up to model some aspects of the complex fluid-phenomena associated with these systems.

This has been performed taking into consideration that the code, based on one-dimensional thermal–hydraulic relationships, has limitations for modelling the thermal–fluidynamics phenomena involved in this geometry.

So, at first, the code was improved with additional correlations valid for single-phase flow that could allow one to overcome these difficulties. Among the correlations available in the literature for helical pipes, Ito's friction factor ones have been used. Moreover, the code was modified to allow also the studies of two-phase flow by using the Lockhart–Martinelli correlations, valid for helical pipes, as modified by Xin et al.

Experimental data obtained at several international research laboratories (Bertani et al., 2007, 2008; Ali, 2001) and especially at the Polytechnic of Torino Department of Energetics, have been used to validate the modified RELAP5 code. These last experimental activities have allowed us to investigate the fluid dynamics behaviour of a helically coiled steam generator that has been designed for the IRIS nuclear power reactor: two test sections with different helical diameters were tested to study the effect of the centrifugal forces on the flow pattern.

The obtained results show that much of the analyzed experimental data are better predicted by the modified RELAP5 code for all the examined helical pipes geometries, as it is confirmed by the results reported in Table 6, where the values of the chi-square test (χ^2) for goodness of fit is reported. This result seem interesting taking into account that the modified code is based on simple structure in comparison with 3D or finite elements ones.

References

Ali, S., 2001. Pressure drop correlations for flow through regular helical coil tubes. Fluid Dyn. Res. 28, 295–310.
Bandini, G., Meloni, P., Polidori, M., Casamirra, M., Castiglia, F., Giardina, M., 2008. Decay heat removal and transient analysis in accidental conditions in the EFIT reactor. Sci. Technol Nucl. Instal., 1.
Banerjee, S., Rhodes, E., Scott, D.S., 1969. Studies on concurrent gas–liquid flow in helically coiled tubes. I-Flow patterns, pressure drop, and holdup. Can. J. Chem. Eng. 47, 445–453.
Bertani, C., De Salve, M., Malandrone, M., Orio, M., Panella, B., 2007. Studio sperimentale del deflusso bifase aria-acqua in un tubo elicoidale. In: XXV Congresso Nazionale UIT sulla Trasmissione del Calore, Trieste, 18–20 June 2007.
Bertani, C., De Salve, M., Malandrone, M., Orio, M., Panella, B., 2008. Cadute di pressione e grado di vuoto in condotti elicoidali: confronto tra risultati sperimentali e modelli semiempirici. In: XXVI Congresso Nazionale UIT sulla Trasmissione del Calore, Palermo, 23–25 June 2008.
Carelli, M.D., et al., 2004. The design and safety features of the IRIS reactor. Nucl. Eng. Des. 230, 151–167.
Casamirra, M., Castiglia, F., Giardina, M., Meloni, P., 2005. RELAP5 Modification for CHEOPE Simulations. In: International Conference Nuclear Energy for New Europe, Bled, Slovenia, 5–8 September 2005.
Casamirra, M., Castiglia, F., Giardina, M., Lombardo, C., 2006. Modifying RELAP5 code to deal with helical coiled ducts. In: XXIV Congresso Nazionale sulla trasmissione del calore, UIT, Napoli, Italy, 21–23 June 2006.
Casamirra, M., Castiglia, F., Giardina, M., 2007. Heat Transfer Prediction of the THX Exchanger in MEGAPIE Facility by Using RELAP5 Code Suitably Modified to Deal with Helical Channel. Technical Report, FPN-P9EH-010, ENEA, Bologna, 20 December 2007.
Casamirra, M., Castiglia, F., Giardina, M., 2009. Lombardo, C. Studio con il codice RELAP5 delle perdite di carico e dello scambio termico in tubi elicoidali interessati da deflussi monofase. XXVII Congresso Nazionale UIT sulla Trasmissione del Calore, Reggio Emilia, 22–24 June 2009.
Cioncolini, A., Santini, L., 2006. An experimental investigation regarding the laminar to turbulent flow transition in helically coiled pipes. Exp. Thermal Fluid Sci. 30, 367–380.
Dean, W.R., 1927. Note on the motion of fluid in a curved pipe. Philos. Mag. 4, 208–223.
GIF, 2002. A Technology Roadmap for Generation IV Nuclear Energy Systems. Issued by the U.S. DOE Nuclear Energy Research Advisory Committee and the Generation IV International Forum, GIF-002-00, December 2002.
Gou, L., Feng, Z., Chen, X., 2001. An experimental investigation of the frictional pressure drop of steam–water two-phase flow in helical coils. Int. J. Heat Mass Transfer 44, 2601–2610.
IAEA, 2005. Innovative small and medium sized reactors: design features, safety approaches and R&D trends. Final report of a technical meeting, 7–11 June 2004, Vienna, IAEA-TECDOC-1451, May 2005.
High Temperature Gas Cooled Reactor Fuels and Materials. International Atomic Energy Agency (IAEA), 2010. IAEA, TECDOC-1645, Vienna.
Ito, H., 1959. Friction factors for turbulent flow in curved pipes. Trans. Am. Soc. Mech. Engrs. 81, 123–134.
Jeschke, H., 1925. Wärmeübergang und Druckverlust in Rohrschlangen. Beih. Tech. Mech., Z.VDI 69, 24–28.
Lockhart, R.W., Martinelli, R.C., 1949. Proposed correlation of data for isothermal two-phase two component flow in pipes. Chem. Eng. Prog. 45, 39–48.
Rippel, G.R., Eidt, C.R., Jornan, H.B., 1966. Two-phase flow in a coiled tube. Ind. Eng. Chem. 5, 32–39.
Ritu Gupta Wanchoo, R.K., Jafar Ali, T.R.M., 2011. Laminar flow in helical coils: a parametric study. Ind. Eng. Chem. Res. 50 (2), 1150–1157.
Xin, R.C., Awwad, A., Dong, Z., Ebadian, M.A., Soliman, H.M., 1996. An investigation and comparative study of the pressure drop in air–water two-phase flow in vertical helicoidal pipes. Int. J. Heat Mass Transfer 39, 735–743.
Xin, R.C., Awwad, A., Dong, Z., Ebadian, M.A., 1997. An experimental study of single-phase and two-phase flow pressure drop in anular helicoidal pipes. Int. J. Heat Fluid Flow 18, 482–488.

4 PRINCIPALI MODELLI E CORRELAZIONI DISPONIBILI IN LETTERATURA PER L'ANALISI DI TRANSITORI IN REATTORI DI IV GENERAZIONE REFRIGERATI A METALLO LIQUIDO E POSSIBILI APPLICAZIONI E IMPLEMENTAZIONI IN CODICI DI CALCOLO

CIRTEN

Consorzio **I**nteruniversitario per la **R**icerca **TE**cnologica **N**ucleare

UNIVERSITÀ DEGLI STUDI DI PALERMO

DIPARTIMENTO DI ENERGIA, INGEGNERIA

DELL'INFORMAZIONE E MODELLI MATEMATICI

PRINCIPALI MODELLI E CORRELAZIONI DISPONIBILI IN LETTERATURA PER L'ANALISI DI TRANSITORI IN REATTORI DI IV GENERAZIONE REFRIGERATI A METALLO LIQUIDO E POSSIBILI APPLICAZIONI E IMPLEMENTAZIONI IN CODICI DI CALCOLO

Autori

F. Mascari, M. L. Richiusa, G. Vella

CERSE-UNIPA RL 1222/2013

PALERMO, Agosto 2013

Lavoro svolto in esecuzione dell'Attività *LP2-A3*
AdP MSE-ENEA sulla Ricerca di Sistema Elettrico - Piano Annuale di Realizzazione 2012
Progetto B.3.1 "Sviluppo competenze scientifiche nel campo della sicurezza nucleare e collaborazione ai programmi internazionali per il nucleare di IV generazione

Indice

1. APPLICABILITY OF ANALYTICAL MODELS FOR GIF-IV LEAD-COOLED REACTOR PROTOTYPES

The aim of this work is to study and identify the main models and correlations of pressure drop and heat exchange used and implemented in thermal hydraulic system codes (TRACE, RELAP5-3D) to simulate steady-state and possible transient conditions of Generation-IV Lead-cooled reactors. Among the six promising reactor technologies being considered by the GIF member countries, the Lead-cooled Fast Reactor (LFR) has been identified as the technology with great potential to meet the needs for both remote sites and central power stations [1]. The LFR system is top-ranked in sustainability because it uses a closed fuel cycle, and in proliferation resistance and physical protection because it employs a long-life core. It is considered good in safety and economics. The safety is enhanced by the choice of a relatively inert coolant at high temperatures. Lead does not react with water or air, so this give the possibility to eliminate the intermediate loop and stringent requirement on reactor leak tightness; steam generators can be installed inside reactor vessel. Lead has very high boiling point and very low partial pressure: these features reduces core voiding risk. Furthermore, Lead is a low moderating medium and has low absorption cross section; these elements permit to increase space between fuel rods reducing core pressure loss and enhancing natural circulation capability, in other words, this means the possibility to adopt passive safety systems [2].

Since Lead is much more abundant and less expensive than Bismuth, in case of deployment of large number of reactors, pure Lead as coolant offers enhanced sustainability. Furthermore, the use of Lead reduces the production of the highly radioactive and, hence, decay-heat generating Polonium in the coolant with respect to Lead-Bismuth Eutectic (LBE). Operation at a higher minimum temperature, required by the use of pure Lead, are necessary also in the case of LBE to improve plant efficiency and to avoid excessive embrittlement of structural material subjected to fast neutron flux at low temperature. The risk of Lead freezing is reduced by the choice of a pool-type configuration.

The LFR system is estimated to be deployed by 2025.

For this reasons most of the civil reactor projects developed in the last years are based on pure Lead as coolant. Among them, BREST-300 and BREST-1200 have been launched in Russia; the European Lead-cooled System (ELSY) and its evolutions European Lead-cooled Fast Reactor (ELFR) and the LFR-Demo Advanced Lead fast Reactor European Demonstrator (ALFRED) have been proposed in the framework of European projects, and the Small Secure Transportable Autonomous Reactor (SSTAR) in USA. LBE is mainly reserved to experimental reactors mainly because of the lower freezing temperature when compared to Lead and for the large power density that can be obtained even at low operating temperature [3].

After a brief introduction about the status of development of LFR, it will follow an overview on the pressure drop and heat transfer models presented in literature, useful to understand the field of applicability of such models and to compare this models with the ones used by the system codes.

1.1. ELSY DESIGN PROJECTS [1], [4]

Design feasibility studies for a LFR are performed within the framework of EURATOM programmes. The LFR system is characterized by a fast-neutron spectrum and a closed fuel cycle for efficient conversion of fertile uranium. The LFR can also be used as a burner of all actinides from spent fuel and as a burner/breeder with Thorium matrices. The design proposed during the past years as candidate for international cooperation and joint development in the GIF framework are the pool-type reactor ELSY.

The ELSY project aims at demonstrating the possibility to design a competitive and safe Lead-cooled Fast power Reactor using simple engineered features, such as compact in-vessel steam generators and a simple primary circuit with all internals possibly removable.

The ELSY power plant is sized at 600 MWe because only plants of the order of several hundreds MWe are expected to be economically affordable on the existing well-interconnected grids of Europe.

Thanks to the suitable neutronic characteristics of Lead as coolant, the fuel rods of a Lead-cooled reactor, similarly to LWRs, can be spaced further apart than in the case of Sodium as a coolant, resulting in a lower pressure drop across the core. As a consequence, in spite of the higher density of Lead, the needed pump head can be kept low (on the order of one to two bars) with a reduced requirement for pumping power.

Figure 1.1. shows the cylindrical inner vessel concept of circular cross section, a first project scheme for the primary system design of ELSY.

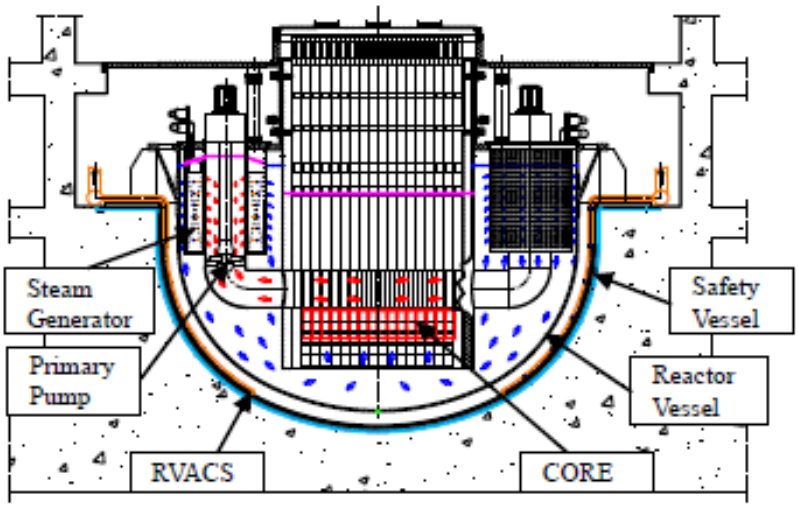

Fig. 1.1. Preliminary scheme of the ELSY Reactor [4].

The vessel containment contains eight steam generators (SGs) and, respectively, eight primary pumps (PP). The SG tube bundle is characterized by a stack of spiral-wound tubes arranged in the annular space between the perforated outer and inner shells of the SG with the inlet and outlet ends of each tube connected to the feed water header and steam header, respectively.The tube spirals (one spiral for each tube, two spirals per layer) are arranged equally spaced one above the other. An axial-flow primary pump, located inside the inner shell of the SG, provides the head requires to force the coolant to enter from the bottom of the SG; then, the hot Lead flows radially through the perforated inner shell and, once past the tube spirals, through the outer shell.

Simplification of the internals will offer the possibility of removable in-vessel components, a provision for investment protection.

Compactness of the reactor building is the result not only of the elimination of the Intermediate Cooling System but also of the reduced height of the vessel; this is the result of forced circulation and the design approach of reduced-height components. For more details about the project design, it can see [1], [4].

However, in March 2010 the activities on ELSY were terminated and the ELSY reference design evolved to a new system configuration identified as ELFR. The new conceptual configuration is developed under the new LEADER project (Lead-cooled European Advanced Demonstration Reactor). Its main aim is to identify the design changes to the ELSY configuration (it becomes ELFR) in order to promote a conceptual design of a small size reactor (300 MWth, the Demonstrator ALFRED), based on available technology to be able to start construction in the short time frame.

Below are reported the primary project scheme of ELFR and ALFRED designs.

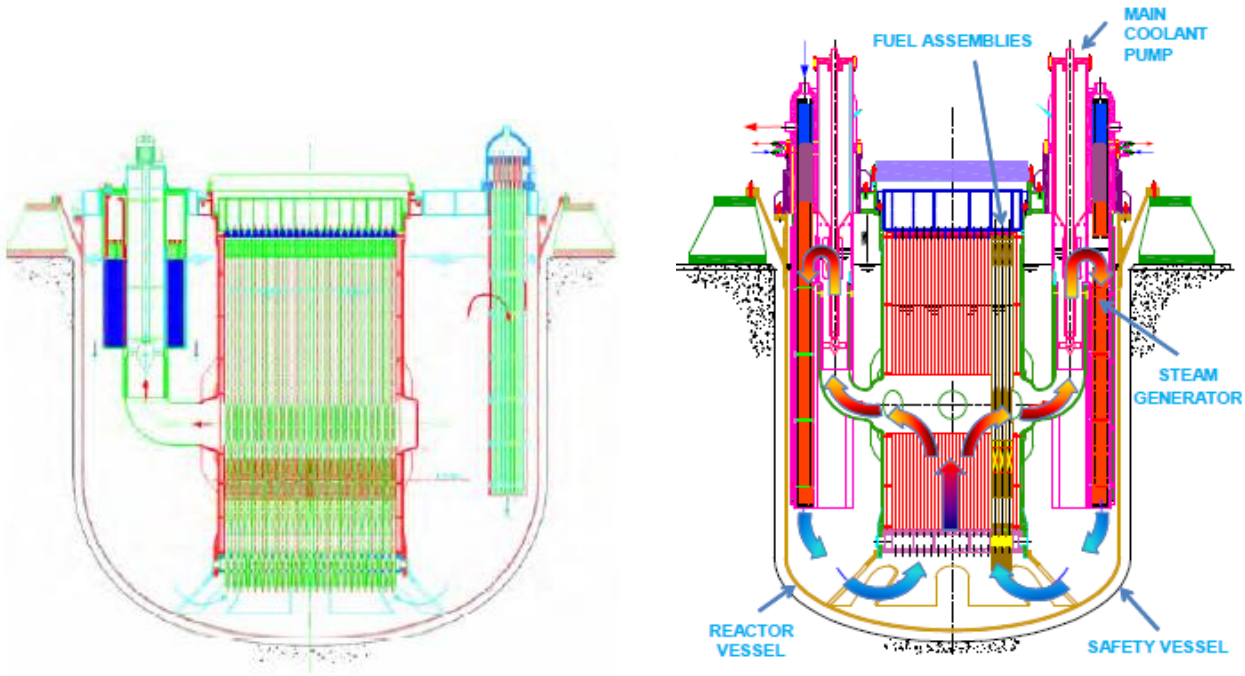

Fig 1.2. Preliminary project of ELFR [2] (to the left) and ALFRED-DEMO [3] (to the right).

2. LIQUID METAL FAST BREEDER REACTORS [5]

Liquid metals used as refrigerant in fast nuclear reactors are characterized by high thermal conductivities, high heat transfer coefficients and high specific heat that permits to remove thermal power with lower temperature gradients and relatively small flow quantities.
Conductive heat transfer is governed by Fourier's equation, in which the heat flux per unit area for laminar and slug flow in a three-dimensional system is given by:

$$\frac{\dot{q}}{A} = -k\bar{\nabla}T \tag{1.1}$$

where:

$\dot{q}$ = rate of heat transfer, W

A= area, m^2

k = thermal conductivity, W/mK

$\bar{\nabla}$T= temperature gradient along the three spacial directions, K/m

and for turbulent flow:

$$\frac{\dot{q}}{A} = -(\alpha + \varepsilon_H)C_p\rho\bar{\nabla}T \tag{1.2}$$

where:

ε_H = eddy diffusivity of heat, m^2/s

α = thermal diffusivity, m^2/s.

Unlike ordinary liquids, the molecular thermal conductivity of liquid metals is so high that it competes with eddy conductivity in transferring heat across the turbulent core in channel flow.
In a convective heat transfer, instead, the heat flux per unit area is calculated according the Newton's equation:

$$\frac{\dot{q}}{A} = h\left(t_w - t_b\right) \tag{1.3}$$

where:

h = surface heat-transfer coefficient, W/m^2K

t_w = wall temperature, K

t_b = bulk coolant temperature, K

Three non-dimensional numbers are useful to study thermal transfer properties of fluids:

The **Reynolds number** $$N_{\mathrm{Re}} = \frac{\rho u D_e}{\mu} = \frac{u D_e}{\nu} \tag{1.4}$$

where:

u=mean velocity of fluid, m/s

μ=absolute viscosity of fluid, Ns/m^2

ρ=fluid density, kg/m^3

ν=dynamic viscosity, m^2/s

D_e = characteristic length for the flow, m

The Reynolds number is a measure of the degree of turbulence of a flowing fluid; this is significant for the kind of flow established inside a channel (laminar or turbulent flow) because it represents the ratio of inertia forces to viscous forces.

The **Prandtl number**

$$N_{\mathrm{Pr}} = \frac{\mu c_p}{k} = \frac{\nu}{\alpha} \tag{1.5}$$

where:

α=thermal diffusivity, m^2/s

The Prandtl number is defined as the ratio of the molecular diffusivities of momentum and of heat. Gaseous and non-metallic fluids have $N_{\mathrm{Pr}} \geq 1$; liquid metals are characterized by $0.001 \leq N_{\mathrm{Pr}} \leq 0.1$ because of their high thermal conductivities. Low Prandtl numbers mean that heat from a solid surface is propagated by conduction much farther into the stream of coolant than it is in a fluid with a higher Prandtl number. Turbulence is less necessary to achieve good heat transfer into the stream and heat transfer coefficients are less dependent on flow rate, whether in forced or free convection.
For forced-convection heat transfer, the heat transfer coefficient is expressed in a dimensionless **Nusselt number**:

$$N_{Nu} = \frac{hD_e}{k} \tag{1.6}$$

that is significant of the way in which the heat transfer takes place (conduction or convection mechanism).
The heat transfer through liquid metals is governed by the **Peclet number**, defined as the product of Reynolds and Prandtl numbers:

$$N_{Pe} = N_{\mathrm{Re}} \times N_{\mathrm{Pr}} \tag{1.7}$$

The Peclet number is the ratio of heat transfer by convection to heat transfer by conduction and the Nusselt number is a function of the Peclet number.
Theoretically, the correlations would be affected by the temperature variations caused by the heat transfer itself; for liquid metals, their thermal properties do not vary greatly with temperature and liquid metals yield high values of h and, consequently, low values of $(t_w - t_b)$. It is seen that fluids with Prandtl number close to 1 have a fractional temperature change that almost coincides with the fractional velocity change. For liquid metals (with low Prandtl number), the temperature variations extend over the entire tube radius: the turbulent or eddy viscosity and the velocity profile exhibit almost no temperature dependence.

3. LIQUID-METAL PRESSURE DROP

The relations that govern the flow behaviour of common fluids, such as water, are also valid for liquid metals. In the same way, the methods by which frictional losses and form losses are calculated for common fluids can be used with liquid metals. The data developed for predicting frictional losses as a function of Reynolds number and form losses as a function of velocity, and velocity profiles in ducts as a function of Reynolds numbers are used to the fast reactor engineering [5].

The Reynolds number describes the character of the flow. In round tubes:

1. For $N_{\mathrm{Re}} < 2000$, all the flow filaments are parallel to the flow axis, and the flow is laminar.
2. For $N_{\mathrm{Re}} > 4000$, the flow filaments present no constant pattern with respect to time and the walls of the duct, and the flow is turbulent.
3. For $2000 < N_{\mathrm{Re}} < 4000$ the flow is in the critical zone with either laminar or turbulent conditions, depending on the absence or presence of irregularities in the duct, vibrations, prior turbulence and other factors.

Liquid-metal flow is no different than that of non-metals; conventional formulas and techniques of calculation can be used in the design of liquid-metal piping systems. The frictional pressure drop across a length *l* of the conduit can be calculated as:

$$\Delta p = f \frac{l}{D} \rho \frac{u^2}{2} \tag{1.8}$$

where *f* is the Weisbach friction factor, a function of Reynolds number and, in a turbulent regime, also of the relative roughness, ε/D, and it can be calculated using the Moody diagram. D represents a characteristic length of the considered geometry: for round tubed, D is the inside diameter; for other geometric configurations, such as noncircular tubes, D coincides with the hydraulic diameter (or equivalent diameter, defined as a function of the flow area and its wet perimeter, $D_e = 4\frac{S}{P}$).

For circular smooth tubes, in laminar flow, $f = \frac{64}{N_{\mathrm{Re}}}$. (1.9)

Pressure losses due to fittings, valves, bends, contractions and expansions are called form losses. These objects cause the flowing fluid to lose energy owing to a sudden change of cross section or change of direction [5]. Such a loss in energy is proportional to $\bar{u}^2$:

$$\Delta p = k \cdot \frac{\rho u^2}{2} \tag{1.10}$$

where k is the velocity head-loss coefficient, calculated for different form losses.

3.1. PRESSURE DROP IN ROD BUNDLES

The total pressure drop along a reactor core includes:

- Entrance and exit pressure between the vessel plena and the core internals;
- The friction pressure drop along the fuel rods;
- The form losses due to the presence of spacers.

The entrance and exit losses are due to a sudden change in flow area; attention here is focused on the friction along the rod bundles and the effect of the spacers [6].

3.1.1. FRICTION ALONG BARE ROD BUNDLES

- **Laminar Flow [6]**

The coolant region in rod array can be represented as an array of equivalent annulus around the rods.
The equivalent annulus approximation is satisfactory for pitch-to-diameter (P/D) ratios greater than 1.3, in a triangular array (see fig. 3.1).

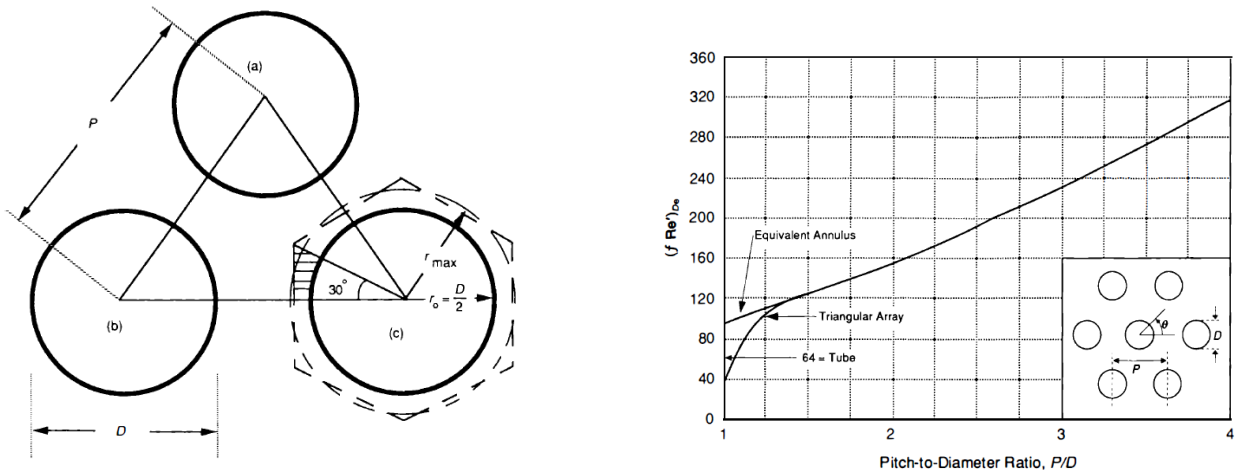

Fig. 3.1. On the left: equivalent annulus around a rod in a triangular array. Cross-hatched area represents an elementary coolant flow section; circle of radius r_{max} represents the equivalent annulus with equal flow area. On the right: product of laminar friction factors and N_{Re} for parallel fully developed laminar flow in a triangular array rod bundle [6].

For fully developed laminar flow for such a kind of triangular subchannel, in a bare (spaceless) rod bundle, the friction factors are been well calculated by Cheng and Todreas through polynomials that have the following form:

$$C_{f_{iL}} = a + b_1\left(\frac{P}{D} - 1\right) + b_2\left(\frac{P}{D} - 1\right)^2 \tag{1.11}$$

where:

$$f_{iL} = \frac{C_{f_{iL}}}{N_{\mathrm{Re}}^n}$$

(1.12)

and for laminar flow n=1.

For edge and corner subchannels, P/D is replaced by W/D, where W is the rod diameter plus gap between rod and bundle wall.

The effect of P/D (or W/D) is separated into two regions; $1.0 \le P/D \le 1.1$ and $1.1 \le P/D \le 1.5$. Tables 3.1 and 3.2 present the coefficients a, b_1 and b_2 for the subchannels of hexagonal and square arrays, respectively.

	$1.0 \le P/D \le 1.1$			$1.1 < P/D \le 1.5$		
Subchannel	a	b_1	b_2	a	b_1	b_2
Laminar flow						
Interior	26.00	888.2	−3334	62.97	216.9	−190.2
Edge	26.18	554.5	−1480	44.40	256.7	−267.6
Corner	26.98	1636.	−10,050	87.26	38.59	− 55.12
Turbulent flow						
Interior	0.09378	1.398	−8.664	0.1458	0.03632	−0.03333
Edge	0.09377	0.8732	−3.341	0.1430	0.04199	−0.04428
Corner	0.1004	1.625	−11.85	0.1499	0.006706	−0.009567

Table 3.1. Coefficients in Eqs 1.11 and 1.13 for bare rod subchannel friction factor constants C_{fi} in hexagonal array [6].

	$1.0 \le P/D \le 1.1$			$1.1 < P/D \le 1.5$		
Subchannel	a	b_1	b_2	a	b_1	b_2
Laminar flow						
Interior	26.37	374.2	−493.9	35.55	263.7	− 190.2
Edge	26.18	554.5	−1480	44.40	256.7	−267.6
Corner	28.62	715.9	−2807	58.83	160.7	−203.5
Turbulent flow						
Interior	0.09423	0.5806	−1.239	0.1339	0.09059	−0.09926
Edge	0.09377	0.8732	−3.341	0.1430	0.04199	−0.04428
Corner	0.09755	1.127	−6.304	0.1452	0.02681	−0.03411

Table 3.2. Coefficients in Eqs 1.11 and 1.13 for bare rod subchannel friction factor constants C_{fi} in square array [6].

- **Turbulent Flow [6]**

For turbulent flow situation, solution of both the exact and the equivalent annulus geometry require assumptions about the turbulent velocity distribution. Cheng and Todreas calculated the friction factor using a polynomial such that:

$$C_{f_{iT}} = a + b_1\left(\frac{P}{D}-1\right) + b_2\left(\frac{P}{D}-1\right)^2 \qquad (1.13)$$

where

$$f_{iT} = \frac{C_{f_{iT}}}{N_{\mathrm{Re}}^{n}} \tag{1.14}$$

and n=0.18. Tables 1.1 and 1.2 list the C_{fi} coefficients for subchannels of hexagonal and square array.

3.2. PRESSURE LOSS AT SPACERS

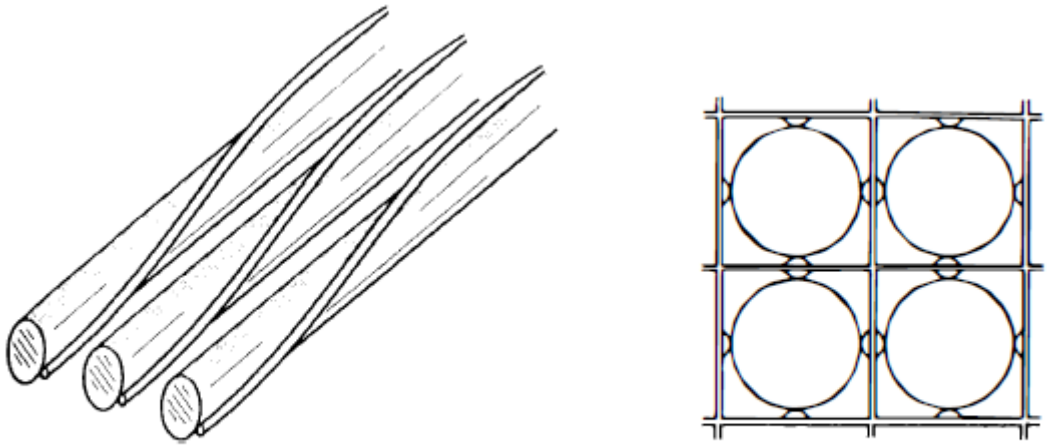

Fig 3.2. Rod bundle fuel element spacers [6].

Pressure losses across spacer grids or wires are form drag-type. The pressure losses can be calculated using pressure-loss coefficients; the spacers' pressure drop can be comparable in magnitude to the friction along the bare rod bundle.

The pressure drop across the spacer grid is given by DeStordeur equation:

$$\Delta p_s = C_s \left(\rho \frac{v_s^2}{2} \right) \left(\frac{A_s}{A_v} \right) \tag{1.15}$$

where

A_s=projected frontal area of the spacers;

A_v=unrestricted flow area away from the grid or spacer;

v_s=velocity in the spacer region.

The grid drag coefficient is a function of the Reynolds number for a given spacer or grid type. At high Reynolds numbers ($N_{\mathrm{Re}} \square 10^5$) honeycomb grids showed drag coefficients of ≈ 1.65.

Rheme founds that the effect of the ratio $\left(A_s / A_v\right)$ is more pronounced than was indicated by DeStordeur, so concluded that grid pressure drop data are better correlated by:

$$\Delta p_s = C_v \left(\rho \frac{v_v^2}{2} \right) \left(\frac{A_s}{A_v} \right)^2 \tag{1.16}$$

where:
C_v=modified drag coefficient;
v_v=average bundle fluid velocity.

The drag coefficient C_v is a function of the average bundle, unrestricted area Reynolds number. For square array, C_v=9.5 at $N_{\mathrm{Re}} \leq 10^4$ and C_v=6.5 at $N_{\mathrm{Re}} = 10^5$.

Recently, Cheng and Todreas (1986) correlated wire-wrapped pressure losses utilizing the large database existing in literature and extracted correlations that cover the laminar, transition and turbulent flow regime; the friction factor for rod bundle is calculated as follow [6]:

Turbulent region: $N_{\mathrm{Re}} < N_{\mathrm{Re},L}$ with $N_{\mathrm{Re},L} = 10^{(1.7P/D+0.78)}$

$$f_T = \left(\frac{C_{fT}}{N_{\mathrm{Re}}^{0.18}}\right)\psi^{1/3} \tag{1.17}$$

Transition region: $N_{\mathrm{Re},L} < N_{\mathrm{Re}} < N_{\mathrm{Re},T}$

$$f = \left(\frac{C_{fT}}{N_{\mathrm{Re}}^{0.18}}\right)\psi^{1/3} + \left(\frac{C_{fT}}{N_{\mathrm{Re}}}\right)(1-\psi)^{1/3} \tag{1.18}$$

Laminar region: $N_{\mathrm{Re}} > N_{\mathrm{Re},T}$ with $N_{\mathrm{Re},T} = 10^{(0.7P/D+3.3)}$

$$f_L = \frac{C_{fL}}{N_{\mathrm{Re}}} \tag{1.19}$$

where:

$$\psi = \frac{\log_{10}\left(N_{\mathrm{Re}}/N_{\mathrm{Re}L}\right)}{\log_{10}\left(N_{\mathrm{Re}T}/N_{\mathrm{Re}L}\right)} = \frac{\left[\log_{10}(N_{\mathrm{Re}}) - (1.7(P/D)+0.78)\right]}{(2.52 - P/D)} \tag{1.20}$$

$$C_{fT} = \left[0.8063 - 0.9022(\log_{10}(H/D))\right] + 0.3256\left[(\log_{10}(H/D))\right]^2 \left(P/D\right)^{9.7} \left(H/D\right)^{1.78-2.0\cdot(P/D)} \tag{1.21}$$

$$C_{fL} = \left[-974.6 + 1612.0\left(P/D\right) - 598.5\left(P/D\right)^2\right]\left(H/D\right)^{0.06-0.085\cdot(P/D)} \tag{1.22}$$

H is the axial step (height of one revolution) of the wire wrap.
All the parameters are bundle average values.
These empirical correlations are applicable for

$$1.025 \leq P/D \leq 1.42, \quad 8.0 \leq H/D \leq 50.0 \text{ and } 50 \leq N_{\mathrm{Re}} \leq 10^6.$$

4. LIQUID-METAL HEAT TRANSFER

A theoretical study of heat transfer with laminar flow through a channel or rod bundle is carried on under boundary conditions of prescribed constant surface temperature or constant heat flux. For laminar flow through rod bundles, the liquid metals around the rods, arranged in a triangular array, can be considered to consist of cells bounded by a hexagonal area surrounding individual rods. Table 4.1 collects the N_{Nu} for laminar flow through rod bundles under specific boundary conditions.

	$(N_{Nu})_L$ **Boundary Conditions**	
Triangular Array P/D	**Uniform wall temperature Circumferentially and Uniform Flux Axially**	**Uniform wall heat flux in all directions**
1.01	1.52	0.26
1.05	2.82	1.06
1.10	4.62	2.94
1.20	7.48	6.90
1.50	11.26	11.22
2.00	15.27	15.26

Table 4.1. N_{Nu} for laminar flow through rod bundles [7].

Heat transfer correlations for steady turbulent flow in channels or rod bundles have the following form [7]:

$$N_{Nu} = A + C\left(N_{Pe}\right)^{\beta} \tag{1.23}$$

if the ratio of eddy diffusivity of heat to that of momentum, Ψ, is assumed to be unity. Instead, if an average value of Ψ along the radial and circumferential directions is defined as $\bar{\Psi}$, the heat transfer is represented by:

$$N_{Nu} = A + C\left(\bar{\Psi} \cdot N_{Pe}\right)^{\beta} \tag{1.24}$$

4.1. PARALLEL FLOW IN BARE ROD BUNDLES (OR TUBE BANKS) [7]

In fuel assemblies liquid metal flows parallel to the fuel elements and removes heat from these elements. The flow inside channels is turbulent. The heat transfer to liquid metals significantly differs from the heat transfer of water. The main reason of this difference stays in the low Prandtl number for liquid metals; as seen before, it means that the contribution to the total heat transfer from the thermal conductivity (compared with the heat transfer for convection) is higher for liquid metals than that of water.

Generally, fuel elements in a Liquid Metal Fast Breeder Reactors (LMFBR) are organized in a triangular array; the P/D ratio varies between 1.20 and 1.50. For such arrangements, heat transfer between fuel elements and coolant (liquid metals) can be calculated using correlations like that:

$$N_{Nu} = A + B \cdot N_{Pe}^{x} \tag{1.25}$$

The first and second terms of equation represent, respectively, the contributions from the thermal conductivity and from the convection. Experimentally, the constant x is found to be close to 0.8, while the coefficients A and B depend on geometry of the heat exchange section (round tube, tube bundle). In particular the following theoretical correlations are used:

$$\begin{aligned} &\text{for } (P/D) > 1.35,\ N_{Nu} = A + 0.0155(\bar{\Psi} N_{Pe})^{0.86} \\ &\text{for } (P/D) \le 1.35,\ N_{Nu} = B + 0.025(\bar{\Psi} N_{Pe})^{0.80} \end{aligned} \tag{1.26}$$

where $A = 6.66 + 3.126(P/D) + 1.184(P/D)^2$ and B is proportional to the N_{Nu} for slug flow through the flow and is a function of P/D. The values of the constants A and B are listed below (see table 4.2).

P/D	**A**	P/D	**B**
1.35	13.17	1.10	7.25
1.40	13.36	1.20	10.65
1.50	14.01	1.30	12.00
1.60	14.69	1.40	12.85
1.70	15.40	-	-

Table 4.2. Constant values in equations 1.26 [7].

The effective ratio of the eddy diffusivity of heat to momentum is

$$\bar{\Psi} = 1 - \frac{1.82}{N_{\mathrm{Pr}} \left(\varepsilon_m / \nu\right)_{\max}^{1.4}} \tag{1.27}$$

and its value ranges between 0 and 1.

Values of $(\varepsilon_m/\nu)_{\max}$ are plotted against N_{Re} for different P/D ratios. Analytical studies have shown that circumferential variations in wall temperature and local heat transfer coefficients increase as the P/D decreases. So, P/D ratio has great influence on variations of wall temperature and local coefficients. At close spacing, the so-called equivalent-annulus model is no longer satisfactory for heat transfer prediction.

In a LMFBR, fuel and blanket assemblies use wire-wrap or spacer grid systems. These elements create increased intrachannel turbulence and enhance interchannel mixing. Both tend to equalize azimuthal temperature along the surface of fuel or blanket elements [7].

A review activity conducted by Konstantin Mikityuk [8] about heat transfer data and correlations for liquid metals in tube lattices shows an overview of the main equations used and the quality of each of these in the field of liquid metal heat transfer. The quality of the selected models is estimated quantitatively by implementing these correlations to the TRACE code and comparing their predictions with selected test data in terms of the wall-to-fluid temperature difference under specific Generation-IV Lead-cooled reactor conditions. The geometry and the power parameters of the test section are chosen to be typical for the Generation-IV Lead-cooled reactor: fuel pin outer diameter of 10 mm, P/D ratio of 1.4, average linear power density of 210 W/cm, axial power peaking factor of 1.3, core inlet coolant temperature of 400 °C.
These correlations, listed below [8], provide a functional dependence of the Nusselt number on the Peclet number and pitch-to-diameter ratio (P/D); some of them are a best fit to experimental data, others are derived theoretically.

- **Dwyer and Tu's correlation (1960) and Friedland and Bonilla's correlation (1961)**

$$N_{Nu} = 0.93 + 10.81(P/D) - 2.01(P/D)^2 + 0.0252(P/D)^{0.273} \cdot (\Psi \cdot N_{Pe})^{0.8}$$
$$N_{Nu} = 7.0 + 3.8(P/D)^{1.52} + 0.027(P/D)^{0.27} \cdot (\Psi \cdot N_{Pe})^{0.8} \quad (1.28)$$

The two equations are used to describe heat transfer to liquid metal flowing in a triangular bundle of circular rods.
The eddy diffusivities of heat and momentum are usually assumed equal in theoretical analyses of turbulent heat transfer, on the basis of the analogy between heat and momentum transfer; so, in these correlations, it is assumed to be $\bar{\Psi} = 1$.
The two correlations have different ranges of applicability: the first is recommended for $70 < N_{Pe} < 10^4$ and for $1.375 < (P/D) < 2.2$, while the second correlation is valid for $0 < N_{Pe} < 10^5$ and $1.3 < (P/D) < 10$.

- **Mareska and Dwyer's correlation (1964)**

$$N_{Nu} = 6.66 + 3.126(P/D) + 1.184(P/D)^2 + 0.0155 \cdot (\Psi \cdot N_{Pe})^{0.86} \quad (1.29)$$

This experimental equation is obtained for a test section consisting of 13 rods of 13 mm (o.d.) arranged in a triangular lattice with (P/D)=1.75 and with mercury as working coolant fluid $(N_{\mathrm{Pr}} = 0.02)$.
This correlation is recommended for triangular bundles in the range of $70 < N_{Pe} < 10^4$ and pitch-to-diameter ratio of $1.3 < (P/D) < 3$. It is assumed to be $\Psi = 1$.

- **Subbotin's correlation (1965)**

$$N_{Nu} = 0.58 \cdot \left(\frac{D_h}{D} \right)^{0.55} \cdot N_{Pe}^{0.45} \tag{1.30}$$

This correlation is recommended for the flow of liquid metal in a triangular lattice of rods with $80 < N_{Pe} < 4000$ and with $1.1 < (P/D) < 1.5$. D_h is the hydraulic diameter while D is the rod diameter. For triangular lattice, the correlation becomes:

$$N_{Nu} = 0.58 \cdot \left(\frac{2\sqrt{3}}{\pi} \cdot \left(\frac{P}{D} \right)^2 - 1 \right)^{0.55} \cdot N_{Pe}^{0.45} \tag{1.31}$$

but it is applied also for the square lattice in the following form:

$$N_{Nu} = 0.58 \cdot \left(\frac{4}{\pi} \cdot \left(\frac{P}{D} \right)^2 - 1 \right)^{0.55} \cdot N_{Pe}^{0.45} \tag{1.32}$$

- **Ushakov's correlation (1977)**

$$N_{Nu} = 7.55 \left(\frac{P}{D} \right) - \left(\frac{20}{(P/D)^{13}} \right) + \left(\frac{0.041}{(P/D)^2} \right) \cdot N_{Pe}^{0.56+0.19 \cdot (P/D)} \tag{1.33}$$

Recommended for a triangular lattice of rods with $1.3 \le P/D \le 2.0$ and $N_{Pe} \le 4000$.

- **Borishanski's correlation (1969)**

$$N_{Nu} = 24.15 \cdot \log\left(-8.12 + 12.76 \cdot (P/D) - 3.65 \cdot (P/D)^2 \right) + 0.0174 \cdot \left(1 - e^{-6((P/D)-1)} \right) \cdot B$$

$$\text{where B} = \begin{cases} 0, & \mathrm{N}_{Pe} < 200 \\ (\mathrm{N}_{Pe} - 200)^{0.9}, & \mathrm{N}_{Pe} \ge 200 \end{cases} \tag{1.34}$$

The equation is recommended for triangular rod bundles in the range of $60 < N_{Pe} < 2200$ and for $1.1 < (P/D) < 1.5$.

This correlation is derived from an experimental apparatus of 22 tubes of 22 mm (o.d.) arranged in equilateral triangular bundles with different P/D ratios (1.1, 1.3, 1.4, 1.5), the heated length of the test section being equal to 800 mm. The temperatures vary from 206 to 236 °C but the working fluid is not specified. The N_{Pr} varies from 0.007, 0.03, 0.024.

- **Graber and Rieger's correlation (1972)**

$$N_{Nu} = 0.25 + 6.2\frac{P}{D} + \left(0.032\frac{P}{D} - 0.007\right) \cdot N_{Pe}^{0.8-0.024\cdot(P/D)} \tag{1.35}$$

Recommended for a triangular lattice of rods with $1.25 \le P/D \le 1.95$ and $110 \le N_{Pe} \le 4300$.

This is based on experimental data obtained from a test section consisting of 31 tubes of 12 mm (o.d.), arranged in equilateral triangular bundles with P/D ratios of 1.25, 1.6 and 1.95., using as working fluid a mixture of 44% Na-56% K at temperatures from 100 to 425 °C; the N_{Pr} varies between 0.011 and 0.024.

- **Zhukov's correlation (2002)**

$$N_{Nu} = 7.55\frac{P}{D} - 14\left(\frac{P}{D}\right)^{-5} + 0.007 \cdot N_{Pe}^{0.64-0.246\cdot(P/D)} \tag{1.36}$$

This is the result of the data obtained from an experimental apparatus consisting of 25 round tubes of 12 mm (o.d.) arranged in a square lattice. Four sets of experimental data were measured for P/D ratios of 1.25, 1.28, 1.34 and 1.46. The working fluid is 22%Na-78%K at 50 °C. The heated length of the assembly is 980 mm; the Peclet number varies in the range $60 < N_{Pe} < 2000$.

As reported in [8], the correlations that give the highest quality results for the considered design and conditions are that of Ushakov and Graber and Rieger.

From this activity of review, a new correlation was derived as a best fit of the experimental data set used; this is reported below [8]:

$$N_{Nu} = 0.047\left(1 - e^{-3.8\cdot\left[(P/D)-1\right]}\right)\left(N_{Pe}^{\ 0.77} + 250\right) \tag{1.37}$$

This correlation is recommended for $1.1 \le P/D \le 1.95$ and $30 \le N_{Pe} \le 5000$.

The important difference of this new correlation from the others presented above is that it provides an asymptotic value for $P/D \to \infty$. This makes the correlation more generally usable in transient analysis code.

5. IDENTIFICATION AND APPLICABILITY EVALUATION OF ANALYTICAL MODELS IN SYSTEM CODES

5.1. RELAP5-3D SYSTEM CODE

5.1.1. PRESSURE DROP RELAP5-3D MODELS [9]

The RELAP5-3D wall friction model contains correlations for the friction factor in laminar, turbulent and transition regions. The laminar friction factor model is based on the exact solution for fully developed flow and constant fluid properties

$$f_L = \frac{64}{N_{\mathrm{Re}} \cdot \phi} \tag{1.38}$$

where $\phi = \frac{64}{C_{fL}}$ is a shape factor that allows the user to account for geometries different from the circular one; this allows the code to exactly match the friction factor for laminar flow.

RELAP5-3D calculates the turbulent friction factor using the Zigrang-Sylvester (1985) approximation to the Colebrook-White (1939) correlation:

$$\frac{1}{\sqrt{f_T}} = -2\log\left(\frac{\varepsilon}{3.7 \cdot D_h} + \frac{2.51}{N_{\mathrm{Re}}} \cdot \left(1.14 - 2\log_{10}\left(\frac{\varepsilon}{D_h} + \frac{21.25}{N_{\mathrm{Re}}^{0.9}}\right)\right)\right). \tag{1.39}$$

The code also uses an alternate turbulent wall friction model in which the friction factor is calculated from:

$$f_T = A + B \cdot N_{\mathrm{Re}}^{-C} \tag{1.40}$$

where A, B and C are constants that the user may specify for each control volume. Setting A=0, B=C_{fT} and C=0.18, it becomes the equation (1.17).

RELAP5-3D assumes that the transition region occurs between $2200 < N_{\mathrm{Re}} < 3000$ and calculates the friction factor by interpolating between the laminar value at a N_{Re}=2200, ($f_{L,2200}$), and the turbulent value at a N_{Re}=3000, ($f_{L,3000}$), obtaining:

$$f = \left(3.75 - \frac{8250}{N_{\mathrm{Re}}}\right) \cdot \left(f_{L,3000} - f_{L,2200}\right) + \left(f_{L,2200}\right) \tag{1.41}$$

A comparison between equations (1.38), (1.40), (1.41) and the correlation of Cheng and Todreas (1986) for P/D=1.3 and H/D=30 (see figure 5.1.) shows that, for these parameters, the transition region identified by the equation (1.18) ($980 < N_{\mathrm{Re}} < 16000$) differs from the one assumed by the code. The friction factor from the RELAP5-3D model is less than that from the correlation, with a maximum error of 40% at a N_{Re}=2200. Below N_{Re}=980 and N_{Re}=16000 the two friction factors are identical. These results indicates that the code's wall friction model needs to be improved to adequately represent wire-wrapped rod bundles in the transition region between laminar and turbulent flow.

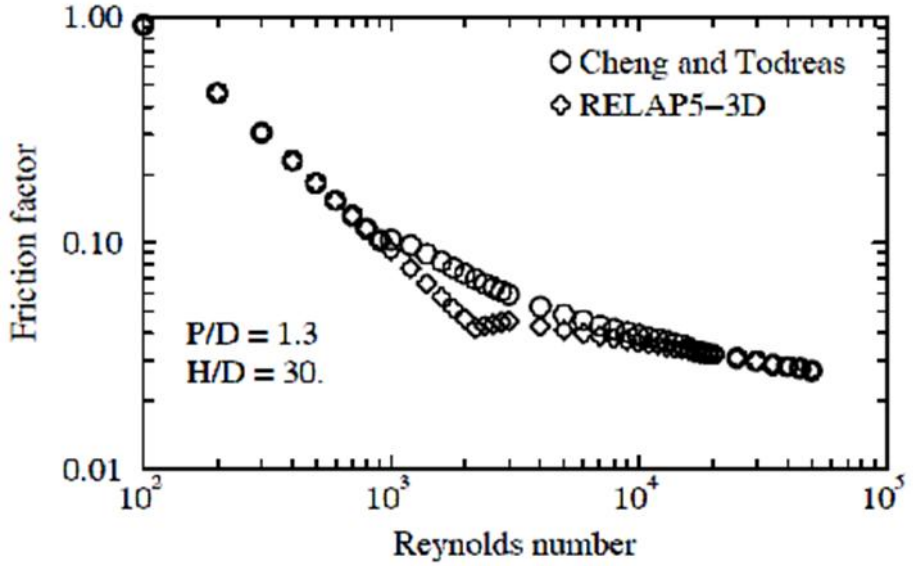

Fig. 5.1. Friction factor comparison for a wire-wrapped bundle [9].

As regard the form loss coefficient, RELAP5-3D requires a more general equation to accurately represent the frictional characteristics of a sharp-edged orifice if a wide range of N_{Re} needs to be simulated.

5.1.2. HEAT TRANSFER RELAP5-3D MODELS [9]

RELAP5-3D was originally developed to simulate thermal hydraulic systems that utilized light water as working fluid; it contains also NaK as working fluid.

Heat transfer through the fuel rod includes heat conduction within the fuel, heat transfer across the gap, heat conduction within the cladding and the heat transfer from the surface of the cladding to the coolant. The existing heat conduction models in RELAP5-3D should adequately represent the heat conduction across the fuel and the cladding. RELAP5-3D has simple models to calculate gap conductance and geometrical changes in light water reactor fuel rods. These models are expected to be applicable to the Lead-cooled reactors if it uses oxide fuel, but will not be applicable if it uses metallic fuel with a sodium bond. In either case, it is expected that a detailed fuel rod performance code will be used to determine appropriate parameters for use in RELAP5-3D system calculations so that the geometry of the fuel rod during normal operation is correctly represented. Thus, no changes are required in RELAP5-3D to model the performance of the fuel rods.

The heat transfer from the surface of the fuel rod cladding to the coolant is governed by the heat transfer correlations used by RELAP5-3D. The default correlation for single-phase heat transfer to liquid metals in RELAP5-3D, for fully developed flow in liquid metals with constant fluid properties, is:

$$N_{Nu} = 5.0 + 0.025 \cdot N_{Pe}^{0.8} \qquad \text{(constant wall temperature)} \qquad (1.42)$$

But fast reactors tend to have relatively flat power profiles and the constant heat flux assumption is expected to be more accurate than the constant wall temperature correlation. Thus, the correlation of Bird, valid for constant heat flux, gives more accurate results for liquid metals:

$$N_{Nu} = 7.0 + 0.025 \cdot N_{Pe}^{0.8} \qquad \text{(constant heat flux)} \tag{1.43}$$

RELAP5-3D also has an optional heat transfer correlation that was developed by Westinghouse for rod bundles with liquid metals; the Westinghouse correlation (Todreas and Kazimi, 1990) is:

$$N_{Nu} = 4.0 + 0.33 \cdot \left(\frac{P}{D}\right)^{3.8} \cdot \left(\frac{N_{Pe}}{100}\right)^{0.86} + 0.16 \cdot \left(\frac{P}{D}\right)^{5.0} \tag{1.44}$$

applies for $1.1 \le P/D \le 1.4$ and $10 \le \mathrm{N_{Pe}} \le 5000$.

Todreas and Kazimi also analysed the correlation of Borishanskii (1969) that gives more accurate results [9] than that written above for larger values of P/D ratio:

$$\begin{aligned} &N_{Nu} = 24.15 \cdot \log\left\{-8.12 + 12.76 \cdot (P/D) - 3.65 \cdot (P/D)^2\right\} \quad \text{for} \quad 1.1 < (P/D) < 1.5 \quad \text{and} \quad N_{Pe} \le 200 \quad \text{and} \\ &N_{Nu} = 24.15 \cdot \log\left\{-8.12 + 12.76 \cdot (P/D) - 3.65 \cdot (P/D)^2\right\} + 0.0174 \cdot \left(1 - e^{(6-6\cdot(P/D))}\right) \cdot \left\{N_{Pe} - 200\right\}^{0.9} \text{ for } 200 \le N_{Pe} \le 2000 \end{aligned} \tag{1.45}$$

So, the equations (1.43) and (1.45) have to be implemented in RELAP5-3D system code.

5.2. TRACE SYSTEM CODE MODELS

5.2.1. HEAT TRANSFER TRACE MODELS IN PIPES TO FLUIDS WITH $N_{\mathrm{Pr}} << 1$

The TRACE correlation used to simulate heat transfer phenomena for fluids with very low Prandtl number has the following form [10]:

$$N_{Nu} = 4.8 + 0.025 \cdot N_{Pe}^{0.8} \tag{1.46}$$

A review of literature, aimed at identifying a correlation which is commonly used and validated, reveals that the most common used correlation is the one of Seban and Shimazaki:

$$N_{Nu} = 5 + 0.025 \cdot N_{Pe}^{0.8} \tag{1.47}$$

5.2.2. HEAT TRANSFER TRACE MODELS IN BUNDLES TO FLUIDS WITH $N_{\mathrm{Pr}} << 1$

For liquid metals, TRACE does not distinguish between pipe and bundle flow, but the two options are available by connecting the hydraulic components to the inner side of a heat structure, that represents a pipe with internal heat source (channel/bundle), or to the outer side, that represents a pipe with heated wall [10].

Since the actual structure of TRACE does not allow differing between quadratic and hexagonal arrays, a general correlation needs to be implemented.

Studies carried out by Pfrang and Struwe and Mikityuk brought to identify the most suitable correlation in the one of Ushakov [10]:

$$N_{Nu} = N_{Nu,L} + \frac{3.67}{90 \cdot \left(\frac{P}{D}\right)^2} \cdot N_{Pe}^{\left[0.56+0.19\cdot\left(\frac{P}{D}\right)-0.1\cdot\left(\frac{P}{D}\right)^{-80}\right]} \cdot \left\{1 - \frac{1}{\frac{1}{6}\cdot\left[\left(\frac{P}{D}\right)^{30}-1\right] + \sqrt{1.15+1.24\cdot\varepsilon}}\right\} \tag{1.48}$$

with

$$N_{Nu,L} = \left[7.88\cdot\left(\frac{P}{D}\right) - 6.3\cdot\left(\frac{P}{D}\right)^{-17\cdot\left(\frac{P}{D}\right)\cdot\left(\frac{P}{D}-0.81\right)}\right] \cdot \left[1 - \frac{6.3\cdot\left(\frac{P}{D}\right)}{\left(\frac{P}{D}\right)^{20}\cdot\left(1+2.5\cdot\varepsilon^{0.86}\right)+3.2}\right] \tag{1.49}$$

These correlations are recommended for $1 < N_{Pe} < 4000$, for $1 < (P/D) < 2$ and for $0.01 < \varepsilon < +\infty$.

This factor is the approximate criterion of thermal similarity of the fuel rods, depending on the geometry and the thermal conductivity of the pin.

A simplified version of equation (1.48) is given below, with the condition that the P/D ration should be greater than 1.3 [10].

$$N_{Nu} = 7.55\cdot\left(\frac{P}{D}\right) - 20\cdot\left(\frac{P}{D}\right)^{-13} + \left(\frac{3.67}{90}\right)\cdot\left(\frac{P}{D}\right)^{-2} \cdot N_{Pe}^{\left[0.56+0.19\cdot\left(\frac{P}{D}\right)\right]} \tag{1.50}$$

BIBLIOGRAFIA

[1] "*The Potential of the LFR and the ELSY Project"*, L. Cinotti, C. F. Smith, J. J. Sienucki, H. Ait Abderrahim, G. Benamati, G. Locatelli, S. Monti, H. Wider, D. Struwe, A. Orden, I. S. Hwang, ICAPP 2007, Nice, France, May 13, 2007 through May 18, 2007.

[2] *"The Lead Fast reactor: Demonstrator (ALFRED) and ELFR Design"*, A. Alemberti, M. Frogheri, L. Mansani. International Conference on FAST REACTORS AND RELATED FUEL CYCLES: Safe Technological and Sustainable Scenarios-FR13, Paris, France, 4-7 March 2013.

[3] *"GenIV-International Forum"*. Annual Report, 2011.

[4] *"Lead-Cooled fast Reactor (LFR): Overview and Perspectives"*, L. Cinotti, C. F. Smith and H. Sekimoto. GIF Symposium, Paris, France, 9-10 September, 2009.

[5] **"***Fast Reactor Technology Plant Design"*, John G. Yevick, A. Amorosi. Prepared under the auspice of the United States Atomic Energy Commission, Division of Technical Information. THE M.I.T. PRESS, 1966.

[6] *"Thermal Hydraulic Fundamentals. Nuclear System I"*, Neil E. Todreas, Mujid S. Kazimi. Massachusetts Institute of Technology, 1990.

[7] *"Thermal Analysis of Liquid Metal Fast Breeder Reactors"*, Y. S. Tang, R. D. Coffield, Jr., R. A. Markley, Jr.. American Nuclear Society, 1978.

[8] *"Heat Transfer to Liquid Metal: Review of Data and Correlations for Tube Bundles"*, Konstantin Mikityuk. Nuclear Engineering and Design, Science Direct, Vol. 239, 2009.

[9] *"Applicability of RELAP5-3D for Thermal-Hydraulic Analyses of a Sodium-Cooled Actinide Burner Test Reactor"*, C. B. Davis, Idaho National Laboratory, July 2006.

[10] *"Improvements and Validation of the System Code TRACE for Lead and Lead-Alloy Cooled Fast Reactors Safety-Related Investigations"*, Wadim Jaeger, Victor Hugo Sanchez Espinoza. NUREG/IA-0421. Prepared as part of The Agreement on Research Participation and Technical Exchange Under the Thermal-Hydraulic Code Applications and Maintenance Program (CAMP), U.S. Nuclear Regulatory Commission, February 2013.

LIST OF ACRONYMS

ALFRED	LFR-Demo Advanced Lead Fast Reactor European Demonstrator
ELFR	European Lead-cooled Fast Reactor
ELSY	European Lead-cooled System
GIF	Generation-IV International Forum
LBE	Lead-Bismuth Eutectic
LEADER Project	Lead-cooled European Advanced DEmonstration Reactor Project
LFR	Lead-cooled Fast Reactor
LMFBR	Liquid Metal Fast Breeder Reactor
O.D.	Outer Diameter
PP	Primary Pump
RELAP5-3D	Reactor Excursion and Leak Analysis Program 5-3 Dimension
SG	Steam Generator
SSTAR	Small Secure Transportable Autonomous Reactor
TRACE	TRAC/RELAP Advanced Computational Engine

Appendice

Breve curriculum scientifico del gruppo di lavoro impegnato nell'attività

Il gruppo di lavoro impegnato nell'attività è costituito da un professore ordinario di Impianti nucleari dell'Università di Palermo (Dipartimento dell'Energia), Giuseppe Vella, da un assegnista Fulvio Mascari e da Maria Lorena Richiusa, laureanda del corso di laurea magistrale in Ingegneria Energetica e Nucleare dell'Università degli Studi di Palermo.

Il prof. Giuseppe Vella , Ordinario del Settore Scientifico Disciplinare ING-IND/19 Impianti Nucleari, è Responsabile del reattore nucleare di ricerca AGN 201 - COSTANZA dell'Università di Palermo. Ha coordinato diversi programmi di ricerca finanziati dal Ministero della Ricerca Scientifica e Tecnologica. E' stato Coordinatore nazionale di un progetto di ricerca di interesse nazionale PRIN-2007 finanziato dal MIUR. E' autore o coautore di più di 150 articoli pubblicati su riviste scientifiche nazionali ed internazionali e/o presentati a conferenze, congressi o simposi. E" anche coautore di diversi rapporti nell'ambito dei PAR trascorsi.. L'attività scientifica del prof. Vella ha riguardato principalmente le seguenti tematiche: tubi di calore al sodio, problemi di ribagnamento di superfici ad elevata temperatura, efflussi critici bifase, analisi termoidrauliche relative alla sicurezza dei reattori nucleari a fissione, analisi neutroniche, termoidrauliche e termomeccaniche del mantello e di componenti ad alto flusso termico di un tipico reattore a fusione di tipo TOKAMAK. E' stato referee per la rivista "Fusion Engineering and Design" e "Nuclear Engineering and Design".

Fulvio Mascari, assegnista di ricerca del S.S.D. ING-IND/19, da circa 6 anni svolge attività di ricerca su problematiche termoidrauliche e nucleari connesse allo sviluppo dei reattori a fissione. Partecipa alle attività di validazione dei codici termoidraulici di sistema TRACE e RELAP5, collaborando con il Department of "Nuclear Engineering & Radiation Health Physics" della Oregon State University, NuScale, l'Università degli Studi di Pisa e ENEA. Recentemente ha preso parte alle attività di un International Collaborative Standard Problem (ICSP) on Integral PWR Design Natural Circulation Flow Stability and Thermo-Hydraulic Coupling of Containment and Primary System during Accidents" promosso dall'IAEA.

I risultati delle sue attività di ricerca sono stati pubblicati su una ventina di memorie in riviste internazionali, capitoli di libro, in atti di congresso nazionali e internazionali e rapporti. E' anche coautore di diversi rapporti nell'ambito dei PAR trascorsi. E' stato referee per le riviste "Nuclear Engineering and Design" e "Science and Technology of Nuclear Installations".

La laureanda Maria Lorena Richiusa, ha conseguito la laurea di primo livello in Ingegneria Energetica – Profilo Sicurezza e Tecnologie Nucleari- presentando la tesi " Reattori integrati di tipo PWR e impianti sperimentali di qualificazione. Analisi delle condizioni di funzionamento in circolazione naturale e preliminari indagini teorico-sperimentali".

Problematiche di scambio termico, in circolazione naturale, tra il sistema primario e il fluido secondario, in presenza di uno scambiatore di calore a tubi elicoidali, sono state affrontate mediante il codice TRACE.